06 OCT 1995

海洋開発及地球科学技術調査研究促進費

地球科学技術特定調査研究

アジアモンスーン機構に関する研究

JAPANESE EXPERIMENT ON ASIAN MONSOON (JEXAM)

（平成元年～平成10年）
（F Y 1989～F Y 1998）

平成６年度　成果報告書
ANNUAL REPORT
(APRIL 1994～MARCH 1995)

LIBRARY
OCT 03 1995
National Marine Fisheries Service
2570 Dole St.
Honolulu, Hawaii

平成７年８月
August　1995

科学技術庁研究開発局
Research and Development Bureau
Science and Technology Agency
Japan

はじめに

大規模な季節変動として知られているアジアモンスーンは、インド洋・東南アジア周辺の海洋とチベット・ヒマラヤを始めとしたアジア大陸の地表面が、大気を媒体として熱・水蒸気等の交換により、相互に影響を及ぼし合っている現象です。その活動の年々変動は、東南アジア地域や、日本を始めとした周辺地域の気候のみならず、大気大循環を介して世界の気候に大きな影響を与えています。また、アジアモンスーンの活動が西部熱帯太平洋域の大気・海洋変動を引き起こし、太平洋規模で発生するエル・ニーニョ／南方振動の引き金になっている可能性があるという指摘もあり、この点からも注目されています。しかし、これらの地域・海域は広大であり、また観測環境が厳しいこと等から観測体制の整備が遅れており、気象・海象・陸象に関するデータの収集は必ずしも十分に行われていませんでした。

このため科学技術庁では、海洋開発及地球科学技術調査研究促進費により「アジアモンスーン機構に関する研究」を平成元年度より開始し、観測・解析を進めてきました。平成５年１月１１日には、「『アジアモンスーン機構に関する研究』プロジェクトに関する日本国科学技術庁と中華人民共和国国家気象局との間の実施取極」が結ばれ、日中の協力体制も整いました。

本研究の成果が、アジアモンスーン機構の解明に寄与し、さらには気候変動に対する理解を深めることを期待しています。

最後になりましたが、本研究に携わられた関係各位に対し感謝するとともに、今後とも御協力をお願いする次第です。

平成７年８月

科学技術庁研究開発局長

加藤　康宏

アジアモンスーン機構に関する研究

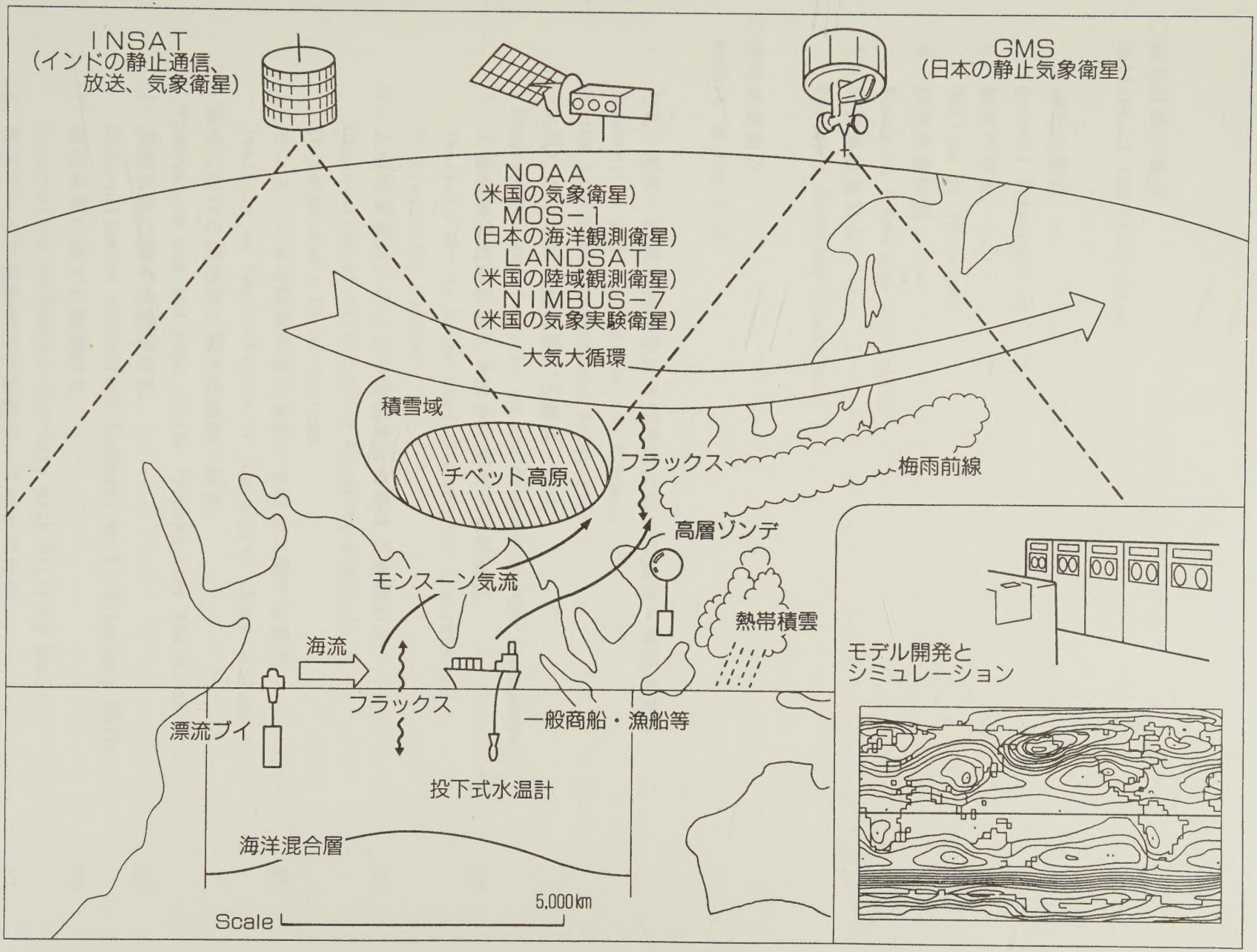

Digitized by the Internet Archive
in 2025

https://archive.org/details/annual-report-japanese-experiment-on-asian-monsoon-jexam_1995-08

目　次
Contents

○研究計画の概要
Outline of the Study Plan

Ⅰ. 研究の趣旨 …… 3
General Introduction
Ⅱ. 研究の概要 …… 5
Outline of the Study
Ⅲ. 研究実施体制 …… 8
Research Items and Institutes
Ⅳ. 研究検討委員会 …… 10
Research Steering Committee

○研究成果報告
Result of the Study

Ⅰ. 大気・海洋・陸域間相互作用の諸過程に関する観測・解析研究
Observation and Analysis on the Process
of the Atmosphere-Ocean-Land Interactions
1. 大気における諸過程に関する観測・研究
Observation and Analysis on the Process in the Atmosphere
(1) 大規模積雲対流活動と降水系に関する解析研究 …… 15
Analysis on the Large scale Convective Activity and
Precipitation Systems
(2) 大規模雲域内における対流雲構造に関する観測研究 …… 25
Observation of Structure of Convective Clouds
in Large-scale Cloud Systems
(3) モンスーン域対流雲の維持過程と水収支に関する研究 …… 35
Analysis on the evolution of Convective cloud systems
2. 海洋における諸過程に関する観測・研究
Observation and Analysis on the Process over the Ocean
(1) 表層水温に関する観測研究 …… 41
Observation on Subsurface Temperature by Voluntary Ships
(2) 海流循環に関する観測研究 …… 73
Observation on Oceanic Currents with Drifting Buoys
(3) 海洋データの標準化及び海洋データ交換の推進 …… 81
Standardization of Oceanic Data and Promotion of Exchange
of Oceanic Data and Information

3．陸域における諸過程に関する観測・研究
Observation and Analysis on the Process over the Land
(1) チベット・ヒマラヤにおける水文変動に関する観測研究 …… 85
Observation on Hydrology over the Tibetan Plateau and Himalayas
(2) 地表面熱収支に関する観測研究 …… 97
Observation on Regional Surface Heat Budget
Observational Study of the Ground Surface Heat Budgets
(3) モンスーン循環広域条件及び雪氷変動状況に関する解析研究 …… 117
Analysis on Environmental Condition and Snow-Ice Cover Changes Affecting Monsoon Cycle in Asia
(4) 地域水収支に関する解析研究 …… 123
Analytical study of water balance on representative river basins
Ⅱ．数値モデルによる大気・海洋・陸域間相互作用の実験研究
Experiment of the Atmosphere-Ocean-Land Interactions by the Use of Numerical Models
1．数値モデルによる4次元資料同化システムの開発に関する研究 …… 129
Development of the Four Dimensional Data Assimilation System by the Use of Numerical Model
2．広域水収支モデルの開発に関する研究 …… 137
Development of the Water Balance Model over the Wide Area
Ⅲ．大気・海洋・陸面間の相互作用に関する総合研究
Synthetic Study on the Atmosphere-Ocean-Land Interactions
1．大規模モデルによる大気・海洋・陸面間の相互作用に関する実験研究 …… 151
Experiment of the Atmosphere-Ocean-Land Interactions by the Use of General Circulation Models
2．モンスーンのエネルギー収支に関する解析研究 …… 159
Analysis of the Energy Balance of Monsoon
3．モンスーン循環系の総合解析 …… 167
Synthetic Study of the Monsoon Circulations

○観測・解析研究ディレクトリー …… 173
Directory of Observation/Analysis Data Set

研究計画の概要

Outline of the Study

Ⅰ．研究の趣旨

アジアモンスーンは、インド洋・東南アジア周辺の海洋とチベット・ヒマラヤを始めとしたアジア大陸の地表面が、その熱的特性の相違により大気を媒体とした熱・水蒸気等の交換を通じて、それぞれ相互に影響を及ぼし合う結果、東南アジア・東アジア地域における季節的な現象として発現している。その活動の年次の変動は、東南アジア地域や、日本を始めとした周辺地域の気候の変動に大きな影響を及ぼすばかりでなく、大気大循環変動を介して世界の気候にも大きな影響を与えている。また最近、アジアモンスーンの活動の異常は西部熱帯太平洋域の大気・海洋変動を引き起こし、これが太平洋規模で発生するエル・ニーニョ／南方振動の引き金となっている可能性があるという研究報告もあり、この点からも注目する必要がある。しかしながら、これらの地域・海域は、対象域の広大さや観測環境の厳しさ等から観測体制が整備されておらず、気象・海象・陸象の基本的な要素に係るデータの収集が必ずしも十分に行なわれているとは言えない。

従って、アジアの一員であり、アジアモンスーンの直接的影響を受け、大気・海洋観測の十分なポテンシャルを有する我が国が、世界の気候を形成する複雑なシステムの一つであるアジアモンスーンの機構を解明するため長期的・総合的な研究を実施することが緊要となっている。本研究を実施することにより、我が国を含むアジア地域における旱ばつや長雨といった異常気象発現の予測技術のみならず、世界的規模の気候変動を予測する技術の発展に寄与することが期待される。

以上のような状況を踏まえて、本研究は１９８９年度から１０年間の計画で行っている。

I. General Introduction

Asian Monsoon is caused by the thermal contrast between the Indian Ocean and surrounding oceans, and the land surface of Asian Continent. These two land and ocean areas interact with each other through the exchange of the heat and moisture. Its consequence is observed as a seasonal phenomenon in the regions of Southeast Asia and East Asia, including Japan.

The year-to-year variation of the Asian Monsoon has a significant influence not only on the climate through the global atmospheric circulations. Furthermore, it is recently reported that the anomalous activities of the atmospheric/oceanic variations over the tropical western Pacific which, in turn, trigger the El Nino/Southern Oscillation events over the whole Pacific Ocean.

Through it is recognized that Asian Monsoon plays an important role in the global climate system, its mechanism has not yet been made clear. This is mainly attributable to the fact that the atmospheric and oceanographic data are sparse over those regions due to the technical difficulties in the observations and the insufficiencies of conventional observation network.

Japan, as a member of the Asian countries, is situated under the direct influence of the Asian monsoon and has a capability to conduct the atmospheric and oceanographic observations. Therefore, it is an important role of Japan to carry out the research projects for the study on Asian Monsoon in cooperation with the countries such as China and India.

This project is expected to make a contribution for the improvement of the long-range forecast of the global climate change as well as the forecasting technique of the unusual weather, such as drought and long spell of rain.

Based on the understandings as mentioned above, Science and Technology Agency (STA) of Japan has launched this ten-year research project since April 1989.

Ⅱ．研究の概要

1．大気・海洋・陸域間相互作用の諸過程に関する観測・解析研究

(1) 大気における諸過程に関する観測・解析研究

・　静止気象衛星資料をデータベース化し、モンスーン活動の年々変動、降水システム、エルニーニョとの関連についての解析を行う。

・　前期に観測した対流雲のデータを解析し、対流雲の構造、対流雲による熱、水、運動量の輸送過程を明らかにする。

(2) 海洋における諸過程に関する観測・解析研究

・　東南アジア周辺海域及びインド洋を航行する公庁船、商船及び漁船により海洋表層水温の通年観測を行う。

・　インド洋に漂流ブイを放流し、大規模海流循環の通年観測を行う。

・　上記で取得した海洋データの標準化、データベース化を促進する。また、インド洋及び東南アジア周辺海域の海洋観測情報交換システムを構築し、取得データを交換する。

(3) 陸域における諸過程に関する観測・解析研究

・　チベット地域における気象及び陸面の観測を行い、大気陸面間のエネルギー収支を見積もる。

・　商船委託により、インド洋から東南アジア周辺に至る海域での海上気象・高層気象観測、及びウィンドプロファイラーにより下層大気の観測を行い、大気海洋間、大気陸面間のエネルギー収支を見積もる。

・　極軌道地球観測衛星資料から、積雪、雲分布、土壌水分量を算出し、解析する。

・　中国の代表流域の水文資料、水文・気象データを収集し、水収支解析及び蒸発発散解析を行う。

2．数値モデルによる大気・海洋・陸域間相互作用の実験研究

(1) 数値モデルによる4次元資料同化システムの開発に関する研究

・　現在の4次元資料同化システムに、現在使用されていない衛星データ等を組み込めるように高度化を図り、得られた物理量からモンスーン機構を考察する。

(2) 広域水収支モデルの開発に関する研究

・　前期に開発した流出量モデル、蒸発散量モデルへの検証・改良を行うと共に、積雪・流出量サブモデルを開発し、積雪地域への広域水収支モデルの適用を図る。

3．大気・海洋・陸面間の相互作用に関する総合研究

(1) 大規模モデルによる大気・海洋・陸面間の相互作用に関する実験研究

・　前期に用いたモデルの改良を行う。また、大気海洋結合モデルを導入し、アジアモンスーンの機構に対する海洋や陸面の役割を評価する。さらに高分解能の大気大循環モデルを開発し、地表面状態や対流活動の影響を評価する。

(2) モンスーンのエネルギー収支に関する解析研究

・　モデルのシミュレーション結果を衛星観測データの解析結果によって検証し、モンスーン機構のエネルギー収支解析を行う。

(3) モンスーン循環系の総合解析

・　海洋や雪氷分布の変動と、モンスーン循環を含む大気大循環や日本の天候の関連を調査する。また、高層・地上・海洋・陸面観測データを用いて総合的に解析することによって、モンスーン循環系を解明する。

Ⅱ. Outline of the Study

1. Observation and Analysis on the Process of the Atmosphere-Ocean-Land Interactions

(1) Observation and Analysis on the Process in the Atmosphere

- To construct a database of the Japanese and Indian satellites and make an analysis of the large scale cloudiness changes.
- To observe and three dimensional structures of the tropical convective clouds related to the heat budget of the atmosphere-ocean interaction by wind Doppler radar.

(2) Observation and Analysis on the Process over the Ocean

- To observe sub-surface temperature throughout the year by voluntary, official, commercial and fishing ships over the Southeast Asia and the Indian Ocean.
- To observe larg-scale oceanic current throughout the year by drifting buoys over the Indian Ocean.
- To standardize and construct a database of the oceanic data and promote a data exchange. To construct an information exchange system concerning to the observation in the Indian Ocean.

(3) Observation and Analysis on the Process over the Land

- To observe weather and land surface conditions over the Tibetan area and estimate an energy budget of the atmosphere-land interaction.
- To observe three dimensional structures of low level air flow related to the heat budget of the atmosphere-land interaction by wind profiler.
- To promote a maritime meteorological observation by voluntary commercial ships and estimate an energy budget of the atmosphere-ocean interaction.
- To construct a database of the polar orbiting earth observation satellites and make an analysis of the atmosphere-ocean-land situations related to the large scale hydrological variations.
- To collect daily hydro-meteorological data over the Yangtze River basin and make an analysis of the long-term variations.

2. Experiment of the Atmosphere-Ocean-Land Interactions by the Use of Numerical Models

(1) Development of the Four Dimensional Data Assimilation System by the Use of Numerical Model

To develop the four dimensional data assimilation system by the use of numerical models for the analysis on the process of the atmosphere-ocean-land interactions.

(2) Development of the Water Balance Model over the Wide Area

To develop numerical models for the investigation of the large scale hydrological budget over the Tibet, India and Southeast Asia related to the heat transport.

3. Synthetic Study on the Atmosphere-Ocean-Land Interactions

(1) Experiment of the Atmosphere-Ocean-Land Interactions by the Use of General Circulation Models

- To perform numerical experiments of the effect of intraseasonal 30-60 day variation on Asian monsoon.
- To perform numerical experiments by the atmosphere-ocean coupled model for the investigation of the effects of oceanic conditions on the long-term variation of the atmosphere-land condition.

(2) Analysis of the Energy Balance of Monsoon

To construct a database of Earth radiation budget through the polar orbiting meteorological satellites and make an analysis of an effect of the monsoon variation.

(3) Synthetic Study of the Monsoon Circulations

To make a comprehensive analysis of the monsoon circulation by the use of the standardized data.

Ⅲ. 研究実施体制
Research Items and Institutes

研究項目 Research Items	担当機関 Research Institutes
Ⅰ. 大気・海洋・陸域間相互作用の諸過程に関する観測・解析研究 Observation and Analysis on the Process of the Atmosphere-Ocean-Land Interactions	
1. 大気における諸過程に関する観測・解析研究 Observation and Analysis on the Process in the Atmosphere	
(1) 大規模積雲対流活動と降水系に関する解析研究 Analysis on the Large scale Convective Activity and Precipitation Systems	気象庁　気象研究所 Meteorological Research Institute (MRI), Japan Meteorological Agency (JMA)
(2) 大規模雲域内における対流雲構造に関する研究 Observation of Structure of Convective Clouds in Large-scale Cloud Systems	気象庁　気象研究所 MRI/JMA
(3) モンスーン域対流雲の維持過程と水収支に関する研究 Analysis on the evolution of Convective cloud systems	科学技術庁　防災科学技術研究所 National Research Institute for Earth Science and Disaster Prevention (NRIESDP), Science and Technology Agency (STA)
2. 海洋における諸過程に関する観測・解析研究 Observation and Analysis on the Process over the Ocean	
(1) 表層水温に関する観測研究 Observation on Subsurface Temperature by Voluntary Ships	水産庁　遠洋水産研究所 Far seas Fisheries Research Laboratory, Fisheries Agency 気象庁　海洋気象部 Marine Department, JMA
(2) 海流循環に関する観測研究 Observation on Oceanic Currents with Drifting Buoys	海上保安庁水路部 Hydrographic Department, Maritime Safety Agency (MSA)
(3) 海洋データの標準化及び海洋データ交換の推進 Standardization of Oceanic Data and Promotion of Exchange of Oceanic Data and Information	海上保安庁水路部 Hydrographic Department, MSA
3. 陸域における諸過程に関する観測・解析研究 Observation and Analysis on the Process over the Land	
(1) チベット・ヒマラヤにおける水文変動に関する観測研究 Observation on Hydrology over the Tibetan Plateau and Himalayas	科学技術庁　防災科学技術研究所 NRIESDP/STA

研究項目 Research Items	担当機関 Research Institutes
(2) 地表面熱収支に関する観測研究 Observation on Regional Surface Heat Budget Observational Study of the Ground Surface Heat Budgets	気象庁　気象研究所 MRI/JMA 郵政省　通信総合研究所 Communications Research Laboratory, Ministry of Posts and Telecommunications
(3) モンスーン循環広域条件及び雪氷変動状況に関する解析研究 Analysis on Environmental Condition and Snow-Ice Cover Changes Affecting Monsoon Cycle in Asia	科学技術庁　防災科学技術研究所 NRIESDP/STA
(4) 地域水収支に関する解析研究 Analytical study of water balance on representative river basins	科学技術庁　防災科学技術研究所 NRIESDP/STA
Ⅱ. 数値モデルによる大気・海洋・陸域間相互作用の実験研究 Experiment of the Atmosphere-Ocean-Land Interactions by the Use of Numerical Models	
1. 数値モデルによる4次元資料同化システムの開発に関する研究 Development of the Four Dimensional Data Assimilation System by the Use of Numerical Model	気象庁　予報部 Forecasting Department, JMA
2. 広域水収支モデルの開発に関する研究 Development of the Water Balance Model over the Wide Area	科学技術庁　防災科学技術研究所 NRIESDP/STA
Ⅲ. 大気・海洋・陸面間の相互作用に関する総合研究 Synthetic Study on the Atmosphere-Ocean-Land Interactions	
1. 大規模モデルによる大気・海洋・陸面間の相互作用に関する実験研究 Experiment of the Atmosphere-Ocean-Land Interactions by the Use of General Circulation Models	気象庁　気象研究所 MRI/JMA
2. モンスーンのエネルギー収支に関する解析研究 Analysis of the Energy Balance of Monsoon	気象庁　気象研究所 MRI/JMA
3. モンスーン循環系の総合解析 Synthetic Study of the Monsoon Circulations	気象庁　予報部 Forecasting Department, JMA
Ⅳ. 検討委員会の開催等 Research Steering Committee	気象庁　気象研究所 MRI/JMA 科学技術庁　研究開発局 Research and Development Bureau, STA

Ⅳ. 研究検討委員会
Research Steering Committee

委員名 Membership	所属 Affiliation
委員長　浅井　冨雄 Chairman: Prof. Tomio Asai	広島大学総合科学部自然環境研究コース教授 Faculty of Integrated of Arts and Sciences, University of Hiroshima
委員　石川　孝一 Member : Mr. Koh'ichi Ishikawa	気象庁海洋気象部海洋課調査官 Marine Department, Japan Meteorological Agency
岩崎　俊樹 Dr. Toshiki Iwasaki	気象庁予報部数値予報課予報官 Forecasting Department, Japan Meteorological Agency
大塚　伸 Mr. Shin Ohtsuka	気象庁気象研究所台風研究部長 Meteorological Research Institute, Japan Meteorological Agency
大畑　哲夫 Dr. Tetsuo Oh'hata	名古屋大学大気水圏科学研究所助手 Institute for Hydrospheric and Atmospheric Sciences, Nagoya University
幾志　新吉 Dr. Shinkichi Kishi	科学技術庁防災科学技術研究所先端解析技術研究部長 National Research Institute for Earth Science and Disaster Prevention, Science and Technology Agency
久保　良雄 Mr. Yoshio Kubo	海上保安庁水路部海洋情報課長 Hydrographic Department, Maritime Safety Agency
住　明正 Prof. Akimasa Sumi	東京大学気候システム研究センター長 Center for Climate System Research, University of Tokyo
鶴田　義成 Dr. Yoshinari Tsuruta	水産庁中央水産研究所企画調整部主任研究官 Central Fisheries Research Laboratory, Fisheries Agency

委員名 Membership	所属 Affiliation
西田　英男 Mr. Hideo Nishida	海上保安庁水路部企画課海洋研究室長 Hydrographic Department, Maritime Safety Agency
新田　勁 Prof. Tsuyoshi Nitta	東京大学気候システム研究センター教授 Center for Climate System Research, University of Tokyo
萩野谷　成徳 Dr. Shigenori Haginoya	気象庁気象研究所物理気象研究部主任研究官 Meteorological Research Institute, Japan Meteorological Agency
増田　悦久 Dr. Yoshihisa Masuda	郵政省通信総合研究所 Communications Research Laboratory, Ministry of Posts and Telecommunications
水野　恵介 Dr. Keisuke Mizuno	水産庁遠洋水産研究所海洋・南大洋部低緯度域海洋研究室長 Far Seas Fisheries Research Laboratory, Fisheries Agency
安成　哲三 Prof. Tetsuzoh Yasunari	筑波大学地球科学系教授 Institute of Geosciences, University of Tsukuba
山形　俊男 Prof. Toshio Yamagata	東京大学大学院理学系研究科教授 Graduate School of Science, University of Tokyo
中村　英俊 Mr. Hidetoshi Nakamura	科学技術庁研究開発局地球科学技術推進室長 Office of Earth Science and Technology, Research and Development Bureau, Science and Technology Agency

研究成果報告

Result of the Study

I. Observation and analysis on the process of the atmosphere-ocean-land interaction

1. Observation and analysis on the process in the atmosphere

(1) Analysis on the Large scale Convective Activity and Precipitation Systems

Japan Meteorological Agency
Meteorological Research Institute,
Masato Murakami, Toshiro Inoue,
Kiyotoshi Takahashi, Minoru Tanaka
Meteorological Satellite Center
Kazuo Itoh, Tomoo Ohno

(Abstract)

The influence of the intraseasonal mode to the diurnal variation was investigated for the summer case around the South China Sea using convective index derived from one degree square mesh mean TBB data with a threshold for reducing the influence of surface temperature variation. It is shown that the contrast between land and sea is not so clear compared with the case using TBB directly.

The analysis of the precipitation systems using 5-day mean GMS high cloud amount data from 1978 to 1992 showed that the phase of the 30-to-60 day intraseasonal oscillation over western north Pacific are linked to SST in the eastern Equatorial Pacific. The onset of convection near 20N,150E are early in the La Nina years and late in the El Nino years. Similar delay in the Baiu rainy season were observed near Japan.

Convective activity defined by brightness temperature (TBB) from infrared measurements is compared with cumulonimbus type cloud area defined by split window (11mm and 12mm) measurements. Colder TBB areas show reasonable agreement with cumulonimbus type clouds areas. However, there are some difference between the two observations. Some colder TBBs in infrared image correspond to cirrus clouds which cover large area over the tropical region. Low level cumulus/strato-cumulus clouds classified by split window are missed in the infrared images.

Contrastive features of convective activity between 1988 and 1991 summer over the mainland China was studied using cumulus type clouds define by split window data. There was severe damage due to heavy rain along the Huaihe river in 1991 and was drought in 1988 over the mainland China. Very active convection area is confined along the Yangtze river and the Huaihe river in July, 1991. While, in July 1988, no significant convection area is seen over the mainland China except over the northern part.

1. Objectives

This study aims at revealing the large scale features of the Asian monsoon by using satellite data and the objective analysis data. The diurnal and intraseasonal variations are known as principle variations in the tropical convective activity. In FY 95 the investigation was carried out to reveal the influence of the intraseasonal mode to the diurnal variation. Efforts were made to reduce the influence of surface temperature variation and to understand the effect in the monsoon activity.

The main objective of this part is also to study characteristic features of SST, water vapor amount and convective activity associated with Asian summer monsoon over the 40S-40N, 40E-150E area using split window (11mm and 12mm) data. Split window measurement is effective in estimating Sea Surface Temperature (SST) and water vapor amount over the cloud free ocean area. Further optically thick (cumulus) clouds and optically thin (cirrus) clouds can be classified objectively using the split window measurements.

2. Methods

The analysis of the diurnal variation was carried out for the summer case. We used the convective index defined with a threshold 255K in the similar way as Nitta and Skine(1994) for cutting off information below the threshold and reducing the influence of surface temperature variation of land and sea. The amplitudes and phases of diurnal variations were calculated by the Fourier analysis of 3 hourly data. The active and inactive phases of the intraseasonal mode were defined at the key region with most variance to the west of the Philippines. The composites were made at both phases respectively, and were compared with each other.

The analysis of the precipitation systems using the 5-day mean GMS high-cloud-amount data was carried out with emphasis on the interannual variation of the intraseasonal oscillation and its relationship to El Nino and La Nina.

Infrared (IR) measurements from satellite give us information on clouds. Therefore, IR data from satellite are widely used for the analysis of convective activity over the tropics. However, we cannot tell the difference between cold non-precipitating cirrus clouds and convective clouds from the single infrared measurements. Split window on board NOAA polar orbiting satellite is effective in classifying optically thin cirrus clouds and optically thick cumulus clouds. Here, we compared infrared images with cloud type map derived from split window measurements. Convective activity over the mainland China was assessed for the year of 1988 and 1991 summer using the mean cloud top temperature for the cumulus clouds which are classified by split window data.

3. Results

Figures 1 and 2 show the differences in amplitudes and phases of the diurnal variations, respectively. Dotted areas denote the values where the diurnal amplitude was enhanced(suppressed) at the inactive(active) phase at key region. One cannot see the contrast between the land and sea clearly in the figures This situation is different from the previous result in which the TBB values were used directly.

In Fig. 2, the length of arrows indicates the absolute values of the amplitude difference between active and inactive phases. The direction of arrows shows the phase difference between the maximum phases of the convective activity. For example, the direction pointing to the north means the zero phase difference and the direction pointing to eastward(westward) means 6 hours advance(behind) in the

inactive(active) phase. The situation in this figure shows that the phase of diurnal variation is not affected so largely by the intraseasonal mode.

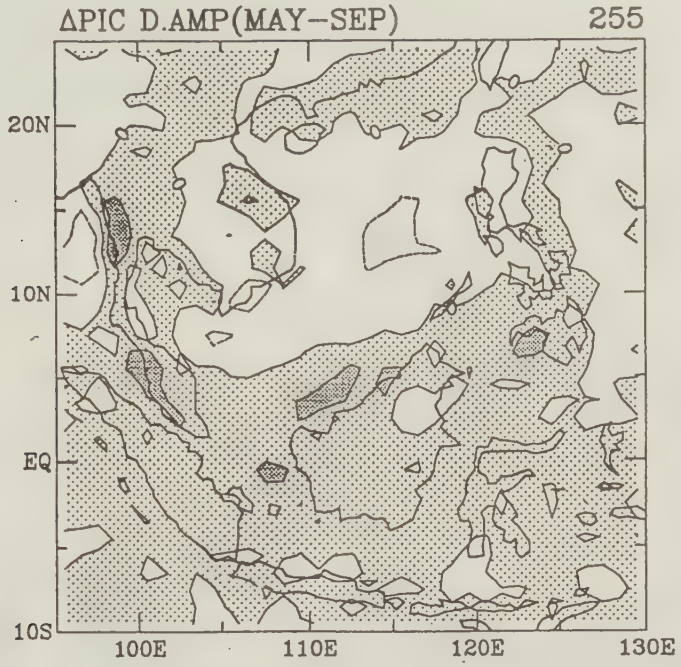

Figure 1 Summer horizontal distribution of differences of diurnal amplitudes defined by subtraction of the active phase's one from the inactive.

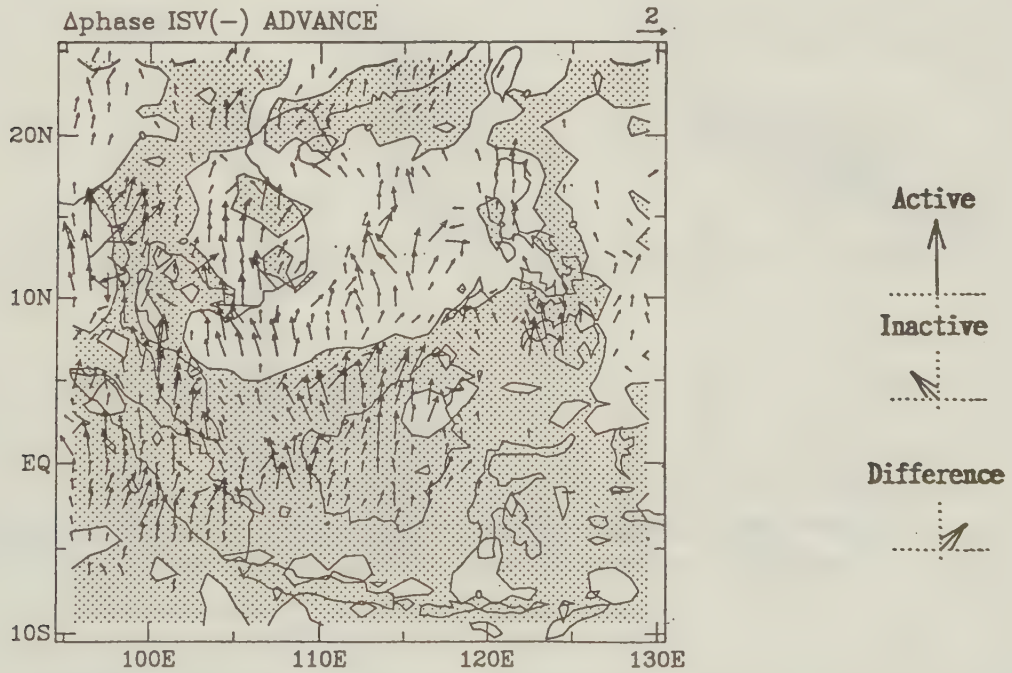

Figure 2 Summer horizontal distribution of differences presented in vector form of phases and amplitudes of diurnal variations between the inactive and active phases.

The analysis of the precipitation systems using the 5-day mean GMS high-cloud amount data from 1978 to 1992 showed that the phase of the 30-to-60 day intraseasonal oscillation over the western north Pacific is linked to the SST in the eastern equatorial Pacific. The onset of convection near 20N, 150E are early in the La Nina years(1978,84,85,88) and are delayed by 20 to 25 days during the El Nino years (Figure 3). Similar delay in the ending dates of the Baiu season were observed near Japan.

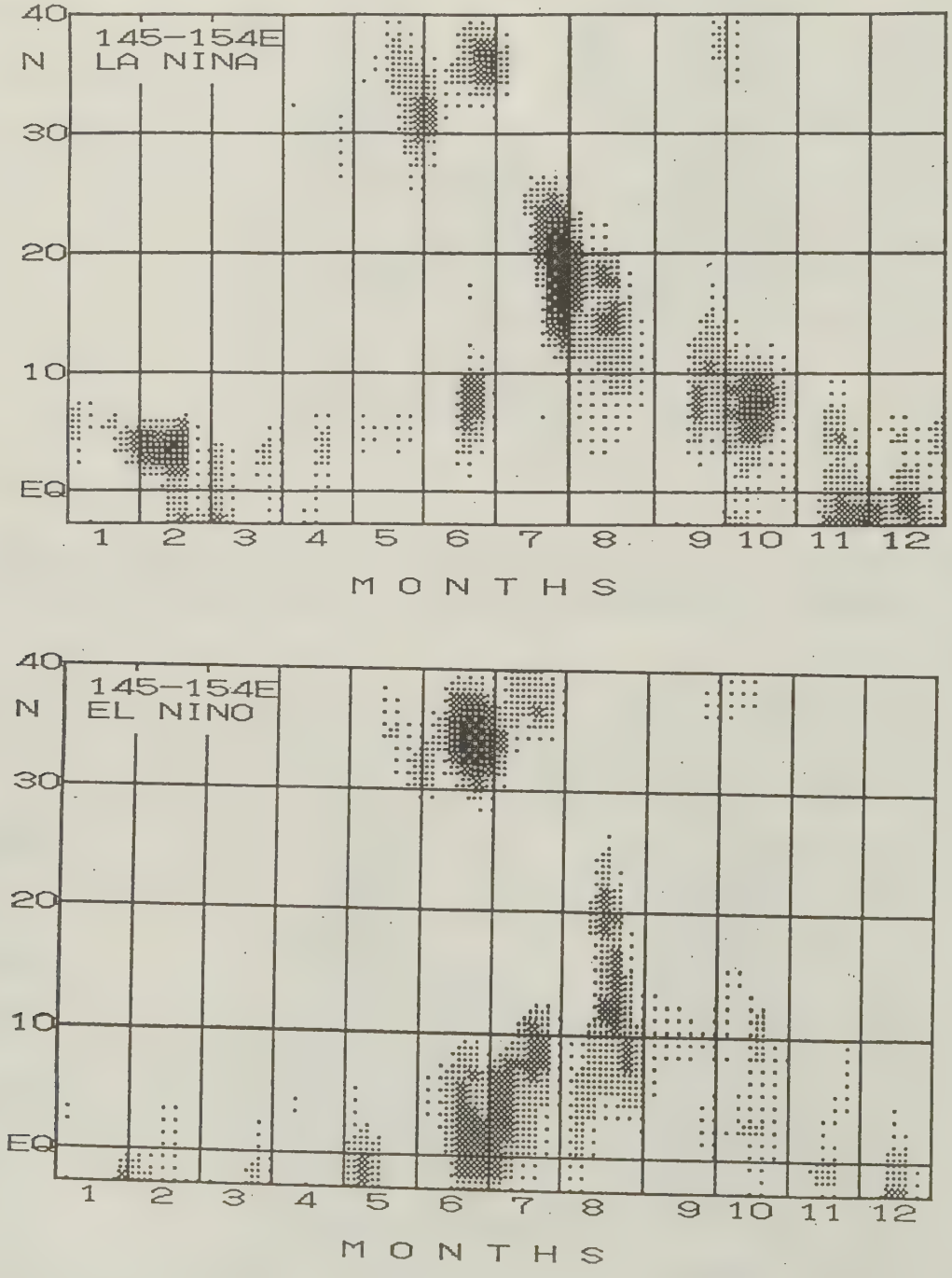

Figure 3 Composite latitude-time cross section of the GMS high-cloud-amount for La Nina years (1978,84,85,88; upper) and El Nino years (1982,83,87,91,92; lower) for the longitude 145-154E.

Figure 4 shows TBB map composed of INSAT and GMS in June 1, 1991 at 06 GMT over the area of 40N-40S, 40E-150E. The TBB colder than 270K are contoured every 10 degree and shaded (colder than 260K) in the figure. Figure 5 shows cloud type map constructed from split window measurements. Five orbits are composed to make the Fig. 5. Therefore, about 10 hours difference between the east side and west side of the map. The orbit over the India corresponds to 06 GMT. The asterisks show cumulonimbus type clouds, the crosses show cirrus clouds and the triangles show low level cumulus/strato-cumulus.

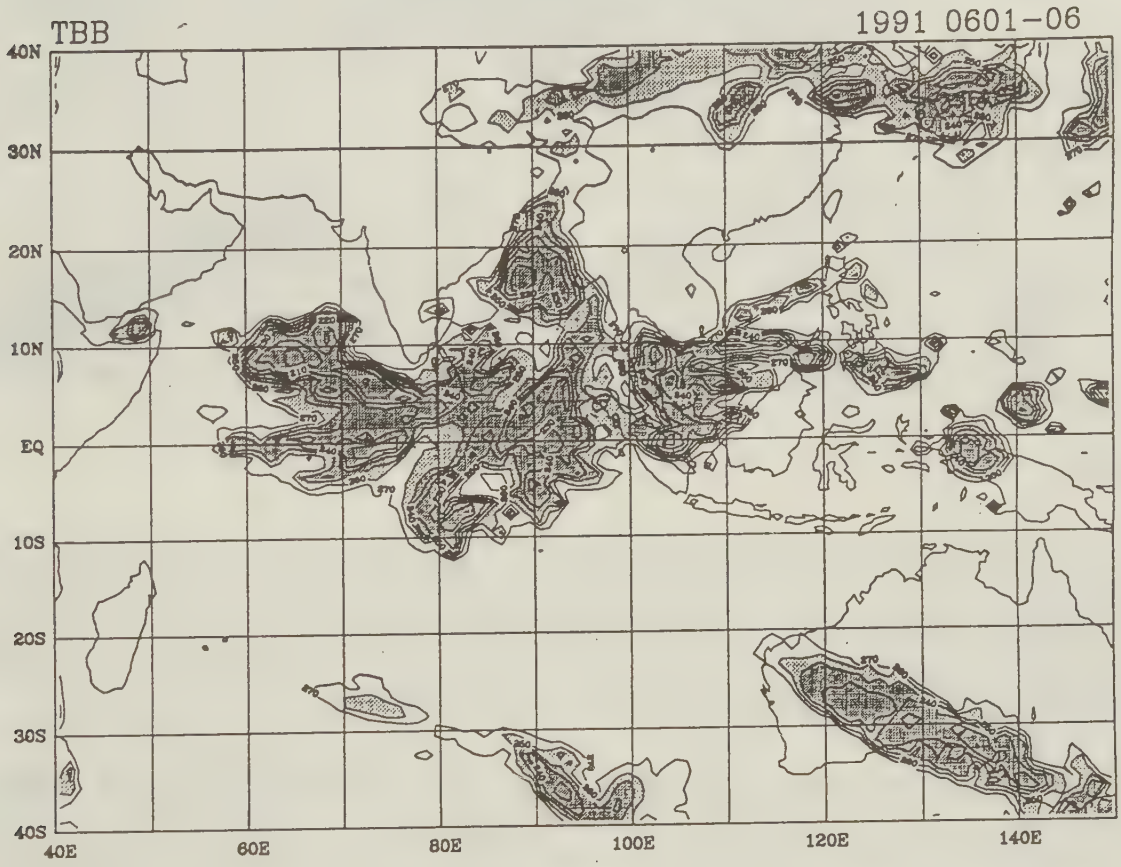

Figure 4 TBB map at 06 GMT on 1 June 1991

Cumulonimbus clouds by split window corresponds to very low brightness temperature (TBB) by infrared observations. However, cold TBB does not necessarily corresponds to cumulonimbus clouds. Over the tropics, cold cirrus clouds are generally associated with cumulonimbus clouds. Relatively cold TBB by single IR measurements show reasonable agreement with the active convection region by split window measurements. The coldest TBBs (<210K) over the south west off the India in Fig. 4 corresponds to the TBB measured by 11mm of the split window. The TBB in Fig. 4 show reasonable agreement with the TBB measured by split window.

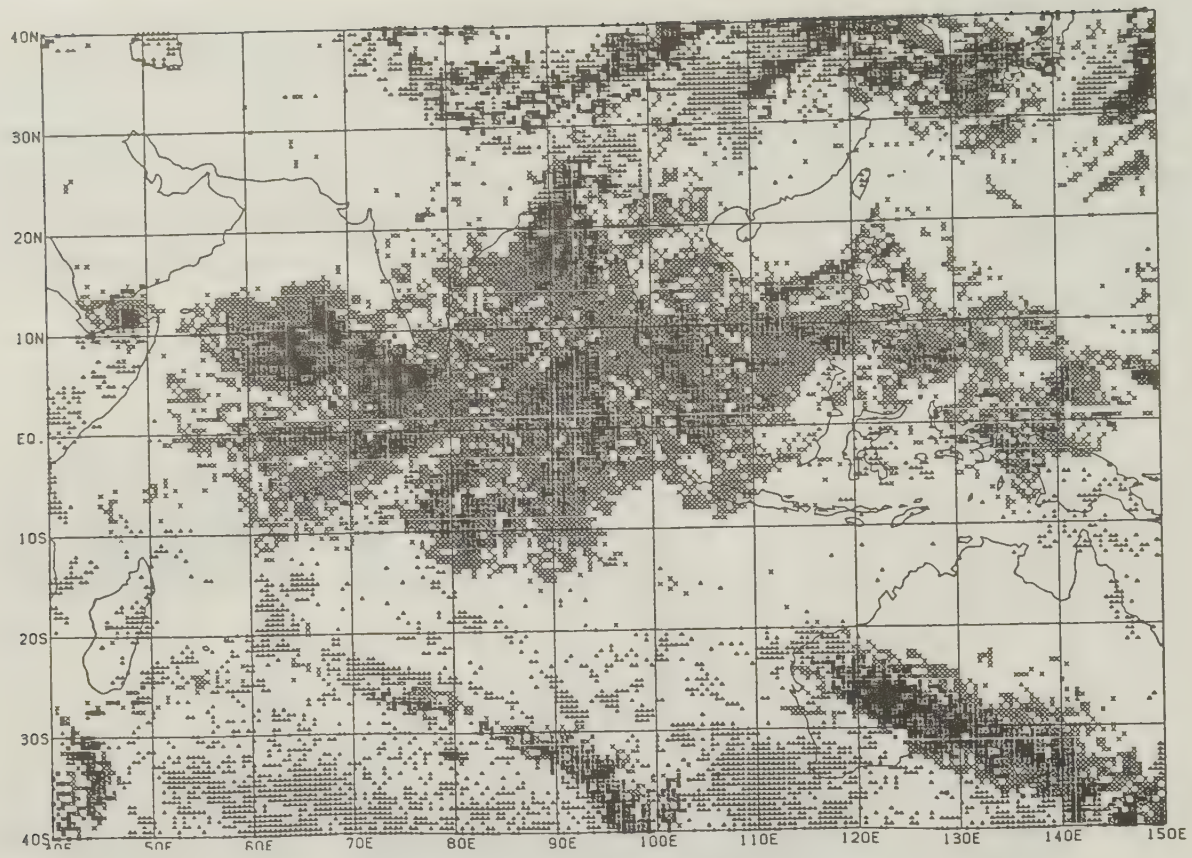

Figure 5 Cloud type map from split window on 1 June 1991

The most significant difference is the low level clouds. The low level cumulus/strato-cumulus clouds classified by split window appear over the ocean east off the Honshu island and west off the Australia, and over the main land China in Fig. 6b. We can identify these low level clouds subjectively from the GMS visible images. These clouds cannot be seen in the Fig.4.

Figure 6a, b show the 10 day (1 July-10 July) mean TBB of cumulus type clouds classified by split window measurements over the mainland China for the year of 1991 and 1988, respectively. In the figure, number shows tenth degree of TBB (7 means 270K). In 1991, severe damage by heavy rain was reported during July over the Yangze river. While, in 1988, abnormally dry and hot weather was reported. Band shape high convective cloud area along the 30N over the mainland China is seen in Fig.6a. We can see that low level cloud (warm TBB) covers widely over the southern part of China in Fig.6b. These cloud features agree well with the fact of heavy rainfall in 1991 and drought in 1988.

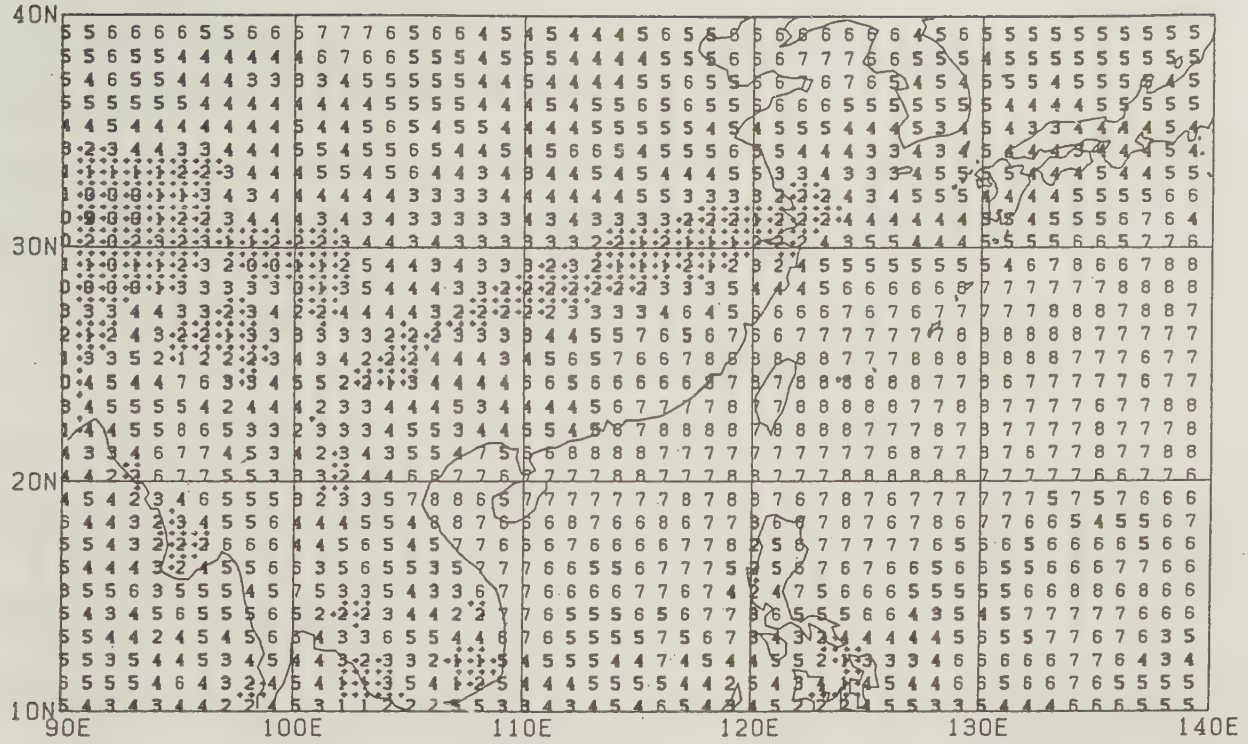

Figure 6a 10 day mean (1 July - 10 July) TBB of cumulus type clouds in 1991

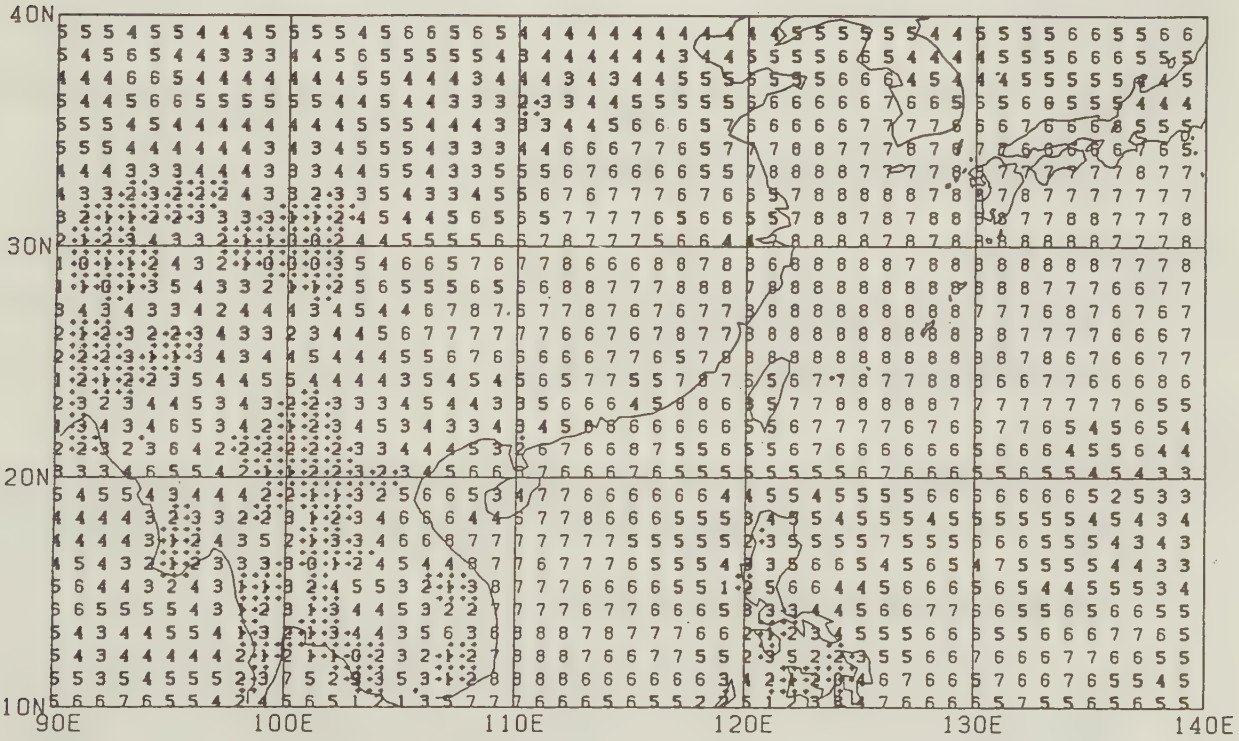

Figure 6b Same as Fig. 6a except for 1988

4. Discussions

Comparing this result on the diurnal variation with the previous result using TBB directly, the difference is seen in the contrast between the land and sea in the diurnal amplitude distribution. This result suggests the following two possibilities. One is that the influence of surface temperature variation cannot be neglected when using TBB directly. Other is that diurnal variation of deep convection may not be affected by intraseasonal mode so drastically. This point is expected to be revealed by using histogram data that include original pixel information. Currently we are also conducting the analysis of the relationship between the GMS high-cloud-amount and the atmospheric circulation pattern.

Cumulus type clouds classified by split window show reasonable agreement with convective rain area. We will study the quantitative representatives of rainfall amount from the cumulus cloud information by split window. So far split window data are available for the NOAA polar orbiting satellite. Since GMS-5 and GOES-I carry split window sensor, further analysis will be possible with high time resolution over the western Pacific. Diurnal, intraseasonal and interannual variation of SST, water vapor and convective activity over the Asian monsoon area will be studied using split window measurements and SSM/I data.

5. References

1) Nitta, T. and S.Sekine, 1994: Diurnal variations of convective activity over the tropical western Pacific, J.Meteor.Soc.Japan, Vol.72, p627-641

6. Publications

Papers in the scientific journals

1) Overseas journal:

T.C.Chen, K.Takahashi: Diurnal variation of outgoing longwave radiation in the vicinity of the South China Sea:Effect of intraseasonal oscillation Mon.Wea.Rev. 1995, Vol.123, 566-577

2) Domestic journal:

M. Tanaka: The onset and retreat dates of the Austral summer monsoon over Indonesia, Australia and New Guinea, J.Meteor.Soc. Japan 1994, vol.72, 255-267

Oral presentations

K.Takahashi, M.Murakami: Analysis of the effect of intraseasonal variation on diurnal variation around the South China Sea using geosynchronous satellite data.
1994 Spring meeting of MSJ, May 1994

T. Inoue: SST and water vapor over the Arabian Sea and convective activity over the south India - conrast between 1987 and 1988 summer -
1994 Spring meeting of MSJ, May 1994

M. Tanaka: Interannual variations of the summer monsoon over East Asia and western North Pacific using GMS high-cloud amount data.
1994 Spring meeting of MSJ, May 1994

M. Murakami: Current and future monsoon research activities in Japan.
PSA International Conference on Weather Analysis and Forcasting in the Asia-Pacific Monsoon Region, June 1994

T. Inoue: Intraseasonal variation of sea surface temperature, water vapor and convection derived from Split Window measurements.
7th Conference on Satellite Meteorology and Oceanography, June 1994

K.Takahashi, M.Murakami: Analysis of the effect of intraseasonal variation on diurnal variation around the South China Sea using geosynchronous satellite data -Part 2-
1994 Autumn meeting of MSJ, October 1994

K.Takahashi, M.Murakami: Analysis of the effect of intraseasonal oscillation on diurnal variation in the vicinity of the South China Sea by using GMS IR data
1st RPC-JAPAN Workshop on Asian Monsoon Mechanism, Ocotber 1994

J.He, Q.Zhu, M.Murakami: Asian-Australian circulation features in wet/dry year uncovered by TBB data.
1st RPC-JAPAN Workshop on Asian Monsoon Mechanism, Ocotber 1994

M.Murakami, K.Takahashi: The seasonal and intraseasonal convective changes over the Asian monsoon area.
International Sysmposium on Asian Monsoon and its Variabilities, November 1994

Q.Zhu, J.He, M.Murakami: Seasonal and intraseasonal variation features of East Asian - North Australian monsoon circulation as revealed with TBB data.
International Sysmposium on Asian Monsoon and its Variabilities, November 1994

M. Murakami: Use of geostationary satellite observations in monsoon research.
WMO Regional Workshop on Asian/African Monsoons, January 1995

M. Murakami: Monsoonal covective system from tropics to middle latitude.
International Workshop on East Asian Monsoon, March 1995

T. Inoue: Rainfall estimation by split window data over the TOGA-COARE region.
3rd Algorithm Intercomparison Project of GPCP, March 1995

7. International Cooperation

The cooperation with China has been carried out based on the agreement signed in 1993 between Japan Science and Technology Agency and China Meteorological Administration. During FY 1994, three Chinese experts were invited to M.R.I. and performed the joint study on the interannual aspects of Asian monsoon by using the GMS satellite data. From Japanese side, two research officials visited China duirng FY 1994 and joined the First P.R.C.-Japan Workshop on Asian Monsoon.

Ⅰ．大気・海洋・陸域間相互作用の諸過程に関する解析・観測研究

1．大気における諸過程に関する解析・観測研究

（1）大規模積雲対流活動と降水系に関する解析研究

気象庁
気象研究所
村上勝人、井上豊志郎、
高橋清利、田中実
気象衛星センター
伊藤和男、大野智生

（要旨）

積雲対流活動の日変化に対する季節内変動の影響を、地表面温度の影響を弱めた積雲活動の指標を用いて、夏季の南シナ海について調査した。赤外の等価黒体温度を直接使用した場合と比較して、海陸のコントラストは明瞭ではなかった。

５日平均のＧＭＳ上層雲量を１９７８年から１９９２年の期間について用いた降水系の解析によれば、３０－６０日周期の西太平洋上の季節内変動は東太平洋赤道域の海面水温と関連している。北緯２０度、東経１５０度付近の積雲対流活動の開始時期は、ラニーニャ年には早く、エルニーニョ年には遅い。同様な遅れは、日本付近の梅雨においても観察される。

赤外の輝度温度（ＴＢＢ）から定義された積雲対流の活動度を、スプリット・ウインドウにより定義された積乱雲タイプの雲域と比較した。低温のＴＢＢ域は積乱雲タイプの雲域と良い対応を示すが、違いも存在する。低温のＴＢＢ域のあるものは熱帯域を覆う絹雲に対応している。スプリット・ウインドウにより定義された下層の積雲や層積雲は赤外画像においては欠落している。

１９８８年と１９９１年の夏の中国本土における対照的な様相を、スプリット・ウインドウにより定義された積乱雲タイプの雲域を用いて調べた。淮河流域においては１９９１年に豪雨、１９８８年には干ばつに見舞われている。非常に活発な積雲の領域が１９９１年７月には揚子江と淮河流域に見られた。一方１９８８年７月には、北部を除いて中国本土には顕著な積雲域が見られなかった。

I. Observation and analysis on the process of the atmosphere–ocean–land interactions

1. Observation and analysis on the process in the atmosphere

(2) Observation of structure of convective clouds in large-scale cloud systems

Meteorological Research Institute,
Japan Meteorological Agency
H.Sakakibara, H.Okamura, K.Akaeda,
K.Mori, Y.Shimazu

(ABSTRACT)

Cloud clusters which form and develop over the warm sea transport upward heat and water vapor added through the sea surface. Latent heat released by condensation of water vapor remains in the atmosphere if the condensed water falls as rain and heats the air in the cloud cluster. This heating is not only the energy source of the cloud cluster but one of the energy sources of monsoon.

In order to reveal the structure of convective clouds in cloud clusters and the interaction between convective clouds and cloud clusters, convective clouds in typhoons and cloud clusters associated with the Baiu front which is a stationary front extending from China to Japan in early summer months were observed by using X-band Doppler radars and omega-sondes in Miyako Island (24.8N, 125.4E) from 1990 to 1992.

Until 1993 we analyzed four typhoons in which the eyewall cloud was observed and eight cloud clusters associated with the Baiu front. Common features of the convective cloud in four typhoons which passed by the island were analyzed. Structure of convective clouds was roughly determined by their location in typhoons. On the contrary, structure of convective clouds in the cloud clusters in the Baiu season showed various types. The variety of the structure of cloud clusters in the Baiu season is probably due to their life stage and their environment.

In 1994 structure of convective clouds in Typhoons 9015 (Abe) and 9119 (Mireille) and in a quasi-stationary mesoα-scale convective system in the Baiu season in 1992 was examined in detail. Typhoon 9015 which passed just over Miyako Island with the central pressure of 955 hPa had a very large eye of about 150 km in diameter. The center of the deeply inclined eyewall cloud was located at about 100km from the typhoon center. The outermost rainband usually located

at about 150 km from the eyewall cloud. The mean distance of rainbands was about 50 km. Structure of rainbands in Typhoon 9015 is examined with Doppler radar data. Outflow at middle levels ascended and formed a convective rainband between 150 to 200km from the typhoon center.

Central pressure of Typhoon 9119 was 935 hPa when it passed 45 km east of Miyako Island. Precipitation area extended to 600 km from the typhoon center. The mean spacing of rainbands on the forward (northwestern) side was about 43km. Part of the air with high equivalent potential temperature did not rise in the eyewall cloud but flowed outward above the boundary layer. Rainbands embedded in the stratiform precipitation area in the inner core region were formed by convergence of the air with high equivalent potential temperature at middle levels.

The stationary mesoα-scale cloud cluster was composed of several mesoscale convective systems (MCSs). They first formed at the western edge of the cloud cluster and moved eastward and then decayed. This process repeated several times and the whole cloud area seems to be stationary. Three MCSs which contained linear convective areas were observed in Miyako Island. In the former two MCSs middle level flow enters from ahead of the system and passes through it to the rear. A convective cloud which developed at the low-level convergence area moved rearward according to the mid-level front to rear flow. After the convective cloud is moved out to the rear, next convective cloud is formed at the low-level convergence area. On the contrary, mid-level inflow from ahead is blocked by rear inflow in the third MCS to form a deep convergence layer up to 8 km. This deep convergence maintains one steady convective band. The structure of these systems can probably explain the precipitation peaks observed in Miyako Island.

1. OBJECTIVES

Cloud clusters which form and develop over the warm sea transport upward heat and water vapor added through the sea surface. Water vapor condenses during the upward transportation. Some fraction of condensed water falls and reach the sea surface as rain. If raindrops reach the sea surface, latent heat released by condensation of water vapor to form the raindrops remains in the atmosphere and heats the air in the cloud cluster. This heating is not only the energy source of the cloud cluster but one of the energy sources of monsoon.

In this study we aimed to reveal the structure of convective clouds in cloud

clusters and the interaction between convective clouds and cloud clusters and to discuss the processes of precipitation and vertical transport of heat and water substances.

2. METHODS

Convective clouds in typhoons and cloud clusters associated with the Baiu front which is a stationary front extending from China to Japan in early summer months were observed by using X-band Doppler radars and omega-sondes in Miyako Island (24.8N, 125.4E) from 1990 to 1992. Until 1993 we analyzed four typhoons in which the eyewall cloud was observed and eight cloud clusters associated with the Baiu front. In 1994 structure of convective clouds in Typhoons 9015 (Abe) and 9119 (Mireille) and in a quasi-stationary mesoα-scale convective system in the Baiu season in 1992 was examined in detail. In the analysis we used operationally observed data such as echo intensity of the Miyakojima, Ishigakijima and Okinawa radars, surface and upper air observation and cloud imagery of Geostationary Meteorological Satellite as well as the specially observed data in Miyako Island.

3. BRIEF REVIEW OF RESULTS UNTIL 1993

Until 1993, we had investigated structures of convective cloud in typhoons and cloud clusters in the Baiu season in order to achieve the objectives by using the Doppler radar and rawin-sonde data which were obtained in Miyako Island. Common features of the convective cloud in four typhoons which passed by the island were analyzed. Outer rainbands were maintained by the low-level convergence between inflow from the outer area and the cold air which was produced by the outer rainbands themselves. Inner rainbands which were embedded in stratiform precipitation areas in the inner core of typhoons are classified into three types: (1) rainbands which were made by upper-level updraft due to middle-level convergence, (2) rainbands which were made by low-level convergence like outer rainbands, and (3) rainbands which were seeded by ice particles from upper levels. Eyewall rainbands were formed just below the slantwise outflow which was returning from the inflow in the boundary layer.

Structure of convective clouds in the cloud clusters in the Baiu season showed various types. Two cloud clusters which occurred along cold fronts had convective area in their front portion and stratiform area in the rear portion. Strong

middle-level wind blew from the stratiform area to the convective area. Two cloud clusters south of a stationary front had extensive stratiform precipitation areas in front of and in the rear of active convective bands. Other cloud clusters showed different structures. The variety of the structure of cloud clusters in the Baiu season is probably due to their life stage and their environment.

4. RESULTS

(1) Structure of Rainbands in Typhoon 9015 (Abe) and Typhoon 9119 (Mireille)

Structure of Typhoon 9015 which passed just over Miyako Island with the central pressure of 955 hPa is described first. This typhoon had a very large eye of about 150 km in diameter. The center of the deeply inclined eyewall cloud was located at about 100km from the typhoon center. The outermost rainband usually located at about 150 km from the eyewall cloud. The mean distance of rainbands was about 50 km. This typhoon did not have active convective rainbands associated with decrease of surface temperature in the outer region of the typhoon system. Only scattered convective clouds were observed on the northwestern side and no convective clouds on the southeastern side.

Rainbands in Typhoon 9015 are examined using Doppler radar data. Precipitation in the eyewall region was convective. It was produced by the slantwise updraft along the upper end of the eyewall cloud. There was a stratiform precipitation area of 40-50km wide outside the eyewall cloud. Convective rainbands with convergence at middle levels were occasionally embedded in the stratiform area. Outflow at middle levels ascended and formed a convective rainband between 150 to 200km from the typhoon center (Fig.1). Environmental air on the southeastern side flowed into a stratiform precipitation area about 300 km from the typhoon center and then descended toward the surface.

Central pressure of Typhoon 9119 was 935 hPa when it passed 45 km east of Miyako Island. The eye of this typhoon was about 50 km in diameter and precipitation area extended to 600 km from the typhoon center. The rainbands on the forward (northwestern) side were analyzed in detail. There were thirteen rainbands on this side and the mean spacing was about 43km. Although surface temperature dropped distinctly during the passage of outer rainbands, it did not change significantly during the passage of rainbands within 300 km from the typhoon center. Furthermore, surface temperature and relative humidity within 180km from

the typhoon center were 25--26 °C and 100%, respectively. This condition was nearly in equilibrium with the sea surface. Equivalent potential temperature at the surface near the typhoon center was as high as 367K. Part of the air with such high equivalent potential temperature did not rise in the eyewall cloud but flowed outward above the boundary layer. Rainbands embedded in the stratiform precipitation area in the inner core region were fairly convective (Fig.2). Convergence was found at middle levels (1.5–5 km). The air with high equivalent potential temperature transported from the eyewall region seemed to ascend there. Divergence was found at lowest levels below the rainbands.

(2) Structure of Convective Clouds in a Stationary Cloud Cluster

This cloud cluster occurred on June 10, 1992. It had triangle–like shape (so–called "tapering cloud"). Several mesoscale convective systems (MCSs) evolved under this cloud area. They first formed at the western edge of the cloud area and moved eastward and then decayed. This process repeated several times and the whole cloud area seems to be stationary. Total rain of 170 mm fell in Miyako Island between 0830 and 2300 JST and it was brought by three MCSs. The precipitation is characterized by several peaks due to convective rain with intervals of 30 or 40 minutes in the former two MCSs and one strong peak surrounded by stratiform precipitation in the third MCS.

These MCSs are mainly composed of linear convective areas. The convective areas are formed by the strong surface convergence between southerly wind ahead and westerly or northwesterly wind in the rear. The motions of these three MCSs are 120°, 6.1m/s; 125°, 6.9m/s; 80°, 11.2 m/s, respectively. The former two MCSs show the similar movement but the third one is different and faster than the others. Though the second MCS consisted of several sub–systems (Fig. 3a), one steady convective band was maintained in the third MCS (Fig. 3b). Figure 4 shows the system–relative horizontal flow in the panel parallel to the movement of each MCS derived by VAD analysis. In these figures, low level convergence is prominent in all cases. Meanwhile, the mid–level flow is different between the former two MCSs and the third one. In the former two MCSs middle level flow enters from ahead of the system and passes through it to the rear. Mid–level inflow from ahead is blocked by rear inflow in the third MCS to form a deep convergence layer up to 8 km. This deep convergence maintains one steady convective band. On the contrary, in the former two MCSs a convective cloud which developed at the

low-level convergence area moved rearward according to the mid-level front to rear flow. After the convective cloud is moved out to the rear, next convective cloud is formed at the low-level convergence area. This repeated formation and translation of convective clouds can probably explain the precipitation peaks with interval of 30 to 40 minutes in the former two MCSs.

5. Discussions

Some typhoon rainbands had their roots at middle levels. The air flowing outward above the boundary layer seemed to be potentially warmer than the air in the boundary layer and to ascend to form the rainbands. One of probable formation mechanisms of the rainbands is conditional symmetric instability. Next year we will examine whether the condition for the symmetric instability was satisfied in the rainbands.

We observed eight cloud clusters associated with the Baiu front. All cloud clusters other than the above-mentioned one are non-stationary. We have to analyze these non-stationary cloud cluster and find the difference of structure between these two types.

6. References

None

7. Publications

None

8. INTERNATIONAL COOPERATION

None

（要旨）

アジアモンスーン域の暖かい海洋上に発生する大規模雲域内の対流雲は暖かい海面から熱、水蒸気を上方に輸送する。水蒸気の凝結（およびその後の降水）による潜熱の放出は大規模雲域のエネルギー源であると同時にモンスーンのエネルギー源でもある。熱、水の輸送過程に関連する対流雲の構造と対流雲と大規模雲域の相互作用を調べる目的で、１９９０年から９２年まで宮古島（北緯２５度、東経１２５度）でドップラーレーダーとオメガゾンデによる大規模雲域（台風と梅雨期クラウドクラスター）内の対流雲の３次元構造の観測を行った。

前年度までに４個の台風および８個の梅雨期クラウドクラスターについてそれぞれ共通する特

徴を求めた。台風では対流雲が台風域内のどこにあるかで構造はおおよそ決まっていた。一方、梅雨期のクラウドクラスターについては構造が多様であった。梅雨期のクラウドクラスターの多様性は観測されたときのライフステージと周囲の環境の多様性によると思われる。

今年度は台風９０１５号と９１１９号および１９９２年梅雨期のほぼ停滞したメソαスケール対流系内の対流雲を詳細に解析した。台風９０１５号は宮古島の真上を通過した台風で、直径約１５０ｋｍの大きな眼を持っていた。大きく外側に傾いた眼の壁雲の中心は台風中心から約１００ｋｍの所にあり、最も外側の降雨帯はそこからさらに１５０ｋｍ外側にあった。降雨帯の平均間隔は約５０ｋｍであった。降雨帯の構造がドップラーレーダーのデータを用いて調べられた。台風中心から１５０～２００ｋｍで中層で外向きに流れてきた空気が上昇し、対流性降雨帯を作っている。

台風９１１９号は非常に強い勢力で宮古島のすぐ東を通過した。降水域は中心から６００ｋｍまで広がっていた。降雨帯の平均間隔は約４３ｋｍであった。台風中心付近の相当温位の高い空気の一部は眼の壁雲で上昇せずに、境界層の上を外向きに流れる。層状性降水域内に埋まっている降雨帯はこの空気が中層で収束し、上昇してできた。

メソαスケールの停滞性クラウドクラスターはいくつかの中規模対流系が風上側で発生し、風下側で消滅することにより停滞していた。宮古島では線状対流域を内部に含む３個の中規模対流系が観測された。はじめの２個の対流系では前方から入った空気が下層収束域の上を通って後方に通り抜けている。したがって下層収束域で発達した対流雲は後方に流され、次の新しい対流雲が再び収束域で発達する。一方、最後の対流系では前方からの流れが後方からの流入によりせき止められ、８ｋｍに達する深い収束域を作る。これにより１本の定常的対流雲を作っている。これらの構造は宮古島で観測された降水強度の時間変化を良く説明する。

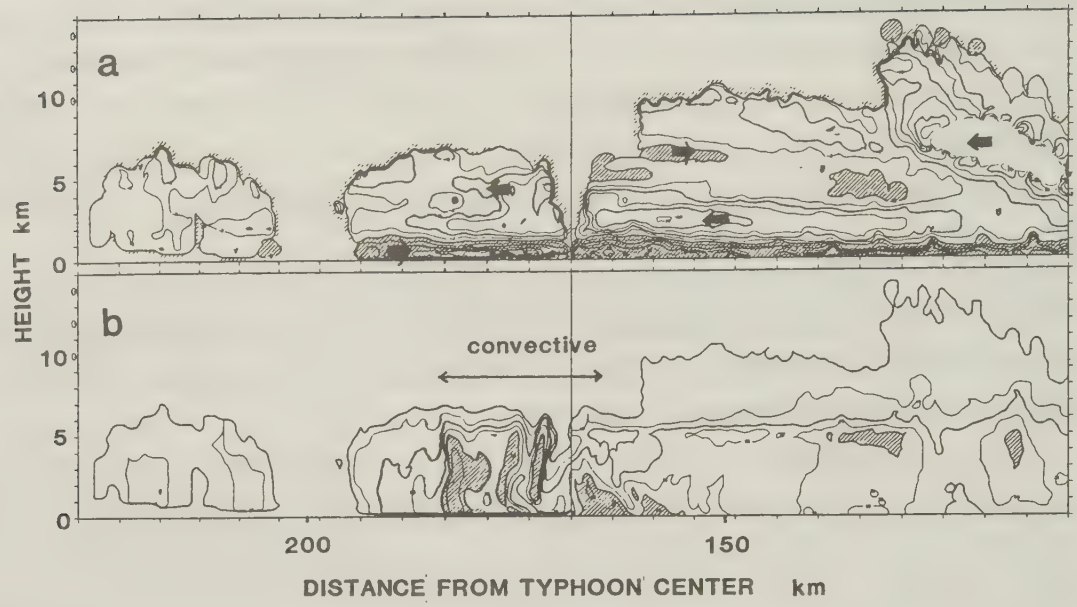

Figure 1. Vertical cross sections of (a) ground-relative horizontal flow nearly normal to the primary circulation of the typhoon and (b) radar reflectivity at 1828 JST, August 29, 1990. Shading in (a) indicates flow from left to right. Shading in (b) indicates reflectivity more than 30 dBZ.

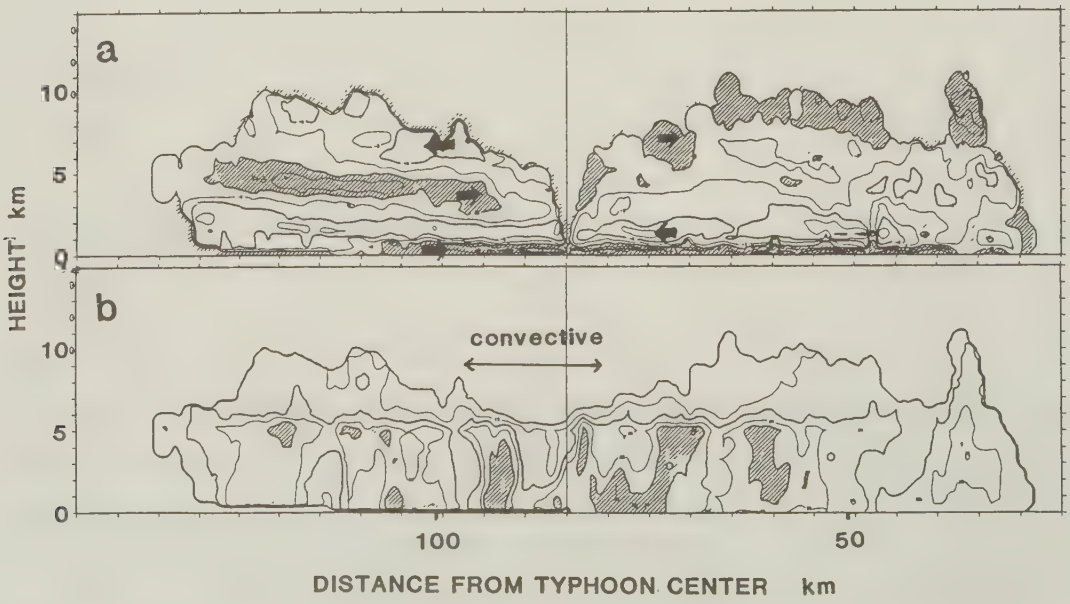

Figure 2. Same as Fig.1 except for 0711 JST, September 26, 1991.

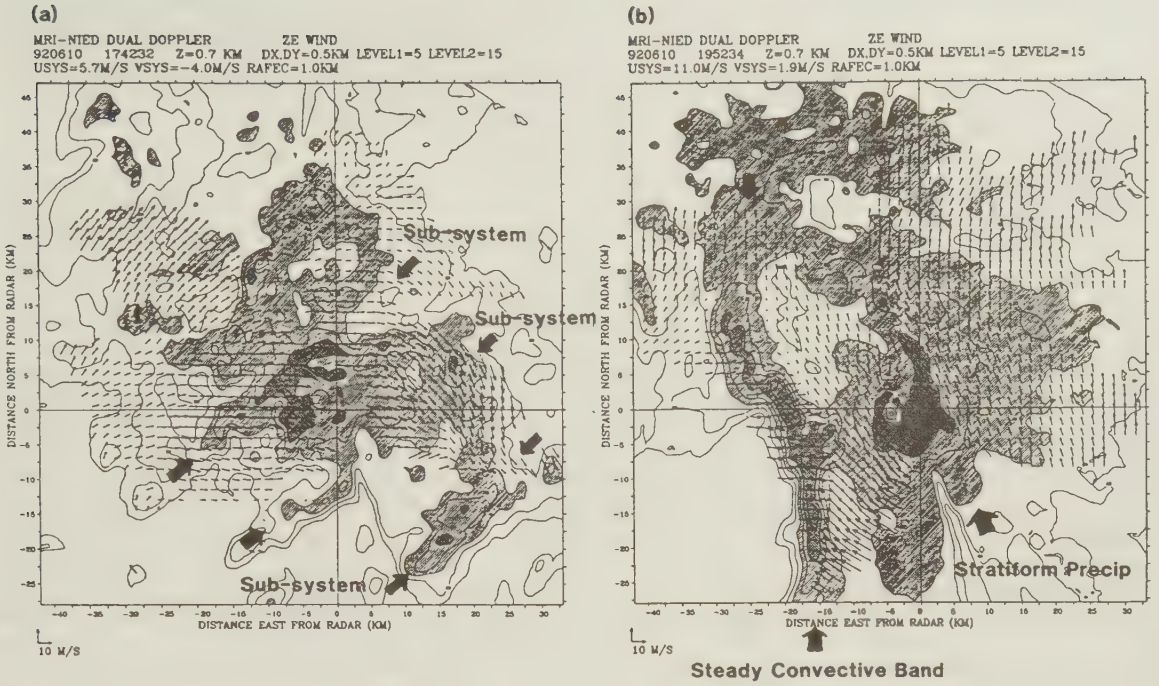

Figure 3. (a) Radar reflectivity with horizontal wind at 0.7 km height at (a) 1742 JST, and (b) 1952 JST. Shading and dark shading indicate reflectivity more than 25 and 35 dBZ.

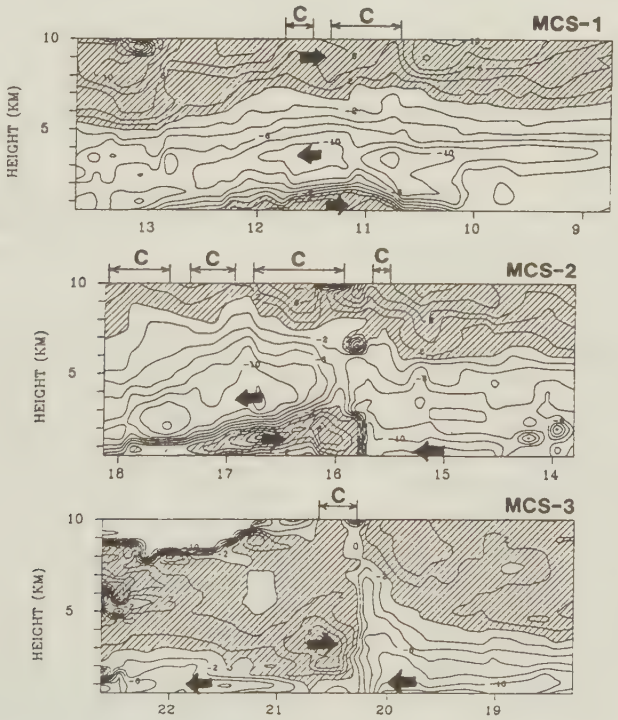

Figure 4. Time-height cross sections of system relative flow along each MCS movement. Shading indicates flow from rear to front. Contour interval is 2 m/sec. "C" in the upper part of each panel indicates convective part.

I. Observation and analysis on the process of the atmosphere-ocean-land interactions
1. Observation and analysis on the process in the atmosphere
(3) Analysis on the evolution of Convective cloud systems

Remote Sensing Laboratory
National Research Institute for Earth
Science and Disaster Prevention (NIED),
Science and Technology Agency
S. Nakai and H. Ohkura

Abstract

Baiu frontal zone over the East China sea and the northwestern Pacific is one of the regions that generate many convective cloud systems. They play an important role on the water cycle of Baiu front. The activity of Baiu front is closely related to the global Monsoon circulation. So, it is important to clarify the water cycle of the Baiu frontal zone focusing on the evolution of convective cloud systems.

In FY1994, we intended to describe the mesoscale wind field accompanying a sequence of mesoscale convective systems (MCSs) and its relation to the convective activity. We analyzed the structure and the wind field of the MCSs observed on 10 June 1992 using single-Doppler radar data. Original Doppler radar data were converted to horizontal/vertical grid data to analyze the evolution of MCSs appeared in the precipitation and horizontal velocity patterns. VAD technique were applied to the conical-scan data at the elevation of 25.2°.

Three MCSs were observed in 10 June 1992. They had common features that stratiform precipitation region surrounded the convective lines, whose typical running direction was southwest-northeast. The convection-cell-relative wind in this direction was northeasterly below 3km and southwesterly above 5km. It is suggested that the wind shear contributed to the evolution of each convection cell. Wind component in northwest-southeast direction indicated convergence and divergence centered at the convective lines at the height below and above 5km, respectively. It is considered that the convergence and the divergence compose the mesoscale circulations accompanying the organization of convection and that the convective lines were in mesoscale updraft regions.

The mesoscale circulation is important to understand the structure and precipitation mechanisms of MCSs observed in the Asian Monsoon region. We will proceed to the detailed data analysis using the observation data on this viewpoint. The analysis of satellite microwave data is promising to clarify the distribution of water in MCS and Baiu frontal zone, and is necessary to be carried out based on the result of observation data analysis.

1. Objectives

The characteristics of the convective clouds vary from place to place in the world. Baiu frontal zone over the East China sea and the northwestern Pacific is one of the regions that generate many convective clouds. Especially, mesoscale convective systems (MCSs) play an important role on the water cycle of Baiu front. The activity of Baiu front closely related to the global Monsoon circulation (e.g., Kato, 1993). It is important to clarify the evolution and the water cycle in MCSs observed in the Baiu frontal zone.

Cooperative observations on the structure of convective clouds were made in June 1992 by Meteorological Research Institute and NIED. We continue the investigation of the observed precipitating clouds mainly using the observation data and the satellite data. Our primary interest is on 1) the process that MCSs vertically transport water, 2) redistribution of water as precipitation, upper level cloud and water vapor, and 3) the mesoscale circulation and its role in the maintainance of MCSs.

In FY1994, we intended to describe the mesoscale wind field accompanying a sequence of MCSs and its relation to the organized convective activity.

2. Methods

We analyzed the structure and the wind field of MCSs observed on 10 June 1992 using single-Doppler radar data. Original Doppler radar data were converted to CAPPI (Constant Altitude Plan-Position Indicator), PPI (Plan-Position Indicator) and RHI (Range-Height Indicator) grid data. Reflectivity structures of MCSs and horizontal velocity fields on vertical planes are used in the subjective analysis. The horizontal velocity was calculated on the low-elevation points neglecting the contribution of vertical air velocity and falling velocity of the precipitation particles.

The VAD analysis was applied to the conical-scan data of the elevation of 25.2°, assuming that the wind field was nearly linear within the circle of analysis. We used conventional VAD method that the divergence and the vertical velocity were not distinguishable. Browning and Wexler (1968) recommended the elevation less than 9° for the rainfall data. However, we selected a higher elevation angle to make the circle as small as possible. The data on the analysis circles were well approximated as linear wind fields (Fig. 1), though the divergence values were contaminated by the vertical velocities. So, we discussed

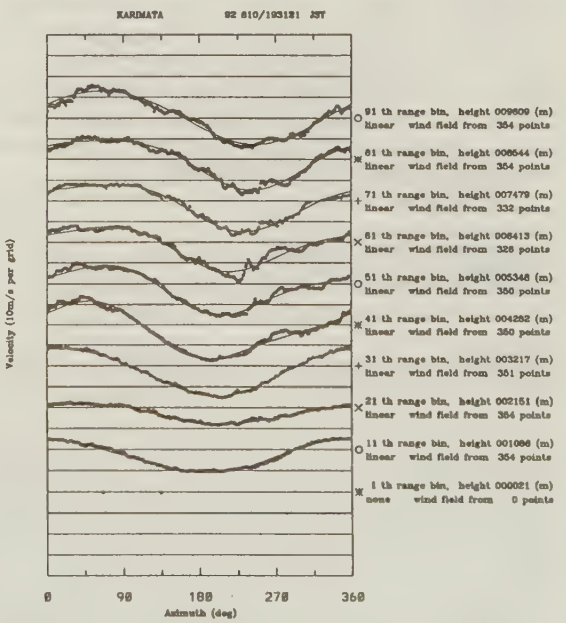
KARIMATA
92 610/193121 JST
91 th range bin, height 009609 (m)
linear wind field from 354 points
81 th range bin, height 008544 (m)
linear wind field from 354 points
71 th range bin, height 007479 (m)
linear wind field from 332 points
61 th range bin, height 006413 (m)
linear wind field from 328 points
51 th range bin, height 005348 (m)
linear wind field from 350 points
41 th range bin, height 004282 (m)
linear wind field from 350 points
31 th range bin, height 003217 (m)
linear wind field from 351 points
21 th range bin, height 002151 (m)
linear wind field from 354 points
11 th range bin, height 001086 (m)
linear wind field from 354 points
1 th range bin, height 000021 (m)
none wind field from 0 points
Velocity (10cm/s per grid)
0
90
180
270
360
Azimuth (deg)

Fig. 1. Example of the velocity-azimuth display at the elevation of 25.2°. Dots and solid lines indicate observed and approximated radial velocities, respectively.

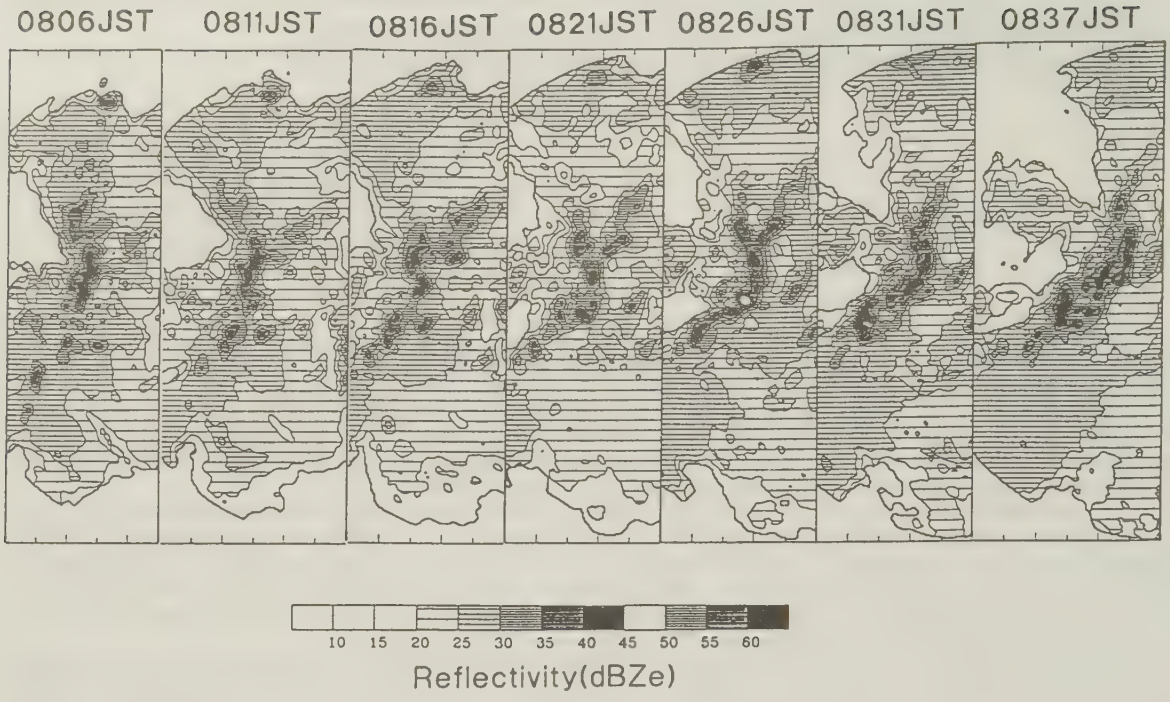

Fig. 2. Reflectivity field at the elevation of 2.8° around the convective line of the second MCS at 5- to 6-minute intervals.

only on the wind speed and wind direction, which were not contaminated by the vertical velocities.

3. Results

Precipitation on 10 June 1992 was brought by three MCSs composed of convective lines and stratiform precipitation (Fig. 2). The stratiform precipitation surrounded the convective lines, different from the squall lines with trailing stratiform precipitation. It was a common feature of the three MCSs.

The third MCS of the three was analyzed intensively and the structure around the convective line has been described (Nakai et al., 1994). There were weak-echo regions on both sides of the convective lines. The wind blew into the convection cell on the front side in the lowest level and diverged to both sides above the melting level. The outflow above the melting level extended to the stratiform precipitation region (Fig. 3).

The third MCS was surrounded by the stratiform precipitation through the period it was observed by NIED Doppler radar. Figure 4 shows the reflectivity field within almost full radar coverage at the height of 2.5km. CR indicates the convective line. The variation of reflectivity field was small in the stratiform precipitation region. The decrease of reflectivity with the distance from the radar was considered as the effect of the attenuation by rain. CR was characterized by the large gradient of the reflectivity. The reflectivity pattern shows that the attenuation by rain was very strong behind the convective region. Fig. 4(a) shows that the Doppler radar was in front of the convective region. The structure of the stratiform region on the front side of CR can be analyzed using the data around 1917JST. Fig. 4(b) shows analogously on the structure of the rear side of CR and the data around 2053JST.

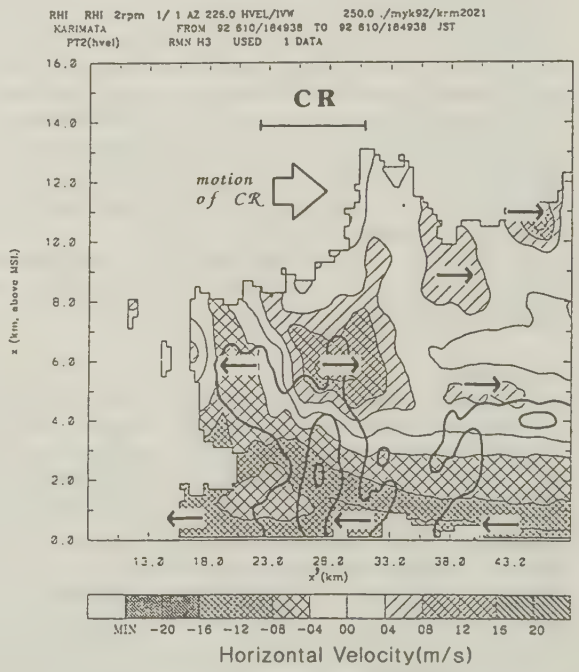
RHI RHI 2rpm 1/ 1 AZ 225.0 HVEL/IVW 250.0 ./myk92/krm2021
KARIMATA FROM 92 610/184938 TO 92 610/184938 JST
PT2(hvel) RMN H3 USED 1 DATA
CR
motion of CR
z (km, above MSL)
x' (km)
MIN -20 -16 -12 -08 -04 00 04 08 12 16 20
Horizontal Velocity(m/s)

Fig. 3. Reflectivity and horizontal velocity fields on a vertical section in 226° - 46° direction around the convective line of the third MCS at 1849JST. The horizontal velocity is relative to the mean motion of the convective cells. The contour lines indicate 22, 30 and 38dBZe. CR indicates the convective line. The horizontal velocity toward right in the figure (from 226° to 46°) is positive.

Reflectivity and horizontal velocity field on a vertical plane at 1915JST is shown in Fig. 5(a) and Fig. 6(a). The convective region was at x'=24km and the front-side stratiform precipitation extended several tens of kilometers wide (Fig. 5(a)). The wind blew toward the convective region (negative in Fig. 6(a)) at the height below 3km and above

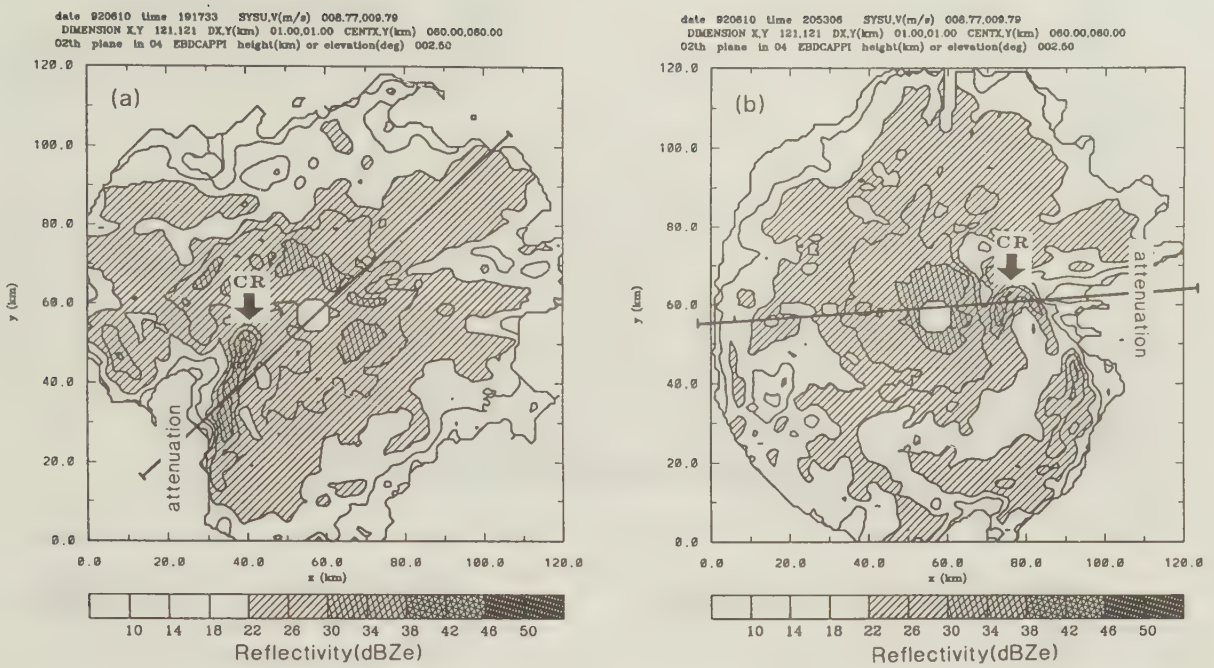
date 920610 time 191733 SYSU,V(m/s) 008.77,009.79
DIMENSION X,Y 121,121 DX,Y(km) 01.00,01.00 CENTX,Y(km) 060.00,060.00
02th plane in 04 EBDCAPPI height(km) or elevation(deg) 002.50
(a)
CR
attenuation
y (km)
x (km)
10 14 18 22 26 30 34 38 42 46 50
Reflectivity(dBZe)
date 920610 time 205306 SYSU,V(m/s) 008.77,009.79
DIMENSION X,Y 121,121 DX,Y(km) 01.00,01.00 CENTX,Y(km) 060.00,060.00
02th plane in 04 EBDCAPPI height(km) or elevation(deg) 002.50
(b)
CR
attenuation
y (km)
x (km)
10 14 18 22 26 30 34 38 42 46 50
Reflectivity(dBZe)

Fig. 4. The reflectivity field at the height of 2.5km. The radar was at the center of each panel and the maximum detectable range was 64km. CR indicates the convective line of the third MCS. Solid line in each panel indicates the position of the vertical plane shown in corresponding panels of Figs. 5 and 6. (a) at 1917JST, (b) at 2053JST.

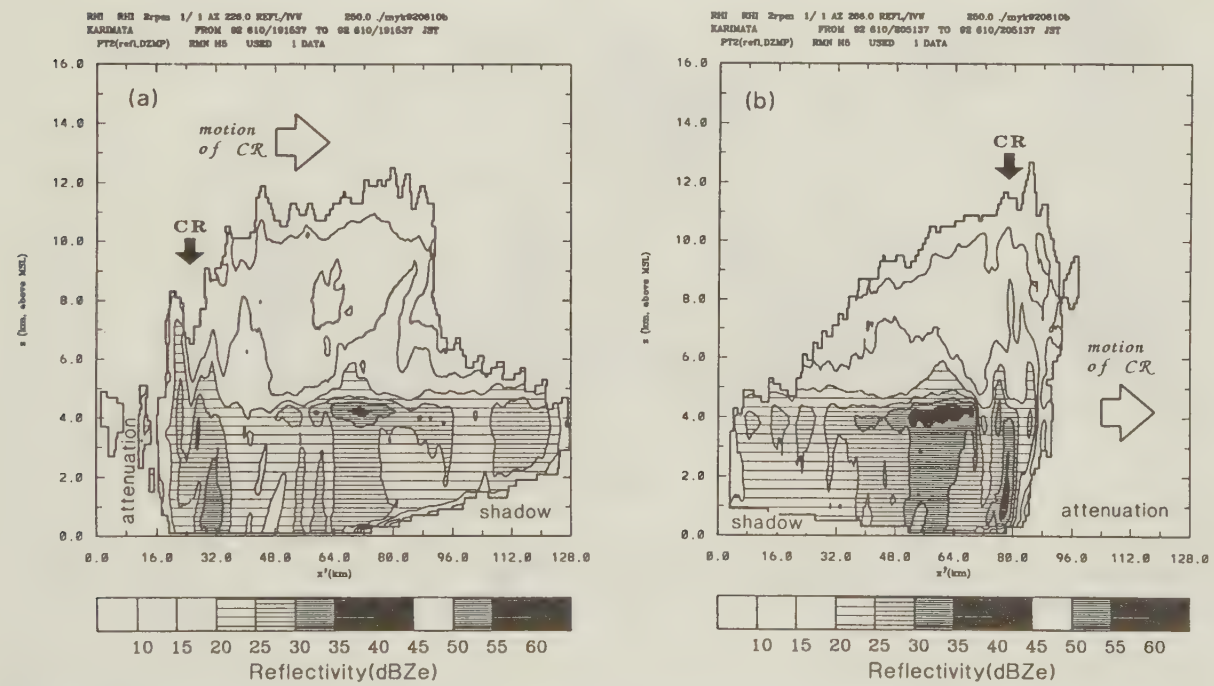

Fig. 5. The reflectivity field in (a) vertical plane along the line shown in Fig. 4(a) at 1915JST, and (b) vertical plane along the line shown in Fig. 4(b) at 2051JST. x' is the direction along the lines. The radar was at x'=64km. CR shows the convective line of the third MCS.

5km, while it blew from the convective region (positive in Fig. 6(a)) at the height between 3km and 5km through the stratiform precipitation region. The horizontally extended area of positive velocity appeared and gradually moved with the motion of CR after 1800JST. This indicates that the positive velocity was part of a mesoscale circulation through the stratiform precipitation region formed in close relation to CR.

Reflectivity and horizontal velocity field on a vertical plane at 2051JST is shown in Fig. 5(b) and Fig. 6(b). The convective region was at x'=80km and the rear-side stratiform precipitation extended several tens of kilometers wide (Fig. 5(b)). The wind blew, in the rear-side stratiform region at 24km<x'<76km, from the convective region (negative in Fig. 6(b)) at the height less than 2km, while it blew toward the convective region (positive in Fig. 6(b)) at the height above 2km. At x'<24km, the wind profile was different, and the maximum height of detected echo was low. This suggests the existence of a mesoscale circulation that closely relating to the rear-side stratiform precipitation, that is,

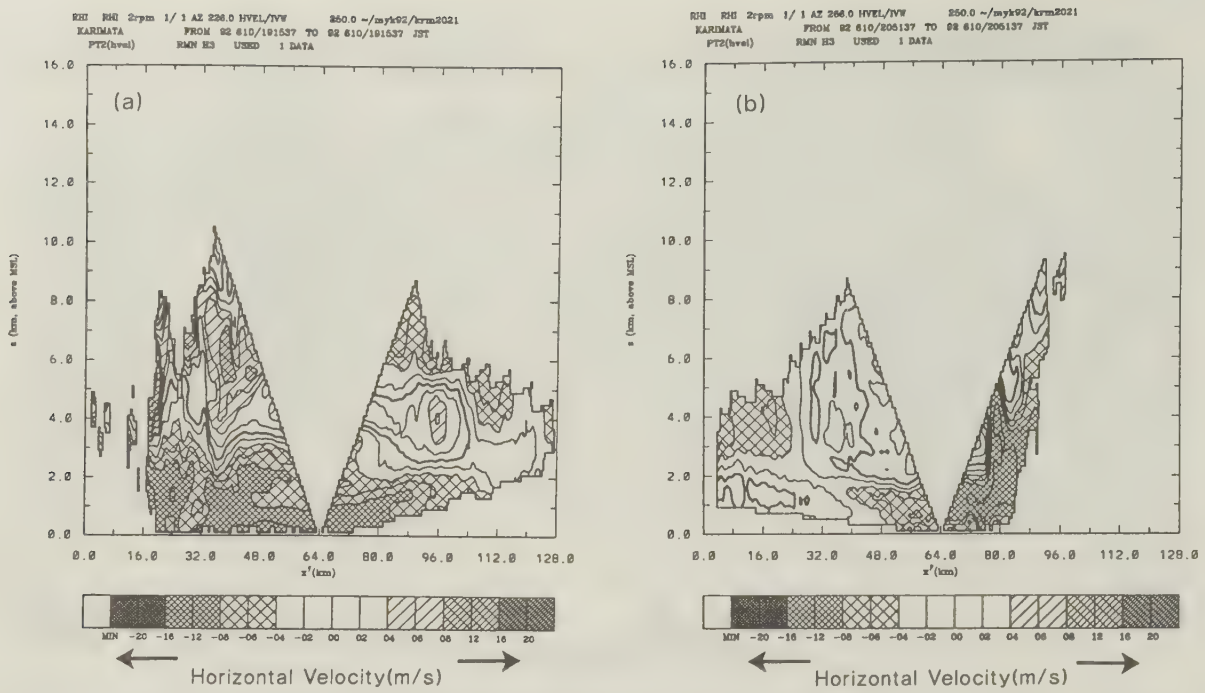

Fig. 6. As in Fig. 5 except for the horizontal wind field relative to the mean motion of the convective cells. The horizontal velocity was calculated where the elevation was less than 20°, suppressing the contamination of the vertical components negligible. The direction of the positive/negative velocity in each panel is shown below the label bar.

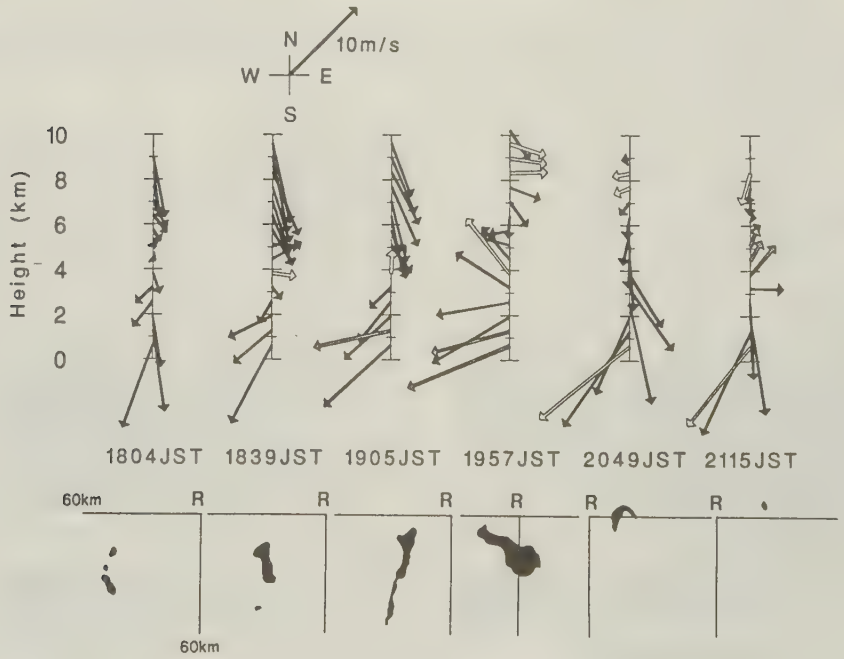

Fig. 7. Upper panel: Wind profile relative to the mean motion of the convective cells obtained from VAD analyses. Hatched and white arrows indicate the winds toward and from CR, respectively. Lower panel: The locations of CR. The radar is indicated by R.

the ice particles generated by the convection in CR entrained to the rear-side stratiform precipitation region in the upper levels.

The results described above were confirmed by the VAD analysis. Fig. 7 shows the time change of VAD wind profile and the location of CR at appropriate intervals. The characteristics of the wind profiles are explained in relation to CR as follows.

The third MCS was too far to influence the wind profile above the radar at 1804JST. The wind direction at the height of 4km changed from westerly at 1839JST to southeasterly at 1957JST, corresponding to the change of location of CR. The wind speed at this height increased as CR approached. These indicate the outflow from CR extended to the stratiform precipitation region. Similarly, on the front side of CR, an inflow existed at the height below 1.5km (1905JST, 1957JST), an outflow existed at the height between 8km and 10km (1957JST). On the rear side of CR, an

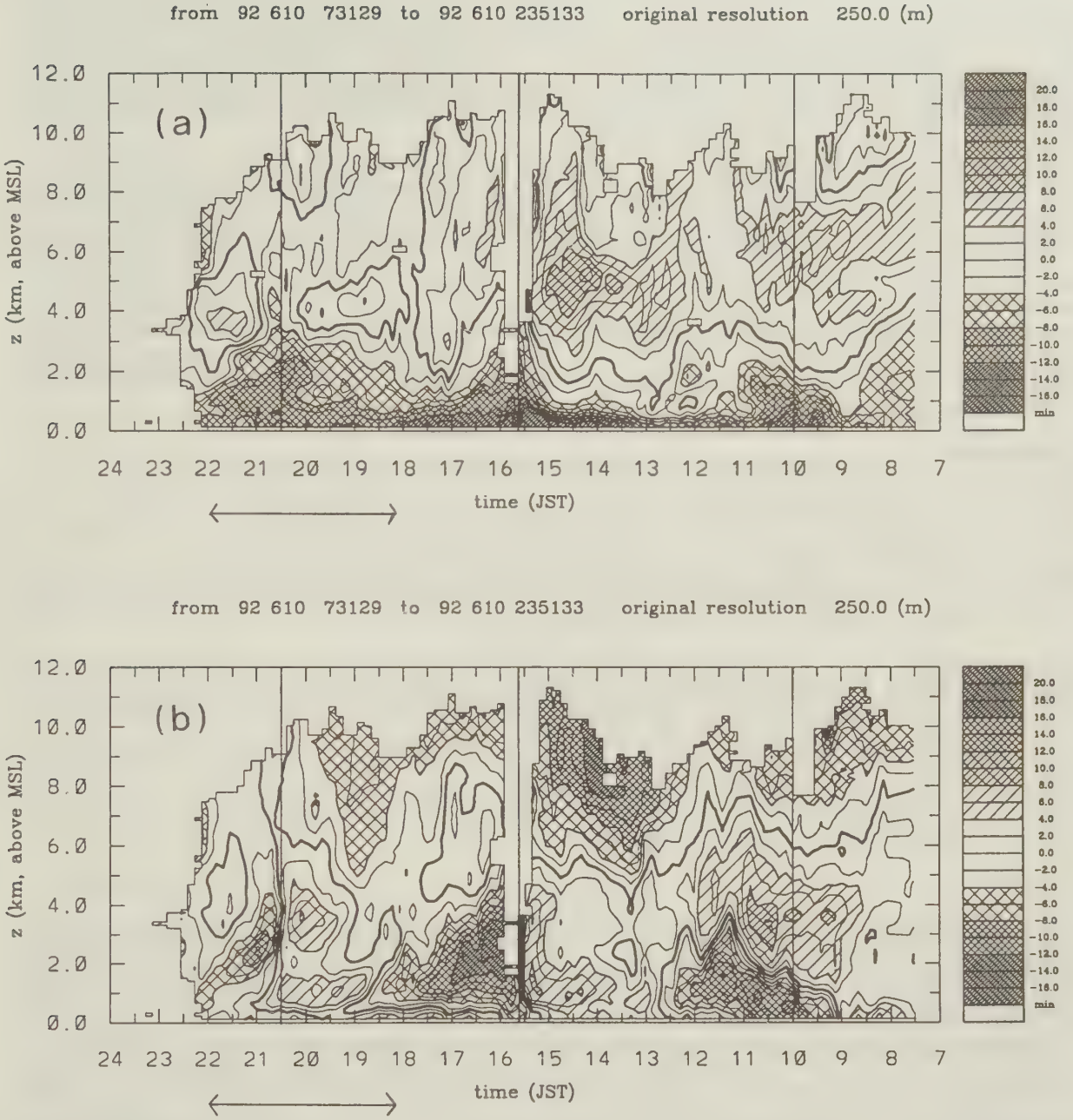

Fig. 8. Time series of the wind relative to the mean motion of the convective cells on 10 June obtained from VAD analyses. Thin vertical lines at 1000JST, 1540JST and 2030JST show the time when CR passed over the Doppler radar site. (a): southwest-northeast component, shown as the southwesterly wind is positive. (b): southeast-northwest component, shown as the southeasterly wind is positive.

outflow existed at the height below 1km, another at the height around 8km (2049JST, 2115JST), and an inflow at the height between 3.5km and 5.5km (2115JST). These characteristic winds disappeared by 2158JST. The wind at 2158JST was similar to that at 1804JST.

4. Discussions

We showed inflow and outflow in various stages of the third MCS. These characteristic winds extended into the stratiform precipitation region and are considered to compose a mesoscale circulation related to the evolution of the MCS. CR was a line of convection whose running direction was not far from southwest-northeast direction.

The time series of convection-cell-relative VAD wind profile on 10 June is shown in Fig. 8. Wind component parallel to the typical running direction of CR (southwest-northeast) showed that northeasterly wind blew below 3km and southwesterly wind blew above 3km (Fig. 8(a)). This direction was also parallel to the motion of convection cells. It is suggested that the wind shear contributed to the evolution of each convection cell. Low-level northeasterly wind strengthened as CR approached, suggesting that each convection cell intensified within CR.

Wind component perpendicular to the typical running direction of CR showed drastic changes when CR passed over

the radar site at 1540JST and 2030JST (Fig. 8(b)). At the height below 5km, the southeasterly and northwesterly wind prevailed before and after the passing of CR, respectively. It means that the wind converged at CR. The wind direction reversed and divergence occurred at the height above 5km. A pair of low-level convergence and upper-troposphere divergence was also recognized around 1000JST though the configuration was different from the later ones. It is considered that the convergence and divergence composed the mesoscale circulation accompanying the organization of convection and that CR was in a mesoscale updraft region.

The mesoscale circulation is important to understand the structure and precipitation mechanisms of MCSs observed in the Asian Monsoon region. MCSs plays an important role in the water cycle of Baiu front and the Asian Monsoon region, for it gathers water vapor more effectively than isolated convection and generate many clouds in the upper troposphere. Detailed data analysis using the observation data on this viewpoint will be needed in the following years.

Satellite microwave data analysis is hopeful to clarify the distribution of water in Baiu frontal zone including MCSs. However, the relation between the precipitation rate and the brightness temperature of microwave radiometer is non-linear and dependent on the distribution of the size and phase of precipitation particles. The knowledge on the structure of MCSs, for example, type of precipitation, the height of melting level, inhomogeneity of precipitation rate within the footprint of the satellite microwave radiometer, are important parameters. It will be needed in the following years to estimate them from the observation data, and to analyze the satellite microwave data based on the result of observation data analysis.

5. References

Browning, K. A. and R. Wexler, 1968: The determination of kinematic properties of a wind field using Doppler radar. J. Appl. Meteor., 7, 105-113.

Kato, K, 1993: The processes of the seasonal transition of Baiu front in East Asia: The effect of Indian Monsoon and the semiarid region around China (Japanese). Kaiyo Monthly, extra issue No.5, 96-101.

Nakai, S., A. Tabata, Y. Yamada, H. Iwasaki and H. Sakakibara, 1994: Vertical structure of a subtropical mesoscale convective system (Japanese). Preprints of the 1994 Spring Semi-annual Meeting of the Meteorological Society of Japan, 24-26 May 1994, Tokyo, D213.

6. Publications

Nakai, S., A. Tabata, Y. Yamada, H. Iwasaki and H. Sakakibara, 1994: Vertical structure of a subtropical mesoscale convective system (Japanese). Preprints of the 1995 Spring Semi-annual Meeting of the Meteorological Society of Japan, 24-26 May 1994, Tokyo, D213.

Nakai, S., 1995: On the analysis method of the Doppler-radar data and the examples of its application: VAD analysis (Japanese). Bosai Kagaku Gijutsu, No. 73, 67-72.

Nakai, S., 1995: Extraction of characteristic mesoscale wind fields by VAD analysis (Japanese with English abstract). Rep. Natl. Res. Inst. Earth Sci. Disast. Prev., No. 55, 9-23.

和文アブストラクト

本研究では、4年度に取得したデュアルドップラー観測データの解析によって対流雲内の雨水量、気流の分布を明らかにすること、およびその結果を基にした衛星データ（主にマイクロ波センサ）の解析によって、対流雲による水蒸気消費量および鉛直輸送量を調査し、対流雲の維持過程、モンスーン雲域の水収支、およびこれらの関係を解明することを目的としている。

平成6年度は、ドップラー観測データを用い、1992年6月10日の3個のMCS(mesoscale convective system)に伴ったメソスケールの循環を解析した。MCS内部には組織化した線状の対流域があり、その代表的な走向は南西－北東であった。対流セルに相対的な風の時系列によると、対流域の走向に平行な成分は高度3kmより下層で北東風、上層で南西風のシアーが定常的に存在し、これは個々の対流の発達・維持に寄与する循環を表すと考えられる。対流域の走向に垂直な成分は、高度約5km以下で収束、高度約5km以上で発散というセンスになっており、鉛直断面の解析によると、これらの収束発散につながる流れが数十kmにわたって層状性降水域に延びていた。このことは、対流が組織化することによってメソスケールの循環が形成されていたことを表すと考えられる。

このようなメソスケールの循環はアジアモンスーン域に出現するMCSの構造と水収支を理解する上で重要であると考えられる。MCSが梅雨前線帯、ひいてはモンスーン域の水収支に果たしている役割は大きいと考えられ、観測データによる詳細な解析がさらに必要である。衛星マイクロ波データによるメソスケールの解析はMCSや梅雨前線の水物質の分布を知るために有効なものであるが、観測データから得られる降水タイプ、降水の不均一の度合などの情報を利用し、より定量的な解析を今後行うことが必要と思われる。

I. Observation and analysis on the process of atmosphere-ocean-land interaction interactions

I. 大気・海洋・陸域間相互の諸過程に関する観測・解析研究

2. Observation and analysis on the process over the ocean

2. 海洋における諸過程に関する観測・解析研究

(1) Observation on Sub-Surface Temperature by Voluntary Ships

(1) 表層水温に関する観測研究

Keisuke Mizuno* , Benny N. Peter, Tomowo Watanabe***

水野 恵介*, ベニー・N・ペーター**, 渡邊 朝生*

*** National Research Institite of Far Seas Fisheries**

遠洋水産研究所

**** School of Marine Sciences Cochin Univertity of Science and Technology**

コチン大学海洋学部

1. Objectives

Large scale oceanographic studies of the Indian Ocean are less compared to the Atlantic or Pacific oceans. Wytrki(1971) presented a comprehensive description of the Indian Ocean using the data collected during the International Indian Ocean Expedition. Later, considerable efforts made on different Parts of the ocean improved our understanding, though the observational data remained sparse. Levitus(1982) prepared a climatology of the subsurface temperature and salinity structure for the entire Indian Ocean as a part of global climatology. The circulation in the upper layers of the North Indian Ocean reverses semi-annually due to the monsoon circulation prevailing over the Indian Ocean. Basic description of the surface forcing fields, and the nature of the mixed layer can be found in Hasternrath and Lamb (1979), Cadet and Dieh (1984), and Molinari et al. (1986). The climatology of the upper layer thermal structure of the tropical Indian Ocean was explained by Rao et al. (1989).

Wyrtki (1973) first found the existence of an equatorial jet in the Indian Ocean and which was validiated by O'Brien and Hurlburt(1974), using a two layer numerical simulation. Numerous modelling efforts have been made to explain the Indian Ocean circulation . After these works, it is recongnized that the wave several kinds of long waves are dominated in the variation of the Indian Ocean. Modelers have made effort to understand the nature of variation in the Indian Ocean. Woodberry et al.(1989) simulated the major features of the large-scale upper

ocean circulation in the southern hemisphere and the equatorial regions, and found the annual signal Rossby wave generated in the shear zone between the South Equatorial Current and South equatorial Counter Current . A similar study on western Indian Ocean circulation was counducted by Kindle and Thompson (1989).

These waves found in the models has not well described in the observed geostrophic field. Although previous observational studies were sucessful in deriving the large scale circulation pattern but the small scale disturbances were left unnoticed due to the paucity of observations. In order to overcome the observational handicap, in the present study it is attempted to make use of temperature profiles in addition to temperature-salinity profiles to estimate the dynamic height.

2. Data and methods

The present investigation employs the historical data set that includes to the region between 30 E - 130 E and 30 S - 30 N. All available hydrographic observations(BT, XBT, CTD, STD and Nansencasts) for Indian Ocean is procured from NODC and INODC data set and the recent NRIFSF cruise reports are merged to form a single data set.

The temperature-salinity profile comprises about 30,000 for the study region. Stations having the first observation within the upper 5m depth are chosen. Then the original observations are interpolated into 20 standard depths(O, 10, 20, 30, 50, 75, 100, 125, 150, 200, 250, 300, 400, 500, 600, 800, 1000, 1200, 1500, 2000). The data set is compared with the Levitus (1982) data set and the stations with even a single bad quality record are discarded with eye inspection. Finally, 11,000 T-S profiles are leftout for analysis (Figure 1A).

The temperature profiles aggregate to about 50,000 for the entire area of interest and observations extending to 400m depth only are considered for the study. Also, observations with no data for more than two consecutive standard depths are rejected. After necessary checkings about 26,000 temperature profiles (Figure 1B)have been selected for further processing.

Stommel(1947) introduced the method of estimating the dynamic height from temperature data by approximating the corresponding salinity from the existing local standard temperature-salinity profile. Using this estimated salinity, he computed the dynamic heights. In the tropical Pacific, Pazan et al.(1986) found good correlation between estimated dynamic hight and island sea level. The dynamic height was estimated by optimally interpolated thermal field based upon XBT data, and climatological T-S curves at the corresponding area. Mitchell et al. (1990) used a simple linear regression between dynamic height and the depth of a specific isotherm in comparing the satellite altimeter data with air-launched XBT transects across the Gulf stream, with a possible error of .07 dynamic meter. Since the upper layer of in the tropical and subtropical Indican is warm, temperature change has important effect to the change of the specific volume. The averaged temperature probably has good correlation with dynamic hight. We excercised this idea in the Indian Ocean.testd to excercise

In the present study, the correlation between heat content and dynamic height with respect 400m depth is examined and this correlation is employed for estimating dynamic height from the temperature data. Using the T-S data, the heat content and dynamic depth is estimated with

reference to 400db. The long term 2x5 latitude/longitude grid averages of heat content and dynamic height are obtained using interpolation with gaussian filter . Then, the correlation between heat content and dynamic height in different parts of the ocean is examined, considering the circulation pattern. Better correlation is obtained by dividing the whole area into nine regions as shown in Figure 2.

To substantiate the correlation between heat content and dynamic height of different regions, T-S diagrams are prepared for the different regions and examined (Figure 3). From the first view itself we can observe the worse correlation in the northern part of Arabian Sea and in Indonesian throughflow region. The influence of high salinity water of Arabian Sea and low salinity water of Bay of Bengal accounts for the wide scatter in the upper layers of region 7 and 6. The water is most homogeneous below the surface layer at region 1 and 2. In the intermediate depths, lateral mixing is predominant but diapycnal mixing is observed at surface.

The presence of low salinity Antarctic Intermediate water is detected in the deeper layers of region 3 and 4. At region 5 much scattering, in the upper layers is due to the waters from Arabian Sea and Bay of Bengal. Towards deeper layers more homogeneous nature is observed.

The incursion of low salinity equatorial Pacific water through the south equatorial current makes the T-S distribution more heterogeneous and wide scattering is observed in the intermediate depths in the Indonesian throughflow region(region 8)

Thus, the T-S characteristics Support the correlation obtained in the different regions. Therefore, Wherever the correlation is found significant, the heat content is reciprocated to dynamic height using the linear fit equations of correlation (Table 1). Annual and bimonthly maps of dynamic height are constructed. The intra-annual and annual variations are discussed by preparing the time-longitude section of dynamic height anomaly.

3. Result and Discussion

3-1. Annual mean

The long term annual mean dynamic topography is presented in Figure 4. The main features observed are the westward flowing South Equatorial Current, eastward Equatorial Counter Current and the South Indian Ocean Current. The North Equatorial Current occurs north of 6 N and is comparatively weak in the annual signal. The eastward flow of the Equatorial Counter Current occupies a broad band of latitude between 6 N to 6 S. The South Equatorial Current is between 10 S and 16 S. The northern part of the Arabian Sea performs anticlockwise circulation whereas clockwise circulation prevails in the northern part of Bay of Bengal. Rest Part of the Bay exhibits lull circulation.

The strong signal of the Indonesian throughflow and the return flow south of it towards western Australia are clearly visible. In the central part of the South Indian Ocean cyclonic eddy circulation is noticed between Madagascar and Australia. Highest steric height is encountered in the Indonesian throughflow region. Eastern part of the equatorial ocean shows high steric heights compared to the west. The southward flowing Leewin Current is visible in the annual mean steric height along the Coast of western Australia. This current is feeded by the South Indian Ocean Current.

Thus, the annual signal exhibits dynamically active condition in the central parts of Arabian Sea, equatorial region and between 20-30 S. The South Equatorial Current and the South Indian Ocean Current are more prominent features. Also, stronger flow is observed in the Arabian Sea compared to the Bay of Bengal.

3-2. Bimonthly dynamic topography

Bimonthly maps of dynamic topograpy is prepard to understand the intra-annual changes in the circulation(Figure 5). During January-February, Northeast monsoon condition prevails in the Indian Ocean. The North Equatorial Current driven by the northeast trades is evident close to the equator. The south equatorial current is between 10 S - 18 S and the Equatorial Counter Current occurs between North equatorial and South equatorial currents.
Anticyclonic circulation prevails in the Bay of Bengal. Arabian Sea exhibits more steric gradient compared to the Bay of Bengal. The South Indian Ocean Current is vivid south of the South Equatorial Current flowing towards east below. A cyclonic eddy activity is noticed in the eastern part of south Indian Ocean where the Indonesian throughflow joins with tropical gyre circulation. The southward flowing Leewin Current is not visible during this period.

In March-April. the northeast winds are much weakened and the equatorial ocean displays a lull condition. The north equatorial current is not evident in the dynamic topography. In turn. the South Equatorial Current and and Equatorial Counter Current are more shifted to north. Another prominent feature noticed is that the Equatorial Counter Current is extended more into the east during this season. High steric height is developed in the eastern part of the equator. The cyclonic eddy noticed in the above period is still present. An increase in the dynamic height is noticed in the Bay of Bengal and in the northern part of the Arabian Sea. But the steric height is reduced in the South Indian Ocean compared to January-February period. The Indonesian throghflow is much weakened compared to the earlier period whereas the Leewin Current is visible off Western Australia.

During May-June. the broad band of eastward flowing Southwest Monsoon Current appeares at the equatorial region. Part of this flow is supplied to the westward flow of SEC and the rest is continuing towards the Pacific through the Indonesian seas. Anticlockwise and clockwise current Patterns are observed in the northern part ofthe Arabian Sea and Bay ofBengalrespectively. High steric heights are developed in eastern part of the Indian Ocean especially. in the Indonesian throughflow region and near Sumatra. The cyclonic cell is still present but its position is slightly shified to the west. The southward flowing Leewin Current is well developed during this period. .

The southwest monsoon condition persists during July-August. The monsoon current is more shifted to the north in the Arabian Sea (upto 15 N) by the stronger southeast trades. In the northern part of the Arabian Sea the low steric heights are observed during this period. The South Equatorial Current becomes more narrow compared to the earlier periods and cover between lOS-15S. Anticlockwise circulation is present in the Bay of Bengal. A prominent decrease is noticed in the steric height in the east near Sumatra. In contrary to the earlier sections. an anticlockwise eddy appears in the region where the Indianesian throughflow joins with the South Equatorial Current. Another interesting feature observed is the weakening of the Leewin Current

off the Western Australia.

Post monsoon characteristics are evident in the September-October topography. The gradual change in the current direction in the northem part of the Arabian Sea is apparent between July-August and September-October periods. Equatorial region still displays the monsoon current. The conspicuous feature observed in this period is the intensification of the Indonesian throughflow with high steric heights extended upto 80 E. The return flow is directed towards the Pacific Ocean and the Leewin Current is not Present in this period. The anticyclonic eddy observed in the earlier period is much weakened. The steric height is reduced in the Bay of Bengal compared July-August.

The Equatorial Counter Current is shifted to the south by the strong northeast trades during November-December. Westward flow is prevailing in the North Indian Ocean between equator and 10 N. The throughfiow is weakened during this period. The North Indian Ocean displays much weaker circulation patten. The Leewin Current is absent in this period.

The main features of the circulation observed is in good agreement with the ship drift: observations of Defant(1961) and the atlas prepard by Wyrtki (1971). Also. similar results were obtained by Molinari et al. (1990) from the compilations ofbuoy trajectories. The South Indian Ocean Current described by Stramma(1992) is identified in the maps. The seasonal variability of SEC with respect to the latitude was documented by Wyrtki (1971) and Rao et al. (1989). The strong throughfolw noticed during September-October period is in consensus with the estimation of Meyers (personal com.) that the maximum transport is noticed in August between Java and Australia. Thus, the one month lag shows the time of throughflow to reach the eastern part of the Indian Ocean. The seasonal variation of the Leewin Current and the eddy circulation between Madgascar and Australia described by Semtner and Chervin (1992) are apparent in the topography.

3-3. Wave phenomenon

The close examination of bimonthly dynamic topography suggests the presence of short period wave like disturbances in the tropical circulation. In order to bring out the nature of these signals, time -longitude section of dynamic anomaly (monthly-annual) along equator and different latitudes (4 N ,4 S, 8 N , 8S, and 12 S) are prepard (Figure 6- 11).

At the equator the anomaly distribution depicts the eastward propagating waves in the pre-monsoon and postnonsoon periods. The first signal generated in the western coast during March-April is propagating to the east in a greater speed and reaches at the eastern coast by June-July, The next wave is originating in September and takes about the same time to arvive at the west.

Away from the equator along 4 N and 4 S, very strong westward propagating biaunual signals are observed. The first signal is initiating in the western side during April -May and it takes about three months time to reach the west. The next signal is originating in October - November. The signals are much stronger in the Northern hemisphere compared to the Southern hemisphere. Also the first one (during summer) is well developed compared to the second signal(winter).

A westward propagating annual signal is obtained along 8 N and S. The signal is much stronger in the southern hemisphere. The signal is initiating inthe east during April-May and it takes about 13 months months to reach west. In the north the propagation is blocked by the Sri Lanka Coast and the eastern part the signal is very weak. Along 8 S. the wave pattern is not shown clearly.

The anomalous dynamic height at 12 S exhibits'strong westward propagating annual signal. The signal is originating in the Indonesian throughflow region in February-March and takes almost one year to reach at 60E ,where its propagation is blocked by the Seychellus-Mauritius Ridge. Between 60 E and African Coast short waves are observed. Studies on equatorial oscillation in the Indian Ocean indicate the existence of different period waves. According to the dispersion relations derived from the linear wave theory. Moore and Philander(1977)classified the equatorial waves in to Kelvin wave, Rossby wave. the inertia-gravity waves and the mixed Rossby-gravity wave(Yanai wave).

The characterstics of the eastward propagating signals obtained at the equator is identified as the fast moving Kelvin waves. Along 4 N, 4 S, 8 N, and 8 S the reflected Rossby waves occurs. The armual signal along 12 S is the Rossby wave travelling from the east along the Indonesian throughflow region. Similar annual oscillations are reported along 12 S in the modelling studies of Woodberry et al. (1989). Kindle and Thompson(1989). This Rossby wave energy is partially blocked by the banks along the Seychellus-Mauritius Ridge at 60 E The variability is generated to the east of 100E and propagates westwdrd as a Rossby wave at approximately 0.1 m/s.

The phase speed of the wave propagation is determined from the figures by estimating the slant of wave pattern. The Kelvin wave at the equator propagates at greater speed of about 1m/s. The Rossby wave speed at 4 degree latitude is about 0.4m/s and the speed is decreasing as the latitude increases. The phase speed of annual Rossby wave obtained is less than 0.2 m/s along 12 S. The phase speed of the wave propagation determined from the figures are to be consistent with the earlier estimations.

Reverdin and Luyten (1986) examined near equatorial meanders beginjng in August - September and westward propagation of 40 ± 15 cm/s. Chang and Philander(1989) ahalyzed the effect of mean currents with weak latitudinal shear on Rossby wave and found that the presence of the baroclinic mean currents can modify the characteristics of wave propagation significantly, a westward current can cause the speed of the long Rossby waves to decrease with decreasing latitude.

4. Summary

The effort to utilize the temperature observations to determine the large scale circulation of the Indian Ocean produces good results. The dynamic heights and the heat content are significantly correlated in the upper 400 m of Indian Ocean except in the Indonesian throughflow region and the northern part of the Arabian Sea. Thus. the correlation permits to compute the dynamic height from the heat content within an estimation error of .03 dynamic meter.

The dynamic topography obtained by this method is clearly depicting the seasonal circulation pattern of the Indian Ocean. The South Equatorial Current and the South Indian

Ocean Current are more well developed in the annual signal. The North Equatorial Current is comparatively weak. The bimonthly distribution displays seasonal changes of the currents. Strong Indonesian throughflow is observed during' September-October period. The seasonal changes in the flow pattern of Leewin Current off western Australia is apparent in the bimonthly maps.

The time-longitude sections of dynamic height anomaly along different latitudes are enables to bring out the annual and semi annual signals of circulation.The semi-annual signal of the Kelvin wave is clearly identified at the equator. Away from the equator the westward propagating Rossby wave signal is obtained and is very strong along 4 N and S. Along 12 S an annual signal of westward propagating Rossby wave generating from the Indonesian throughflow region is distinguished. The phase speed ofthe Rossby wave obtained at 12 S is less than 0.2m/s. whereas 0.4m/s speed is found at 4 N and S. The equatorial Kelvin wave is propagating at a greater speed of about 1 m/s.

5. References

Cadet, D.L. and B.C. Diehl (1984) Interannual variability of suface fields over the Indian Ocean during recent decades. Mon. Weath. Rev. 112, 1921-1935.

Defant, A(1961): Physical Oceanography. Pergamon Press, NewYork,N.Y.,1,567-568.:

Hastenrath, S. and P.J. Lamb (1979) Climatic Atlas of the Indian Ocean, Part II: the oceanic heat budget. The University of Wisconsin Press.

Kindel,J.C. and J.D.Thompson (1989) The 26- and 50-Day Oscillations in the Western Indian Ocean: Model Results. J.Geophys.Res., 94,(C4),4721-4736.

Largerloff,G.S.E. (1994): An Alternate Method for Estimation Dynamic Height from XBT Profiles Using Empirical Vertical Modes. J.Phys.Oceanogr.,24,205-213.

Levitus, S. (1982) Climatological atlas of the World Ocean. NOAA Professional Paper 13. U.S. Department of Commerce.

Mitchell, J.L., J.M.Dastugue, W.J.Teague, and Z.R.Hallock (1990): The estimation of geoid profiles in the northwest Atlantic from simulaltaneous satellite altimetry and airborne expendable bathythemograph sections. J.Geophys.Res., 95C, 17965-17977.

Molinari,R.J., J.F.Festa, and J.C.Swallow (1986) Evolution of near-surface thermoal structure in the western Indian Ocean during FGGE,1979, J.Mar.Res.,44,739-762.

Molinari, R.L.. D. Anson and G. Reverdin 1990: Suface cucent distributions in the tropical Indian Ocean derived from compilations of suface buoy trajectories, J. Geophys. Res.95, 7217-7238.

Moore,D.W. and S.G.H.Philander(1977):Modelling of the Tropical ocean circulation, in The Sea, vol6,319-361. Wiley Interscience, NewYork.

O'Brien,J.J. and H.E.Hurlburt (1974) An equatorial jet in the Indian Ocean: Theory. Science, 184, 1075-1077.

Rao, R.R., R.L. Molinari and J. Festa (1989) Evolution of the climatological near surface thermal structure of the tropical Indian Ocean. Part I: Description of mean monthly mixed layer depth and sea surface temperature, surface current and surface meteorological fields. J. Geophys.

Res. 94, 10801-10815.

Reverdin, G. and J. Luyten (1986) Near-surface meanders in the equatorial Indian Ocean. J. Phys. Oceanog. 16, 1088-1100.

Semtner, A.J. and R.M Chervin (1992) Ocean general circulation from a global eddy-resolving model. J. Geophys. Res. 97, 5493-5550.

Stommel,H. (1947): Note of the use of the T-S correlation for dynamic height anomaly computation. M.Mar.Res.,5,85-92.

Stramma, L. (l992): The South Indian Ocean Current. J. Phys. Oceanog. 22, 421-430.

Woodberry, K.E., M.E. Luther and J.J. O'Brien (1989) The wind-driven seasonal circulation in the southern tropical Indian Ocean. J. Geophys. Res. 94, 17985-18002.

Wyrtki, K. (1971) Oceanographic Atlas of the International Indian Ocean Expedition. National Science Foundation .

Wyrtki, K. (1973) An equatorial jet in the Indian Ocean. Science 181, 262-264.

6. Publications

Nattional Research Institute of Far Seas Fisheris, Fisheries Agency, Hdrographic Department, Marintime Safety Agency, and Marine Department, Meteorological Agency.(1994): Surface currents and Upper Ocean Thermal Structure in the Indian Ocean. 57pp.

Mizuno K. (1995): Seasonal Variation in the Indonesian Throughflow by using Historical Longline Drift Data. Annual Meet.ing of Fisheries Oceanography. (oral presentation in Japanese).

Mizuno K. (1995): Annual and Interannual variation in the subsurface temperature in the Indian Ocean. Annual Meet.ing of Fisheries Oceanography. (oral presentation in Japanese).

7. International Cooperation

1) WCRP Indian Ocean Panel meeting (May 14 - 18 ; Trieste ,Italy)

Attend the meeting, and roported the current sityation of the Indian Ocean studies in Japan. and discussed the future plan in terms of international cooperative scientific research.

2) Cooperative Stukiy with Indian Scientist.

Indian Scientist, Benny N. Peter at Cochin University stayed 1 year at NRFSF, and studied on the Indian Ocean under the support of STA fellow ship.

和文要旨

インド洋において４００ｍまでの積算水温とダイナミックハイトとの相関を検討した。アラビア海北部とインドネシア通過流の影響下にある海域をのぞき、ほぼ全域で良い相関が得られた。相関の良い海域で、水温プロファイルデータから推定し、他は水温・塩分から計算してダイナミックハイト（０／４００ｄｂ）の分布の年平均および周年変化を調べた。赤道海流系やインドネシア通過流およびルーイン海流の季節変化の特徴がとらえられた。赤道上に半年周期で発生するケルビン波や、低緯度のロスビー波の存在が確認され、１２Ｓでは１年周期のロスビー波が西進がみられた。

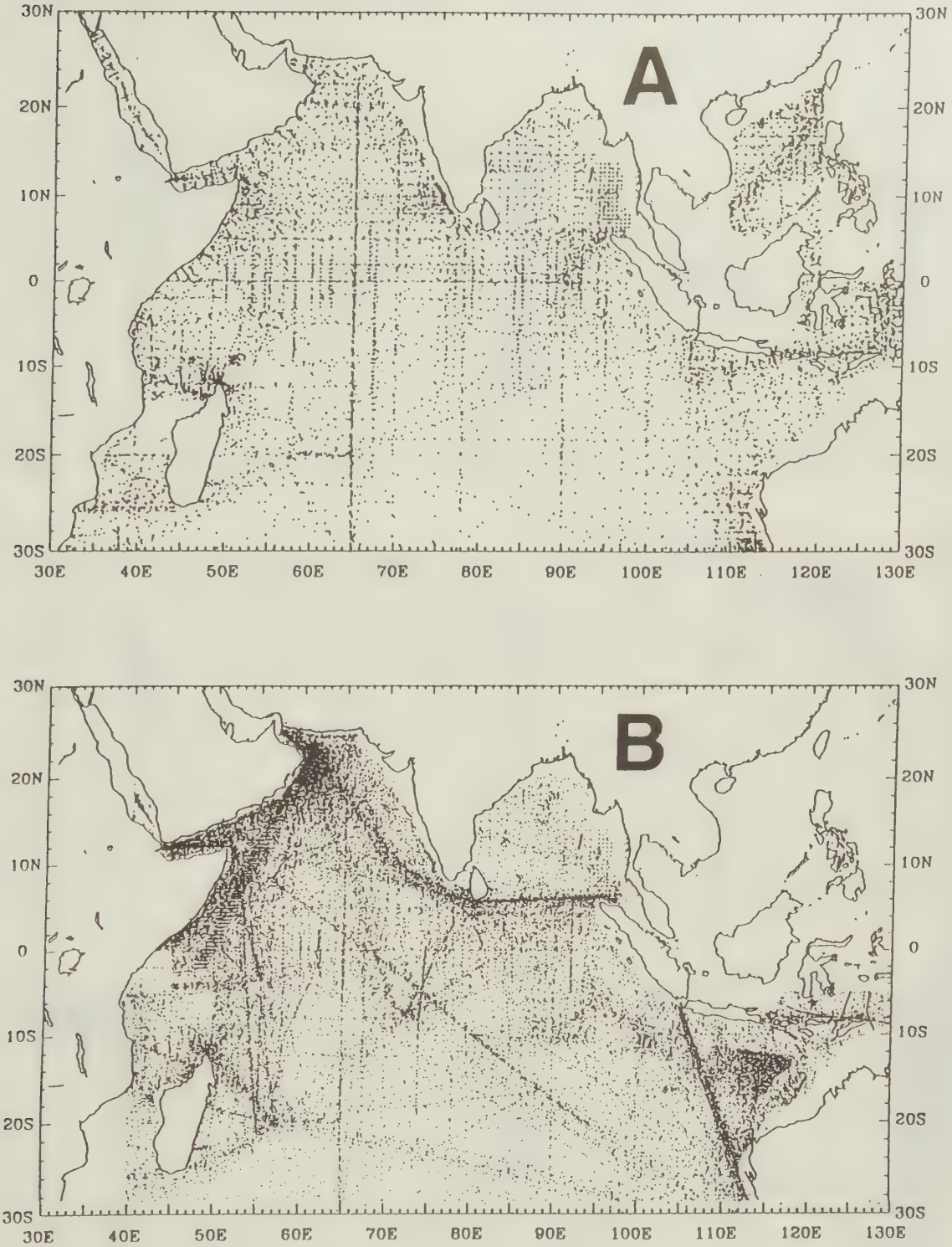

Figure 1. Upper panel; Geographical distribution of historical temperature/salinity/depth data..
Lower panel; Geographical distribution of historical temperature/depth data.

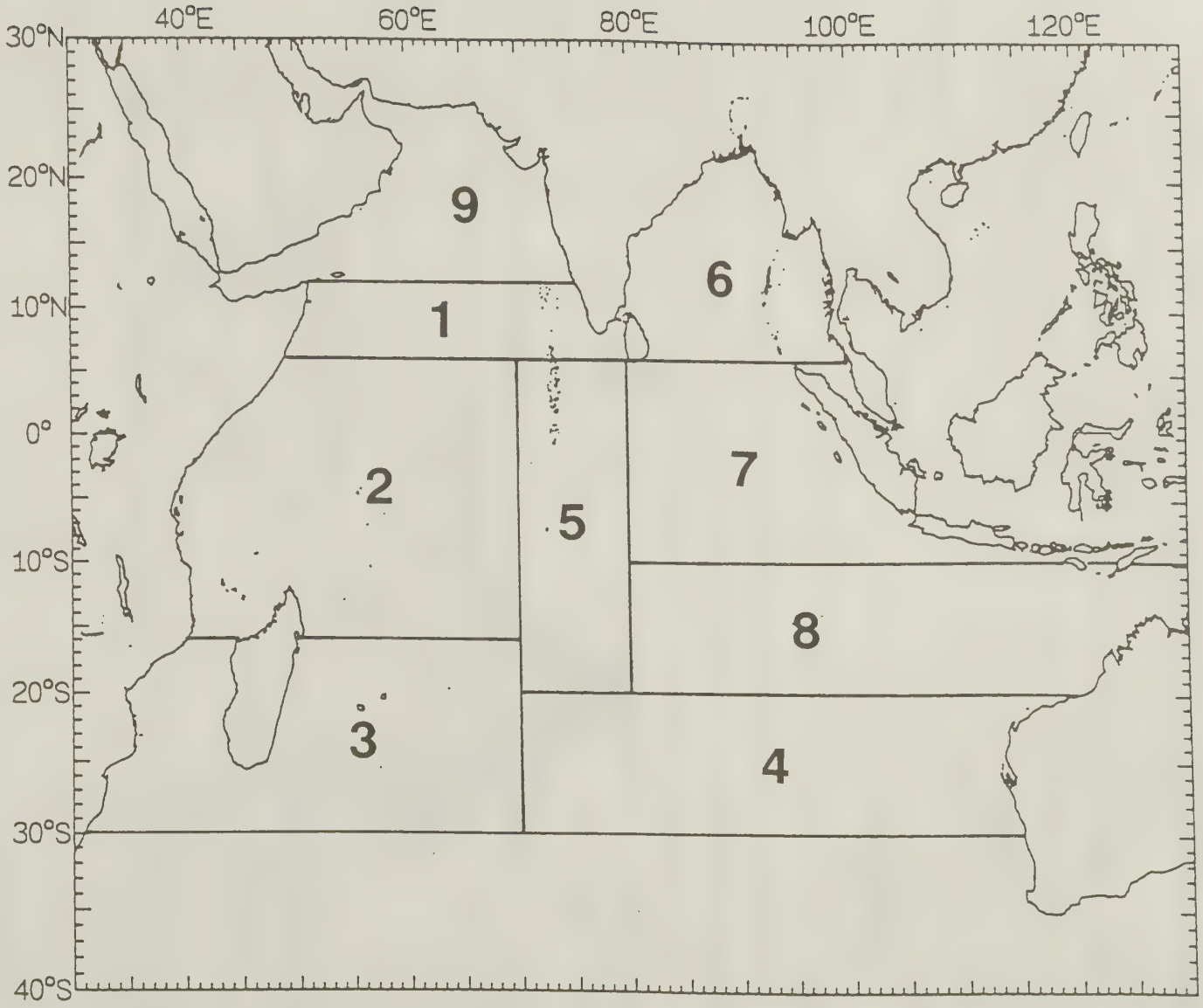

Figure 2. Sectors to estimate dynamic height from averaged temperature of upper 400m.

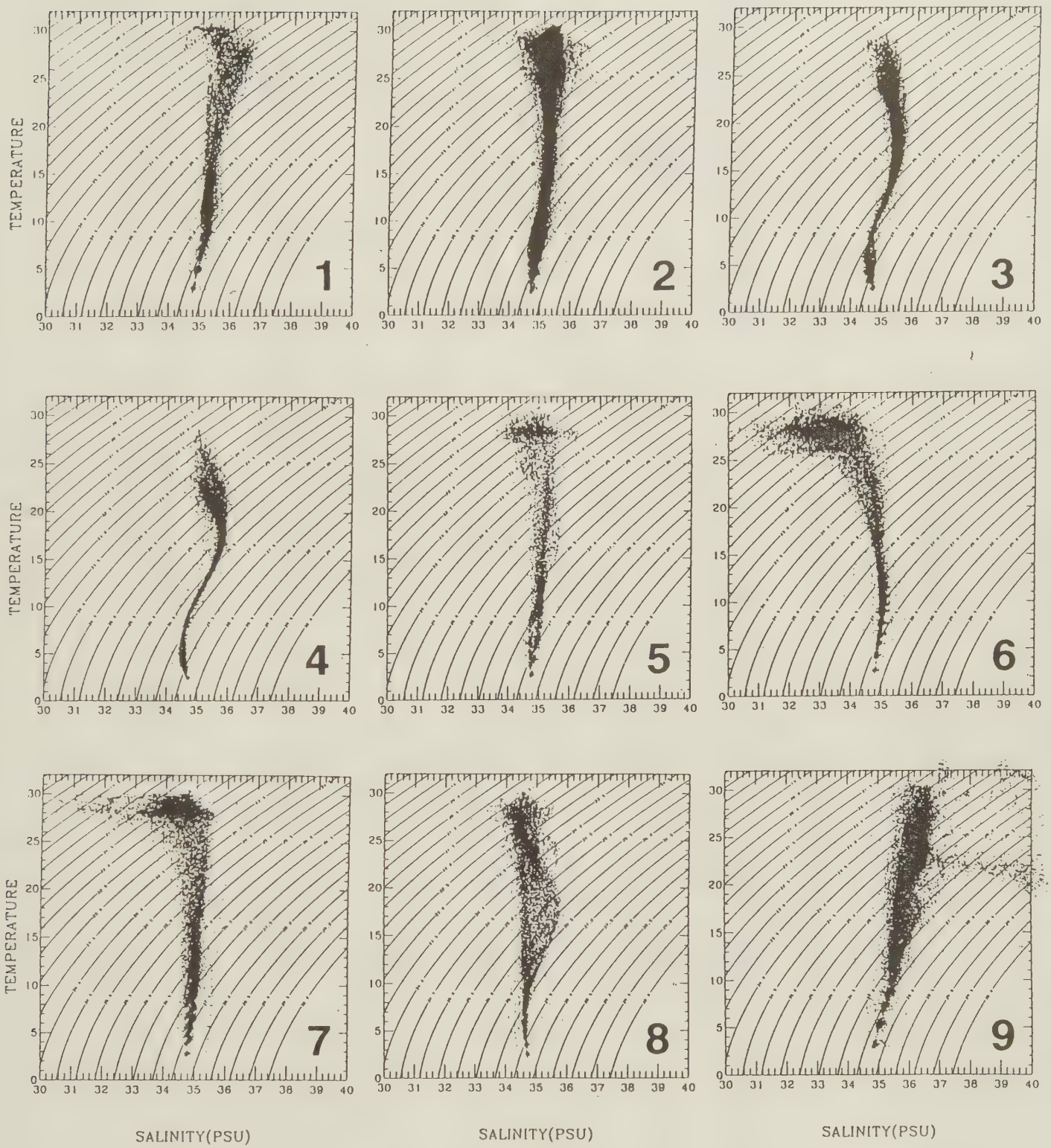

Figure 3. T-S scatter of individual temperature/salinity observation for each sector (1-9 in the previous figure).

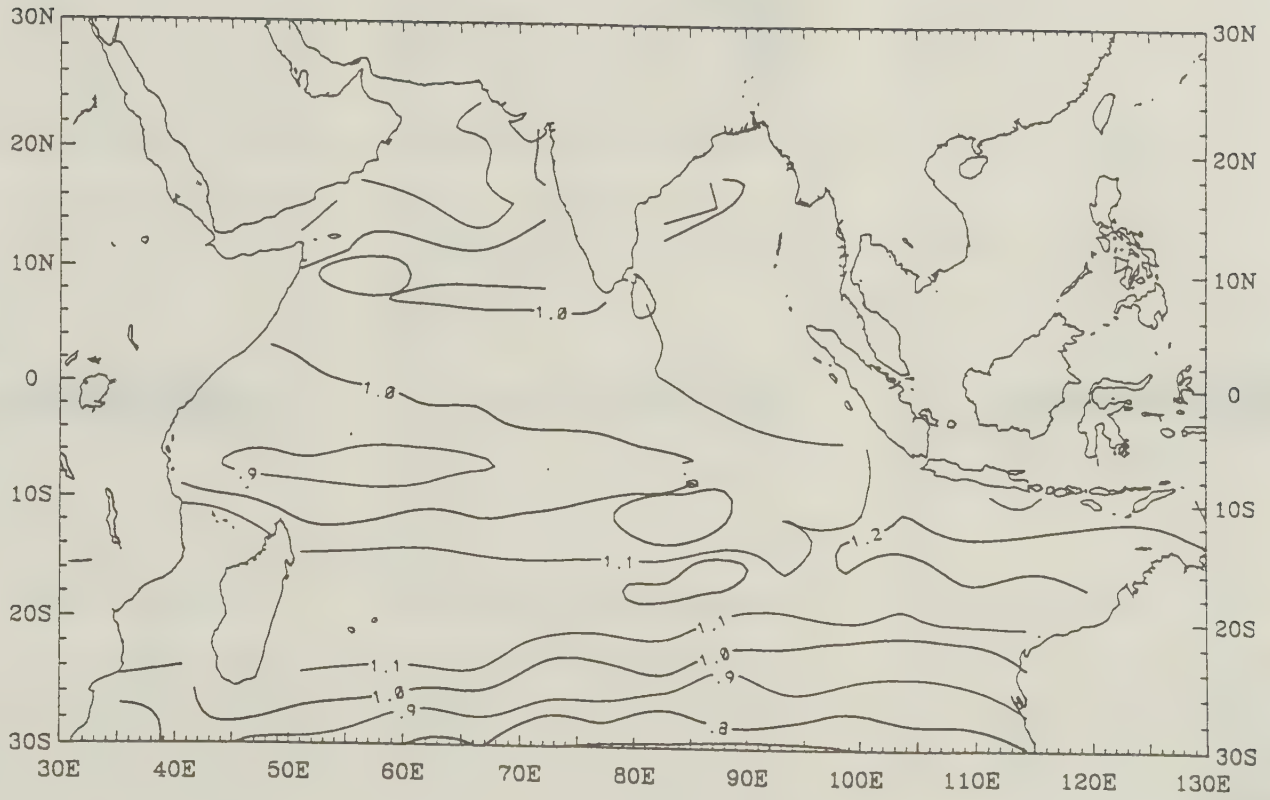

Figure 4. Long-term annual mean dynamic height (0-400db).

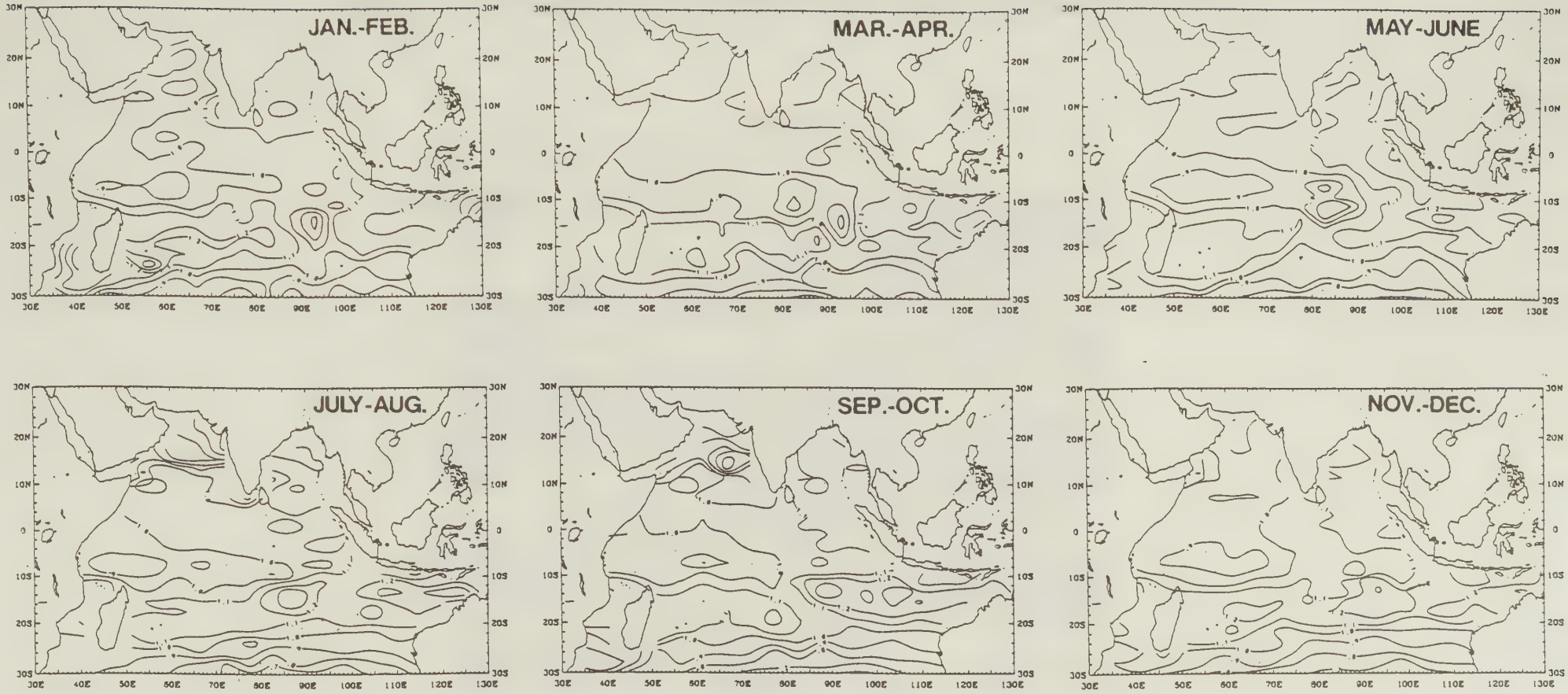

Figure 5. Long-term bimonthly mean dynamic height (0-400db).

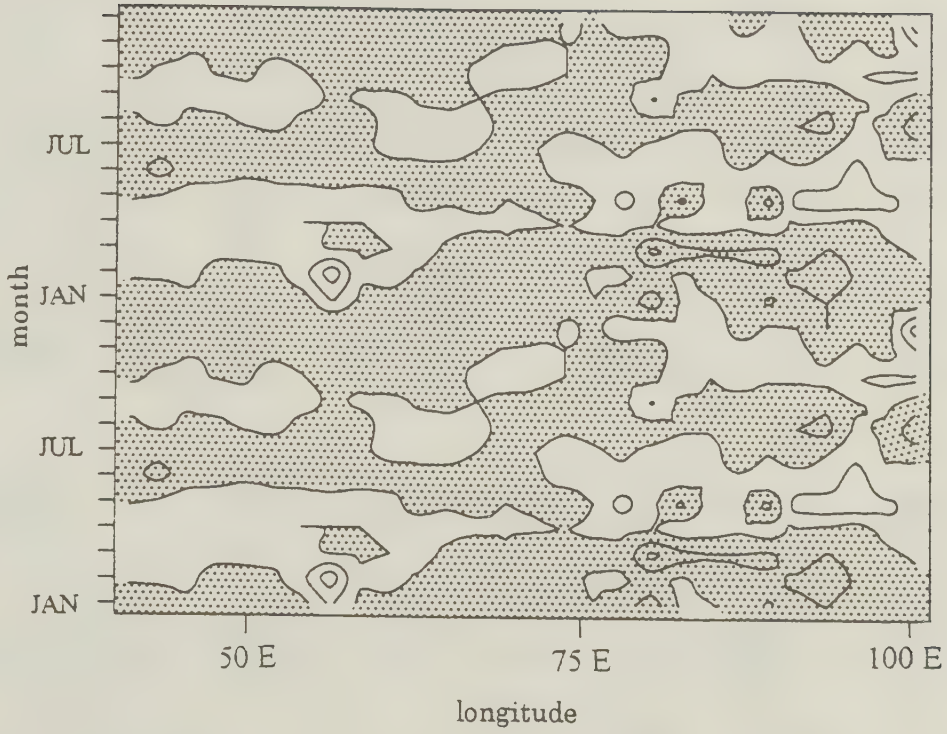

Figure 6. Time-longitude matrix of anomalous dynamic height anomaly along the equator. Contour interval is 10dyn. cm, negative anomalies are shaded.

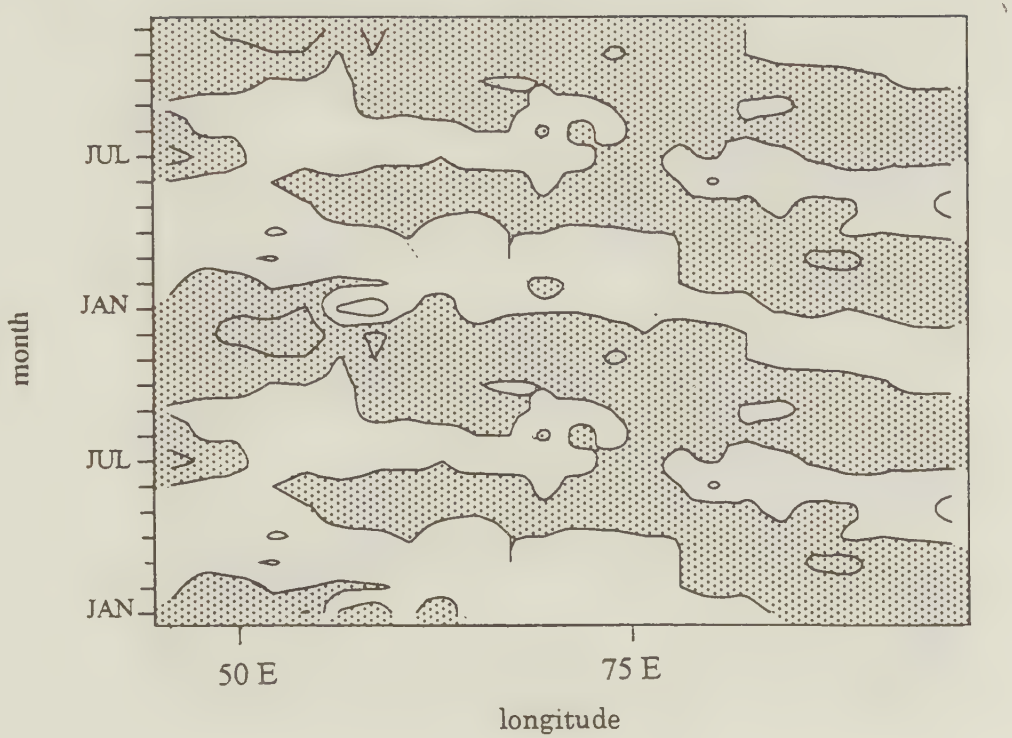

Figure 7. Time-longitude matrix of anomalous dynamic height anomaly along 4N. Contour interval is 10dyn. cm, negative anomalies are shaded.

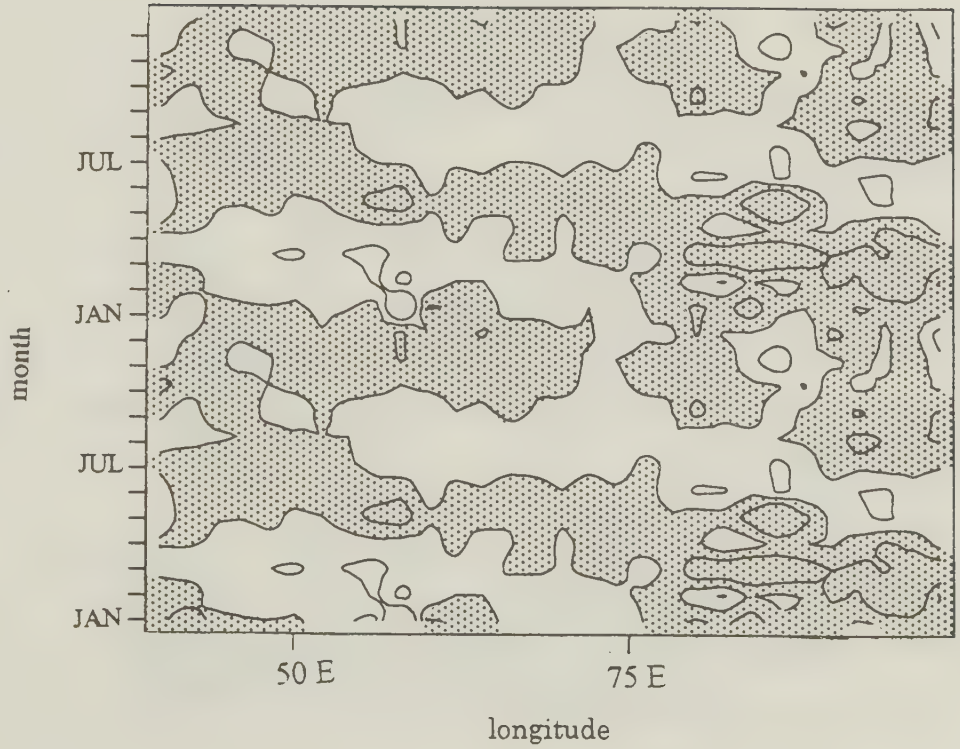

Figure 8. Time-longitude matrix of anomalous dynamic height anomaly along 4S. Contour interval is 10dyn. cm, negative anomalies are shaded.

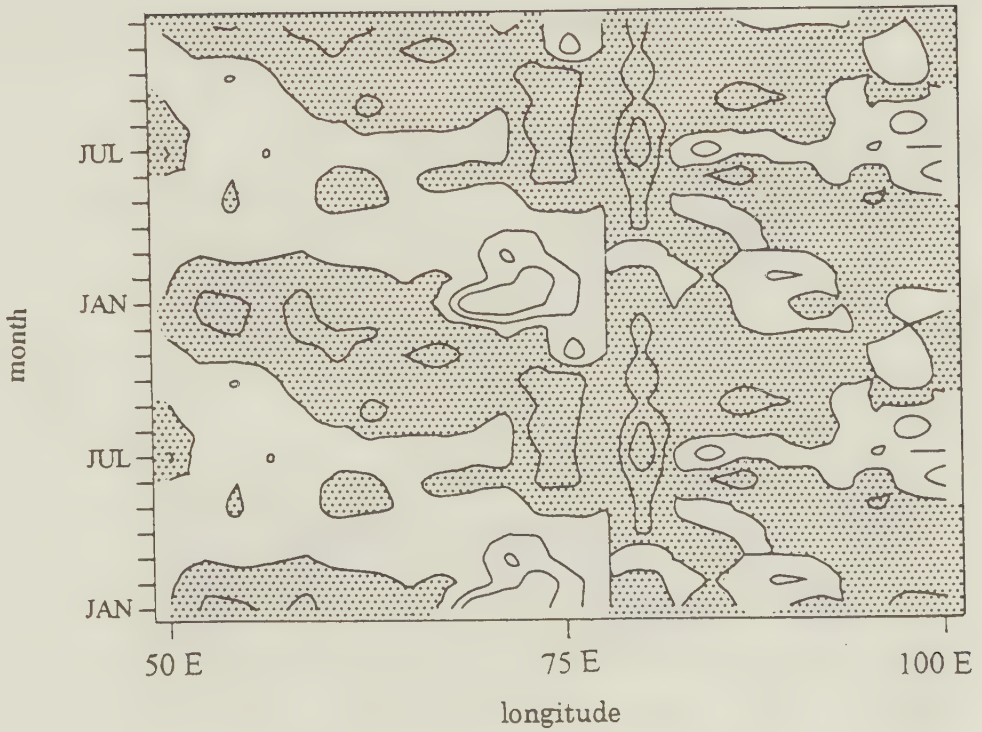

Figure 9. Time-longitude matrix of anomalous dynamic height anomaly along 8N. Contour interval is 10dyn. cm, negative anomalies are shaded.

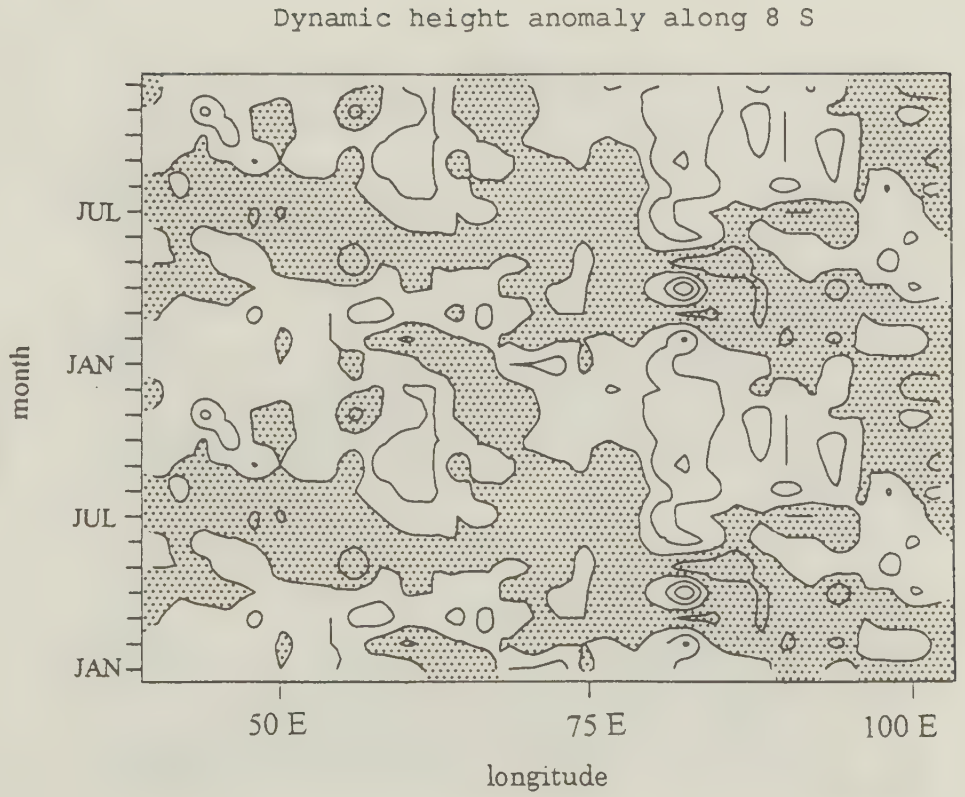

Figure 10. Time-longitude matrix of anomalous dynamic height anomaly along 8S. Contour interval is 10dyn. cm, negative anomalies are shaded.

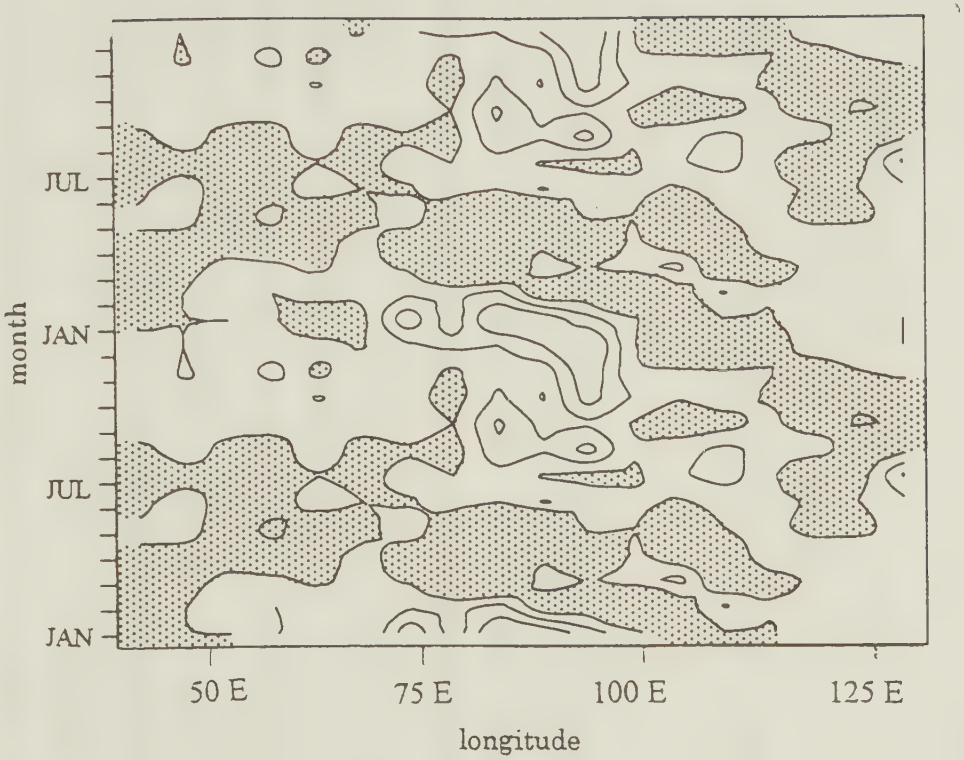

Figure 11. Time-longitude matrix of anomalous dynamic height anomaly along 12S. Contour interval is 10dyn. cm, negative anomalies are shaded.

Ⅰ．大気を媒体とした海陸相互作用及び長期変動に関する観測・解析研究

Observation and analysis on the process of the atmosphere-ocean-land interactions

2．海洋に関する観測研究

Observation and analysis on the process over the ocean

(1)表層水温に関する観測研究

Observation on Subsurface Temperature by Voluntary Ships

気象庁海洋気象部　三河哲也、石川孝一

Tetsuya Mikawa and Koichi Ishikawa

Marine Department, Japan Meteorological Agency (JMA)

(Abstract)

Subsurface temperature observations with XBT have been made by two voluntary observing ships "Kashimasan-Maru" and "Delmas Tourville" in the Indian Ocean since 1990. XBT data collected via GTS including these data were analyzed to investigate the thermal structure of the Indian Ocean using the Ocean Data Assimilation System developed by JMA.

In the eastern Indian Ocean, surface warm water masses accumulate during both transition periods between the two monsoons, thus seasonal variation of the ocean subsurface corresponds with the change of the wind system. On the other hand, the state of ocean of the western Indian Ocean changes semiannually, although the monsoon circulation shows annual variation. The phase of seasonal variation of the depth of the 20°C isotherm and ocean heat content in the upper layer is one month or two ahead of one of the sea surface temperature .

1. Objectives

The Asian Monsoon over the Indian Ocean and the seas around Southeast Asia is considered to relate to El Niño events which affect the global climate (Barnett 1983[1]), Nicholls 1984[2])). Recently, understandings of the ocean structure in these regions, and explanations of relation between the Asian Monsoon and El Niño have been urged. However, in these regions, amount of oceanographic data are too sparse to fully understand the state of the ocean. The subsurface temperature observed with XBT and reported by a crude oil tanker between Japan and the Persian Gulf and by a cargo carrier between Japan and the Cape of Good Hope via the Strait of Malacca have been distributed to national meteorological/oceanographical services throughout the world via the Global Telecommunication System (GTS) of World Meteorological Organization (WMO) since October 1990. XBT data collected via GTS including those of the crude oil tanker and the cargo carrier are analyzed to investigate annual and seasonal variation of subsurface waters in this region. These data are being used to explain not only the structure of Asian Monsoon but also related phenomena.

2. Methods

Subsurface temperature in the Indian Ocean and the South China Sea is observed four times a day by a crude oil tanker "Kashimasan-Maru" which makes a fifty days round trip between Japan and Persian Gulf via the Strait of Malacca and by a cargo carrier "Delmas Tourville" which makes a fifty days round trip between Japan and the Cape of Good Hope via the Strait of Malacca. The latter ship was consigned to make such observations cooperatively by Japan Meteorological Agency (JMA) and Organization of Research on Science and Technology Outside Marine (ORSTOM, Brest, France). Fig. 1 shows the routes of the two ships.

JMA has developed the Ocean Data Assimilation System (ODAS) and commenced its operational use at the beginning of 1995. The ODAS consists of a dynamical ocean general circulation model and a sea surface and subsurface temperature analysis system. The output of the ODAS using XBT data collected via GTS including those of two ships mentioned above are used to investigate

the structure and its variation of subsurface waters in the Indian Ocean. The system output is used for the analysis of the structure and its variation of the ocean. A global ocean general circulation model follows Bryan's (1969)[3] formulation for its dynamical framework. The horizontal resolution is 2.0° in latitude and 2.5° in longitude except 20°S-20°N equatorial band, where latitudinal grid spacing is smoothly decreased to a minimum of 0.5° in order to resolve complicated current system there. The model has 20 vertical levels, of which 13 lie in the upper 300 meters. The computational domain is global, except for the Arctic Ocean. Topography and grid spacing of the model are shown in Fig. 2. External forcing to drive the model is estimated with bulk formula, using the JMA Global Data Assimilation System (GDAS). As thermal boundary condition on the model, instead of heat fluxes derived from GDAS, temperature of the uppermost level is forced to be analyzed SST by nudging. The seasonal variation in the tropical Indian Ocean is investigated using normals every 5 days computed from 1987-1994 base period (Yoshikawa et al. (1995)[4]).

3. Results

(1) Observation of subsurface temperature by voluntary observing ships

As many as 1583 subsurface temperature data were obtained by "Kashimasan-Maru" in the South China Sea, the Bay of Bengal and the Arabian Sea since October 1990 to December 1994. The total number of data obtained by "Delmas Tourville" between the Strait of Malacca and the Cape of Good Hope since April 1990 to December 1994 amounts to 490.

(2) Analysis using results derived from the ODAS

① Results derived from the ODAS

In case of little observed data, it is difficult to explain the variation of three-dimensional ocean structure continuously. Data assimilation into models makes it possible to see three-dimensional ocean structure. Fig. 3 shows the time-longitude sections obtained using the JMA's ODAS along the equator in

the Indian Ocean 8-year mean (1987-1994) values for the following parameters:

(a) Sea Surface Temperature (SST)

(b) Depth of the 20°C isotherm (D20)

(c) Ocean Heat Content (OHC)

(d) Surface zonal wind stress

The OHC is defined as follows:

$$OHC = \Sigma \rho_i T_i D_i / \Sigma \rho_i D_i$$

ρ : density T : temperature D : layer thickness

i : layer number (1-12 , i.e. 0m-260m)

OHC is roughly considered to be averaged temperature from the surface to the depth of 260m.

② Seasonal variation along the equator in the eastern Indian Ocean

As shown in Fig. 3a, SST along the equator east of 80°E in the Indian Ocean (south of the Bay of Bengal) is around 28 and 29°C and changes little throughout the year. However the depth of 20°C isotherm (D20) corresponding to the thickness of the warm surface layer changes distinctly (Fig. 3b). D20 in June when the North-East (NE) monsoon shifts to the South-West (SW) monsoon is more than 140m and is deepest in the year. In October/November when the SW monsoon shifts to the NE monsoon, D20 is more than 120m. D20 in the east of the equatorial Indian Ocean is deeper than in the central. On the other hand, D20 in February/March is less than 90m and is shallowest, when D20 in the east of the equatorial Indian Ocean is shallower than in the central. In September during the SW monsoon, D20 is shallower than the previous and the following months. Such features also appear in OHC (Fig. 3c). The seasonal variation of the zonal wind stress is shown in Fig. 3d. Westerly prevails around 80°E along the equator from April to November, especially in May/June. In October/November, westerly is stronger than the previous and the following months. The periods of strong westerly correspond with ones of accumulation of surface warm water. These features are caused by the surface warm water accumulated by strong eastward jet flow along the equator (Wytki, 1973[5]). ODAS shows well

this ocean structure.

③ Seasonal variation along the equator in the western Indian Ocean

As can be seen in Fig. 3a, SST in the equatorial Indian Ocean west of 80°E (south of the Arabian Sea) has a remarkable change all the year round in contrast to east of 80°E. SST during the period of the monsoon transition (April to May) is more than 29°C throughout the equatorial Indian Ocean and highest in the year. SST west of 60°E in November/December is slightly higher than in the previous and the following month. On the other hand, in January/February and in August/September, SST is low west of 60°E, thus the semiannual variation is dominant. The semiannual variation can be seen in the variation of D20 (Fig. 3b) and OHC (Fig. 3c) as well as SST. But the variations of SST and D20/OHC are out of phase. Fig. 4 shows averaged seasonal variation of SST, D20 and OHC at the equator 45°E in the Indian Ocean. D20 and OHC's higher period in March/April goes one month ahead of SST's higher period in April/May, and D20 and OHC's lower period in August/September goes two months ahead of SST's lower period in June/July. Higher SST in November/December and lower SST in January/February have one ore two months lag to D20/OHC.

Westerly which appear around 80°E during the transition period from SW monsoon to NE monsoon is not found off the Somalia Peninsula east of 60°E, so that the variation of wind is annual. But Fig. 3b suggests semiannual variations of ocean in the western tropical Indian Ocean. Westerly doesn't correspond with surface and subsurface temperature.

4. Discussions

It is difficult to investigate the ocean structure of the Indian Ocean, because of less observed data there than in the Pacific and the Atlantic. The output derived from the ODAS revealed it to be available to analyze the variation of the mean ocean structure in the tropical Indian Ocean. More *in situ* data such as the XBT data by "Kashimasan-Maru" and "Delmas Tourville" is needed for understanding the ocean structure in the Indian Ocean. It is necessary to

investigate the long-term variations of the mean ocean structure in not only the equatorial region but also other regions in the Indian Ocean and to explain the relation to El Niño.

5. References

1) Barnett, T. P, 1983: Interaction of the Monsoon and Pacific Trade Wind System at Interannual Time Scales. Part I: The equatorial Zone, *Mon. Weather Rev.*, **111**, 756-773.

2) Nicholls, N., 1984: The Southern Oscillation and Indonesian Sea Surface Temperature, *Mon. Weather Rev.*, **112**, 424-432.

3) Bryan, K., 1969: A Numerical Method for the Study of the Circulation of the World Ocean, *J. Comput. Phys.*, **4**, 347-376.

4) Yoshikawa, I., M. Kimoto and M. Ishii, 1995: Ocean Data Assimilation System for Climate Monitoring at JMA, WMO/TD-No. 651, volume II, 561-564.

5) Wyrtki, K., 1973: An Equatorial Jet in the Indian Ocean. *Science*,**181**, 262-264.

6. Publications

None

7. International Cooperation

Japan Meteorological Agency (JMA) and Organization of Research on Science and Technology Outside Marine (ORSTOM, Brest) have entrusted cooperatively XBT observation and its report to a cargo carrier recruited.

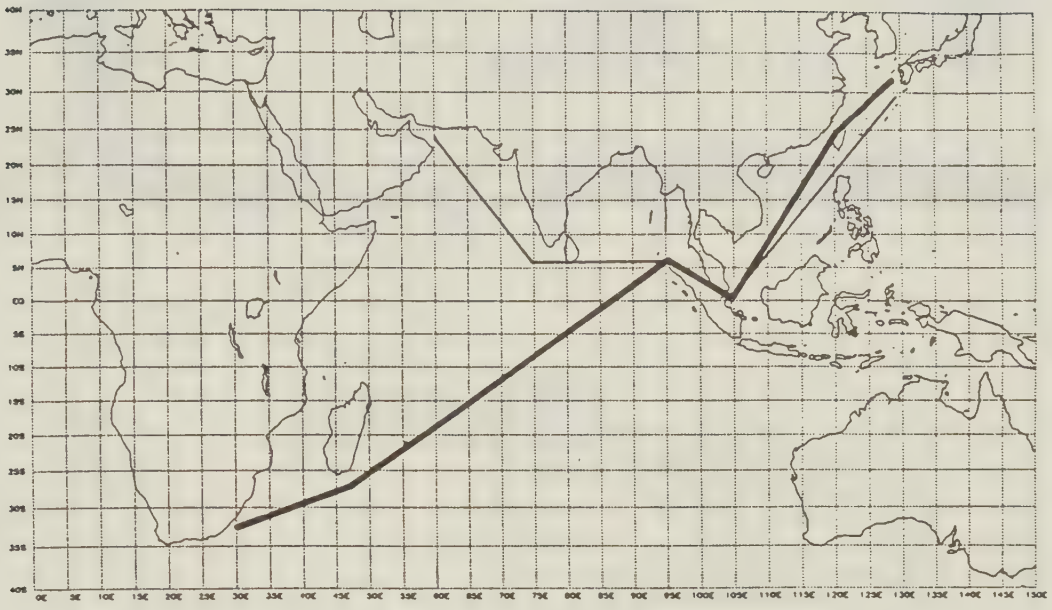

図１　委託商船の航路。細線は「鹿島山丸」、太線は「Delmas Tourville 」。

Fig. 1 Cruise tracks of "Kashimasan-Maru" (thin line) and "Delmas Tourville" (thick line).

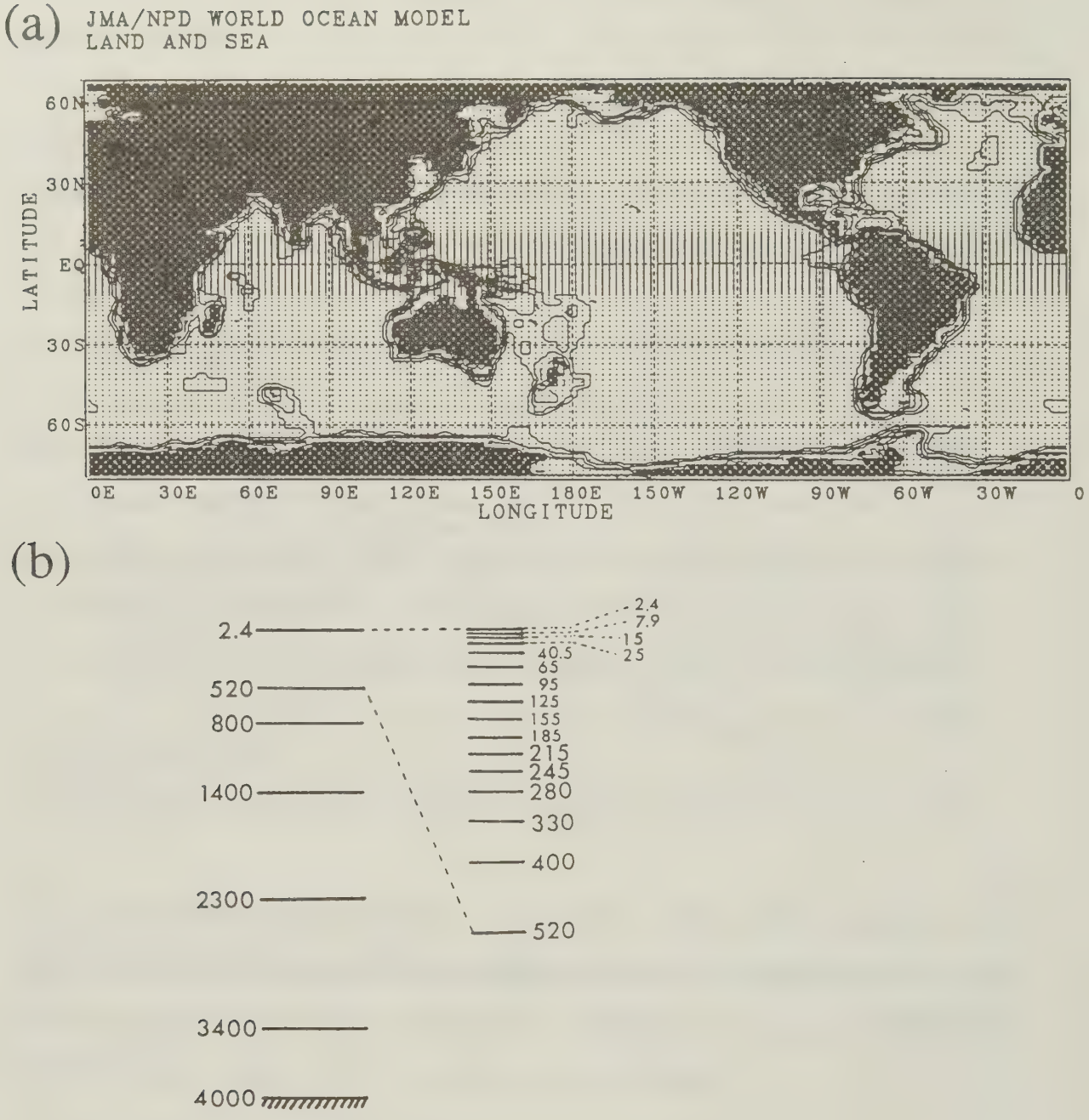

図2　海洋大循環モデルの地形及び格子点

(a) 陸域をタイルパターンで、水平の格子点分布をドットで示す。等深線は1000m間隔で最深4000m。

(b) 鉛直の層のとりかたを示す。単位はメートル。

Fig. 2 Topography and grid spacing of the ocean general circulation model

(a) Each grid point is shown as a dot. Depth contours of 1000, 2000, 3000 and 4000 m are shown.

(b) Vertical layers (m)

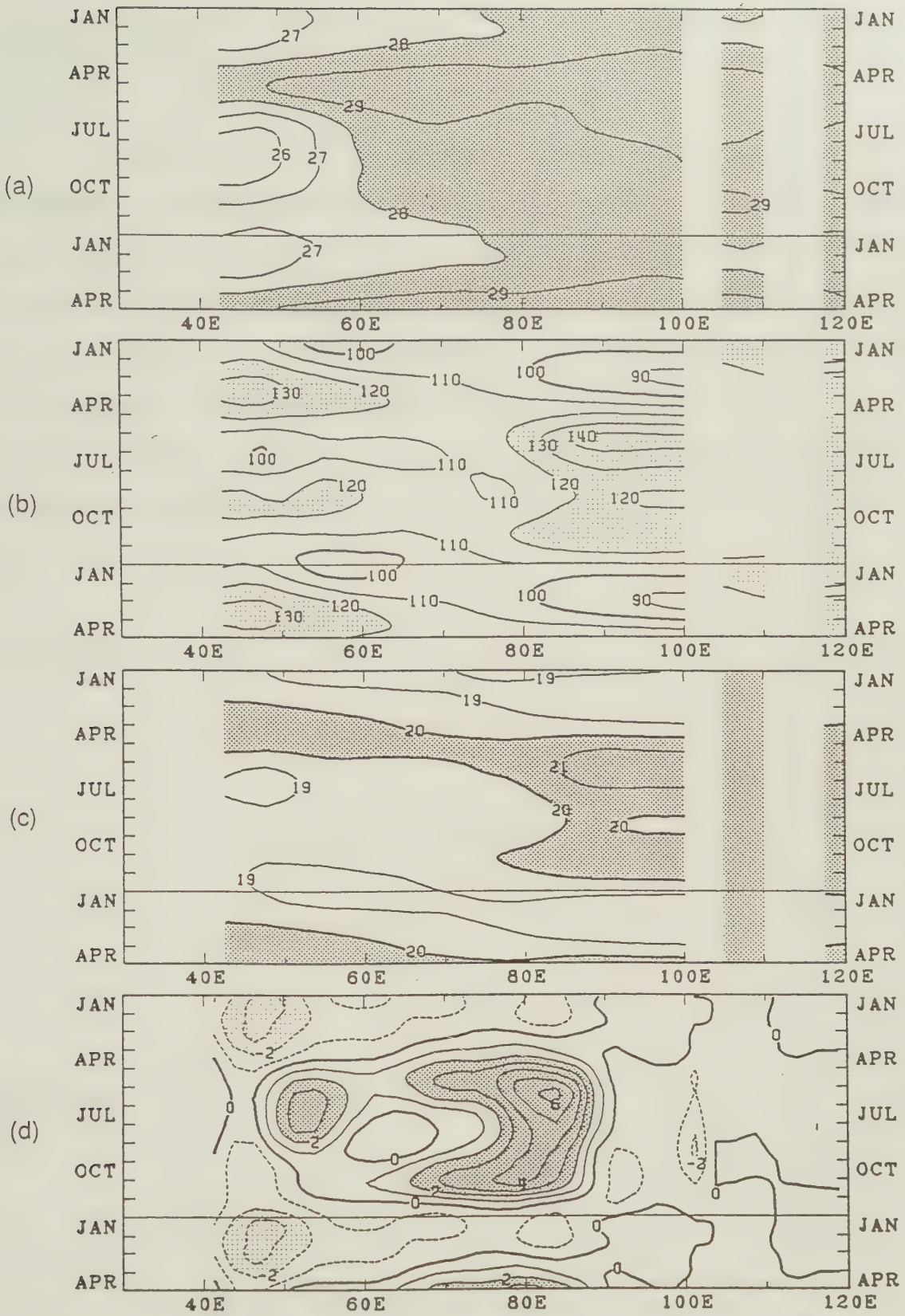

図3　インド洋の赤道に沿った(a)海面水温(℃),(b)20℃深度(m),(c)貯熱量(℃)および(d)風の応力の東西成分(0.01N/m^2)の季節変動の平均値（ODASによる1987～1994年の8年間平均値）

Fig. 3 Averaged seasonal variation of (a) Sea Surface Temperature (°C), (b) Depth of the 20°C isotherm (m), (c) Ocean Heat Content (°C) and (d) Surface zonal wind stress (0.01N/m^2) along the equator in the Indian Ocean. Data are derived from ODAS for the period from 1987 to 1994. Note duplication from January to April in each figure.

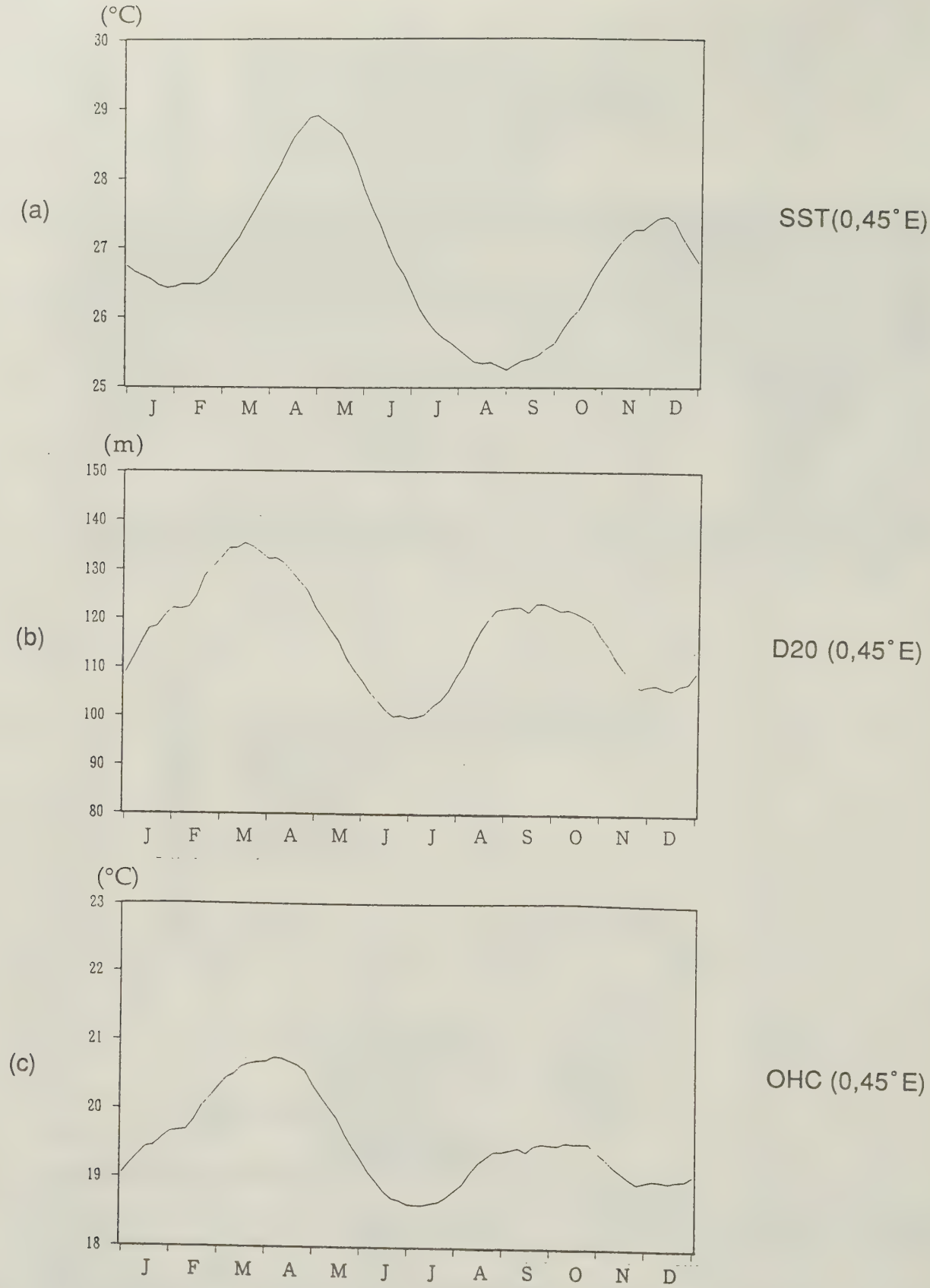

図4　インド洋の西部赤道上の東経45度における(a)海面水温(℃)，(b)20℃深度(m)，および(c)貯熱量(℃)の季節変動の平均値（ＯＤＡＳによる1987～1994年の８年間平均値）
Fig.4 Averaged seasonal variation of (a) Sea Surface Temperature (°C), (b) Depth of the 20°C isotherm (m) and (c) Ocean Heat Content (°C) at the equator 45°E in the Indian Ocean. Data are derived from ODAS for the period from 1987 to 1994.

アブストラクト

本研究によって1990年よりインド洋を航行する「鹿島山丸」と「Delmas Tourville」の２隻の篤志船によって表層水温が観測されてきた。これらの観測データと世界気象機関(WMO)の全球気象通信網(GTS)を通じて取得した他の商船などによる観測データを併せ、気象庁で開発した「海洋データ同化システム」を用いてインド洋の赤道上の海洋構造の変化を解析した。その結果、インド洋東部赤道域では、海面水温には顕著な季節変化は見られないが、表層の構造には年に２回の明瞭な暖水蓄積が見られ、南西／北東のモンスーンの移行期に見られる西風と良く対応している。一方、インド洋西部海域では、海面水温にも表層の構造にも半年周期の変動が見られ、20℃深度や表層の貯熱量の変化の位相が、海面水温より１～２か月先行している。

I. Observation and analysis on the process of the atmosphere-ocean-land interactions

2 Observation and analysis on the process over the ocean

(2) Observation on Oceanic Currents with Drifting Buoys

Hydrographic Department
Maritime Safety Agency
Yutaka Michida and Hideki Kinoshita

(Abstract)

The purpose of this study is to elucidate the ocean circulation including its temporal (annual, interannual) and spatial variation in the Indian Ocean, particularly in the tropical region. For this purpose, Lagrangian observation of the surface currents has been carried out with satellite-tracked ARGOS drifters since 1989. The results of the investigation for the fiscal 1994 are described in this paper.

Six drifters were deployed in the equatorial area east of Sumatera Island in November 1994 under cooperation with R/V 'Kagoshima-maru' of Kagoshima University. It was anticipated that these drifters would visualize the surface current of the region where the coverage of the drifter trajectories within JEXAM programme had not been dense enough to see the current system. Their tracks are described together with those of the former drifters.

Surface currents in the Indo-Pacific throughflow area flowing from the Indian Ocean toward the Indonesian Seas in boreal winter, to the opposite direction to other seasons, are traced with the drifters deployed in the region south of the Indonesian Archipelago in 1993. In particular, northward flows in Lombok Strait in boreal winter that has been presented by a numerical model is clearly displayed by a drifter which drifted from the Indian Ocean to Flores Sea through Lombok Strait in December 1993.

1. Objectives

Interannual variation of the Asian Monsoon, which has big influence upon the climatical variabilities in the region of south east Asia, may play an important role in the global climate change through the atmospheric general circulation. Some of previous studies have suggested that the Aisan Monsoon would cause changes in the oceanographic condition in the western tropical Pacific and should have close relationship with ENSO events. As a successful example of oceanographic research related to climate change, TOGA(Tropical Ocean and Global Atmosphere), whose major field was the tropical Pacific, provided so much knowledge on ENSO mechanism. In the Indian Ocean, on the other hand, there have been very few oceanographic data available in comparison with other oceans.

Thirty-seven surface drifters were deployed by the end of 1994 in the Indian Ocean and tracked with ARGOS system within this research programme, Japanese EXperiment on Asian Monsoon (JEXAM) to illustrate the surface current system of the tropical Indian Ocean and the Seas adjacent to Indonesia, which is very interesting issue for oceanographers from the view points of, for examples, mass/heat/salt exchange between the Pacific Ocean and the Indian Ocean, or air-sea interactions there.

A schematic representation of the Indian Ocean currents and their seasonal changes has been proposed by *Molinari et al.*[1990], who have presented a monthly climatology of surface

currents by analysing historical drifter data. To investigate thier results and to complement thier study, trajectories of the drifters which are uniformly designed according to the recommendation of WOCE/TOGA SVP (Surface Velocity Programme) have been analysed in this study. The results of analysis for the drifters deployed in 1993 and 1994 are mainly described in this paper.

2. Methods

Six to ten drifters have been deployed in the Indian Ocean every year since 1990, the commencement of JEXAM programme. The drifters are designed according to the WOCE/TOGA SVP standard. A holey sock drogue of 8.6m in length whose drag center is at 15m below the sea surface is attached to the surface float that contains a processing unit for sensor data (sea surface temperature, on/off of the drogue and battery voltage) and a transmitter for ARGOS system. There is also a small subsurface float, which would reduce the tension of the tether between the surface float and the drogue (cf. *Michida and Ishii*, 1993).

Five drifters were deployed south off Java Island and one in Makassar Strait in December 1993, to see the currents in the area of Indo-Pacific throughflow. Six drifters were deployed in the equatorial region east of Sumatera Island in October-November 1994, to cover the area where very few buoys have been tracked in JEXAM programme. All the above drifters were released from a training vessel '*Kagoshima-maru*' of Kagoshima University by officers onboard.

3. Results

3-1 Drifter Tracks in 1994

Figure 1 shows the trajectories of the six drifters deployed in the central tropics of the Indian Ocean in 1994. Five of them were released along 90E line, and one was approximately 2 degrees east away from the line.

Two released at the points north of the equator generally drifted eastward; one seemed to be driven ashore near the northernmost of Sumatera around December 5, 1994, and the other also seemed to get ashore at the west coast of Sumatera during the end of December to early January 1995.

One released at the point near 2.5S drifted west or southwestward for a while after deployment, turned east gradually in the middle of November, then drifted eastward along 5S. It further drifted southeast and was still at the sea south of Java Island at the end of March 1995.

Three released at the points south of 3S drifted westward in the South Equatorial Current until January 1995. One of them reached 80E and turned east around January 13, 1995, the second one reached 74E and turned east around January 16, 1995, and the third one reached 77E and turned east around January 15, 1995. They visualized eastward flow of the Equatorial Counter Current, which appeared in the south of the equator during the boreal winter. The turning occured almost in the same period, when the wind field should have changed. The observational fact that they drifted rather northeastward after the turning would support the description that the Equatorial Counter Current has a northward component east of about 80E (*Molinari et al.*,1990). All the three drifters were still alive and drifting eastward as of the end of March 1995.

3-2 Currents in the area of Indo-Pacific throughflow

Five drifters were deployed south of Java Island in 1993, and four of them were conveyed by the ocean current toward Indonesian Seas from the Indian Ocean. This result should be of interest to oceanographers as an important observational fact that would tell us the seasonal change of the surface current in the region (*Michida and Yoritaka*, 1994a,b). Tracks of the drifters deployed in 1993 are given in Figure 2, and those deployed in 1991 are also shown in Figure 3, to see the seasonal difference of the current. The drifters for 1991 were released in boreal spring (May) and drifted west or southwest in boreal summer, except for one that was driven ashore at the south coast of Java in August or September. The drifters for 1993, on the other hand, released in boreal autumn (November) were drifted east or northeast, though the release points were close to those for 1991.

Masumoto and Yamagata [1993] have carried out numerical experiments on the mechanism of the seasonal variations of the Indo-pacific throughflow and made investigation into the current structure in the seas adjacent to Indonesia. They mainly discuss about the seasonal change of the volume transport in some channels. We compare the drifter tracks with the numerically simulated current by *Masumoto and Yamagata* [1993] to examine the current field.

The annual cycle of numerically simulated surface current field at a depth of 5m presented by *Masumoto and Yamagata* [1993] is shown in Figure 4. Seasonal contrast in the surface current can be easily seen in Figure 4. In the area where our drifters were tracked, there can be also found big seasonal differences. In Lombok Strait, in particular, there are northward flows simulated in February, while stronger southward flows are simulated in other seasons. It is pointed out for the currents west of 110E that the currents are generally weak in February though the current directions are not very different from those in other seasons. As for the currents east of 110E, it is suggested as a remarkable seasonal change that they have northward components in February and southward in other seasons.

A time series of daily drifting velocity of a buoy which drifted through Lombok Strait is shown in Figure 5. The drifter was at about 150km south of Java Island in early December, 1993, after deployment in November. Then it was drifted along the south coast of Java with a speed of 50-90 cm/s in a eastward current. The northward velocity in Lombok Strait was over 130 cm/s as seen in Figure 5, showing a strong current in the strait. After passing the strait, it was further drifted eastward in Flores Sea and Banda Sea with a speed of about 50cm/s, sometimes over 100cm/s, from January to March, 1994.

4. Discussions

With comparison between the surface current system in the area of Indo-Pacific throughflow derived from drifters experiments and that numerically simulated by *Masumoto and Yamagata*[1993], we would conclude that the numerical model has well simulated the surface currents there including seasonal variations, as far as in qualitative words. In some quantitative comparison, we could also suggest that the stronger eastward flows in Java Sea and Flores Sea appeared in February in the numerical model (Figure 4) should agree with the trajectories of a drifter which passed Lombok Strait northward and had a eastward drifting speed of about 50cm/s to 100cm/s.

To examine the sea level difference between the Pacific and the Indian Ocean which will drive the currents in the Indonesian Seas, the mean sea levels observed by a satellite altimeter on TOPEX/POSEIDON are calculated for the area shown in Figure 6, two box areas of ten-degrees square are selected as representatives for both oceans. After the standard procedures of correction for TOPEX/POSEIDON data, for examples, correction for atmosphere, ionosphere, earth/ocean tides and so on, the time series of averaged sea level for each box

area and difference between the two areas are obtained as shown in Figure 7. As a good assumption, we do not take the spatial fluctuation of the geoid into account in the above calculation, because the fluctuations of the ground tracks of the satellite are small enough. And, of cource, the temporal fluctuation of the geoid should be negligible in such an analysis for 1 or 2 years. It is suggested from Figure 7 that the sea level in the Pacific Ocean was lower ralative to the Indian during the period when the drifter experiment has been carried out in 1993 to 1994, although a trend of sea level rising can be observed in the series for both oceans for which the reason is not clear. The lower sea level in the Pacific in boreal winter may be a coincident phenomenon with the reversal in the surface current in the Indonesian Seas. *Masumoto and Yamagata* [1993] have numerically shown that the depth-integrated volume transport through Lombok Strait always flows out from the Pacific but the flow in the surface layer changes its direction by seasons. The reversal of the surface current in the region, which will transport much heat because of its high temperature, should affect not little on the inter-ocean heat transport, even if the volume transport always comes from the Pacific toward the Indian Ocean.

5. References

Masumoto, Y. and T. Yamagata, Simulated seasonal circulation in the Indonesian seas, *J. Geophys. Res.*, 98, 12501-12509, 1993.

Molinari, R. L., D. Olson and G. Reverdin, Surface current distributions in the tropical Indian Ocean derived from compilations of surface buoy trajectories, *J. Geophys. Res.*, 95, 7217-7238, 1990.

Michida, Y. and H. Ishii, Observation of ocean circulation with surface drifters, *Kaiyo monthly*, extra 4 ,115-122,1993 (in Japanese).

Michida, Y. and H. Yoritaka, Annual report of JEXAM 1993, 33-39, 1994a(in Japanese).

Michida, Y. and H. Yoritaka, Surface current field in the tropical Indian Ocean and the seas adjacent to Indonesia observed with surface drifters, *Proc. IOC/WESTPAC 3rd International Scientific Symposium*, 1994b.

6. Publications

①Scientific Journals

2) International

Y. Michida and H. Yoritaka, Surface currents in the area of Indo-Pacific throughflow and tropical Indian Ocean observed with surface drifters, *J. Geophys. Res.* (in preparation).

③Oral Presentations

Y. Michida and H. Yoritaka, Surface current observation in the Indian Ocean with drifters, *1994 Fall meeting of Oceanogr. Society of Japan*, Matsuyama, Oct. 1994, (in Japanese).

Y. Michida, Drifter tracks in the Indian Ocean, *WOCE/TOGA SVP 7th session*, La Jolla, Nov. 1994.

Y. Michida and H. Yoritaka, Surface current field in the tropical Indian Ocean and the seas adjacent to Indonesia observed with surface drifters, *IOC/WESTPAC 3rd International Scientific Symposium*, Bali, Nov. 1994.

Y. Michida, Drifter experiment for the throughflow, *ASEAN-Australia Economic Co-operation Program Major International Symposium*, Lombok, Jun. 1995 (planned).

7. International Cooperation

The United States has a plan to deploy many drifters in the Indian Ocean within WOCE/TOGA Surface Velocity Programme in 1995 and 1996. It is strongly required for us to provide our experiences and knowledge acquired in JEXAM Programme to the international scientific communities and to keep close contact and relationship with the drifter group in US in exchanging information on each other's deployments or cooperative deployment.

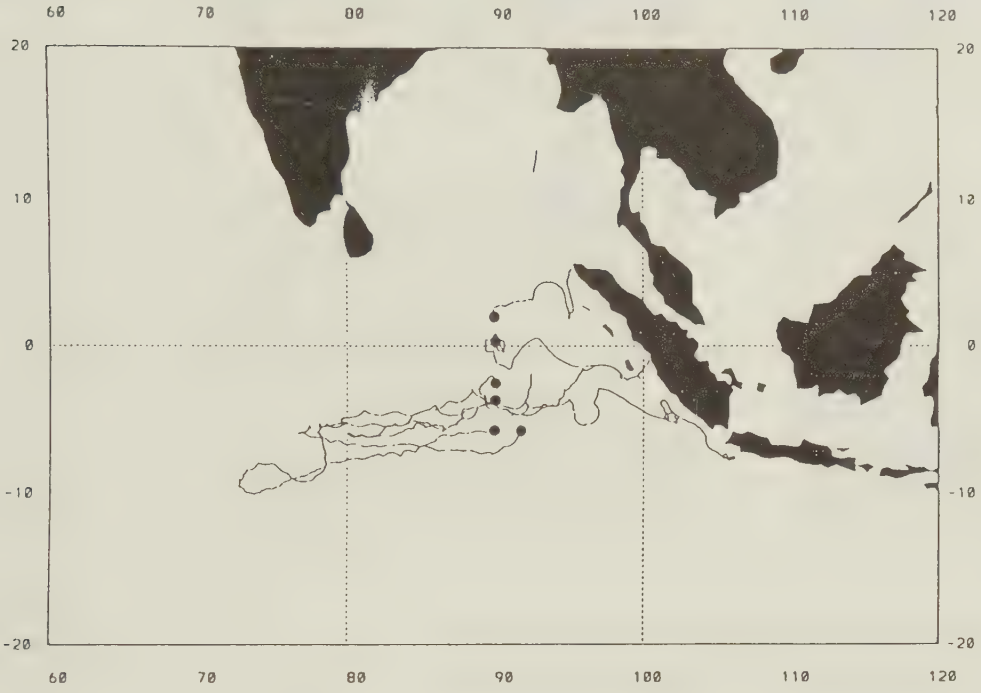

Figure 1. Trajectories of six drifters deployed in October-November 1994. Solid circles indicate the location of deployment.

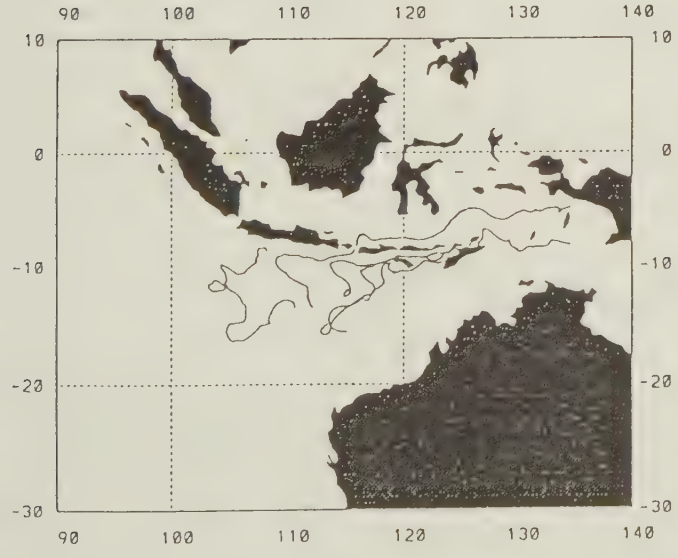

Figure 2. Trajectories of the drifters deployed in the area south of Java Island in November 1993.

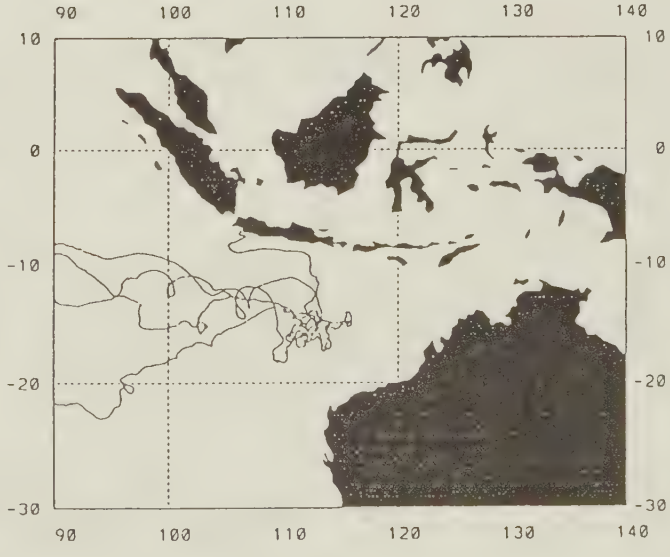

Figure 3. Trajectories of the drifters deployed in the area south of Java in May 1991.

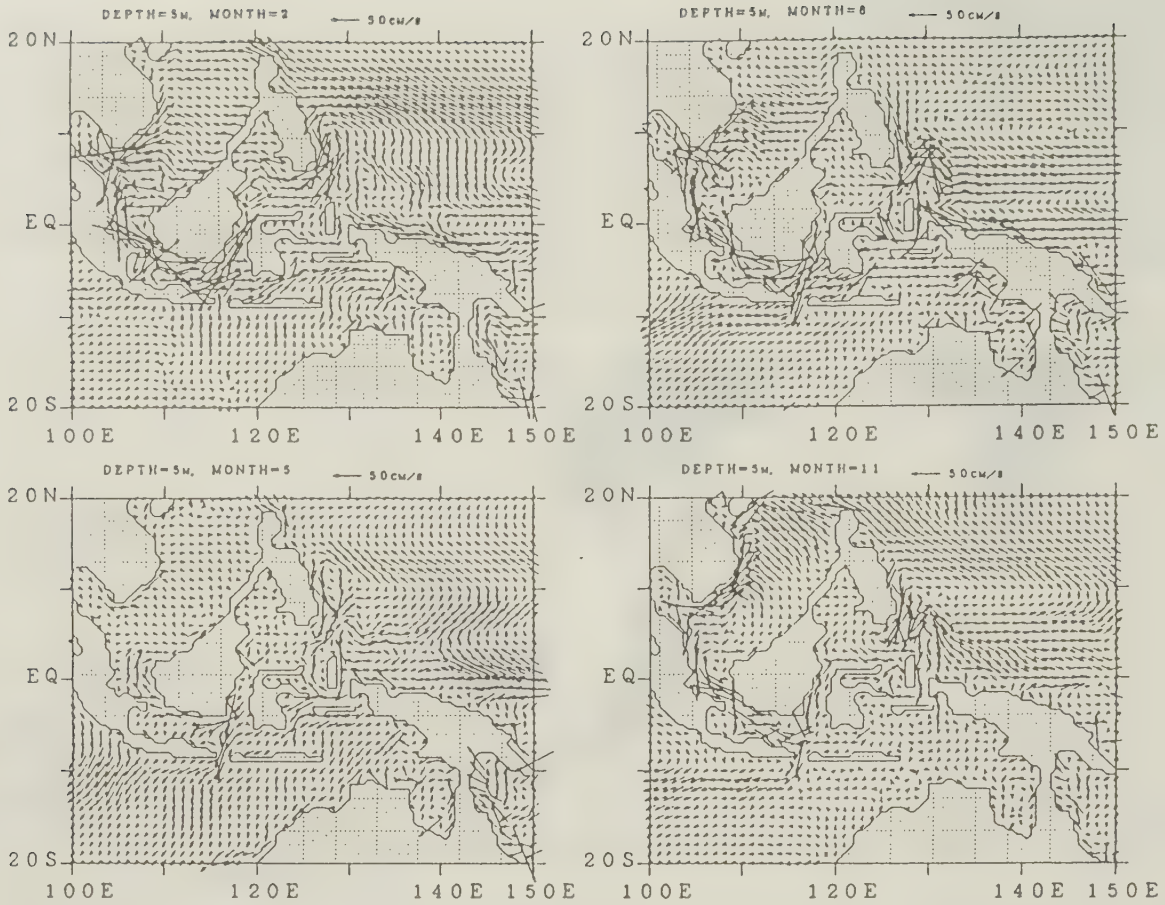

Figure 4. Annual cycle of numerically simulated surface current field at a depth of 5m in the Indonesian Seas (after Masumoto and Yamagata[1993]).

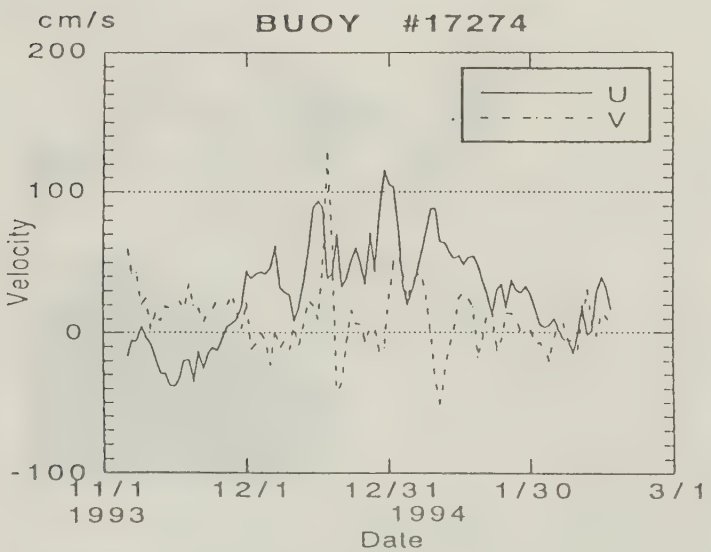

Figure 5. Time series of daily drifting velocities for drifter #17274, which drifted into Flores Sea north through Lombok Strait.

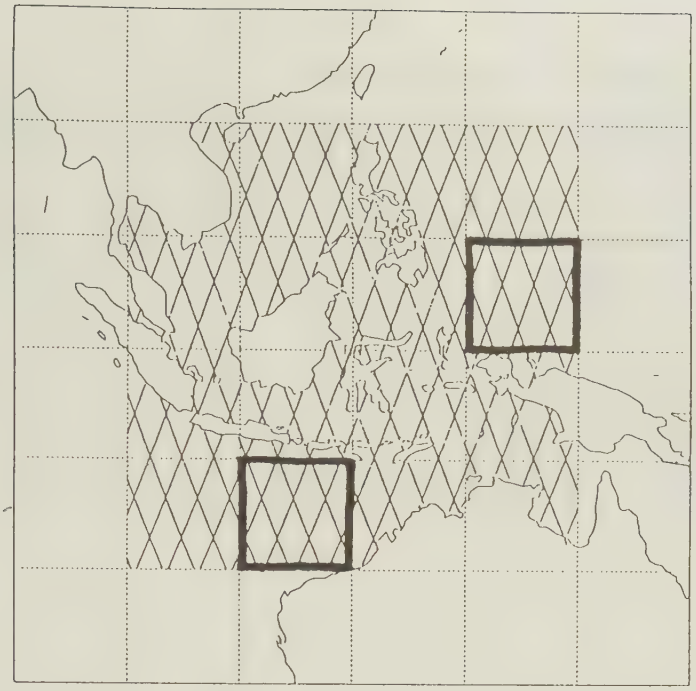

Figure 6. Available data points for TOPEX/POSEIDON satellite altimeter for a cycle in the area of Indonesian Seas. Solid squares indicate two ten-degrees boxes for which mean sea levels are calculated.

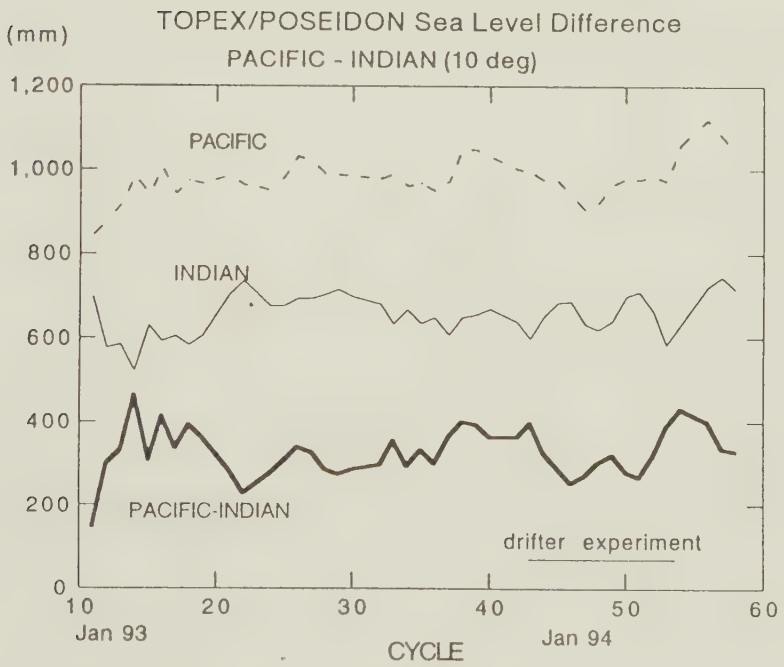

Figure 7. Time series of averaged sea level for each box area shown in Figure 6 and difference between the two areas, i.e. between the Pacific and Indian Ocean, calculated from TOPEX/POSEIDON data.

（要旨）
アジアモンスーンの変動に大きな影響を及ぼすインド洋、特にインド洋熱帯域の海流循環の実態とその時間空間的な変動を解明するため、海上保安庁水路部は「アジアモンスーン機構に関する研究（JEXAM）」の一環として、1989年以来表面漂流ブイを放流して海流の追跡観測を行っている。ここでは、平成６年度の研究成果について述べる。
1994年11月に、鹿児島大学水産学部の「かごしま丸」の協力を得て、スマトラ島当方沖のインド洋熱帯域に表面漂流ブイを６個放流した。従来この海域はJEXAMで放流したブイがあまり流れておらず海流像の把握が進んでいないが、今回のブイによって当該海域の海流の可視化が進み、南緯5度付近を東に流れる赤道反流が捉えられた。
インドネシア通過流の海域の表層の流れは、北半球の冬季には他の季節と異なり、インド洋から太平洋側に向かって流れることが、1993年にジャワ島南方で放流したブイによって確認された。特に、ロンボク海峡の強い北向きの流れが北半球の冬季に現われることが数値実験によって示されていたが、この流れも漂流ブイによって存在が確認された。

I. Study on Air-Sea-Land Interactions and their Long Term Variations
2. Observation in the Indian Ocean
(3) Standardization of Oceanic Data and Promotion of Exchange of Oceanic Data and Information

Japan Oceanographic Data Center
Hydrographic Department
Maritime Safety Agency
Taiji Imoto, Norio Baba

(Abstract) The purpose of study is to provide a sufficient data set and timely information for promoting the JEXAM study. In order to suffice this goal, sub-themes have been established; data standardization and quality controlof JEXAM data; collection of existing data from other nations; establishment of international on-line network system for data and information exchange.

The JODC Online Information and Data Exchange Service (JOIDES) was added with information exchange system for NODCs, and JODC collected the information of oceanographic data resources for JEXAM in 1994.

1. Purpose of study

The purpose of this study is to provide researchers engaged in the "Japanese Experiment on Asian Monsoon" (hereinafter referred to as JEXAM) and research study on the Indian Ocean with the best available data set as well as information on research in order to be carried out those studies smoothly and effectively.

To achieve this purpose, oceanic data such as water temperature obtained through the "Observation in the Indian Ocean", one of the research subjects of JEXAM, will be standardized so that researchers can share their data with each other smoothly. In addition, existing oceanic data and information will be collected in order to provide full basic data for each study of JEXAM. Efforts will be also made to improve the accuracy of quality control of data by enhancing the reliability of statistics based on the obtained data.

In addition to such data management activity, a data base will be built, which permits on-line input/output or retrieval of information to check the state of data management or marine research programs with the view of speeding up distribution of information. Furthermore, a data information network system will be established between national oceanographic centers of various countries and JODC to allow it to easily obtain cooperation from various countries for acquisition of data and information while another system will be established to allow Japan and other countries to share consistent oceanic data and information. Those systems will contribute to easy, fast and smooth use of oceanic data for JEXAM and to effective use of such data for various projects related to global environment.

2. Methods for study

(1) Support the system for fast and smooth distribution of data in this project through on-line computer network system, JOIDES.

(2) Standardize obtained data (water temperatures, ocean currents, drifting buoys), and building a data base of such data.

(3) Collect information and data on the marine research in the Indian Ocean.

3. Results of study

(1) On-line computer network system JOIDES

The system for fast and smooth distribution of information for this project is supported by the on-line computer network system JOIDES.

(2) Building a data base of observation data on the Japanese Experiment on Asian Monsoon

JODC received surface water temperature data (XBT, DBT) observed at 780 points from March 1992 to May 1994 through "Observation and Analytical Study on Various Processes in the Indian Ocean" of JEXAM from Far Seas Fisheries Research Laboratory via Internet, an international computer network.

Observation points for the received data are shown in Fig. 1.

(3) Data related to the sea area covered by the project

① As for a set of data on the Indian Ocean, JODC received a set of seven CD-ROMs containing observation data obtained from 1985 to 1990 by the Tropical Ocean Global Atmosphere Program (TOGA), an international joint research project, from the Jet Propulsion Laboratory ; NASA, US in August 1994. Data contained in this data set is shown in Table 1.

② JODC received "The World Ocean Atlas 1994", a set of nine CD-ROMs, from the World Data Center A in December, 1994. This data set is the revised version of data set, what is called Levitus data set, and has been processed by the data the World Data Center received until 1993 spring.

This data set also contains the data already subjected to quality control, in addition to statistics of global temperatures, salinity and nutrients in one-degree mesh. The results of statistical processing contained and the number of observation points are shown in Table 3.

4. Summary

(1) Recently, there has been a sharp increase in use of Internet among researchers in Japan, and interconnection from Internet to JOIDES as well as access to data bases owned by JODC from JOIDES is hoped for. Thus, it is necessary to review the possibility of interconnecting Internet with JOIDES and of accessing data bases contained in JODC from JOIDES.

(2) JODC is planning to make a data set in CD-ROMs for the data obtained in the first half period of this project in 1995. Although JODC plans to include mainly oceanic data in the set, it is possible to contain data other than oceanic data as there is sufficient capacity. Thus, it is necessary to review the composition of the data set through coordination with the agencies concerned.

（要　約）

本研究は、「アジアモンスーン機構に関する研究」（以降JEXAM）及びインド洋に関する調査研究の円滑かつ効果的な実施を図るため、当該研究に携わる研究者に対し、利用可能な最良のデータセット及び調査に係る情報を提供するためのものである。
この目的を達成するために、JEXAMの一研究項目である「海洋に関する観測研究」において取得される水温等の海洋データの標準化を行い、研究者間のデータ相互利用の円滑化を図った。また、JEXAMの各研究における基礎資料の充実を図るため、インド洋及び周辺海域における既存の海洋データ及び関連情報の収集を行い、さらに、得られたデータにより統計値の信頼度を増すことによってデータ品質管理の精度向上を図った。

一方、これらのデータ管理活動のほかに、情報流通の迅速化を図るため、データの管理状況及び海洋調査計画等に関する情報のオンライン入出力・検索が可能なデータベースを構築した。さらに、データ・情報提供に関する各国の協力を得やすくするため、各国国立海洋データセンター等とJODCとの間に海洋データ・情報交換のためのデータ情報ネットワークシステムを構築し、国内から国外まで一貫した海洋データ・情報交換のためのシステムを確立し、JEXAMにおける海洋データの迅速・容易かつ円滑な利用、さらに、その他の地球環境関係の各種プロジェクトでの有効利用に寄与している。

Fig. 1　Observation points for data received from Far Seas Fisheries Research Laboratory

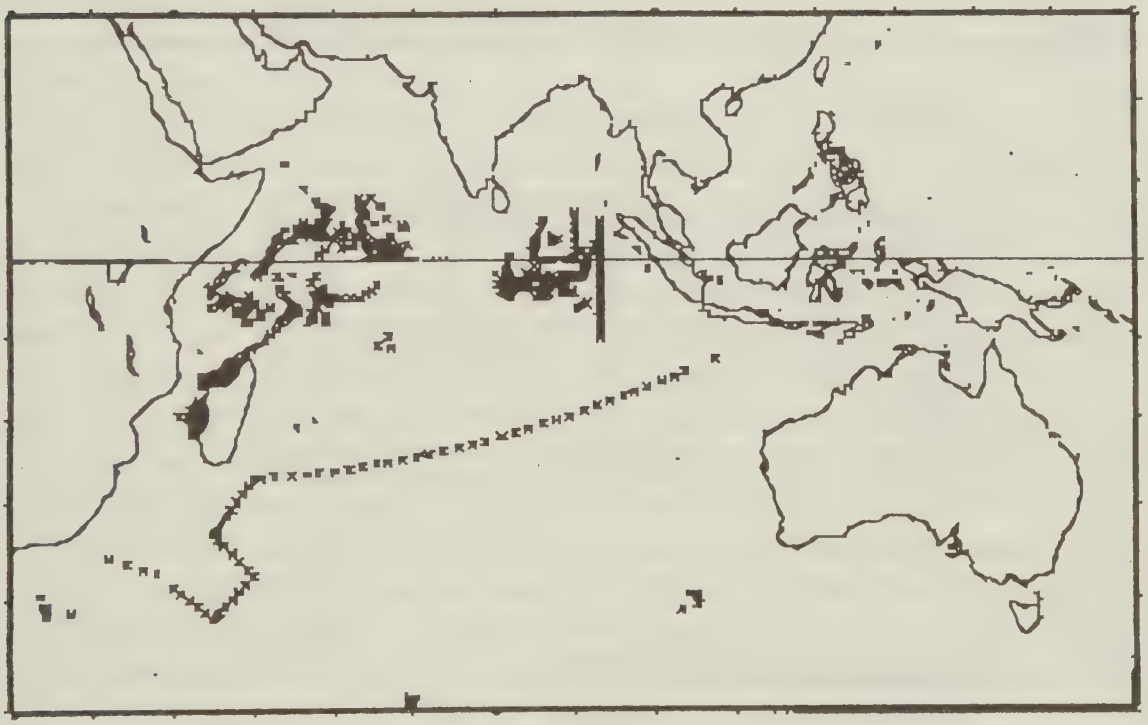

Table 1 Data in TOGA CD-ROM data set

Data Set Name	Providing Institution	Format	Contents
AOML	NOAA Atlantic Oceanographic and Meteorological Laboratory	ASCII	Drifting Buoy data
CAC	NOAA National Meteorological Center (NMC)	ASCII	Sea surface temperature
ECMWF	European Center for Mediumrange Weather Forecasts	GRIB	Numerical model results
FSU	Florida State University	ASCII	Wind pseudo-stress
GEOSAT	NOAA National Ocean Service	ASCII	Sea-surface height
GPCP	NOAA NMC	ASCII	Precipitation estimates
IFREMER	TOGA Subsurface Data Center	ASCII	Subsurface data
ISCCP	NASA Climate Data System	GRIB	Cloud products
LODYC	Universite Pierre et Marie Curie	ASCII	Atlantic model data
MEDS	Marine Environmental Data Service, Canada	ASCII	Drifting buoy
NCAR	National Center for Atmospheric Research	ASCII	CORDA climatologies
ORSTOM	Center ORSTOM de Brest	ASCII	Wind Pseudo-stress
PMEL	NOAA Pacific Marine Environmental Laboratory	ASCII	Moored current and temperature data
UHAWAII	University of Hawaii	ASCII	Sea level
UKMO	United Kingdom Meteorological Office	ASCII	Surface data

Table 2 Types of statistical processing of "The World Ocean Atlas 1994"

PARAMETER	ANUNAL	SEASON	MONTH
Temperature	*	*	*
Salinity	*	*	*
Dissolved oxygen	*	*	
Apparent Oxygen Utilization	*	*	
Oxygen Saturation	*	*	
Phosphate	*		
Nitrate	*		
Silicate	*		

Table 3 "The World Ocean Atlas 1994" data already subjected to quality control

Parameter	Number of Profiles
Temperature	4,553,426
Salinity	1,254,771
Oxygen	367,635
Phosphate	184,153
Silicate	110,413
Nitrate	75,403

I. Observation and analysis on the process of the atmosphere–ocean–land interactions

3. Observation and analysis on the process over the land

(1) Observation on Hydrology over the Tibetan Plateau and Himalayas

Shinjo Branch of Snow and Ice Studies,
National Research Institute for Earth Science
and Disaster Prevention,
Science and Technology Agency
Takeshi Sato

(Abstract)

In this study, three automatic observation sites of snow weight (water equivalent of snow), ground temperature, and frozen ground depth were established in the Tibetan Plateau. Based on their long term records, variations of snow cover and frozen ground together with and their relation to the Asian Monsoon will be analyzed.

In July, 1993, three sets of snow weight and frozen ground depth meters were set at Lhasa, Rikeze, and Nagqu, and continuous measurements started. These works were done in cooperation with Chinese scientists. At the same time, Meteorological Research Institute started micrometeorological observations at these three sites. The first data collection was carried out in July, 1994. The frozen ground depth data at Lhasa and the ground temperature data at Nagqu were missed due to trouble of the instruments.

Analyzing the records from July, 1993 to July, 1994, following results were obtained : The frozen ground depth meter at Nagqu recorded reasonable diurnal variations of freezing and melting of the ground, and seasonal variations of frozen ground. The maximum frozen ground depth was 158cm, which appeared from the end of Feb. to the beginning of Mar., 1994. Analysis of the growth rate of frozen ground at Nagqu showed that the frozen ground developed in proportion to the square root of the accumulated freezing index and the proportional constant was about 3. Since the snow weight meter is not so sensitive, it detected only the snow cover lasting for several days at Nagqu twice in Jan., 1994. However, it did not detect the snow cover lasting for a few days at Nagqu. Also, the snow cover at Lhasa and Rikeze was not detected. The snow weight values observed at Nagqu were 9kg/m^2 and 21kg/m^2. Assuming the density of accumulated snow is 100kg/m^3, the maximum depth of snow cover are estimated to be about 0.1m and 0.2m, respectively.

1. Objectives

Snow cover and frozen ground in the Tibetan Plateau have great influence not only on the Asian Monsoon activity but also on the global climate system. In order to understand the mechanism of the Asian Monsoon, seasonal and annual variations of the snow cover and frozen ground should be clarified and the relationship between them and the Asian Monsoon activity should be studied. Though areal and quantitative investigation of snow cover and frozen ground is required, present remote sensing technology has not yet made such measurements possible. In this study, automatic observation of accumulated snow and

frozen ground are continued for several years at three sites in the Tibetan Plateau. The data will be analyzed to clarify the relationship between the snow cover and frozen ground conditions and the Asian Monsoon.

2. Methods

The snow weight meter [1] to measure the weight (water equivalent) of accumulated snow is almost the same as that commonly used in Japan [2] . Four metal wafer units are used to support the accumulated snow, in which unti-frozen liquid is filled. The accumulated snow on the metal wefer units leads to the change of inner pressure within the units. A pressure sensor detects this pressure change, which is processed electrically and converted to the output voltage by a control unit. The ground temperature just below the metal wafer unit is measured by Pt resistance thermometer. These data are stored in a data logger every hour.

The frozen ground depth meter consists of a cylindrical sensor unit, 225cm long and 1.6cm in diameter, and a processing and recording circuit [3] . The sensor unit has 104 detection terminals separated 2cm from each other and one common terminal on the surface. The sensor unit is in a Silicon rubber tube and water is filled between the sensor unit and the tube. The thickness of the water around the sensor unit is 1mm. The resistance between the detection and common terminals changes largely according to the state of the water (water/ice), which is scanned and frozen portion is distinguished. The scanning is made every two hours and results are stored in an EPROM.

The training of operations of the instruments and data collection was carried out for Chinese scientists in June, 1993 at Chengdu Meteorological Institute. After that, the instruments were set at three sites (Lhasa, Rikeze, and Nagqu) in the Tibetan Plateau and continuous measurements started in July, 1993 [1] . At every site, the instruments were installed in the precinct of the meteorological observatory. Meteorological Research Institute (MRI) installed the instruments for the micrometeorological observations at the same sites. Visual inspection of the instruments is carried out every month by the staff of the meteorological observatory. Data collection is made every year using personal computer.

3. Results

3.1. Observation in 1993/94 winter

The first data collection was made in July, 1994. During the period from July, 1993 to July, 1994, the instruments worked normally except that the frozen ground depth meter at Lhasa and the ground temperature sensor at Nagqu broke, and some ambiguity was found in the data (Table 1). The calibrations of the snow weight meter in July, 1994 showed that the sensitivity to the snow weight did not change during one year.

3.2. Frozen ground depth

Figure 1(a)-(d) are the raw data of the frozen ground depth meter at Nagqu. Hereafter, the time in the figures denotes GMT. The Beijing standard time is GMT+8hours and the local time at the sites are about GMT+6hours. At the beginning of winter (Fig.1(a)), the soil froze only in the nighttime, and the whole frozen ground layer melted in the daytime. After that, the frozen ground layer developed downward (Fig.1(b)).

However, the layer near the surface, a few centimeter in depth, melted in the daytime. In this report, the layer which melts in the daytime is designated as a daily active layer. The frozen soil did not melt even in the daytime in the midwinter as shown by Fig.1(c). In spring (Fig.1(d)), near surface layer did not freeze all day and the frozen ground layer was left in the ground. Fig.1(a)−(d) represent typical diurnal variations of frozen ground layer at different stages of frozen ground formation.

Figure 2 shows a seasonal variation of the daily frozen ground depth at Nagqu, where the white bar indicates a daily active layer and the black bar indicates a frozen ground layer. The bottom of the daily active layer corresponds to the daily maximum depth of the melted layer during the period from 00Z to 22Z. The bottom of the frozen ground layer corresponds to its daily maximum depth during the period from 02Z of the previous day to 00Z. At the beginning of winter, the daily active layer often formed. This stage continued for about twenty days. After that, frozen ground layer developed and it attained maximum (158cm) from the end of Feb. to the beginning of Mar., 1994. In spring, the frozen soil melted rapidly both from the surface and from the bottom. Nagqu meteorological observatory routinely observes the frozen ground depth at 00Z (Fig.3), which corresponds to the early morning. Though the data of 1994 is not available at present, seasonal variation of frozen ground layer almost agrees with the measurement by the frozen ground depth meter. The routine data cannot give the information about the daily active layer since it is observed once a day, around the time when the frozen ground depth becomes maximum in the diurnal variation.

In Fig.2, the daily frozen ground depth sometimes changed stepwise. The frozen ground depth meter scans the resistance between the detection and common terminals by eight paired terminals. The stepwise change may be due to this scanning method. In July, 1995, the scanning method is going to be altered to the scanning by one paired terminals. At Rikeze, the daily frozen ground depth was smaller than the routine observation. The reason for this discrepancy is not clear.

3.3. Snow Weight

Lhasa and Rikeze are not located in snowy area of the Tibetan Plateau. In 1993/94 winter, no significant records of accumulated snow were found at Lhasa and Rikeze. Only at Nagqu, snow accumulation was detected.

The snow weight meter used is suitable for the heavy snow accumulation in relatively warm area, such as Japan. Under such conditions, the temperature at the ground surface below the accumulated snow is almost 0 ℃ and it is not necessary to consider the temperature dependence of the snow weight meter. In case of the Tibetan Plateau except for high mountain, however, snow accumulation is not thick and diurnal temperature variation is very large. So, temperature dependence of snow weight meter should be corrected to get true snow accumulation record. Figure 4 is an example of diurnal variations at Nagqu of the air temperature at z=2.5m measured by MRI and the output of the snow weight meter which is converted into the snow weight value. Since the ground temperature sensor broke, air temperature is compared with the apparent snow weight value. There was no accumulated snow in these three days, and the cange of apparent snow weight is caused by the temperature dependence of the snow weight meter. The apparent snow weight is almost in phase with the air temperature. But hysteresis can be

found in the apparent snow weight variation.

To obtain the temperature dependence of the snow weight meter, the periods without snow accumulation were selected on referring to the albedo values measured by MRI. Apparent snow weight values during these periods were plotted against the air temperature at z=2.5m (Fig.5). Two regression lines can be drawn for negative and positive air temperatures. The data are scattered within a range of about $\pm$ 8kg/m^2 due to the hysteresis of the snow weight meter. If the ground temperature is used instead of the air temperature, the data may be less scattered. Note that the temperature dependence of the snow weight meter is caused by the thermal inertia of metal wafer units and the temperature drifts of pressure sensor and control circuit. The regressive relationship obtained at Nagqu between the snow weight meter output and temperature is not general, and it should be determined at every site.

By applying these regression lines to the hourly values of snow weight meter output at Nagqu, the snow weight values from Jan. to Apr., 1994 were calculated. Time series of the hourly snow weight is plotted in Fig.6. Because of the hysteresis, noise-like behavior exists and negative values remain. To reduce this, daily snow weight values were obtained by averaging twenty-four values (Fig.7). For comparison, time series of the albedo is shown in Fig.8, in which the data are plotted when the global solar radiation exceeds 200W/m^2. Snow accumulation lasting for several days is found twice in Jan., 1994, and that lasting for a few days is found several times from Feb. to Apr. The snow weight meter detected the accumulated snow in Jan. The first one is about 9kg/m^2 and the second one is about 21kg/m^2. But it could not detect that from Feb. to Apr., since the snow weight was very light and less than the accuracy.

4. Discussion

The frozen ground depth D (cm) can be estimated by the following equation [4] :

$$D=\alpha\sqrt{I}\ , \qquad (1)$$

where I (℃·day) is an accumulated freezing index defined b

$$I=\sum T\ . \qquad (2)$$

Though T (℃) is a ground surface temperature, air temperature is often used instead of it. The temperature is a daily mean value, and the summation is made for only negative values. The coefficient α is found to be 4-6 when air temperature is used [5] . The value of α depends on the physical property of the soil, especially on the soil moisture. The accumulated freezing index of Nagqu were calculated from the routine observation of the ground surface temperature, measured at an interval of 6hours (00Z, 06Z, 12Z, and 18Z). The measured frozen ground depths are plotted against the accumulated freezing index from Nov. to Dec., 1993 in Fig.9. Routine data after Jan., 1995 is not available at present, and Fig.9 is not completed. Until the accumulated freezing index attained about 70 ℃·day, the frozen ground depth did not exceed about 10cm, and the daily active layer existed almost everyday (see Fig.2). After this early stage, the frozen ground depth increased in proportion to the square root of the accumulated freezing index. This agrees to the Eq.(1) and the coefficient α seems to be about 3. Interannual variation of α, especially its

dependence on the soil moisture, will be analyzed in the future based on the long term observation in this study.

At Lhasa and Rikeze, similar analysis was made using the routinely observed frozen ground depth. But the accumulated freezing index did not reach 100 ℃·day and the proportional constants were not determined.

The measured snow weights in Jan. 1993 at Nagqu were 9kg/m^2 and 21kg/m^2. If the density of accumulated snow is assumed to be 100kg/m^3, the snow depths are estimated to be about 0.1m and 0.2m, respectively. After receiving the routinely observed snow depth data, in turn, the snow density will be calculated and its change after the snowfall will be discussed taking account of the heat budget on the snow surface.

5. References

1) Sato, T. and T. Kimura, 1994 : Observation on hydrology over the Tibetan Plateau and Himalayas., *Annual Report of Japanese Experiment on Asian Monsoon*, Research and Development Bureau, STA, 69−76. (in Japanese with English abstract)
2) Kimura, T., 1983 : Observation of water equivalent of snow cover by metal wafer., *Report of the National Research Center for Disaster Prevention*, **31**, 203−217. (in Japanese with English abstract)
3) Kimura, T., 1992 : Observation on hydrologic variations in Tibet−Himalaya area., *Annual Report of Japanese Experiment on Asian Monsoon*, Research and Development Bureau, *STA*, 80−83. (in Japanese)
4) Kinosita, S. (ed.), 1982 : *Physics of frozen ground.*, Morikita Shuppan, 227pp. (in Japanese)
5) Kinosita, S., K. Horiguchi, K. Tanuma, and T. Ohno, 1968 : Frost heave in Kitami (1967−1968)., *Low Temperature Science*, Ser.**A**, **26**, 363−381. (in Japanese with English summary)

6. Publications

Author	Title	Name of Publications	Notes
(oral)			
T. Sato *et al.*	Continuous measurements of snow weight and frozen ground depth in the Tibetan Plateau (2)	Japanese Society of Snow and Ice. Preprints of the presentation, Sept., 1994.	

7. International cooperation

The observations of the snow weight and frozen ground are carried out as the cooperative study with China Meteorological Administration. National Research Institute for Earth Science and Disaster Prevention invited Prof. Li Weiliang (Chinese Academy of Meteorological Sciences) for 25 days in 1994. At the same time, Meteorological Research Institute invited Mr. Gong Yuanfa (Chengdu Institute of Meteorology). During their stay in

Japan, we discussed the cooperative study, for example, results of the action items in 1994 F.Y., working plan in 1995 F.Y., research themes and so on. They were summarized in the memorandum and approved in the 3rd Working Group Meeting held from 3 to 5 Mar., 1995 in Tianjing, China.

（要旨）

本研究ではチベット高原に３ヶ所の積雪重量（相当水量），地温，凍結深度の自動観測点を設置し、長期間のデータを蓄積するとともに、積雪、凍土の変動ならびにそれらとアジアモンスーンの関係を解析する。

１９９３年７月に積雪重量計及び凍結深度計をラサ、シガセ、ナチュの３ヶ所に設置し、連続観測を開始した。又、同時期に気象研究所は同じ観測点で接地気象の観測を開始した。第１回目のデータ回収は１９９４年７月に行われたが、ラサの凍結深度及びナチュの地温データは測器のトラブルのため取得できなかった。

１９９３年７月から１９９４年７月のデータを解析し、以下の結果を得た。ナチュにおいて観測された土壌の凍結・融解の日変化及び凍土の季節変化は妥当なもので、最大凍結深度は１５８cm（１９９４年２月下旬～３月上旬）であった。またナチュの凍土の発達過程を積算寒度をもとに解析した結果、凍結深度と積算寒度の平方根の比例定数として約３を得た。積雪重量計の感度はさほどよくないため、ナチュで１９９４年１月に数日間継続した積雪を観測できたが、２～３日しか継続しない積雪は観測不能であった。観測された積雪重量は９kg/㎡および２１kg/㎡であった。積雪密度を１００kg/m^3と仮定すれば、これらはそれぞれ０．１mおよび０．２mの積雪深に相当する。

Table 1 Summary of observation in 1993/94 winter
(from July, 1993 to July, 1994).
○ : no trouble, △ :see captions , × : sensor broke.

Site	Frozen Gound Depth	Snow Weight	Ground Temperature
Lhasa	×	○	○
Rikeze	△*1. *2	△*3	○
Nagqu	○*1	○	×

*1 : Total number of data disagrees with snow weight data.
*2 : Disagrees with routine data.
*3 : Drift is large.

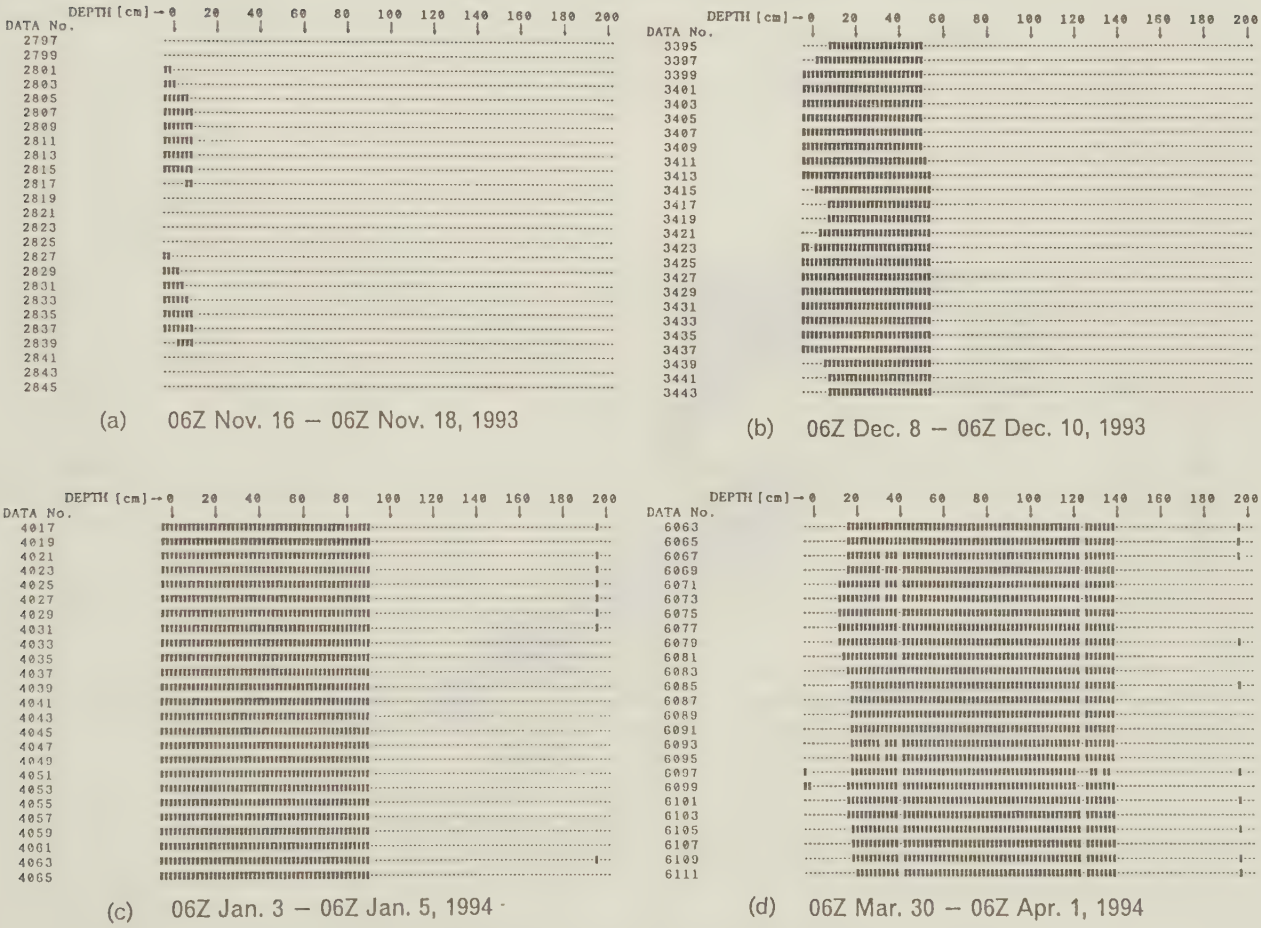

Figure 1 Examples of the raw data of the frozen ground depth meter at Nagqu.
Black mark denotes a frozen portion of the ground.

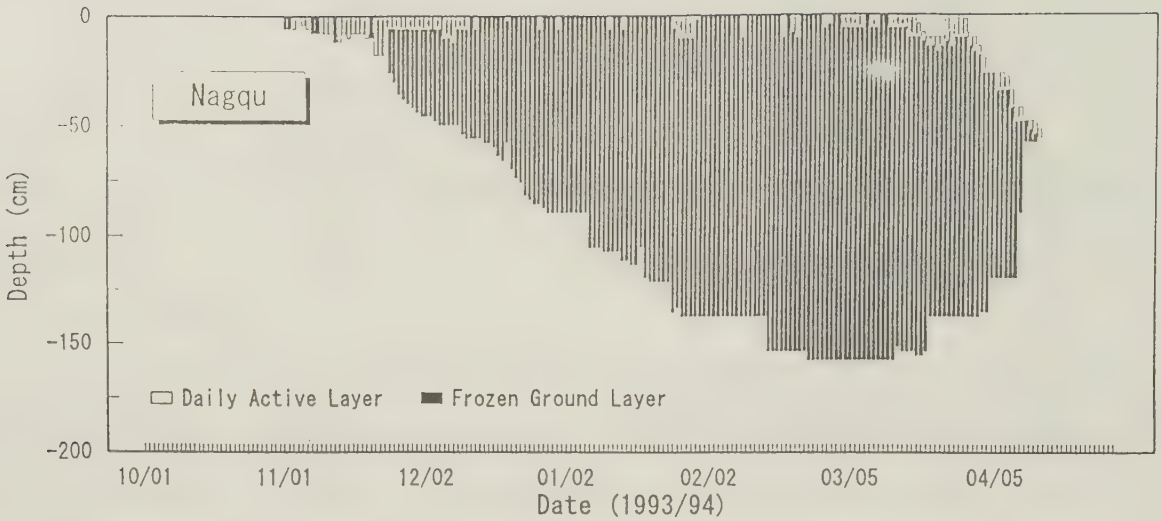

Figure 2 Seasonal variation of the daily frozen ground depth at Nagqu.

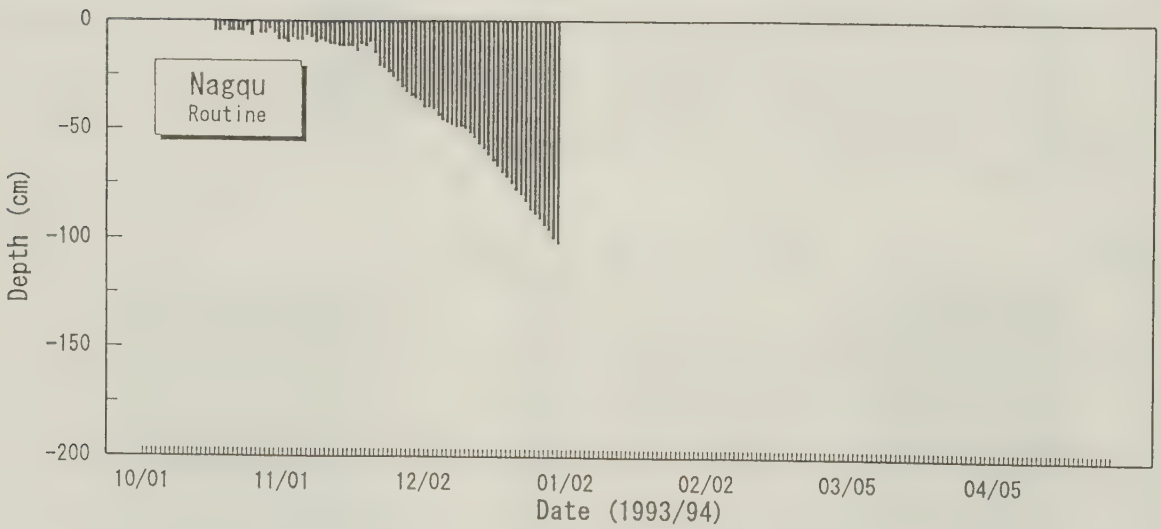

Figure 3 Routinely observed frozen ground depth at Nagqu.

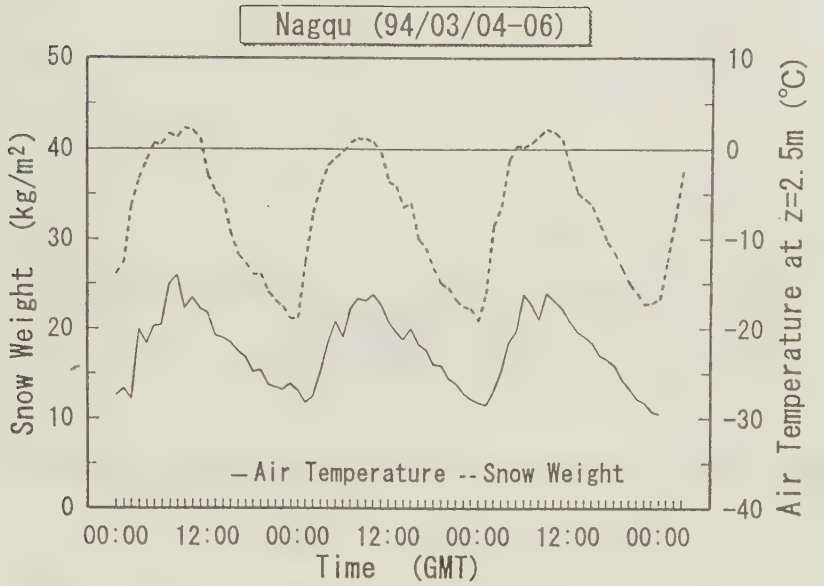
Nagqu (94/03/04-06)
Snow Weight (kg/m²)
Air Temperature at z=2.5m (°C)
—Air Temperature -- Snow Weight
00:00 12:00 00:00 12:00 00:00 12:00 00:00
Time (GMT)

Figure 4 Diurnal variations of the air temperature at z=2.5m and the apparent snow weight (Nagqu).

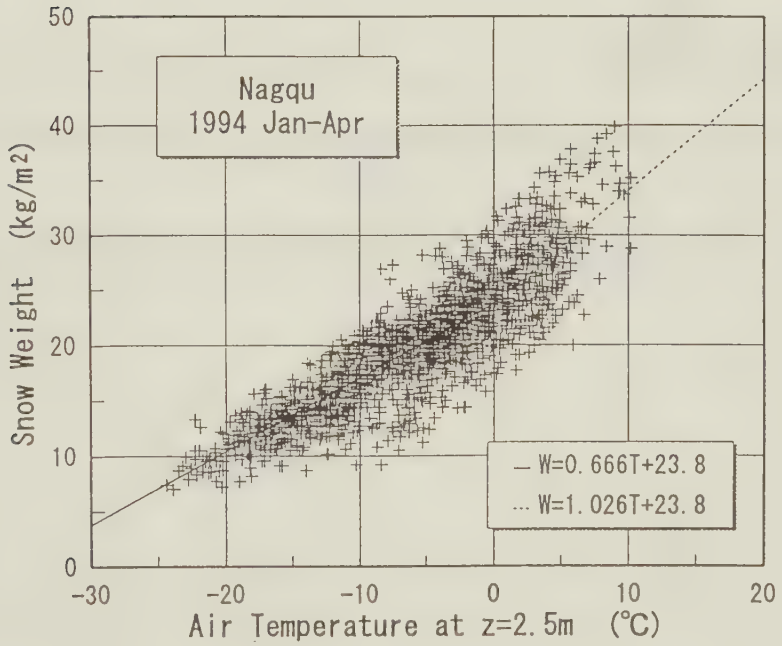

Figure 5 Relationship between the apparent snow weight and the air temperature at z=2.5m (Nagqu).

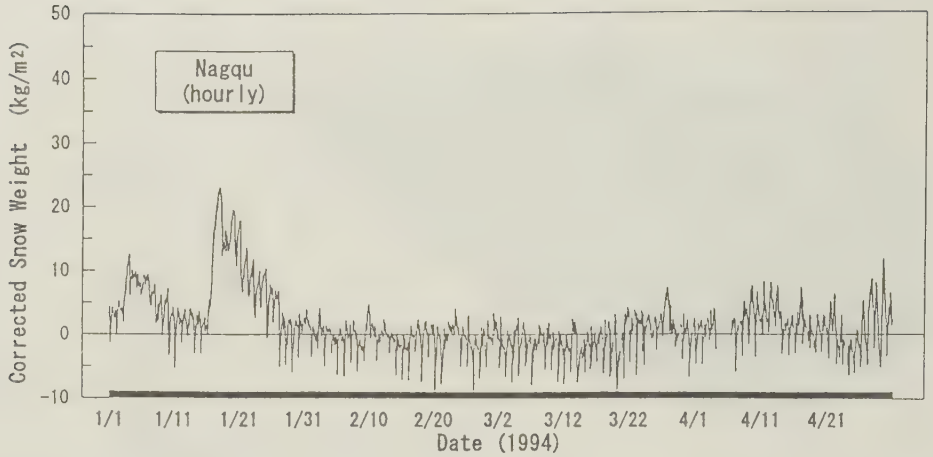

Figure 6 Time series of snow weight (hourly vaule) at Nagqu.

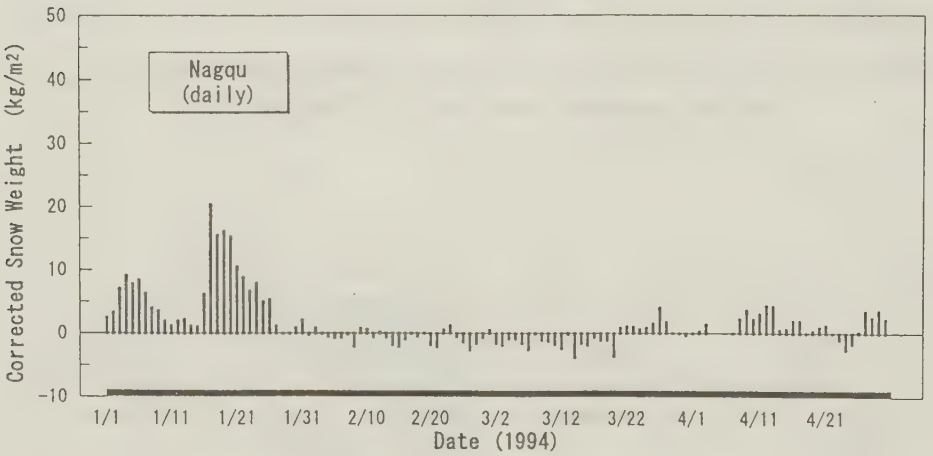

Figure 7 Time series of snow weight (daily averaged vaule) at Nagqu.

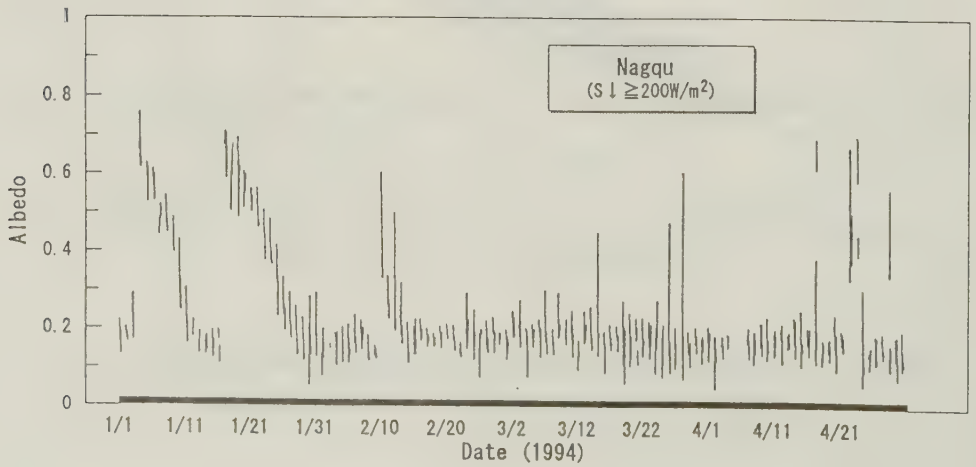

Figure 8 Time series of the albedo at Nagqu.

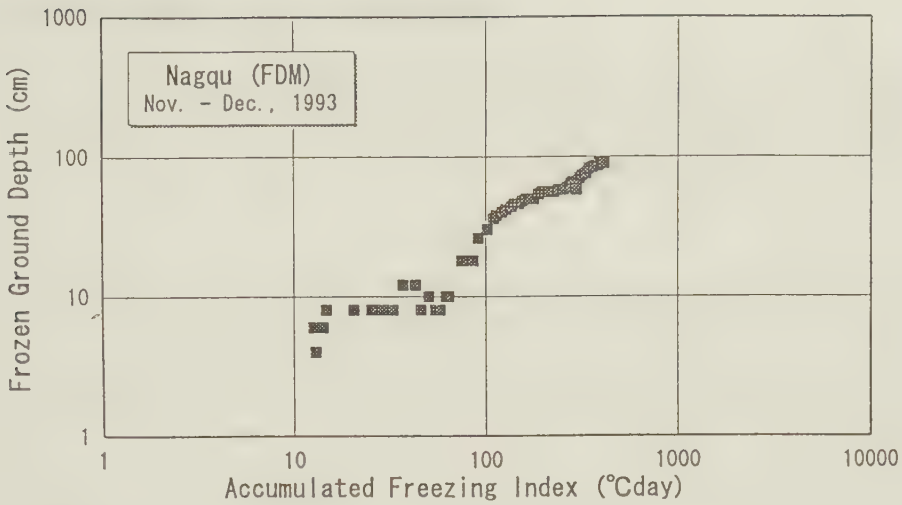

Figure 9 Relationship between the daily frozen ground depth and the accumulated freezing index at Nagqu.

Ⅰ. Observation and analysis on the process of the atmosphere–ocean–land interactions

3. Observation and analysis on the process over the land

(2) Observation on Regional Surface Heat Budget

Meteorological Research Institute, Japan Meteorological Agency
S. Haginoya, N. Kinosita, M. Kato, H. Niino,
T. Fujitani, M. Mikami, I. Takayabu and H. Mouri

Abstract

The purpose of this study is estimating the large–scale heat budgets over the two different areas by using of the meteorological data obtained by the on–site observation in order to clarify the mechanism of the Asian Monsoon caused through Air–Sea–Land interactions. One of the two budgets is the land surface fluxes on the tibetan–Himalayan Mountains area. Another is the sea surface fluxes on the Indian Ocean.

In relation to tibetan–Himalayan Mountains area, the Automatic Weather Stations(AWS) were set up at the four observation sites. The observation has been continued since the summer in 1993. The on–site investigations were carried out for Lhasa and Rikeze to survey the surrounding topography. The routine meteorological data in this area were obtained. The Chinese researchers were invited to Japan. The data obtained by the AWSs to December 1993 were collected and analyzed.

The aerodynamic roughnesses on the AWS sites were estimated. Measuring the vertical distribution of the wind velocity near the surface and using the data obtained during the strong wind were important for the estimation.

The daily variation of the air pressure showed the influence by the local topography. The daily variation of the wind velocity indicated that the westerly wind in the upper air went down in the daytime. The magnitude of solar radiation is in order of Rikeze , Lhasa, Nagqu and then Lingzi. The albedos at the AWS sites varied from 0.1 to 0.2. They were small in summer and large in winter. The influence of snow was found only at Nagqu.

In relation to the Indian Ocean, the observation by the AWS on the Osaka–Maru(31,382 tons) was continued along her regular line on the Indian Ocean. Omega sonde observation was carried out on the Chofu–Maru(430 tons) that is a meteorological observation ship of JMA. The observation area was between 13 and 29 degrees north latitude and between 126 and 128 degrees east longitude. The atmospheric boundary layer was surveyed by the upper air soundings. The height of the atmospheric mixed layer reached above 1600m in January and February. That in October was below 1000m.

1. Objectives

In order to clarify the mechanism of the Asian Monsoon caused through Air–Sea–Land interactions, the large–scale heat budgets over two different areas should be estimated: Tibetan–Himalaya Mountains Area and the Indian Ocean–South China Sea Area. Because of the vastness of the areas and of their unsuitable conditions for observations, observatories or ships in these areas are very sparsely distributed. Therefore the basic meteorological data to clarify the mechanism of the Asian Monsoon has been lacking. This study aims to collect these basic data and estimate large–scale heat budgets over the two areas.

2. Methods

Since the heat budgets in two areas are studied by different methods, they are described separately.

(1) Tibet

The four sets of Automatic Weather Station (AWS) were installed in the Tibetan area in summer 1993. Observation sites are Lhasa, Rikeze, Nagqu and Lingzi (see Table 1). The observation were carried out continued from last fiscal year. Japanese scientist visited Lhasa and Rikeze in July 1994. He investigated the observation sites and around topography. He also supported data collection. Chinese side checked AWS every month and collected data twice a year. Chinese side finished the first data collection in August 1994, the second data collection from December 1994 to January 1995. Collected data were sent to Japan by mail. Routine meteorological data of 20 stations in Tibetan area from May to September 1993 were collected.

(2) Indian Ocean

Omega sonde observation (aerological observation) was carried out on the Meteorological Observation Ship, Chofu−Maru (430GT) of JMA in October 1994 in the East China Sea. AWS observations were made on the Osaka−Maru (31,382 GT), which made six times round trips between Japan and Republic of South Africa through the South China Sea, the Strait of Malacca and the Indian Ocean in this fiscal year continued from last fiscal year. When the Osaka−Maru came back to Yokohama, the data were collected. AWS were exchanged once a year for maintenance. Observation data from April 1994 to March 1995 were analyzed.

3. Results

(1) Tibet

The preliminary results of test observation at Lhasa showed the followings. Daily variation of air pressure is about 5hPa and is in phase with the daily variation of air temperature. Heat balance analysis suggests the existence of local circulation at Lhasa[1]. This section shows the more detail results.

① Table 1 summarized the observation sites. Lhasa site is located at the bottom of valley. The length of valley is 40km in the east−west direction. Its width is 7km−8km at the bottom and is 25km at the ridge lines of mountains. Average height difference between the bottom and the ridge line is 1500−2000m. Nagqu is located over a plateau, about 220km north east of Lhasa. This site is representative place in Tibet which is located in the rural area on the opened plateau. Other sites are located in a valley or a basin. The most of routine meteorological observatories in Tibetan plateau are generally located in a valley, so that average wind velocity is generally weak.

Aerodynamic roughness z_0 is one of the important parameter to estimate the surface heat budget. We obtained z_0 from the log + linear profile relationship[2]. The observational data using the analysis is temperature and wind profile (10m, 5m, 2.5m) observed by AWS. Near neutral condition data are selected. z_0 at Lhasa is larger than any other three sites, but wind speed is the smallest in the four sites.

② Pressure and temperature variation in each AWS site are compared. Figure 1 shows

the surface pressure and temperature variation in AWS sites. The amplitude of pressure variations at Lhasa and Rikeze are large (about 4hPa), on the other hand that at Nagqu is small (about 2hPa). The amplitude of temperature variations of three sites are nearly equal to each other. These facts are likely to be caused by the difference in topography around the site. Lhasa and Rikeze sites are located at the bottom of valley or basin, Nagqu is on the hill. The amplitude of surface pressure variation at Lhasa is of similar amplitude to that observed at the bottom of basin or a valley in Japan when the mountain–valley circulation is fully developed on a clear and calm day. The surface pressure variation is measure the heating or cooling of air column. The surface temperature variation only depends on the near surface condition. So that the pressure difference in each site indicates the different depth of atmospheric boundary layer in each site [3].

③ Diurnal variation of wind velocity in Tibetan Plateau. Figure 2 shows the time series of AWS wind data at Nagqu. One can easily find the daily cycle of wind speed. Surface wind velocity reaches above 10m/s in the daytime and it becomes below 2m/s in the nighttime. Figure 3 shows the hodograph of 15 days vector average. It changes the clockwise. Diurnal strong wind is westerly. Its direction is the same as 500hPa or 400hPa level at Lhasa. 500hPa level is about 1200m height from Nagqu ground level, 400hPa is about 3000m height. It is conceivable that diurnal convective mixing transports the upper layer momentum to the ground surface level [4]. The mechanism of daily cycle is as follows. Mixed layer develops in the daytime. Momentum of westerly wind is transported downward. Then, the ground surface wind velocity increases. In the nighttime, the atmospheric boundary layer stabilizes, the momentum transfer from the upper layer stops, then wind is weakened.

④ Global solar radiation was measured by two kinds of systems. One system can store the instantaneous value at every 10 minutes to the memory. Another system can store the hourly accumulated value. To check the data quality, these two observational data were compared each other. Figure 4 shows the time series of the daily mean global solar radiation which are obtained from the hourly accumulated value. In summer period, the fluctuation of solar radiation is large. This is caused by the influence of cloud which indicates convective activity. On the other hand, that in winter period is small. The ratio of solar radiation at the ground surface to that at the top of atmosphere is large in winter because of small water vapor in the air mass. The solar radiation of the western part of Tibet is larger than other area. The magnitude of solar radiation is in the order of Rikeze > Lhasa > Nagqu > Lingzi.

⑤ Albedo of AWS sites were analyzed. Albedo is defined by the ratio of reflective solar radiation to global solar radiation. Used data are instantaneous value at every 10 minutes. Global solar radiation below 400W/m^2 data were excluded from the monthly mean calculation. Figure 5 shows the monthly mean albedo of each site. Albedo changes periodically. Its cycle is one year. Its value is from 0.1 to 0.2. In summer, albedo is small because of plant activity and relatively wetted ground surface conditions. Winter albedo becomes larger than summer one, because of dried bare soil conditions. All sites has no snow except for Nagqu, so that albedo and their error bar are small. As Nagqu has snow in winter, albedo and its error bar are larger than other sites. Snow

is observed from November to April.

(2)Indian Ocean

Chofu–Maru's Omega sonde system observed atmospheric boundary layer in the East China Sea and Pacific Ocean area. Observation area is from 13 degree north latitude to 29 degree north latitude along 128 degree east longitude line. Observation is carried out two times. One is from January to February 1994, another is October 1994. Height of atmospheric mixed layer were obtained from potential temperature profile [5]. Mixed layer height in January to February reached above 1600m. That in October was below 1000m (Figure 6).

4. Discussions

It is necessary for estimating the roughness to a certain accuracy to measure wind profile even between 2.5 m and the ground surface and to use the relatively strong wind data. Since Lhasa, Rikeze and Lingzi are located at the bottom of a valley, local circulations seem to heat up the air in the valley very effectively and produce a pressure variation of a large amplitude. To clarify local circulations over Tibet seems to be an important subject. Solar radiation is the important element of heat balance equation. To maintain the data accuracy, sensors must be calibrated periodically. AWS observation sites are located in the eastern part of Tibetan Plateau. It is necessary to establish AWS in the western part of Tibet to estimate an energy balance over the Plateau.

5. References

1)Haginoya, S. et al.: Observational Study on the Regional Surface Heat Budget over the Tibetan Plateau. Preprints of The First PRC–Japan Workshop on the Asian Monsoon Mechanism, CAMS, Beijing, 33–36. (1994)

2)Li Guoping: Private Communication. (1995)

3)Kuwagata, T., M.Sumioka, N.Masuko and J.Kondo: The Daytime PBL Heating over Complex Terrain in Central Japan under Fair and Calm Weather Conditions. Part I : Meso–scale Circulation and the PBL Heating Rate. J. Meteor. Soc. Japan, 68, 625–638. (1990)

4)Zhang Jiacheng and Lin Zhiguang: Climate of China. John Wiley & Sons, Inc. pp.376 (1992)

5)Haginoya, S. et al.: Observation on Regional Surface Heat Budget. Annual Report of Japanese Experiment on Asian Monsoon, Research and Development Bureau, STA, 47–59. (1994)

6. Publications

name	Title	paper name	memo
(report) S.Haginoya et al.	Observation on Regional Surface Heat Budget.	Research and Development Bureau, Science and Techno-logy Agency, Japan. Annual Report of Japanese Experiment on Asian Monsoon (1992), March 1994, 63-73.	
S.Haginoya et al.	Observation on Regional Surface Heat Budget.	Research and Development Bureau, Science and Techno-logy Agency, Japan. Annual Report of Japanese Experiment on Asian Monsoon (1993), August 1994, 47-59.	
(oral) S.Haginoya et al.	Automatic Meteorological Observation over Tibetan Plateau (2).	Meteorological Society of Japan. Preprints of the presentation, October 1994.	
S.Haginoya et al.	Observational Study on the Regional Surface Heat Budget over the Tibetan Plateau.	Chinese Academy of Meteorological Sciences. Preprints of The First PRC-Japan Workshop on the Asian Monsoon Mechanism, Beijing, 33-36, October 1994.	
S.Haginoya et al.	Observational Study on the Regional Surface Heat Budget over the Tibetan Plateau.	Chinese Academy of Sciences. Preprints of International Symposium on the Asian Monsoon and Its Variabilities, Gangzhou, November 1994.	
S.Haginoya et al.	Automatic Meteorological Observation over Tibetan Plateau (3).	Meteorological Society of Japan. Preprints of the presentation, October 1994.	

7. International cooperation

Meteorological observation over the Tibetan Plateau is carried out the cooperative study with China Meteorological Administration. Meteorological Research

Institute invited one Chinese scientist named Mr. Gong Yuanfa (Chengdu Institute of Meteorology) for 25 days. In the same time, National Research Institute for Earth Science and Disaster Prevention, Science and Technology Agency invited another scientist named Prof. Li Weiliang (Chinese Academy of Meteorological Sciences). Japanese side discussed the Tibet observation above two scientists. Japanese and Chinese sides examined the results of 1994 F.Y. and the plan of 1995 F.Y. They summarized the results of discussion as "Working Plan". Japanese side and Chinese side agreed the "Working Plan" in the 3rd Working Group Meeting held from 3 March to 5 March, 1995 in Tianjing, China. Details concerning the above are summarized in the Appendix 1 of "SUMMARY REPORT ON THE 3RD WGM OF PRC–JAPAN COOPERATIVE PROGRAM ON ASIAN MONSOON".

アブストラクト

本研究は，大気を媒体とした海洋と陸面間の相互作用として発現しているアジアモンスーンの機構を解明するため２つの異なる地域における広域のエネルギー収支を評価するものである．そのうちの１つはチベット・ヒマラヤの山岳地帯の地表面フラックス，もう１つはインド洋・東南アジア地域の海面フラックスである．熱収支解析に必要な気象要素を現地観測により収集し，それに基づいて広域熱収支解析を行うことを目的としている．

チベット関連：４ヶ所の観測地点に山岳用自動気象観測装置(AWS)を設置し，1993年夏から観測を継続して実施している．ラサとシガセの現地を視察し，周辺の状況を調査した．チベット地域のルーチン観測所のデータを入手した．中国人研究者を日本に招聘した．1994年12月までの観測データを回収・解析した．

AWS設置地点の周辺状況や空気力学的粗度を求めた．粗度を求めるには地面付近の風速分布を測定すること，比較的強風時のデータを使用すること，が重要である．気圧の日変化から局所地形の影響が見られることが示唆された．風速の日変化から上空の偏西風が日中地表面付近まで下降することが確認された．年間の日射量は大きい順からシガセ＞ラサ＞ナチュ＞ニンチの順になっている．アルベードは積雪のない時は0.1から0.2の間を変動し，夏期に小さく，冬季に大きくなる．積雪の影響はナチュのみに現れ，他の３地点には現れなかった．

インド洋関連：大阪商船三井船舶株式会社の定期コンテナ船「大阪丸(31,382t)」に船舶用ＡＷＳを搭載し，インド洋航路の観測を継続して実施した．「長風丸(430t)」を用いて東シナ海～太平洋上（東経128度［±２度］線を北緯13度～29度まで観測）でオメガゾンデによる高層観測を実施し，大気境界層の構造を調べた．１月～２月の大気混合層高度は1600m以上に達し，10月は1000m以下であった．

Table 1 Summary of the sites. $S\downarrow/S\downarrow_0$ means the ratio of annual mean global solar radiation at the ground surface to that at the top of atmosphere.

site name		Lhasa	Nagqu	Rikeze	Lingzi
location	latitude	29° 40'N	31° 29'N	29° 15'N	29° 34'N
	longitude	91° 08'E	92° 04'E	88° 53'E	94° 28'E
altitude(m)		3649	4507	3836	3000
topography		valley	plateau	basin	valley
conditions around the site		city	rural	rural	rural
roughness length(cm)		8.2	2.5	4.5	5.8
friction velocity(m/s)		0.11	0.22	0.19	0.19
wind speed at 10m(m/s)		1.5	3.7	3.0	2.8
$S\downarrow/S\downarrow_0$		0.64	0.57	0.73	0.48

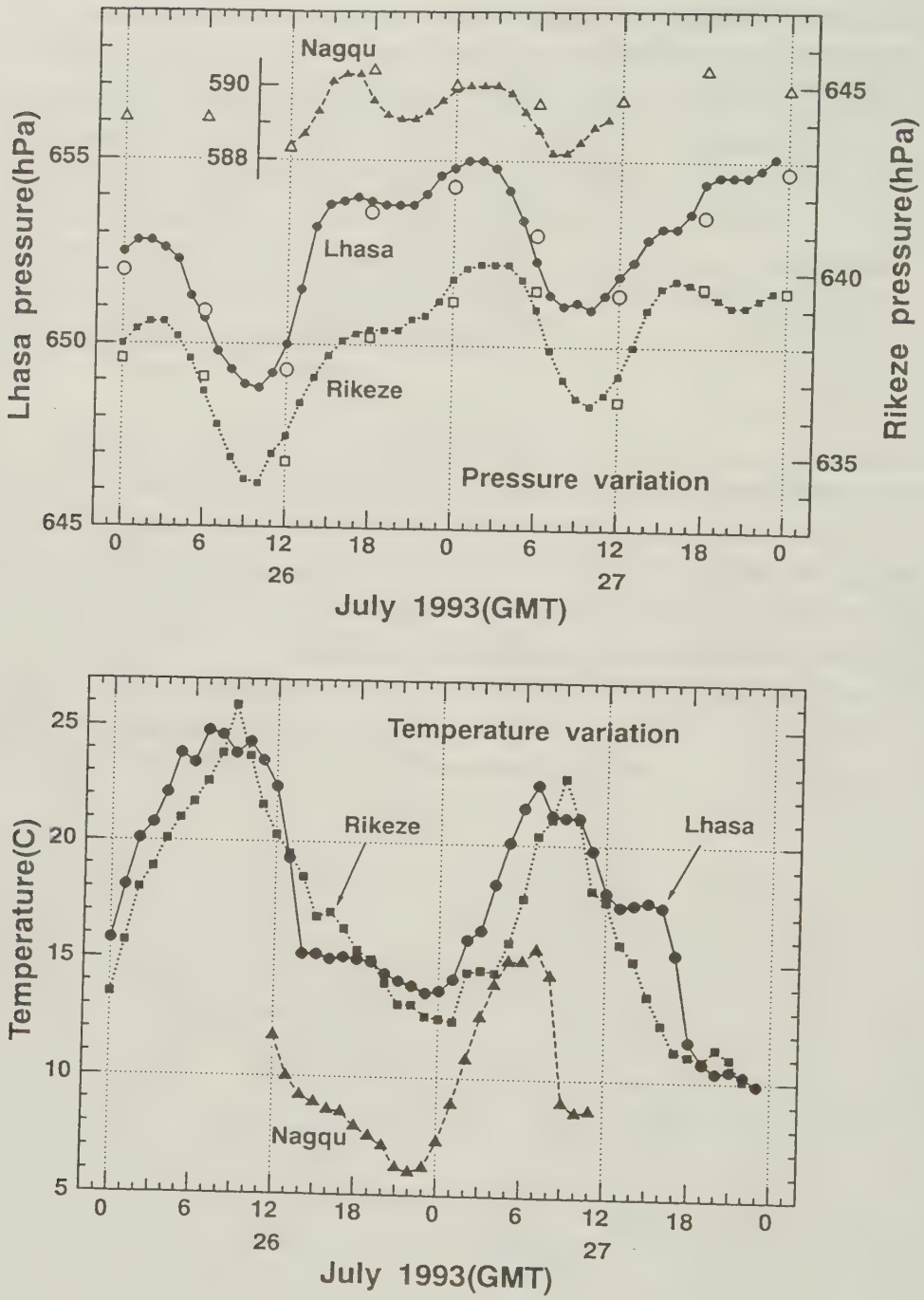

Figure 1 Surface pressure and temperature variation. Circle, square and triangle indicate Lhasa, Rikeze and Nagqu, respectively. Filled marks indicate hourly average AWS data and open marks 6 hourly routine data. Pressure value of each site correspond to each vertical axis.

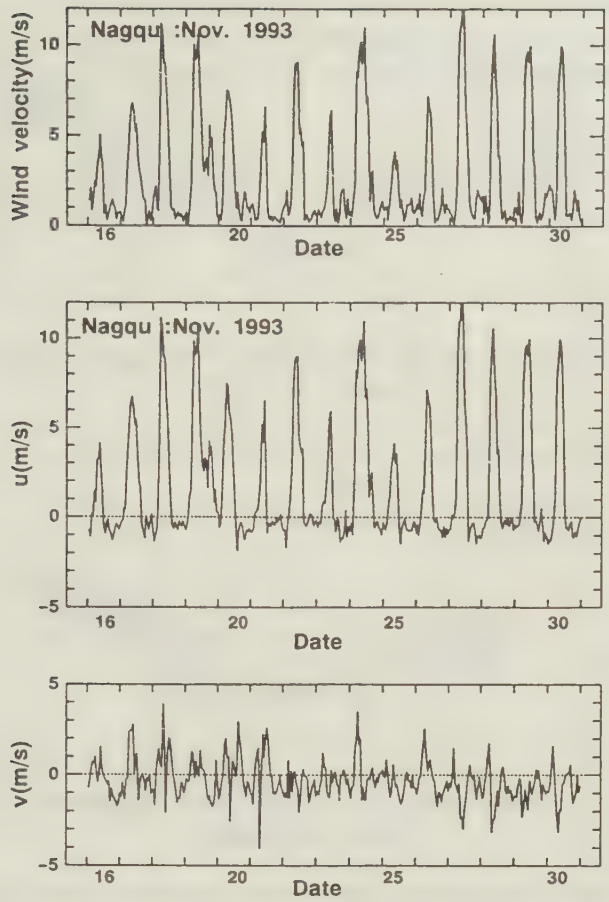

Figure 2 Wind velocity of 10m height at Nagqu. Data are hourly average.

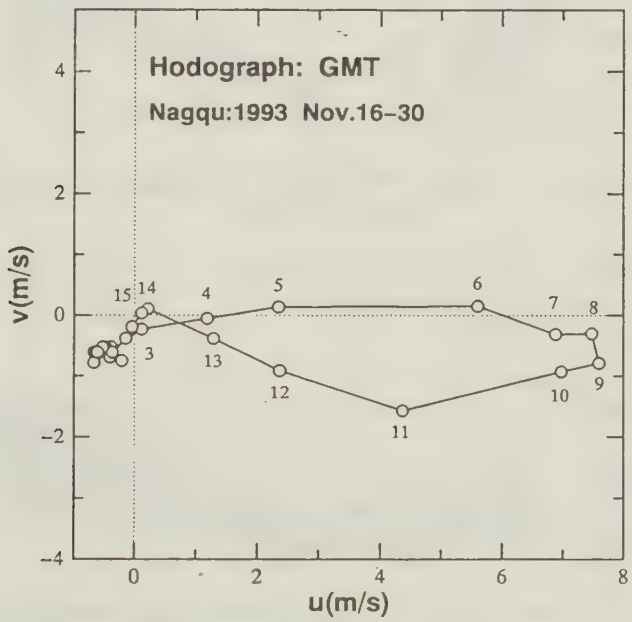

Figure 3 Hodograph at Nagqu. Data are the same period as Figure 2. Number indicates GMT. Local time is GMT+6.

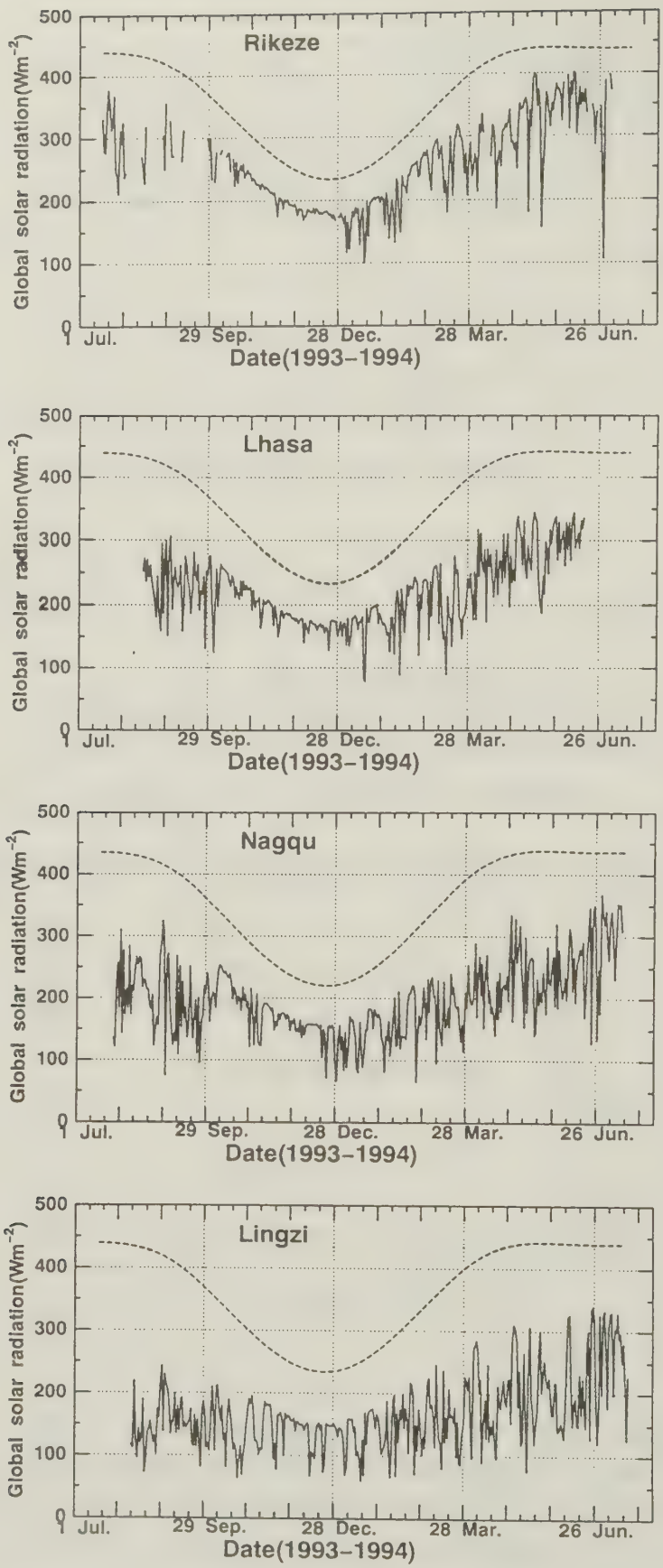

Figure 4 Daily mean global solar radiation which are obtained from the hourly accumulated value. Solid line shows the observational data. Broken line shows the calculated value at the top of atmosphere.

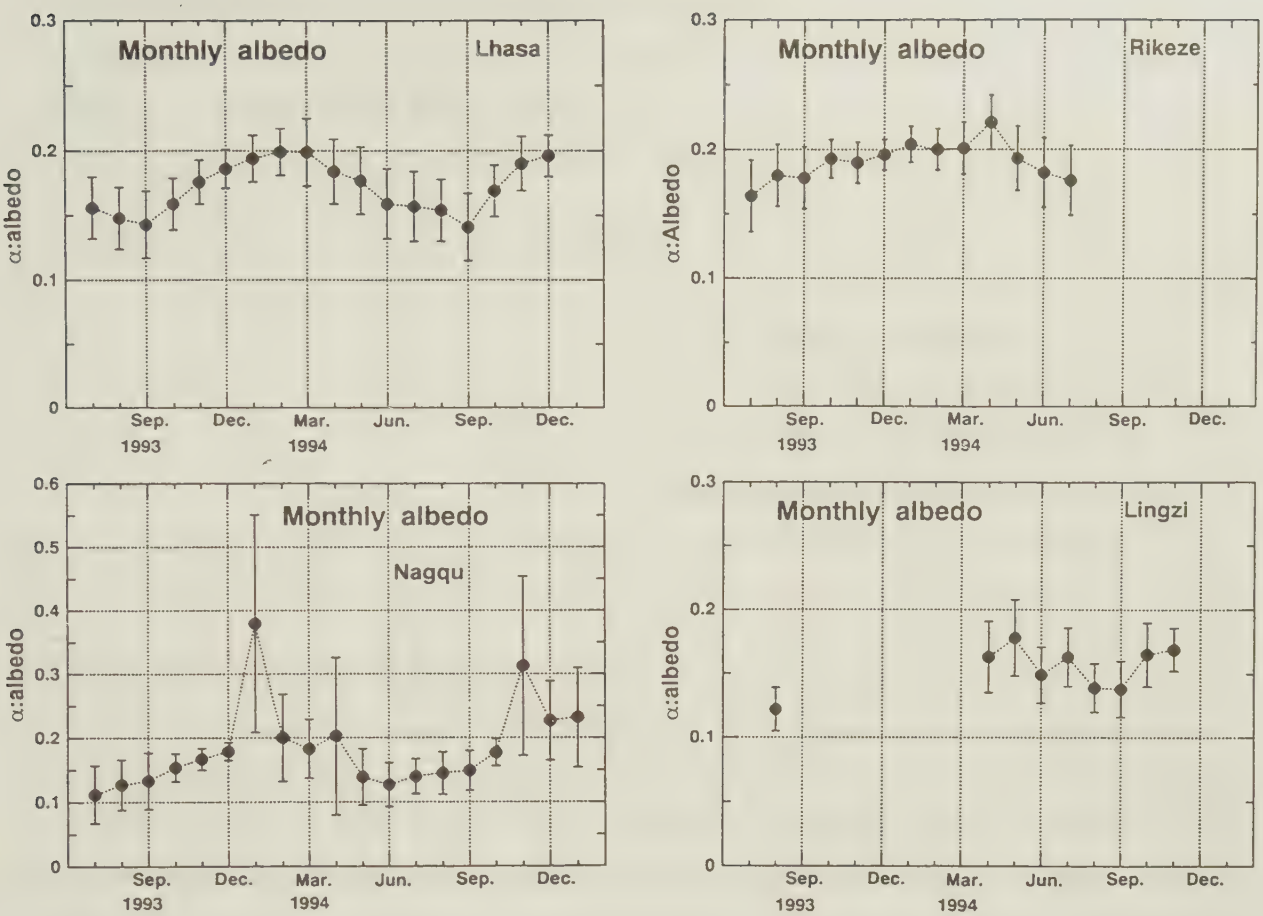

Figure 5 Monthly mean albedo.

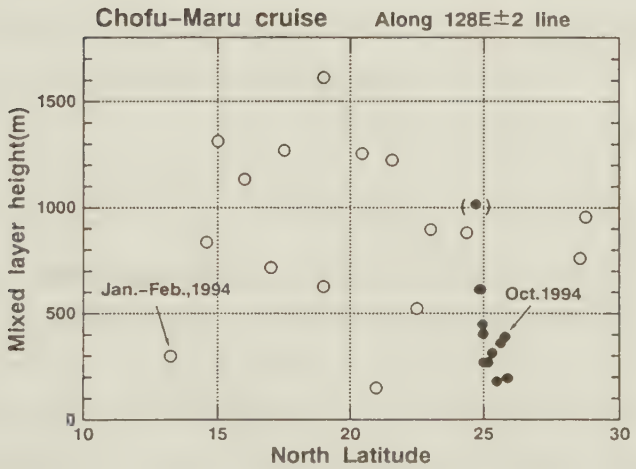

Figure 6 Latitudinal variation of atmospheric mixed layer height. (●) indicates the questionable data.

Ⅰ. 大気·海洋·陸域間相互作用の諸過程に関する観測·解析研究

Observation and analysis on the process of the atmosphere-ocean-land interactions

3. 陸域における諸過程に関する観測·解析研究

Observational and analysis on the process over the land

(2) 地表面熱収支に関する観測研究

Observational study of the ground surface heat budgets

郵政省通信総合研究所

大崎　祐次、増田　悦久

Communications Research Laboratory

Ministry of Posts and Telecommunications

Yuji Ohsaki and Yoshihisa Masuda

(Abstract) Wind profilers developed by the Communications Research Laboratory (CRL) are operating at the Okinawa Radio Observatory (ORO) of CRL and at King Mongkut's Institute of Technology Ladkrabang (KMITL) in Thailand. A wind profiler is a Doppler radar for measuring the vertical profile of the three-dimensional wind vectors from the echo signal scattered by clear air turbulence. This article describes two research topics. One is the rejection of clutter in the Doppler spectrum measured by the ORO wind profiler. Vegetation will have a motion caused by wind, and this motion will produce signals contaminating the Doppler spectrum. The ORO is located in a wooded area, and such clutter makes it difficult to identify the echo signal in a Doppler spectrum. A software-based clutter filter was therefore developed. The other topic is the temperature profiling using a wind profiler with a Radio Acoustic Sounding System (RASS). Comparison at KMITL of experimental results obtained with a wind profiler and with radiosonde data shows that a wind profiler with a RASS can measure the temperature profile with an accuracy within 0.8 ℃.

1. Objectives

Vertical heat flux is defined by the quantity of heat passing a unit horizontal plane in a unit time, and to better understand global heat balance, we need to know the global distribution and temporal variation of this flux. Heat flux can be estimated from atmospheric parameters measured by the conventional radiosonde, but, it is difficult to obtain it global distribution from radiosonde measurements. Remote sensing is the most suitable technique for global monitoring, and the development of a suitable heat flux sensor would make it possible to measure the global distribution of the heat flux with spaceborne or airborne sensors. Although several algorithms for estimating the heat flux from wind profiler data have been proposed[1)2)], these algorithms have not be well established. This study therefore evaluates the accuracy with which a wind profiler with a Radio Acoustic Sounding System (RASS) measures wind vectors and temperature, and develops the

algorithm for estimating the heat flux.

2. Methods

The Doppler spectrum will be contaminated with clutter signals that are due to the motion of shrubs or trees, and that are received by antenna-sidelobe. Because vegetation will have a back-and-forth motion due to the wind, the Doppler spectrum from such clutter will be distributed on both sides of the zero Doppler frequency. Since the Okinawa Radio Observatory is in a wooded area, the peak power of such clutter is sometimes larger than that of echo signal from clear air turbulence, and It is difficult to distinguish the echo signal from the clutter. But because the Doppler spectrum of clutter is generally symmetrical about the zero Doppler frequency, it can be canceled by subtracting a side of the Doppler spectrum without the echo signal as a target from that with a target, and the asymmetrical target spectrum will be extracted[3]. It is found that the wind vector estimated from wind profiler measurement using this software-based clutter rejection corresponds well to that estimated from radiosonde measurement.

A wind profiler with a RASS measures the Doppler signals reflected from actively radiated acoustic wave. The speed of an acoustic wave estimated from measured Doppler signals is a function of temperature, and can be used to evaluate the vertical profile of temperature. We therefore compared measurements made with a wind profiler and measurements made with radiosondes, and found that a wind profiler with a RASS can measure the temperature profile with an accuracy within 0.8 ℃.

3. Results

Figure 1(a) shows an example of the Doppler spectrum composed of 128 data points. The Doppler frequency here is transformed to wind speed, and such figure is called a wind spectrum. Positive and negative wind speeds mean approaching and receding wind along the antenna radial direction, respectively. The clutter spectrum around zero wind speed is clearly found, and the target spectrum is at the left side of the clutter spectrum. The closed circle indicates the mean wind speed estimated from a first-moment calculation without the clutter rejection. It is because of the clutter spectrum that the mean wind speed is not estimated correctly. Figure 1(b) shows a clutter-rejected wind spectrum generated from Fig. 1(a). The symmetrical clutter spectrum is canceled by subtracting the right part of the wind spectrum without the target from the left part of the spectrum with target. Five-point running averaging is done to enhance the symmetry of the clutter spectrum. As shown by the closed circle, the mean wind speed in Fig. 1(b) is estimated almost correctly.

The horizontal wind vector estimated from the wind-profiler data was compared to the corresponding vector measured by the radiosonde. Initial and last range, range resolution, and time interval for measurements can be selected on the wind profiler operation. In this comparative experiments, the wind profiler measured from heights of about 0.3 km to about 2.4 km with 150-m

resolution and at 5-minute intervals. Radiosondes were launched from the Okinawa Meteorological Observatory of Japan Meteorological Agency at 3, 9, 15, and 21 hour of Japan Standard Time. Hourly means of the horizontal wind vector at these times were calculated from the wind-profiler data and compared with the radiosonde data. The distance between Okinawa Radio Observatory and Okinawa Meteorological Observatory is about 15 km. Wind at lower heights (about less than 1 km) will blow independently at each observatory, higher than this wind will blow uniformly over a wide area. Wind vectors estimated from wind-profiler data at heights of 1.5, 1.95, and 2.4 km can be compared directly with no interpolation in the vertical direction with vectors estimated from radiosonde data. Wind vector data for comparison was obtained from December 1992 to November 1993. Figure 2(a) shows a scatter-diagram for the north-south component of wind speed derived from radiosonde data and from wind-profiler data without clutter rejection. Positive and negative wind speeds means north-to-south and south-to-north directions, respectively. Figure 2(b) is the same as Fig. 2(a), but for the west-east component. Positive and negative wind speeds mean west-to-east and east-to-west directions, respectively. As shown in Fig. 2, the wind speed estimated from the wind-profiler data is less than that estimated from the radiosonde data. This difference is due to the clutter effect. Figures 3(a) and 3(b) are the same as Figs. 2(a) and 2(b), respectively, but with clutter rejection, and they show closer correspondence between the wind-profiler-derived and radiosonde-derived wind speeds.

A wind profiler with a RASS can measure the vertical profile of temperature, and a comparison of wind-profiler-derived and radiosonde-derived profiles was made in Thailand on the 17th and 18th of December 1994. The wind profiler measured from heights of about 0.15 km to about 4.65 km with 75-m range resolution. Figure 4 shows a scatter-diagram of the virtual temperatures (T_V) derived from radiosonde data and from data obtained using a wind profiler with a RASS. The Doppler spectrum of the RASS echo can not be detected at heights more than about 1 km. A wind profiler with a RASS can measure the virtual temperature with a accuracy of 0.82 ℃.

4. Discussions

The clutter spectrum was canceled by software-based clutter rejection, and the horizontal wind vector was well estimated. The vertical wind velocity will be quite close to the clutter spectrum around zero wind speed, so that this software-based clutter rejection will not well operate for estimating the vertical wind velocity. However, this can not be checked because wind profiler is a unique instrument to measure the vertical wind velocity. That is, there is no reference data.

The temperature profile measured by a wind profiler with a RASS will be useful in developing an algorithm for estimating heat flux from remotely sensed data, but these temperature profile measurements will be reached to heights of less than 1 km. Higher than this, the variance of the vertical wind velocity or radar received power will be used to estimate the heat flux.

5. References

1) W. M. Angevine, D. A. Carter, W. L. Ecklund, and K. S. Gage: Temperature Profiling Using 915 MHz Wind Profiler with RASS, Extended Abstracts of Second International Symposium on Tropospheric Profiling, pp. 43–44, 1991.
2) G. Peters and H. J. Kirtzel: Measurements of the Flux Diffusion Coefficient on Momentum in the Lower Atmosphere, Extended Abstracts of Second International Symposium on Tropospheric Profiling, pp. 97–98, 1991.
3) H. P. Kalmus: Doppler Wave Recognition with High Clutter Rejection, IEEE Trans., Vol. AES–3 in Supplement, No. 6, pp. 334–339, 1967.

6. Publications

① Oral presentations

1) Y. OHSAKI and M. KANESHIRO: Data Analysis of Lower Atmosphere Measurements with a Wind Profiler, Proc. 20th Remote Sensing Symposium conducted by SICE, pp. 39–42, 1994.
2) Y. OHNO, Y. MASUDA and K. NAKAMURA: Boundary Layer Measurements Using a 1357 MHz Wind Profiler, Extended Abstracts of Third International Symposium on Tropospheric Profiling, pp. 310–312, 1994.
3) Y. OHNO, A. MANYAON, N. LEELARUJI, N. HEMMAKORN and Y. MASUDA: Tropical Boundary Layer Observations using Lower Atmosphere Observation Radar in Thailand, Proc. Second International Study Conference on GEWEX in Asia and GAME, pp. 121, 1995.

7. International Cooperation

A wind profiler with a RASS is operating at KMITL in Thailand to study the atmospheric phenomena in a tropical region. This research is a joint project between CRL and KMITL and is sponsored by the Ministry of Posts and Telecommunications.

和文アブストラクト

通信総合研究所が開発したウィンドプロファイラは、当研究所の沖縄電波観測所とタイのモンクット王工科大学において運用されている。ウィンドプロファイラは、大気乱流からの散乱波を受信することにより、風の三次元ベクトルの高度分布を観測することができるドップラレーダである。本報告では二つの研究成果について述べる。はじめは、ソフトウェアによるドップラスペクトラム中のクラッタ除去について述べる。そして、ウィンドプロファイラにRadio Acoustic Sounding Systemを併用して観測した気温高度分布の精度について述べる

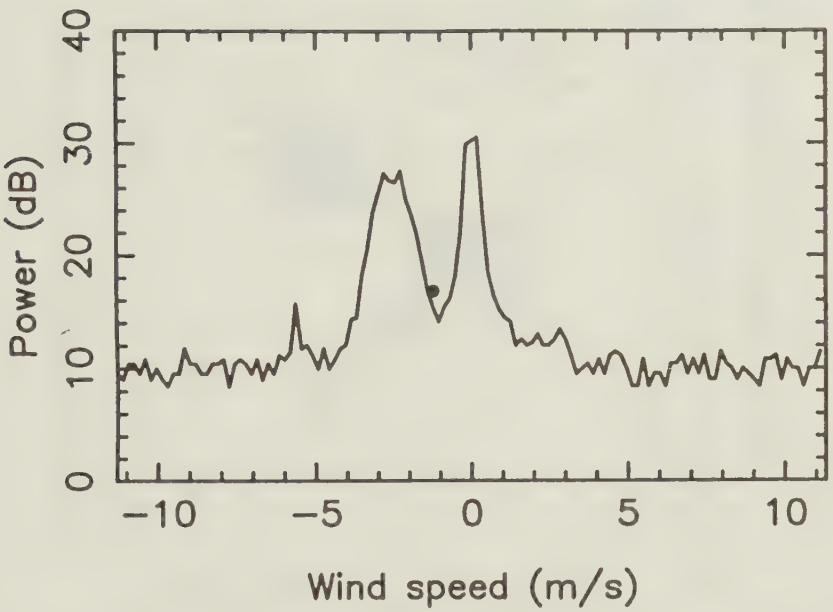

Fig. 1(a). An example of the wind spectrum measured at 0937 LT on December 4, 1992. Azimuth and zenith angles are 225 and 10 degrees, respectively, and the measurement range is 0.9 km. The closed circle the mean wind speed estimated from a first-moment calculation.

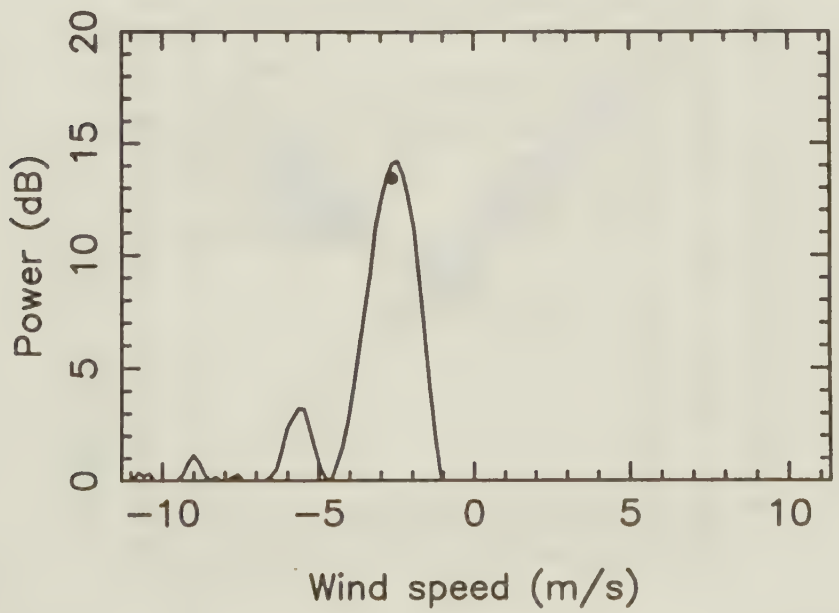

Fig. 1(b). Same as Fig. 1(a) but with clutter rejection and plotted as 5-point running average.

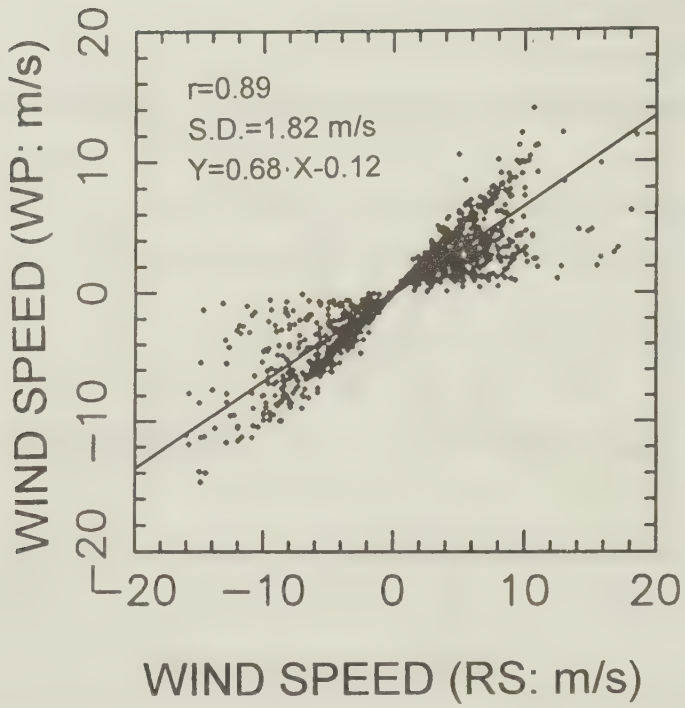

Fig. 2(a). North-south component of wind speed derived from radiosonde (RS) data and from wind-profiler (WP) data without clutter rejection. Positive and negative wind speeds mean north-to-south and south-to-north directions, respectively. The equation of the least-squares-fitted line is also shown (r = correlation coefficient, and S.D. = standard deviation).

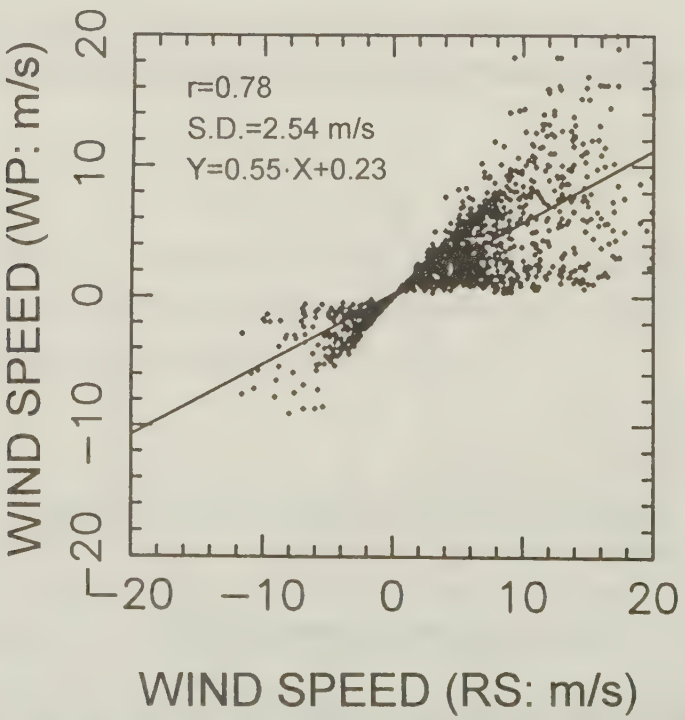

Fig. 2(b). Same as Fig. 2(a) but for the west-east component. Positive and negative wind speeds mean west-to-east and east-to-west directions, respectively.

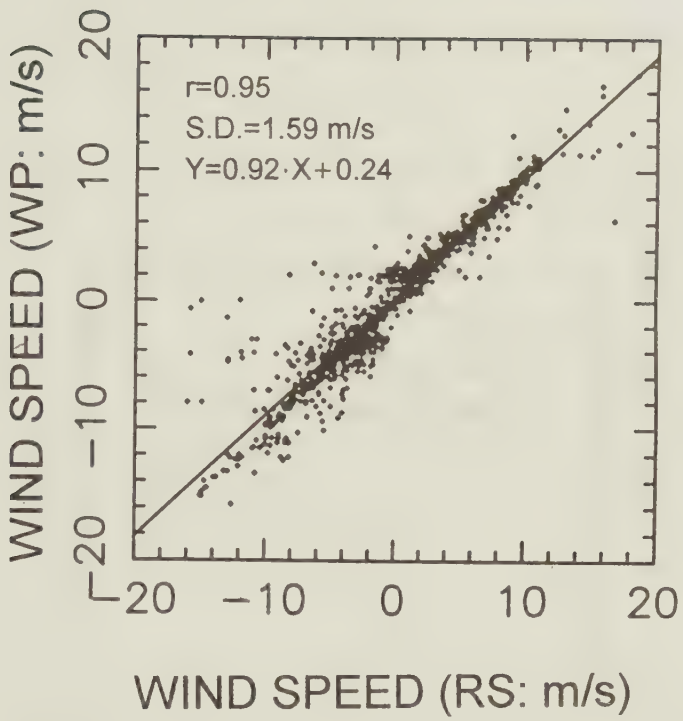

Fig. 3(a). Same as Fig. 2(a) but with clutter rejection.

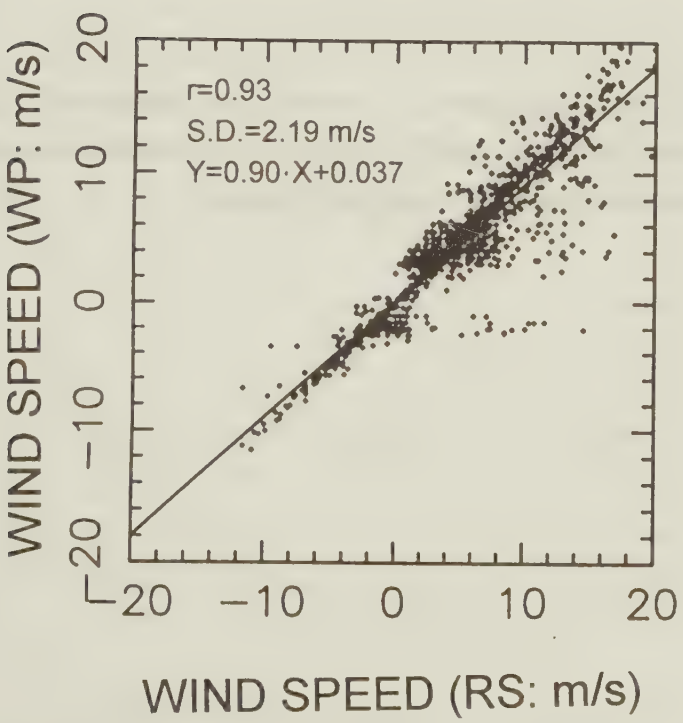

Fig. 3(b). Same as Fig. 2(b) but with clutter rejection.

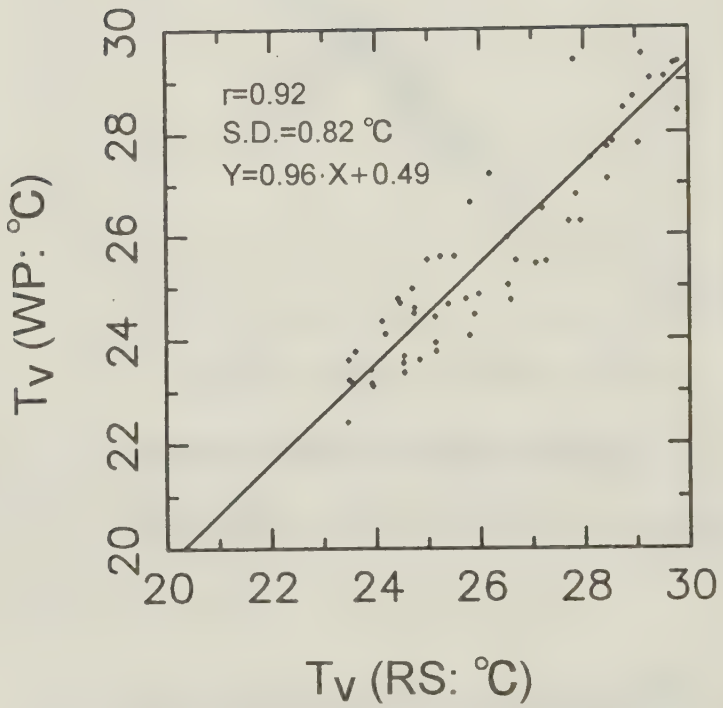

Fig. 4. Scatter-diagram of virtual temperatures (T_V) derived from radiosonde (RS) data and from data obtained by a wind-profiler (WP) with a RASS. The equation of the least-squares-fitted line is also shown (r = correlation coefficient, and S.D. = standard deviation).

I. Observation and Analysis on the Process of the Atmosphere-Ocean-Land Interactions

3. Observation and Analysis on the Process over the Land

(3) Analysis on Environmental Conditions and Snow-Ice Cover Changes Affecting Monsoon Cycle in Asia

National Research Institute for Earth Science and Disaster Prevention, Science and Technology Agency

S.Yazaki, K.Nakane, T.Morohosi, S.Kishi

(Abstract) The mode of Asian monsoon activities is said storongly affected by the environmental conditions of the area especially SST of Indian ocian and snow-ice cover over the continent. This study aims to make clear the relation between the both mainly by analyzing satellite data.

1.Objective

It is commonly known that the Asian monsoon activity is largely affected by the see surface condition of the Indian Ocean and the west Pacific Ocean and the snow cover on the Euro-Asian continent. And the rainfall sutimulated by the monsoon gives much influence to the amount of water resource, disasters and vegetations. The objective of this study is first to detect various earth surface conditions: sea surface temperature, land surface temperature, vegetation index, snow cover, sea ice, cloud top temperature, soil moisture and so on with analizing various kind of polar orbital earth observation satellites data. And the target is to clearify the relationship between those conditions and monsoon activity.

2.Method

(1) NOAA AVHRR/GAC original data are geometrically corrected then synthesized over the range:30E to 160E, 20S to 60N. The synthesized satellite image data are made in every 7 days and archived. Algolisms to detect above mentioned conditions are developed. The system to make the land condition images with the synthesized satellite images through the algolisms for each items is developed.

(2) Precise Analysis of snow-ice condition over Tibetan-Himarayan area with LANDSAT/TM data and MOS-1/MESSR data.

(3) Annual and seasonal change of the environmental conditions is analized with the image data archives. The relationship between those conditions and monsoon activity especially rainfall characteristics is clearified.

3. Result

(1) The method to detect and monitor snow cover change in Himarayan area with NOAA AVHRR data is improved. For the monitoring of snow cover change with satellite data, it is important to detect snow automatically and with high accuracy from cloud contaminated image. Most of cloud is distinguishable from snow by using visible and thermal band information. But some of the cloud still remains undistinguishable by spectral information alone. Cloud boundary generally move faster than that of snow. The new method is to utilize both spacial and temporal information besides spectral one to remove cloud. The AVHRR/HRPT data offerd by Satellite Meteorological Center(SMC)/China Meteorological Administlation are used for this study.

(2) A method for resolution improvement of NOAA AVHRR/GAC data with HRPT data are developed. The method is to get temporal variation information from coase GAC data(resolution:4km) and precise spacial variation information from HRPT data(resolution:1km). Only one clear HRPT data are neccesary for every season.

The several existing methods are examined and improved for our pourse and sufficient result are obtained. This study was carried out as a cooperative research work between NIED and SMC . The HRPT data used for this study was recieved and processed by SMC.

(3) Seasonal and annual changes of glacial lakes in Himarayan area since 1972 are analized with LANDSAT/MSS,LANDSAT/TM and MOS-1/MESSR data. Among many lakes in the area two representative lakes are analized. By making color composit images with visible, near infrared and thermal infrared bands, four lake surface states: clean water, muddy water,frozen and snow covered are found distinguishable. By analizing the same lake for nearly twenty years, change of its shape can be monitored.

4. Discussions

We are concentrating our study field to snow-ice condition in Tibet and Himaraya area. For snow cover detection the spacial resolution of GAC is not sufficient and time interval of data of 7 days is also too long. So we are investigating an utilization of every day's HRPT data of the area recieved and

processed by SMC.

5. References

None

6. Publications

Sheng, Yazaki, Zhu: Method on resolution improvement of NOAA AVHRR/GAC data in Asian monsoon studies, China-Japan workshop on Asian monso on mechanism, Beijin, Sept., 1994

7. International cooperation

We are sharing one sub-subject "The analysis of environmental conditions and snow-ice cover changes affecting monsoon cycle in Asia" with Satellite Meteorological Center, PRC under the bilateral research project "Japan-PRC cooperative program on Asian monsoon"

One researcher of our research group visited SMC and we invited one researcher from SMC to promote coorerative research.

We and SMC are also continueing cooperative measurement of soil moisture in Hubei province, China.

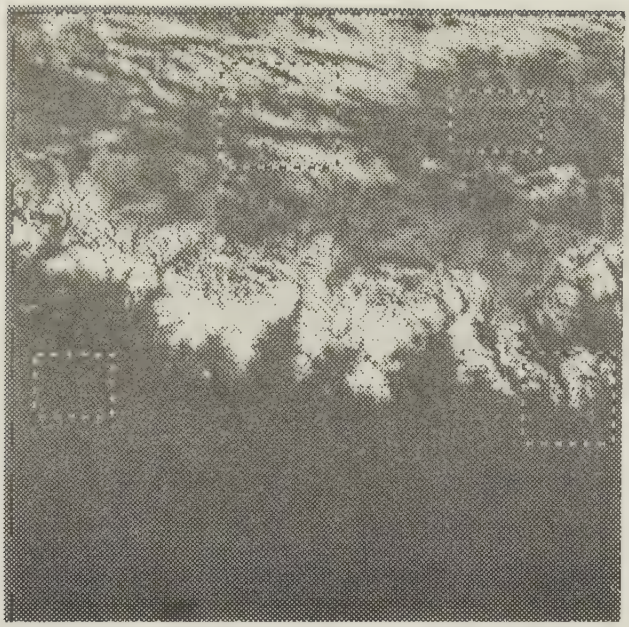

(a)

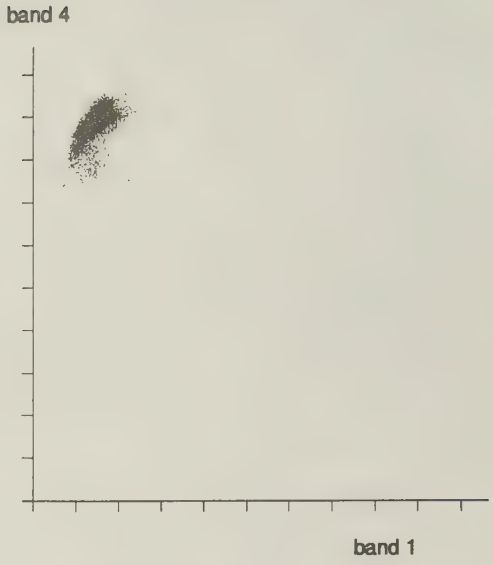

(b)

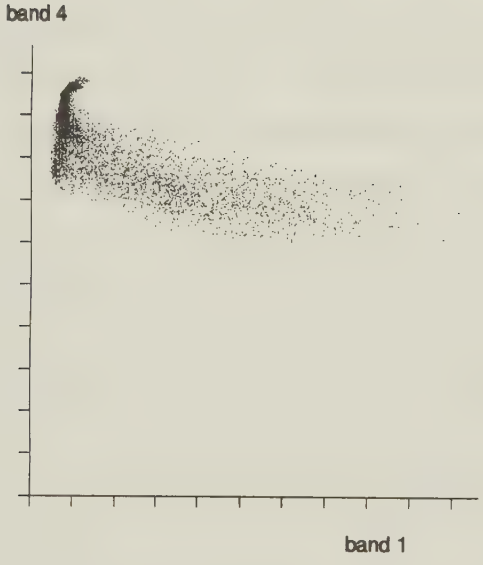

(c)

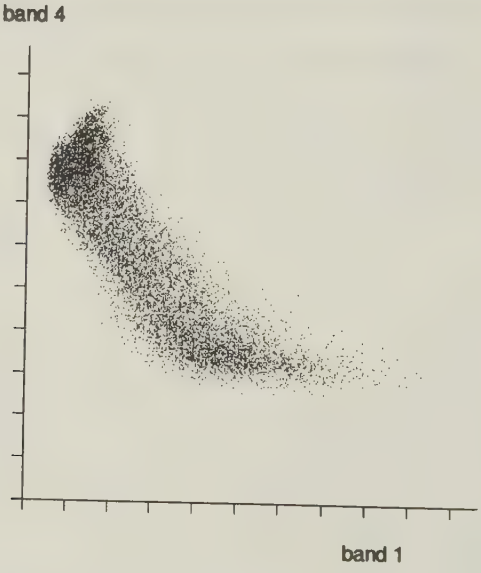

(d)

Fig.1 Distribution in Feature Space of Visible Band(Band 1) and Thermal Band(Band 4)

(a) Training areas

(b) Land(no Snow, no Cloud)

(c) Land and Snow (but no Cloud)

(d) Land and Cloud (but no Snow)

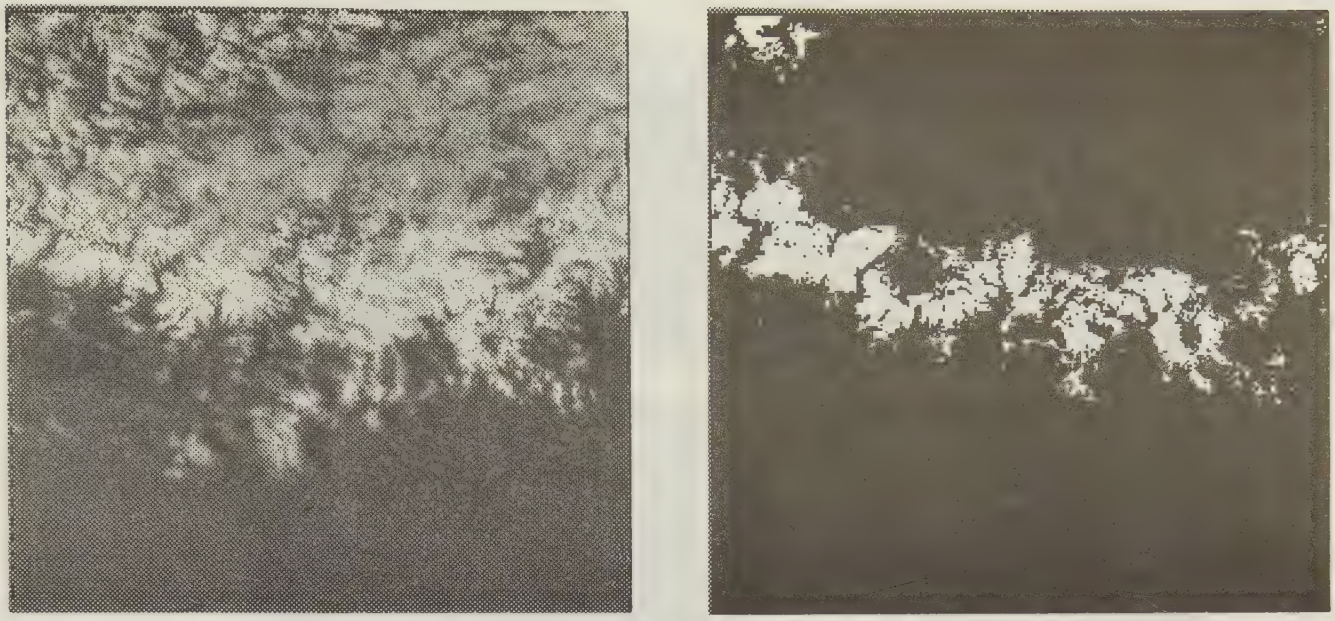

Fig. 2 Cloud contaminated image(left)
and detected snow covered area(right)

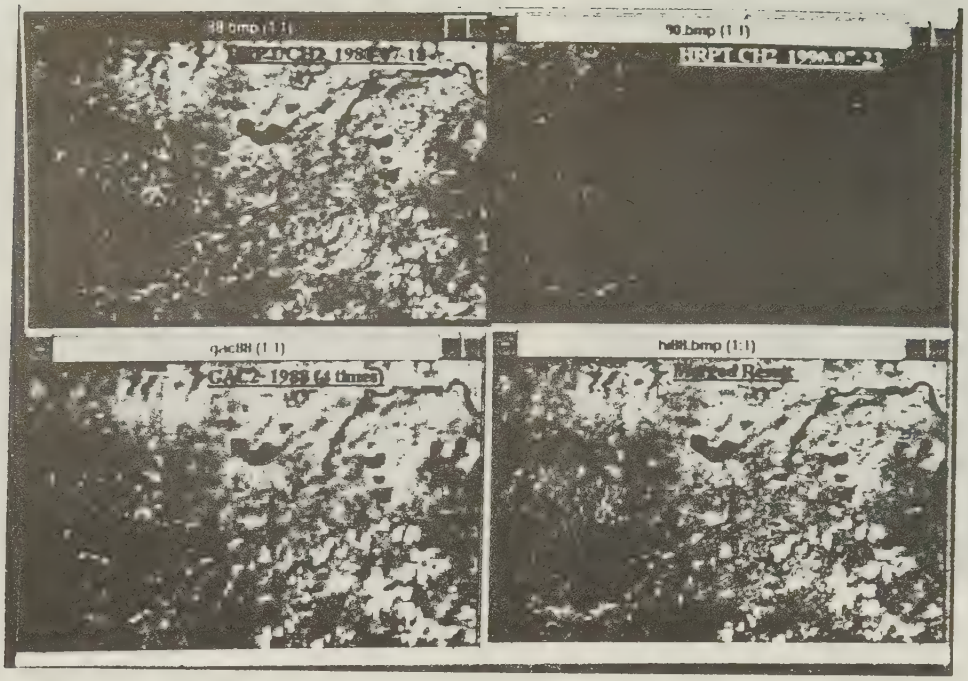

Fig.3 Resolution improvement of GAC image using HRPT image

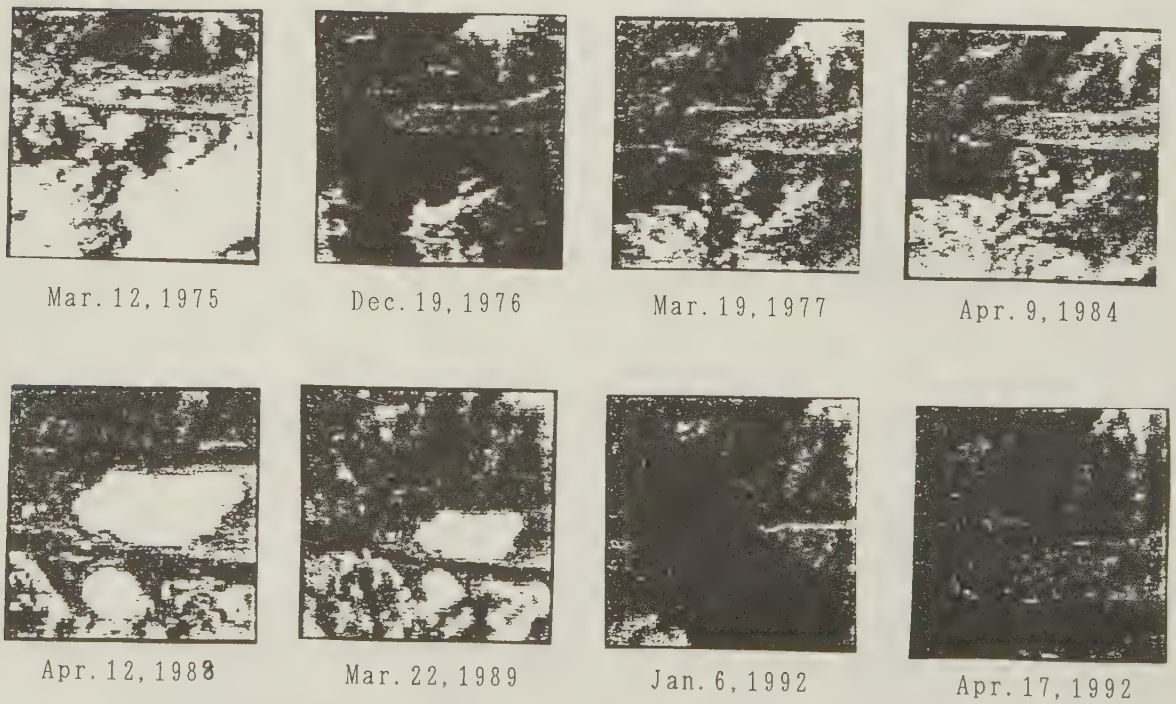

Fig.4 Annual change of Imjya glacial lake in Himaraya by Landsat/TM (1975-1992)

I. 大気・海洋・陸域間相互作用の諸過程に関する観測・解析研究

Observation and analyses on the process of the atmosphere-ocean- land interactions

3．陸域における諸過程に関する観測・解析研究

Observation and analysis on the process over the land

（4）地域水収支に関する解析研究

Analytical study of water balance on representative river basins

科学技術庁防災科学技術研究所

岸井　徳雄、葛葉　泰久、矢崎　忍

杉田　文（客員研究官）

National Research Institute for Earth Science

and Disaster Prevention,

Science and Technology Agency

T. Kishii, Y. Kuzuha, S. Yazaki

and F. Sugita (Visiting researcher)

(Abstract)

The activity of Asia monsoon is influenced by water cycle and the change of water cycle affects Asia monsoon. This study aims to clarify water balance of the regional scale in China. For this purpose hydrological data base, the elements, that is precipitation, runoff, evaporation, temperature, humidity wind velocity and radiation have been collected. Using this data base rainfall and runoff relation are analyzed. Further more the experimental basin was established and the detailed analysis of water balance on the basin has started.

This report shows the result of the analysis on the evapotranspiration and discharge-duration curves in the basin. The source of data is "The monthly meteorological data in China(1987)".

The result is following. The annual rainfall loss of the basin is 800 mm and the potential evapotranspiration also shows similar value. But there are a difference between both values in the seasonal change. The amounts of the potential evapotranspiration range from 3.8 mm/month in winter season and 161 mm/month in summer season. The discharge-duration relation has a tendency that the larger the basin area, the smaller the x day runoff. The amounts of the runoff of 355 day runoff are 0.069 to 0.187 mm/month that correspond basins area from 1.2×10^5 km^2 to 1.0×10^4 km^2. The smallest basin area corresponds that of the Tone River in Japan.

1. Objectives

The activity of Asia monsoon is influenced by water cycle and the change of water cycle affect Asia monsoon. This study aims to clarify water balance of the regional scale in China. For this purpose hydrological data base, the elements, that is precipitation, runoff, evaporation, temperature, humidity wind velocity and radiation have been collected.

This report shows the change of the seasonal evapotranspiration and the state of the discharge (flow) conditions in the representative basin, that is, Huai He River Basin.

2. Methods

The discharge data for this analysis used here were given by the Remote Sensing Technology Center, Department of Water Resources in China. Four discharge stations are selected in the middle to upper stream in the Huai He River. The location of the station are shown in the Fig. 1.

Data of temperature for the calculation of potential evapotranspiration come from "The monthly meteorological data in China(1987)". are used. The stations for the temperature used here are indicated as white circles in the Fig. 1. The "Thornthwaite method" is used for the calculation of evapotranspiration.

3. Results

The result of the calculation of potential evapotranspiration is following.

Monthly potential evaporation ranges from 1.21 mm/month in January to 166 mm/month in four stations. Monthly temperature of five stations ranges from 1.5 ℃ to 27.3 ℃ in 1987. The averaged values of evapotranspiration of the stations corresponds to 3.77 mm/month to 161 mm/month as shown by Fig. 2.

The flow regime is analyzed by use of the discharge - duration curve in 1987. The station analyzed are Paupu(basin area:121,330 km^2) , Rutai(88,630 km^2), Huaipin(16,005 km^2) and Shishen(10,190 km^2) indicated as Fig.1. The runoff (mm/day) of 95 day, 185 day, 275 day and 355 day are calculated. The results are shown by Fig. 3 to Fig. 6 and Table1. For example, the 95 day runoff (mm/day) of each stations become to 0.997, 1.209, 1.555 and 1.543.

4. Discussions

The potential evapotranspiration of the year has the value of 830 mm. The rainfall loss from the estimation by water balance is 808 mm. So both values show similar one in annual period. But the value in winter season is considerably smaller than that of the value

balance method. So it is estimated that the seasonal value is different to the observed one.

The flow regime shows the tendency that the larger basin areas becomes, the larger x day runoff is. The ratio of 95 day runoff to 355 day runoff is about nine times in Huapin. That ratio of the Tone River basin in Japan, similar area of the Huaipin, is about twice. So the flow regime of the Huai He River is unstable as compared with the Tone River.

5. Publications

T. Kishii and S. Cao : Water balance of Huai He River in China. IAHS/IAMAS Workshop HJW3, XXI General Assembly of IUGG 1995.

6. International Cooperation

Information exchange and discussion about cooperative research were carried out by invitation to our institute on March 1995. One researcher was invited from "Remote sensing technology application center", Ministry of water resources in China

要約

アジアモンスーンの変動は、アジア地域の水収支に大きな影響を及ぼし、同時に水収支の変動は、アジアモンスーンに影響を与える。本研究の目的は、この水収支の特性を明らかにするためであり、同時に水文データベース作成のため、降水、流出、蒸発、気温、湿度及び風速等のデータが収集された。さらに詳細な水収支解析を行うため、淮河代表流域が設置された。

本報告は、淮河代表流域における蒸発散の季節変化及び流況について解析したものである。

その結果、水収支解析による年損失は、800mmであり、ほぼ、可能蒸発散量に等しい。 ただし、季節毎、特に冬期における両者の差は大きい。

又、流況曲線を利用した解析の結果、流域面積の増大と共に、流況は良くなる。、95日流量と355日流量との比は、ほぼ、9である。わが国の利根川では、ほぼ2であり、淮河代表流域は、利根川に比べ流況は良くない。

図１．淮河流域と水文観測点（C:蚌埠,B:魯台子,F:淮濱,H:息县）
FIG.1 Huai He River basin and hydrological stations
(C:Paupu,B:Rutai,F:Huaipin,H:Shishen)

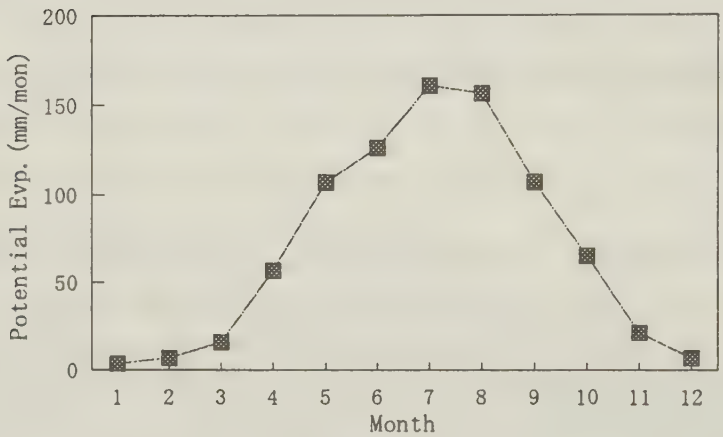

図２Paupu 上流域の可能月蒸発散量(1987年)

Fig. 2 Monthly potential evapotranspiration on the upstream basin at Paupu(1987)

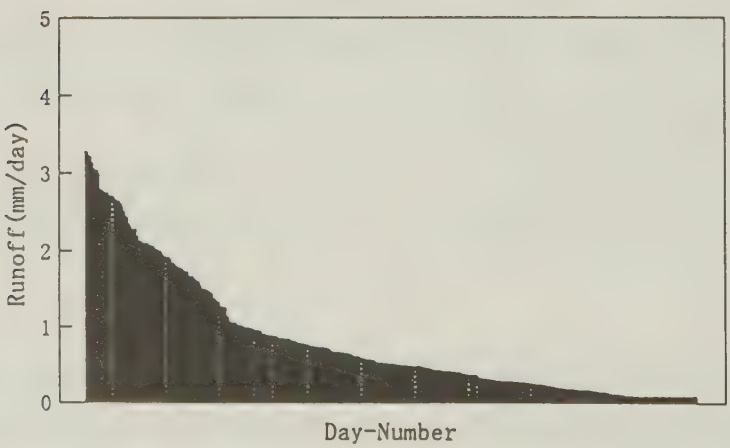

図３Paupu 地点の流況曲線(1987年)

Fig. 3 Discharge duration curve at Paupu (1987)

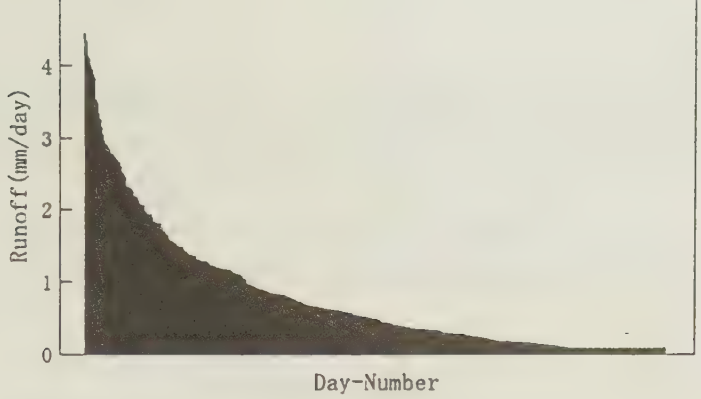

図 4 Rutai 地点の流況曲線(1987年)

Fig. 4 Discharge duration curve at Rutai (1987)

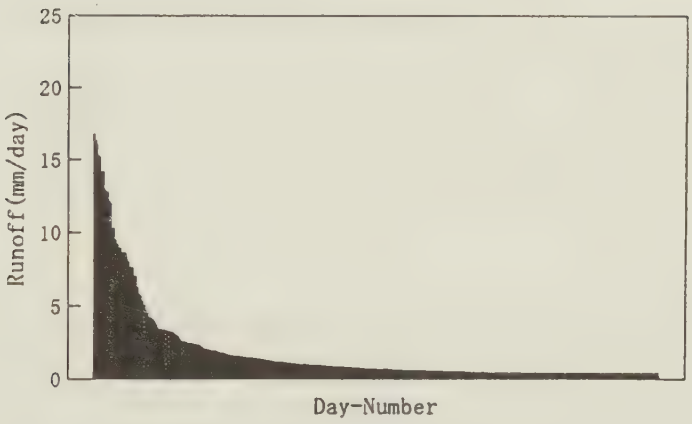

図 5 Huaipin 地点の流況曲線(1987年)

Fig. 5 Discharge duration curve at Huaipin (1987)

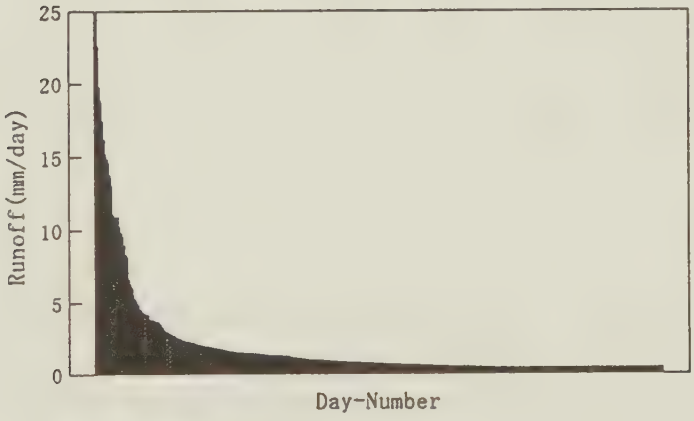

図 6 Shishen 地点の流況曲線(1987年)

Fig. 6 Discharge duration curve at Shishen (1987)

図 7 淮河代表流域の流況一覧

Table 1 Discharge - duration values of four stations in the Huai He River in China.

	C:Paupu	B:Rutai	F:Huaipin	H:Shisen
95 day runoff	0.997	1.209	1.555	1.543
185 day runoff	0.512	0.601	0.724	0.752
275 day runoff	0.241	0.268	0.449	0.433
355day runoff	0.069	0.094	0.172	0.187

II. 数値モデルによる4次元資料同化システムの開発に関する研究

Development of the four dimensional data assimilation (4DDA) system by the use of numerical model

1. --4次元資料同化システムによって評価した水循環--

--Global water circulation estimated through the 4DDA system --

気象庁　予報部
岩崎俊樹、隈健一
気象庁　気象研究所
中沢哲夫、柴田彰
Forecast Department,
Japan Meteorological Agency
Toshiki Iwasaki, Ken-ichi Kuma
Meteorological Research Institute,
Japan Meteorological Agency
Tetsuo Nakazawa and Akira Shibata

Abstract

For the purpose of understanding the physical mechanism of the Asian monsoon, a dataset of describing global water circulation is compiled from the 4-dimensional data assimilation (4DDA) products at the Japan Meteorological Agency. It reasonably presents significant diurnal variations over the south-east Asia and could be useful for the monsoon reseaches.

To improve the 4DDA system, a preliminary validation is made of this dataset. The long-term water balance represented by the 4DDA products weakly breaks down due to systematic difference between the objective analysis and the first guess in the 4DDA system. The discrepancy arises from sparsity of moisture observation data and systematic errors of the numerical weather prediction (NWP) models. We must develop methods of retrieving the global moisture field from satellite observations and reduce model climatic drifts of the NWP model.

1. Objectives

As was studied by many scientists, water circulation is one of the key factors to understand the Asian summer monsoon. Land-sea heat contrast and high mountain range induce large moisture convergence and then enormous precipitation occurs south-east of the Asia. This is the world-wide convection center and an important thermal forcing of driving the atmospheric general circulation. The Asian monsoon has temporal transitions such as an onset characterized by the low-level flow change from easterlies to westerlies. In addition, it has a diurnal cycle, in which evaporation, moisture divergence and precipitation link with each other successively. Thus, the monsoon research must place high priority in the construction of high quality dataset of water circulation.

In this work, we compile a dataset of global water circulation from the four dimensional data assimilation (4DDA) system at the Japan Meteorological Agency (JMA). The 4 DDA system produces a uniformly-spaced and well-defined meteorological and hydrological parameters through the objective analyses and model diagnostics. This dataset will be used for understanding the mechanism of the monsoon and for upgrading the long-range forecasts. We

are also planning to distribute these data to scientists participating in this project.

The 4DDA system, however, is seriously subject to sparsity of observation and forecast errors. In particular, the Asian summer monsoon is very complicated phenomena to be carefully analyzed. In the early stage of this project, we intend to refine the 4DDA system based on detailed validation of its products.

Here, a preliminary validation study is made of a dataset of water circulation obtained through the 4DDA system. First, consistency of long-term water balance is checked, which shows systematic differences between the first guesses and observations. Secondly, objective analyses of total precipitable water are compared with the SSM/I-derived data. The SSM/I data, which is not used in the operational analysis, may give independent information on the performance of the 4DDA. In the 4DDA system, the analyzed fields depend on the NWP model through the first guesses. Among many parts of the NWP model, we study sensitivity of moisture analysis to the cumulus parametrization scheme. Finally, future plans of improving the 4DDA system are discussed in accordance with this validation study.

2. Methods

Since March 1994, we have been compiling a dataset of precipitable water amount (TPW), vertically-integrated horizontal water vapor flux (**F**), precipitation rate (P) and evaporation (E) at every 2.5*2.5 latitude-longitude grid from the 6-hourly 4DDA products. These are complete enough to check the following atmospheric water balance in a column-integrated form;

$$TPW(t_2) - TPW(t_1) = \int_{t_1}^{t_2} \left(- \nabla \cdot \mathbf{F} - P + E \right) dt. \qquad (1)$$

In this analysis, vertical integrations of precipitable water and horizontal water vapor flux are not estimated from objective analysis at mandatory pressure levels but from η-level (model-level) data. Because the model-level data can represent the conservation of water substances much better than the mandatory-level data, including topographic effects and boundary-layer effects. To assess the water balance based on the equation (1), water vapor flux, precipitation and evaporation should be accumulated during the time interval of forecast-analysis cycle. The P and E are accumulated in the NWP model. In the current system, the water vapor flux **F** is not accumulated. Instead, it is estimated from snap shots of 6-hour forecasts. It may cause random errors in the water balance. In the next system starting from 1996, we will store the accumulated value of moisture flux **F**.

In this work, we figure out the long-term water balance (1) evaluated from the 4DDA products in 6-hourly forecast-analysis cycle. There appears residual terms (2) due to systematic differences between the first guesses and analysis, so-called ' analysis increment'. That is,

$$\begin{aligned} \text{Residual} &= TPW(t_{n+1},\text{anal}) - TPW(t_1,\text{anal}) - \sum_{k=1}^{n} \int_{t_k}^{t_k+6} \left(- \nabla \cdot \mathbf{F} - P + E \right) dt \\ &= TPW(t_{n+1},\text{anal}) - TPW(t_1,\text{anal}) - \sum_{k=1}^{n} \{TPW(t_k+6,\text{fore}) - TPW(t_k,\text{anal})\} \\ &= \sum_{k=2}^{n+1} \{TPW(t_k,\text{anal}) - TPW(t_k,\text{fore})\} \end{aligned} \qquad (2)$$

where 'anal' and 'fore' indicate objective analyses (initial condition) and 6-hour forecast (the first guess), respectively. The systematic biases of the NWP model and observation cause imbalance in the water circulation reproduced from the 4DDA products.

In the current objective analysis, moisture data is very sparse especially over the ocean. In data-sparse regions, the objective analysis must be affected by the first guess and needs validation with independent observations. Recently, total precipitable water retrieved from the SSM/I is n ade available. We validate the total precipitable water obtained from the 4DDA products with that from the SSM/I.

3. Results

Figure 1 shows diurnal cycles of precipitation, moisture flux divergence and evaporation averaged over 3 months, June, July and August. Around the monsoon Asia, precipitation has a large diurnal cycle with its maximum in the evening, where the moisture is mainly supplied by convergence. Possibly, the diurnal cycle around the monsoon Asia may play an important role in the atmospheric global circulation.

To check consistency of the atmospheric water balance, Fig. 2 shows monthly averaged zonal mean of each term of the equation (1) in May 1994. Missing or excessive budgets arise from analysis increments. In mid-latitudes, the first guesses of total precipitable water may be lager than observations and then excessive water is removed in the objective analysis. The NWP model may have systematic errors, contradict with the observation and bring the imbalance of water circulation. Sometimes, observations also have systematic biases. Then, the 4DDA products should be validated with independent observations.

The analysis of total precipitable water is compared with that from the SSM/I. Figure 3 shows monthly means of SSM/I-derived (top) and analyzed (bottom) total precipitable water around the tropical Pacific region in July 1994. East of 170W, near the ITCZ and SPCZ total precipitable water obtained from the 4DDA is overestimated in comparison with the SSM/I data. This kind of error is not found west of 170W. The difference between the eastern and western sides of 170 W is attributed to the moisture data retrieved from the GMS (Geostationary Meteorological Satellite) infrared images (Baba[1], 1987). Outside of the GMS observing area (east of 170W), we get temperature observation from the SATEM but few data of the moisture over the ocean. There appear unrealistic feedbacks between the observed temperature and the first guess of relative humidity , because the current operational NWP model has climate drifts of cooling and moistening biases in the tropics. The SATEM data may correct low-level cooling bias in the objective analysis and activate the convection in the course of time integration. Accordingly, enhanced horizontal convergence increases total precipitable water in the first guess. This feedback is avoidable when moisture observation is simply introduced into the objective analysis.

Figure 4 shows sensitivity of the moisture analysis to cumulus parametrization scheme of the NWP model, where the Arakawa-Shubert (A-S) cumulus parametrization scheme is implemented in the experimental system. Top, middle and bottom panels show 10-day averaged global distributions of total precipitable water obtained through the operational and the experimental 4DDA systems and their difference, respectively. Comparing the experimental 4DDA products with the operational one, analyzed total precipitable water

around the ITCZ is considerably reduced. On the other hand, the moisture is increased off the west-coast of major continents, where the SST is relatively low. The difference between two analyses may be related to the sensitivity of parametrization scheme to the static stability. For performing the more realistic 4DDA products, physics packages of the NWP model must be tuned up to reduce its climate drifts.

4. Discussions

To make detailed analysis of the Asian monsoon, the current 4DDA system should be refined as follows.

1) Increase the number of moisture observations. Satellite measurements have no-doubt to be promising ways of observing global moisture with appropriate retrieved methods. Recently, in the ECMWF, a retrieval method of TOVS data has been developed using one-dimensional variational method and its implementation into the 4DDA system is shown to have positive impacts on the moisture analysis especially over the tropical ocean (Eyre et al.[2], 1993). The implementation of the TOVS is also under development at the JMA. The SSM/I data, which is used only for validation in this work, has a great potential to be assimilated. Unfortunately, the SSM/I data is not distributed in real-time basis. We must establish a real-time data transfer system of the SSM/I data. The SSM/I does not inform us of vertical profile but only of the total precipitable water. For its assimilation, vertical profiles need to be assumed referring to the first guess field.
2) Reduce systematic errors of the NWP model. The 4DDA products are affected by the characteristics of the NWP model through the first guess. In this work, we have shown the sensitivity of moisture analysis to cumulus parameterization scheme of the NWP model. In addition to the cumulus convection, we are investigating physics packages of land-surface process, cloud formation (prognostic cloud fraction and cloud water scheme) and cloud-radiation. These may have large influences on the land-sea contrast and change diurnal variations of the Asian monsoon. In this project, we will examine their impacts on the 4DDA products and long-range predictions of the Asian summer monsoon.

5. References

1) Baba, A., 1987: Improvement of estimation method of moisture data from satellite cloud sounding. JMA/NPD technical report No. 16, 54pp.
2) Eyre J. R., G. Kelly, A.P. McNally, E. Andersson and A. Persson, 1993: Assimilation of TOVS radiance information through one-dimensional variational analysis. Q. J. Meteor. Soc., **119**, 1427-1463.

6. Publications

T. Iwasaki, 1995: An estimation method of atmospheric water balance with 4-dimensional data assimilation., Proceeding of 'Second International symposium on assimilation of observations in meteorology and oceanography', TOKYO JAPAN, 13-17 March, 1995.

（要旨）

アジアモンスーン機構を理解するために、気象庁の４次元資料同化結果に基づいて全球水循環の格子点値のデータセットを作成中である。このデータセットは東南アジア地域の日変化も良く表現しており、アジアモンスーンの研究にとって有益である。

さらに４次元同化システムを改善するために、得られた水循環データの検証を行った。データ４次元資料同化システムにおいて第一推定値と客観解析が系統的に異なるため、このデータによって記述された長期水循環は僅かに収支が合わない。この矛盾は水蒸気データの少なさと予報モデルの系統的誤差によって生じる。全球衛星観測から水蒸気データの抽出方法を開発し、予報モデルの気候値を改善する必要がある。

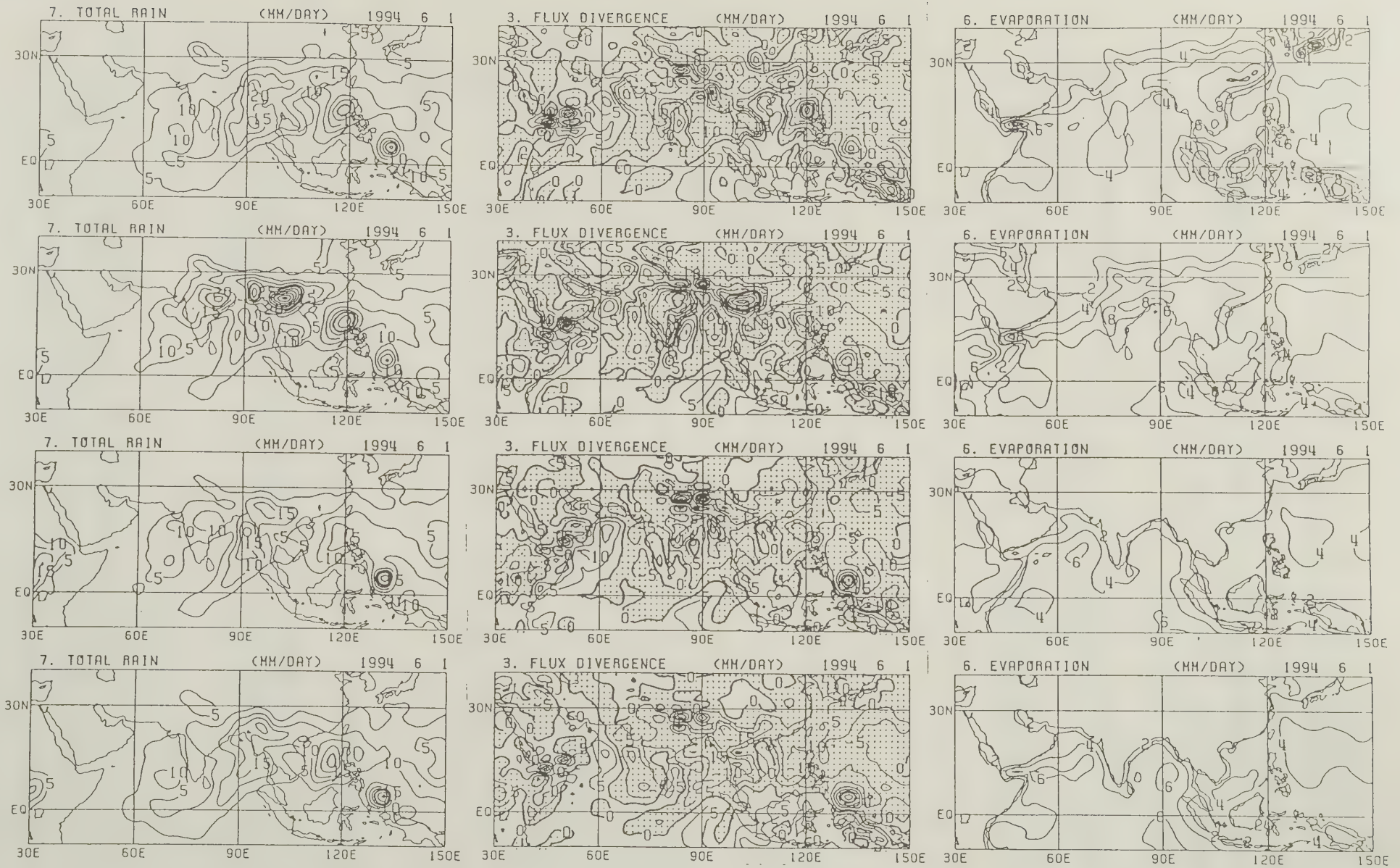

Fig. 1 6-hourly (0-6, 6-12, 12-18 and 18-0UTC) geographical distributions of precipitation (left), divergence (middle) and evaporation (right) averaged over June, July and August, 1994, where contour intervals are 5 mm/day for precipitation and divergence and 2 mm/day for evaporation.

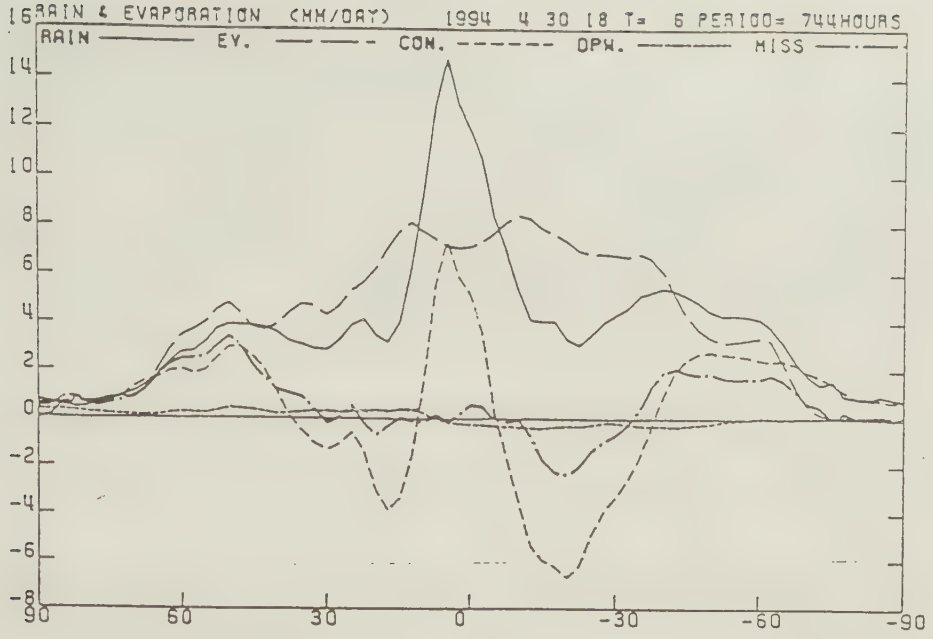

Fig. 2 Monthly averaged (May, 1994) zonal mean tendencies of precipitable water amount due to precipitation, evaporation, horizontal flux convergence, change of precipitable water amount and residual (unit: mm/day).

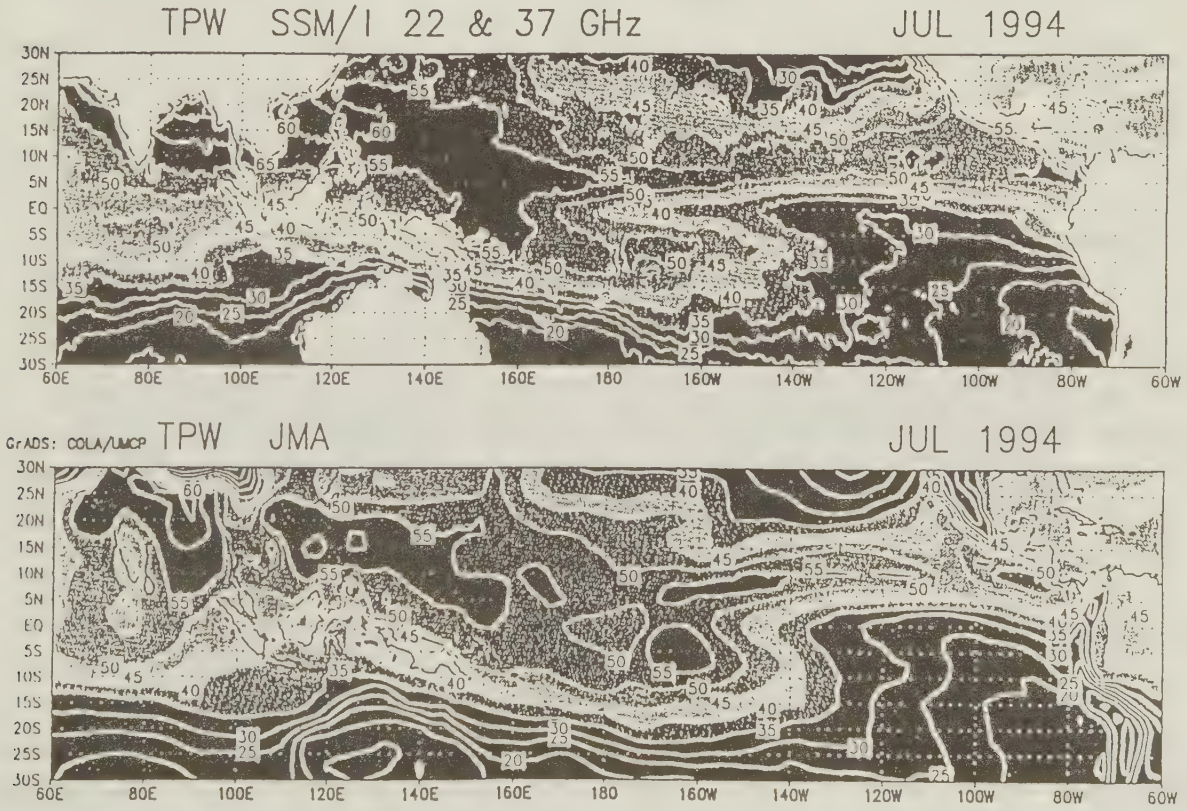

Fig. 3 Total precipitable water (mm) averaged over July 1994. Top and bottom panels show results of SSM/I and 4DDA, respectively.

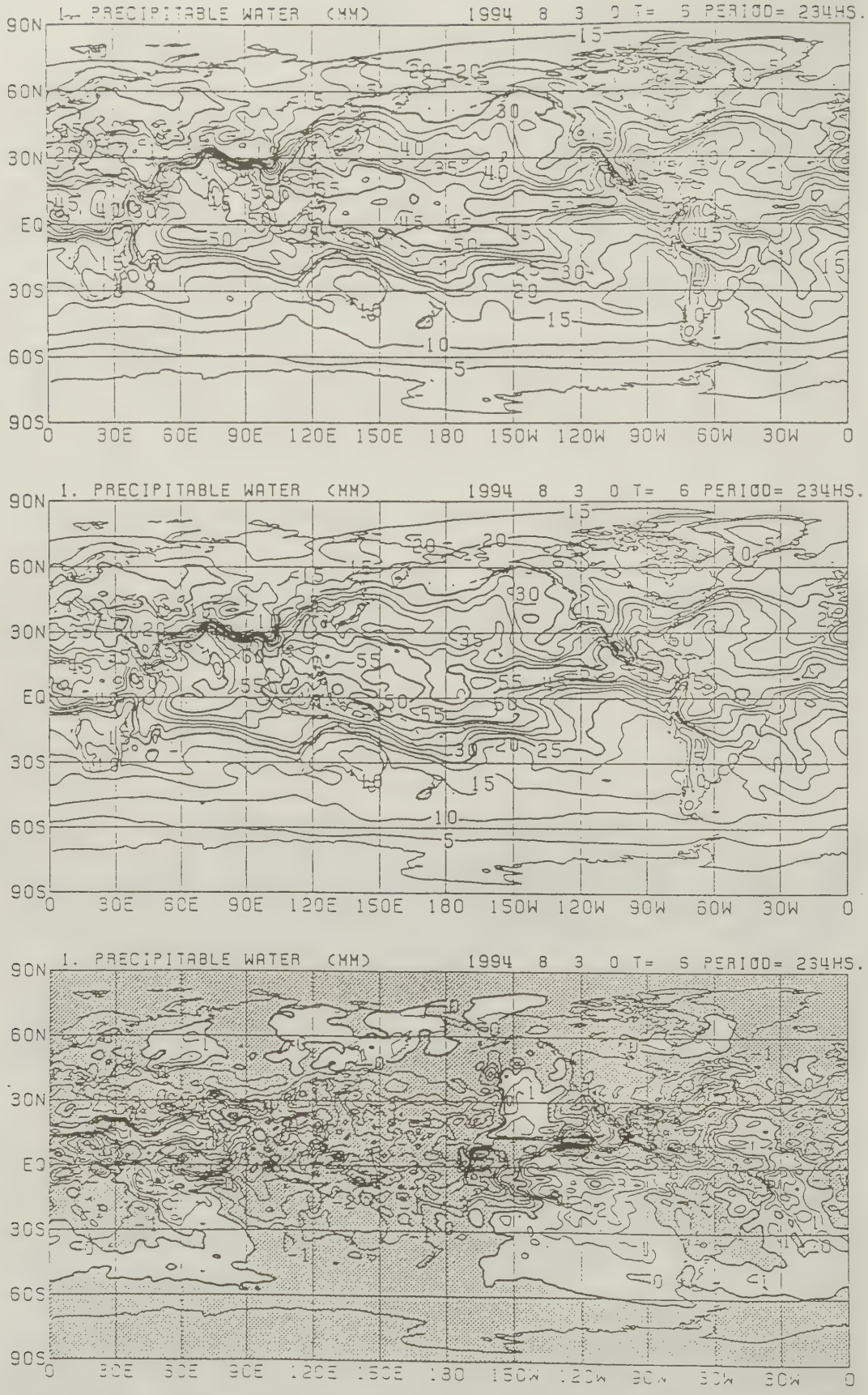

Fig. 4 Total precipitable water (mm) averaged over 10 days from 10 th August. Top, middle and bottom panels show results of experimental and operational 4DDA systems and their difference, respectively. Arakawa-Shubert cumulus convection scheme is implemented in the experimental model, while Kuo cumulus convection scheme has been used in the operational system.

Ⅱ．数値モデルによる大気・海洋・陸域間相互作用の実験研究
Experiment of the atmosphere-ocean-land interactions by the use of numerical models

2．広域水収支モデルの開発に関する研究
Development of water balance model over the wide area

科学技術庁防災科学技術研究所
中根 和郎、幾志 新吉
National Research Institute for Earth Science and Disaster Prevention, Science and Technology Agency.
K. Nakane, S. Kishi

(Abstract) The purpose of this study is to develop the Regional Water Balance Model for assessing the variation of water resources and soil moisture over the wide area due to the fluctuation of Asian Monsoon activity. The model could predict river discharge, water contents in the soil, storage amount of water in the ground, snow deposit, snow melt and actual evapotranspiration on each area with 0.5° x 0.5° in latitude and longitude. The model is made on the basis of the concepts of Tank Model. The prototype of the Regional Water Balance Model had developed and had been applied to Chaophraya River basin in Thailand, where analyzing area is 110 thousand km^2. The results were satisfied, though the dry season and the wet season come alternately in this region. Now, the model is going to be applied to Huaihe River basin in China, where analyzing area is 121 thousand km^2 and Ohyodo River basin in Japan, where analyzing area is 2 thousand km^2.

The model should use huge observed data as input data. It is difficult, however, to acquire the densely data over the wide area, especially evaporation. Therefore, it is necessary to estimate evaporation in wide area by using satellite data. Satellites could observe physical values related with evaporation on the land from the space globally and frequently. Evaporation relates with air-temperature strongly. The air-temperature is derived from split window data of infrared channel on NOAA AVHRR GAC data potentially. Up to this time, the new regression equation estimating the monthly mean air-temperature had been obtained. Now, generalizing the regression equation is curried out for utilizing in various places.

These results in this fiscal year are summarized as follows;
(1) Input data, which are precipitation, evaporation, data set of river system and parameters of the model, have been prepared for applying the regional water balance model to Huaihe River basin in China and Ohyodo River basin in Japan.
(2) Preliminary result of the application to Huaihe River basin were obtained, and simulated river run-off in several points were compared with observed data. Though most of acquired rainfall data located along the river, results of estimation in much rainy year is reasonable. While, results in small rainy year is rather bad.
(3) The new regression equation deriving monthly mean air-temperature has four coefficients. Though, these coefficients are variable from place to place, it was found these coefficients depend on the amount of water vapor in the atmosphere. Relations between coefficients and annual mean water vapor pressure have been obtained. This discovery made the way to apply the regression equation to various places.

1. Objectives

The purpose of this study is to develop the RWB Model(Regional Water Balance Model) with 0.5 degrees x 0.5 degrees resolution. The model is used to assess the variation of water resources and soil moisture over the wide area exactly due to the fluctuation of Asian Monsoon activity. General circulation models are used in general for predicting the climatic change over the world, which could predict not only meteorological conditions, but also hydrological conditions over the land, such as actual evapotranspiration, water contents in the soil, etc. However, these could still not predict the local hydrological regime because of the large grid size of computing by 2 degrees to 5 degrees and simpler modeling hydrological processes over the complicated land. The RWB Model could predict river discharge, water contents in the soil, storage amount of water in the ground as potentially utilizable water, snow deposit, snow melt and actual evapotranspiration on each area with 0.5 degrees x 0.5 degrees in latitude and longitude. The study had started with developing the model. Through applying it to various places, the simulation over the Asian Continent will be carried out as the final goal of this study.

2. Methods

The RWB Model is made on the basis of the concepts of Tank Model(Sugawara, 1984). The Tank Model have been applied to many river basins in the world, such as tropical humid area, snow covered area, semi-arid area, etc. As shown in Figure 1, the RWB Model is composed of four submodels, namely, a discharge submodel, an evaporation submodel, a submodel of snow-pack and snow-melt, and a precipitation submodel. The discharge submodel is composed of many field models and river models. The field models, which are composed of four tanks arranged vertically in series respectively, are applied to each grid areas on simply categorized fields. Field models are four types according to the categorization of fields, such as mountainous type, hilly type, diluvial type and alluvial type. River models composed of one tank are used as the river runoff model on the simplified river system. River models are also three types according to river conditions, such as mountainous type, plain type and swampy type. These field models and river models are coupled like a tree structure. The evaporation submodel calculates the evaporation in a grid area by combining conventional pan-evaporation data at some points and estimated regional evaporation from satellite data. The submodel of snow-pack and snow-melt calculates water equivalent of snow-pack and snow-melt on grid areas using daily precipitation and daily mean air temperature, which has some local factors related to humidity and wind. The precipitation submodel calculates the areal precipitation on grid areas by combining conventional rain-gage data and seasonal patterns of the cloud cover, which are derived from satellite data. Up to this time, the prototype of the discharge submodel had been developed. The submodel had been applied to Chaophraya River basin with 110 thousand km^2 in Thailand. The results were fairly good, though the weather condition in the basin change from dry to wet alternately in annual cycle. Now, the same model are going to be applied to Huaihe River basin with 121 thousand km^2 in China and Ohyodo River basin with 2 thousand km^2 in Japan.

The model should use huge observed data as input data. It is difficult, however, to acquire the densely data over the wide area, especially evaporation. Therefore, it is necessary to estimate evaporation in wide area by using satellite data. Because the satellite could observe physical values related with

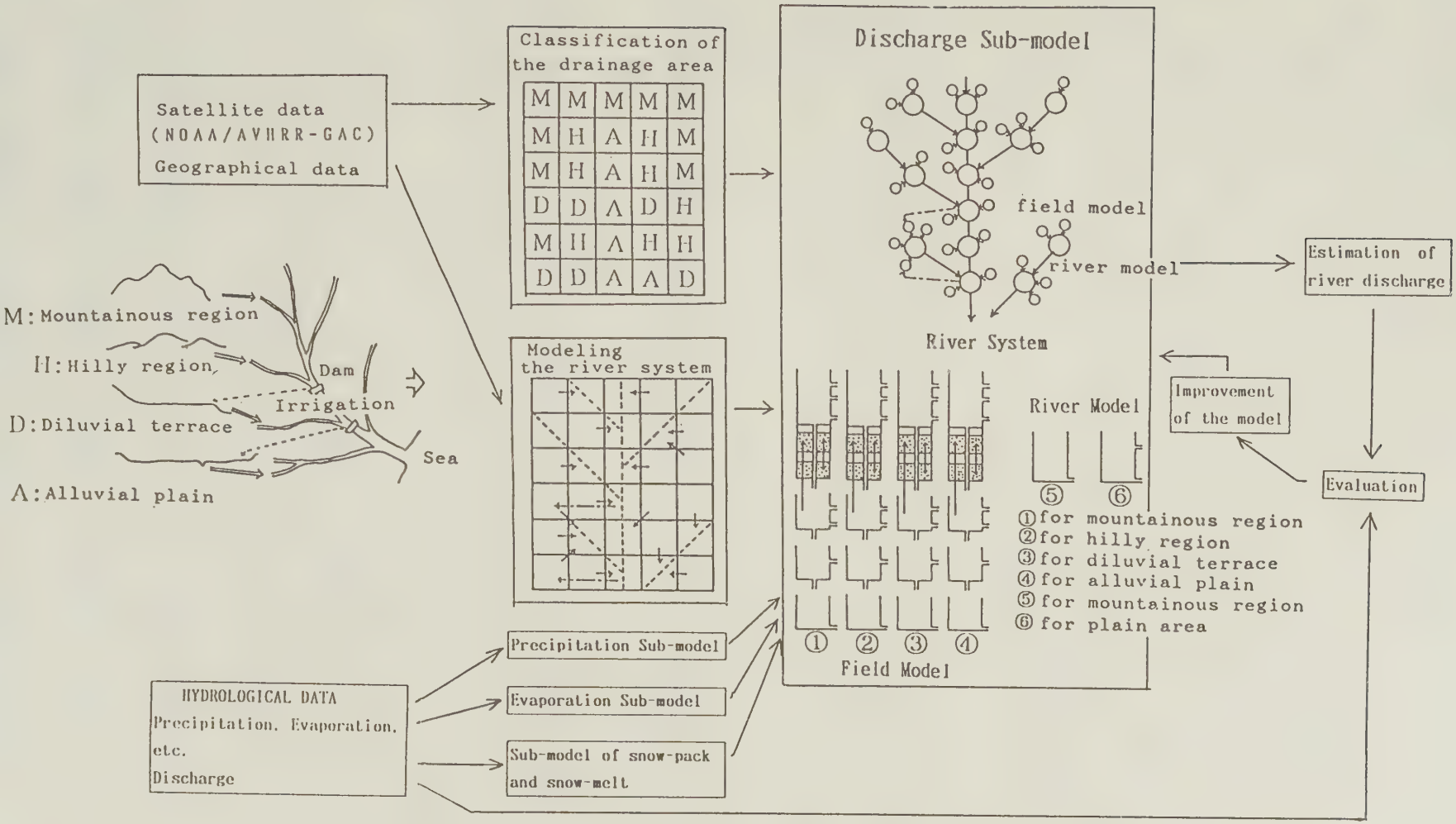

図1　広域水収支モデルの概略
Fig.1 Outline of the Regional Water Balance Model

evaporation on the land from the space globally and frequently. Evaporation relates with air temperature strongly(Thornthwaite, 1948). The air temperature is potentially derived from split window data of infrared channel on NOAA AVHRR GAC data. In our institute(Yazaki, 1990 and Nakane, 1990), W-RSI(Weekly Regional Satellite Image) data covering the area from 60° N to 20° S in latitude and from 30° E to 160° E in longitude are being made from NOAA AVHRR(Advanced Very High Resolution Radiometer) GAC(Global Area Coverage) data in weekly basis, for analyzing land surface conditions related hydrological environment in long terms. The map projection of W-RSI data is a grid coordinate system with 2 minutes equal inter-vals of latitude and longitude. W-RSI data unfortunately contain many cloud, which prevent to transmit information from land surface to satellite due to absorbing radiation and reflection from the land. Therefore, M-RSI(Monthly Regional Satellite Image) data are made by mosaicking data of cloud free area on W-RSI data during a month. M-RSI data could be used for estimating M-AT(monthly mean air-temperature) successfully(Nakane, 1991). Up to now, the new regression equation described in Equation 1 had been obtained for estimating the M-AT from M-RSI data.

$$T_{ave} = K1 \times SR + K2 \times T_{ch4} + K3 \times (T_{ch4} - T_{ch5}) + K0 \quad ----(1)$$

$$SR = \cos(\theta - \delta)$$

$$\delta = 0.4093 \times \sin(0.01698 \times (JDAY - 80))$$

Where, T_{ch4} and T_{ch5} are brightness temperature(unit: degree Celsius) of Channel 4(wave band: 10.5～11.5μm) and Channel 5(wave band: 11.5～12.5μm) on NOAA AVHRR data respectively, SR and θ are the seasonal coefficient of outer solar radiation and latitude at the particular point respectively, δ is declination, JDAY is Juli-an Days. K0, K1, K2 and K3 are coefficients of regression equation.

The equation has four coefficients. These coefficients are unfortunately variable from place to place. Now, relations between coefficients in the equation and climatic conditions on the particular points are investigated for utilizing in various places.

3. Results

In this fiscal year, data set for applying the RWB Model to basins were made and application of the RWB model to Huaihe River basin. Climatic conditions related with coefficients of the regression equation, which is used for estimating M-AT from NOAA AVHRR GAC data, were also investigated. These results are summarized as follows:

(1) Preparation of data set

In order to apply the RWB Model to Huaihe River basin in China and Ohyodo River basin in Japan, precipitation data and evaporation data were acquired. In Huaihe River basin, 16 rainfall data, which are almost located along the river unfortunately, 7 evaporation data and 9 discharge data had acquired. Grid data of both precipitation and evaporation on 0.5 degrees x 0.5 degrees area were made over the basin by interpolating acquired point data. Data set assigning field models and river models to grid area over the basin were also made. In Ohyodo River basin, 36 rainfall data and 8 discharge data had acquired. Grid data on 2 minutes x 2 minutes area and data set assigning models to the basin are still being made. Figure 2 and 3 shows simply categorized fields and simply river system respectively in Huaihe River basin.

(2) Application of the RWB Model to Huaihe River basin

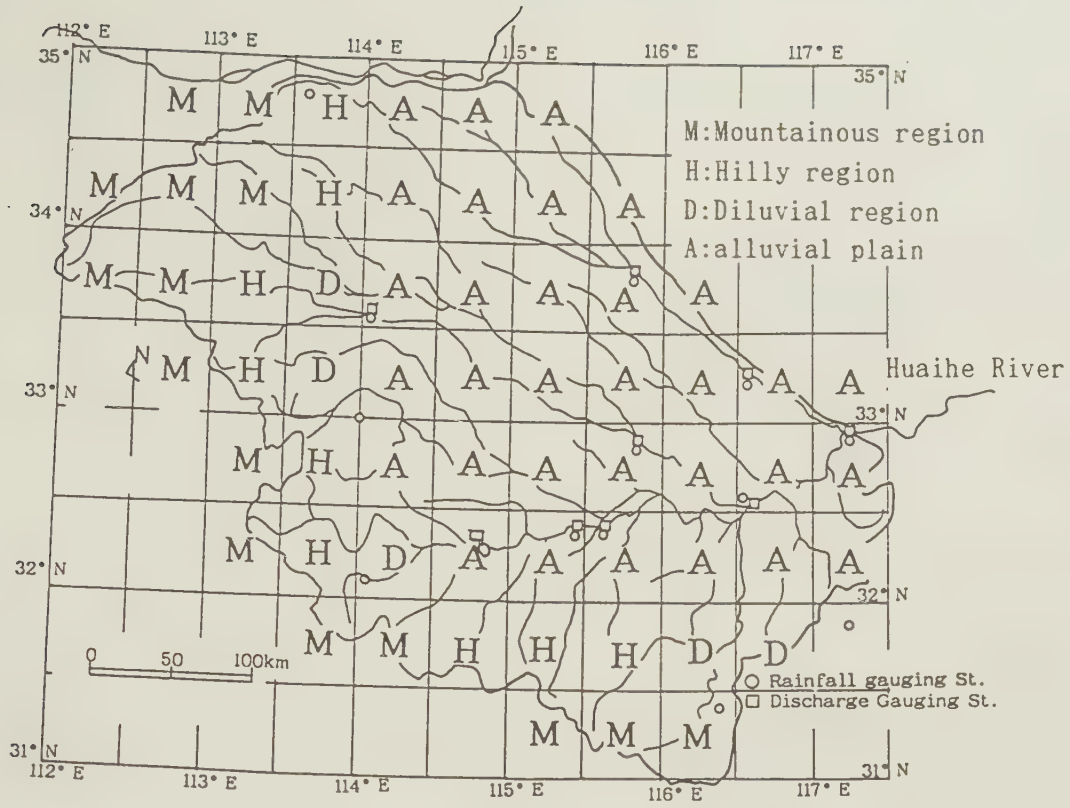

図２　淮河流域（対象流域面積:121,330km²）の分割領域の分類
Fig.2 Simply categorized field in in Huaihe river basin, where analyzing catchment area is 121,330 km2

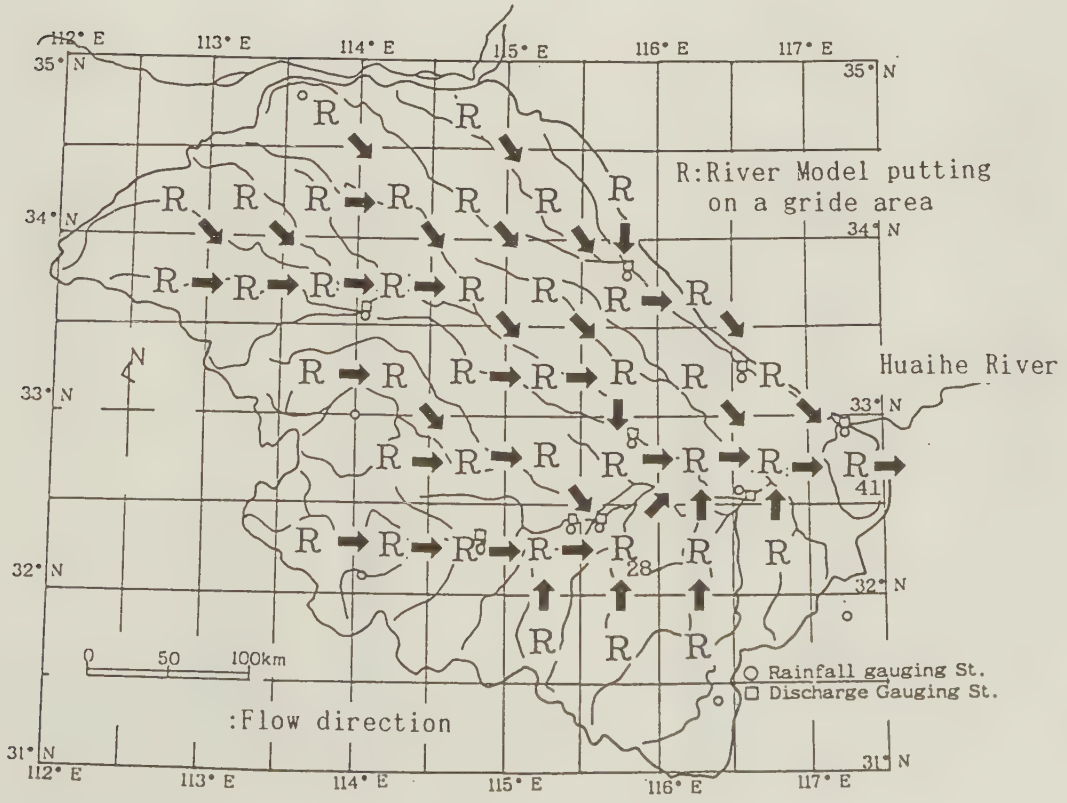

図３　淮河流域（対象流域面積:121,330km²）の単純化した河川網
Fig.3 Simplied river system in Huaihe river basin

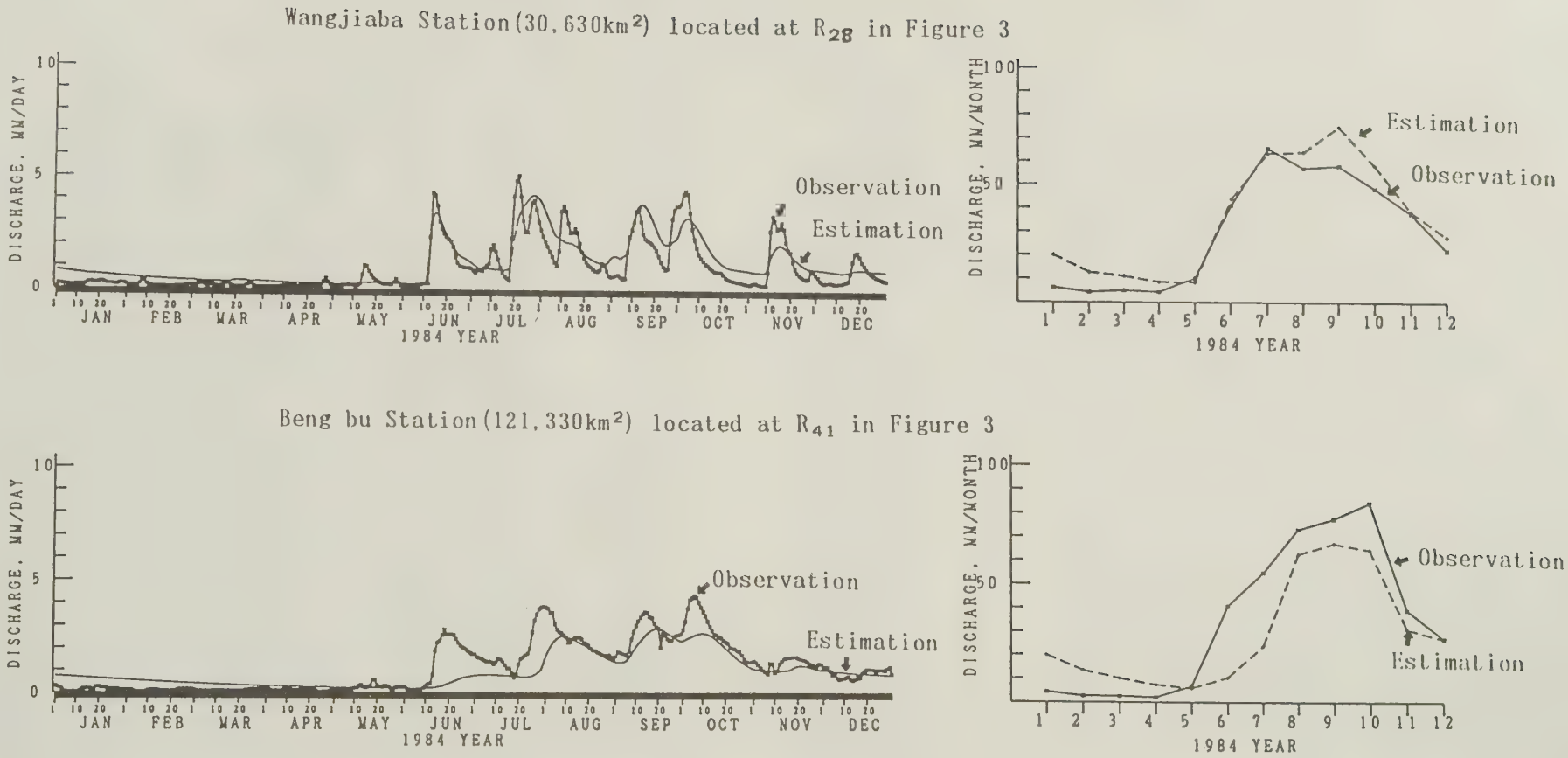

図４　淮河流域における雨の多い年(1984年)の日及び月流量推定結果

Fig.4 Estimation of both daily and monthly discharge by applying the regional water balance model to Huaihe river basin in 1984, when it was much rainy year.

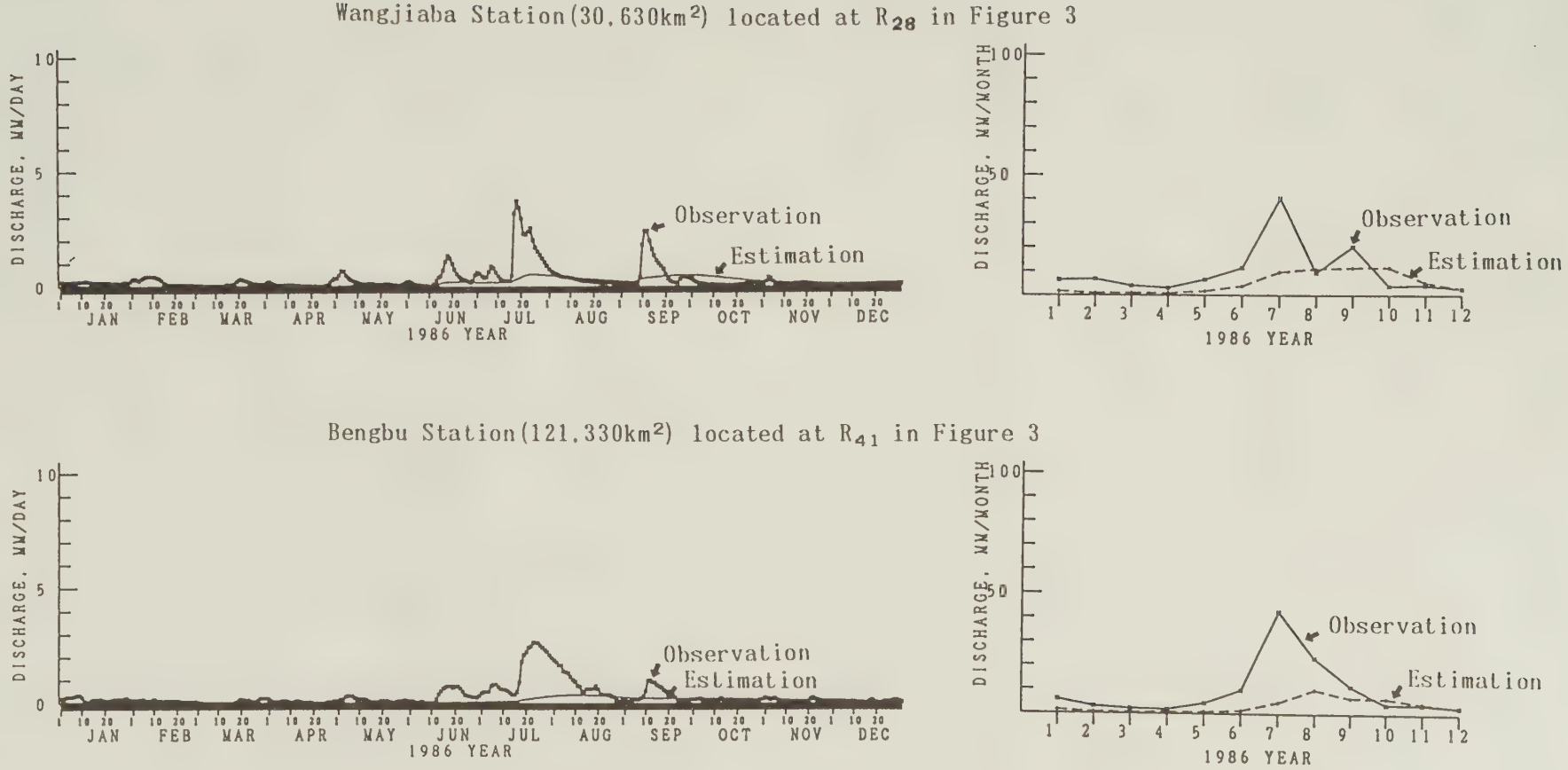

図5　淮河流域における雨の少ない年(1986年)の日及び流量推定結果

Fig.5 Estimation of both daily and monthly discharge by applying the regional water balance model to Huaihe river basin in 1986, when it was little rany year.

Estimation using the RWB Model in Huaihe River basin were curried out on daily basis from 1984 to 1988. Parameters of both field models and river models on the RWB Model were used as same as the models in Chaophraya River basin, Thailand. Though the RWB Model could predicts many hydrological elements, such as river discharge, water contents in the soil, storage amount of water in the ground, snow deposit, snow melt and actual evapotranspiration, only estimated discharge could compare to observed data. Figure 4 shows results in 1984, when it was wet year, were reasonable. In that year, mean annual rainfall in the basin was 1,218 mm and annual discharge at Bengbu, where the catchment area is 121,330 km^2, was 414 mm. Results in 1987, when it was also wet year, were reasonable as same as in 1984. Figure 5 shows results in 1986, when it was dry year, were rather bad. In that year, mean annual rainfall in the basin was 638 mm and annual discharge at Bengbu was 126 mm. Results in 1985 and 1988, when these were dry year, were also rather bad as same as in 1986.

(3) Coefficients, which are in the regression equation deriving M-AT, depending on water vapor in the atmosphere

Through the multiple regression analysis among M-AT, seasonal variation coefficient of solar radiation at the particular point and both brightness temperature of thermal infrared band(10.3 - 11.3μm) and brightness temperature difference between two thermal infrared bands(10.3 - 11.3μm and 11.5 - 12.5μm) on M-RSI data, and desirable coefficients in the regression equations, which could derive M-AT from the M-RSI data, were obtained at 47 points over the Asian Continent(see Figure 6).

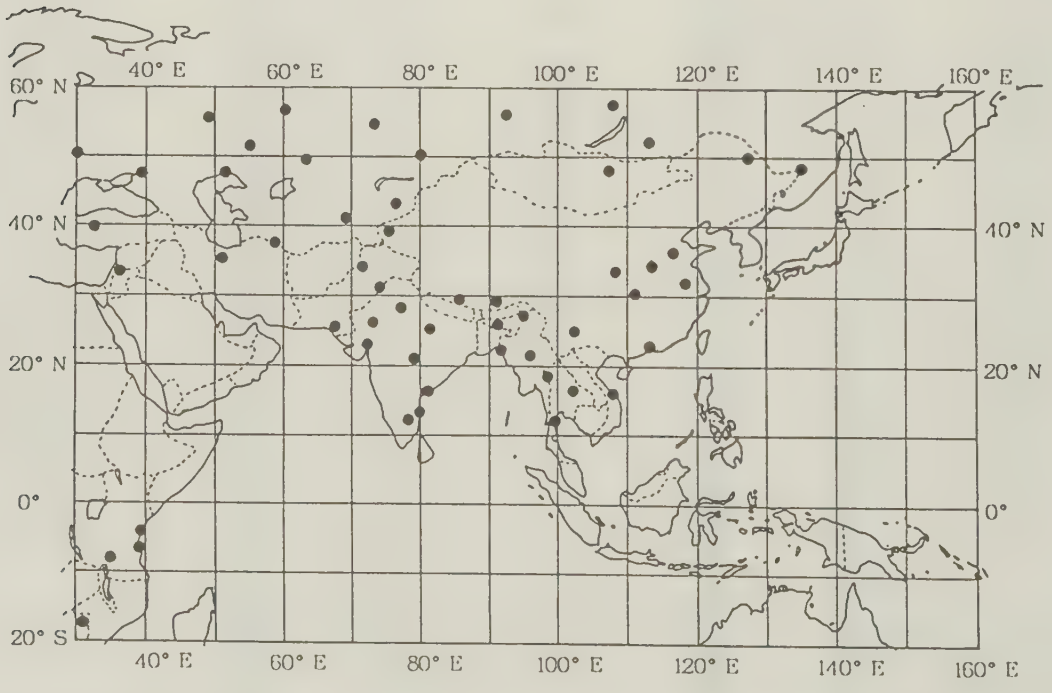

図6　NOAA AVHRR GACデータを用いた月平均気温を求める回帰式が得られた地点の分布
Fig.6 Distribution of particular points, where regression equations estimating the monthly mean air-temperature from NOAA AVHRR GAC data were derived.

These coefficients were variable from place to place. However, it was found coefficients relate with water vapor in the atmosphere. This discovery made the way to apply the regression equation to wide Asian Continent. Figure 7 and 8 show relations between K0 coefficients and latitude and between K2 coefficients and latitude at particular points respectively. Figure 9 and 10 show relations between K0 coefficients and A-WVP(annual mean water vapor pressure) on the surface and between K2 coefficients and A-WVP at particular points respectively. Where, A-WVP was calculated as the average of monthly mean water vapor pressure in a year. The monthly mean water vapor pressure were derived by Tetens Equation (1930) from M-AT and monthly mean relative humidity, which are climatic values described in Science Annual Data Book(1991).

4. Discussions

The RWB Model, which had been applied to Chaophraya River basin in Thailand successfully, was examined in Huaihe River basin. Though input data of rainfall and evaporation were very limited, results in wet year, such as 1984 and 1987, were reasonable. While, estimated discharge in dry year, such as 1985, 1986 and 1988, were very small comparing observed data. It seems four causes as follows;
a) Input rainfall data were too small comparing actual amount of rainfall in the basin. Rainfall amount in dry year is very different between in the field and in the mountainous area. While, rainfall amount in wet year is not so much different between in the field and in the mountainous area.
b) Use of ground water and/or storage water in the reservoir increase in dry year. These water seem to be maintain river flow more than estimated discharge.
c) Actual evapotranspiration was too small comparing observed evaporation. In dry year, temperature becomes relatively higher and evaporation increase. As the results, the RWB Model could not estimate appropriate actual evapotranspiration.
d) Huaihe River basin could drain rain-water easier than Chaophraya River basin. Drainage and irrigation system seem to be developed more than in Chaophraya River basin. The RWB Model could not estimate large river discharge in spite of comparatively heavy rainfall.

It will be clear that which causes are more affecting, if rainfall data in the mountainous area are acquired and use of ground water amount and/or released water amount from the reservoir are surveyed.

Coefficients(K0, K1, K2 and K3) in regression equations deriving M-AT relate with particular latitude respectively. According these relations, K0 coefficient becomes maximum around equator, where water vapor in the atmosphere seems to be much, and become minimum around 40 degrees north, where water vapor seems to be low considering deserted area spread around this latitude. While, K1 becomes minimum around equator and maximum of K1 appears around 40 degrees north. K2 and K3 have similar relation with particular latitude. K2 and K3 are stable in lower latitude than 20 degrees north. The higher the latitude than 20 degrees north, K2 and K3 increase gently. These fact indicate that strong relations between coefficients and A-WVP. Therefore, relations between coefficients and A-WVP on the surface were investigated.

Relations both between K0 and A-WVP and between K1 and A-WVP. K0 and K1 are stable in lower A-WVP than nearly 15 hPa. While, the more the A-WVP than nearly 15 hPa, K0 increases and K1 decreases contrary. These results are reasonable because of following reasons: The more the water vapor in the atmosphere, contribution rate of solar radiation to M-AT decreases and bias of M-AT increases gen-

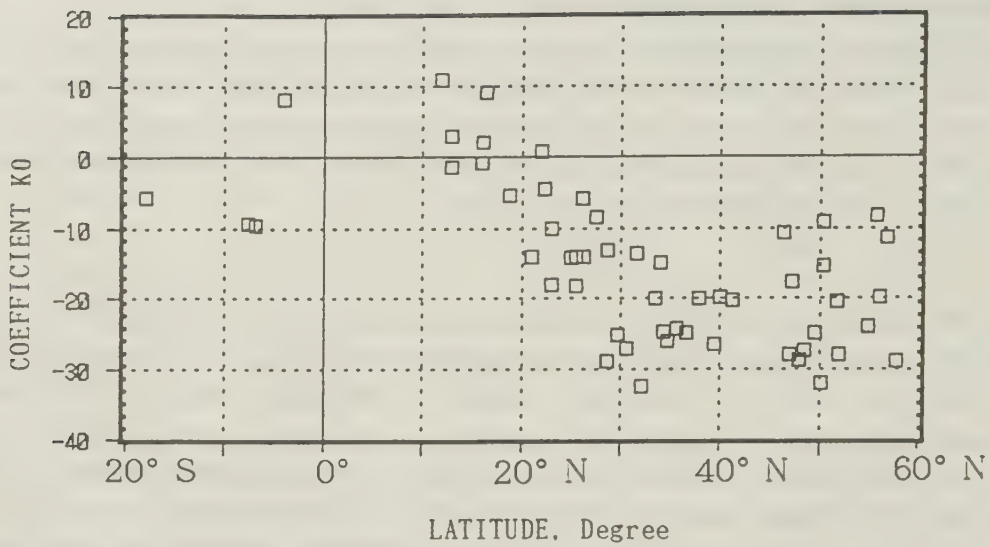

図７　回帰式の係数K0と対象地点の緯度との関係

Fig.7 Relation between K0 Coefficients on the regression equations depending on the latitude of the particular points.

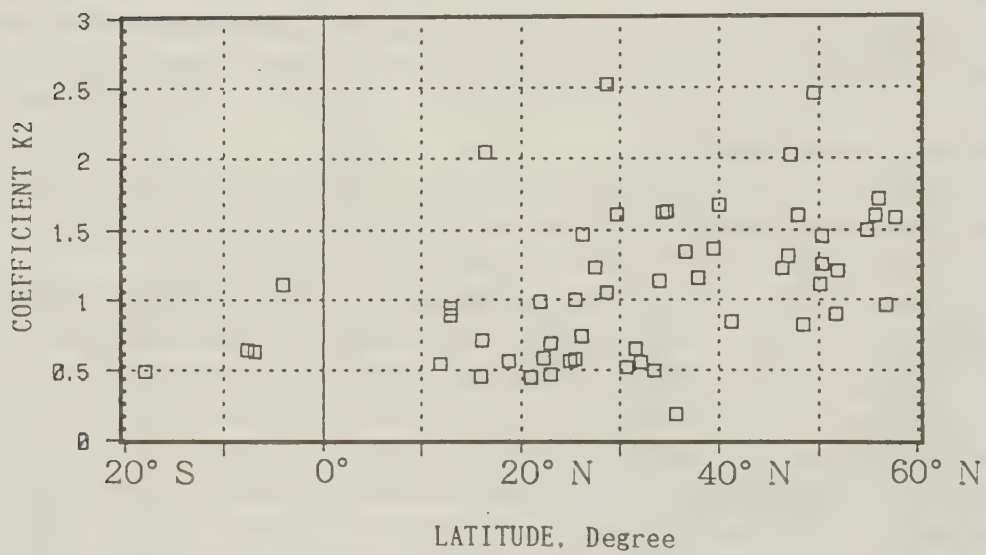

図８　回帰式の係数K2と対象地点の緯度との関係

Fig.8 Relation between K2 Coefficients on the regression equations depending on the latitude of the particular points.

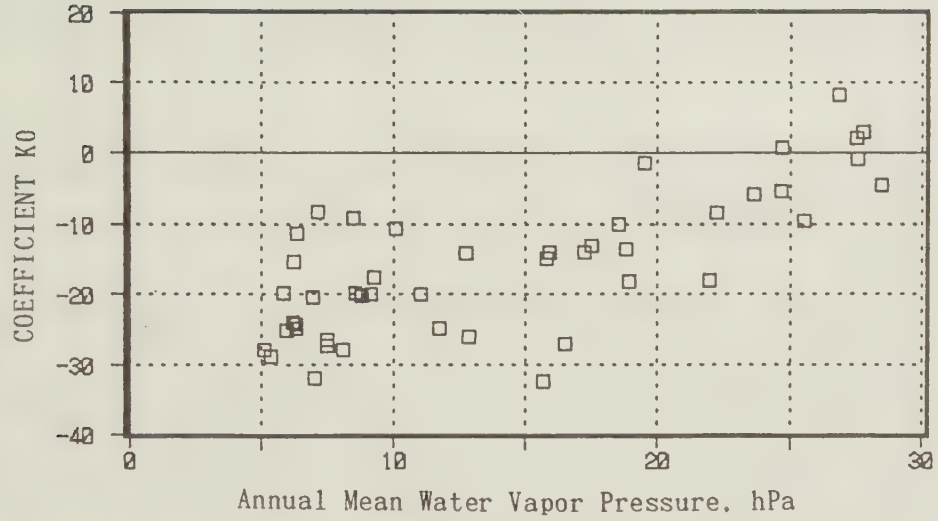

図９　回帰式の係数K0と対象地点の年平均水蒸気圧との関係

Fig.9 Relation between K0 Coefficients on the regression equations and annual mean water vapor pressure on the land surface of particular points.

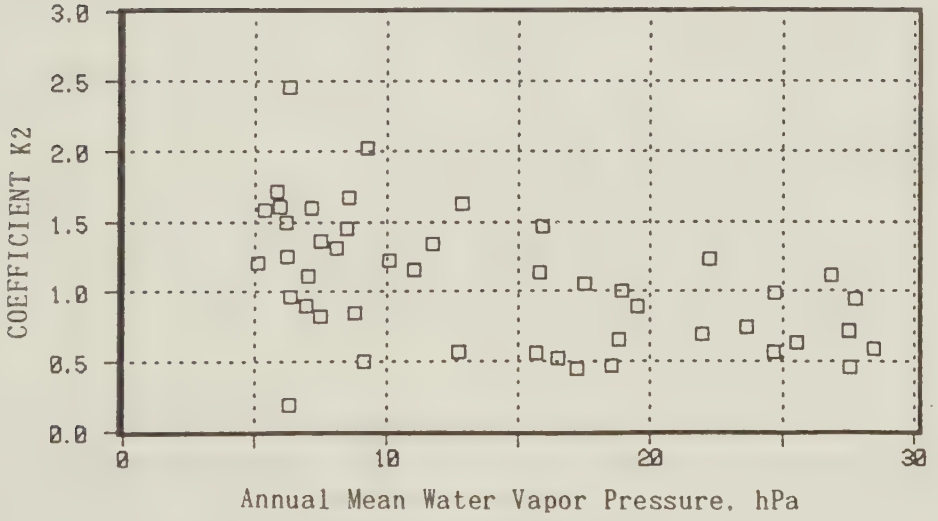

図10　回帰式の係数K2と対象地点の年平均水蒸気圧との関係

Fig.10 Relation between K2 Coefficients on the regression equations and annual mean water vapor pressure on the land surface of particular points.

erally. K1 functions as the contribution rate of solar radiation and K0 is bias in the regression equation.

K2 and K3 have similar relation with A-WVP. K2 and K3 become stable in higher A-WVP than nearly 15 hPa. The lower A-WVP than nearly 15 hPa. K2 and K3 increase respectively. These seem to cause from variation of surface emissivity to thermal infrared radiation depending on land surface condition, such as vegetation cover and soil wetness. The more study is still necessary to make clear the relations.

5. References

1)K. Nakane et al.; Regional Image Processing for NOAA AVHRR data Part II - Composition of the wide Regional Image, Report on the 16th Remote Sensing Symposium,67-70(1990).
2)K.Nakane; Monthly mean air temperature derived from GAC Data of NOAA-11 AVHRR, Proceedings of the 12th Asian Conference on Remote Sensing Vol.II J7.1-6(1991).
3)National Astronomical Observatory; Science Annual Data Book,(1991).
4)M. Sugawara et al.; Tank Model with Snow Component, Research Notes of the National Research Center for Disaster Prevention No.65, 1-293(1984).
5)C.W. Thornthwaite; An Approach Toward a Rational Classification of Climate, Geographical Review Vol.38, 55-94(1948).
6)S. Yazaki et al.; Regional Image Processing for NOAA AVHRR data Part I - Geometric Correction and Map Projection, Report on the 16th Remote Sensing Symposium, 63-66(1990).

6. Publications

1)K. Nakane; Estimation of Potential evaporation using GVI data on NOAA AVHRR, Report on the 19th Remote Sensing Symposium, 31-34(1993).
2)K.Nakane; Estimation of Monthly Mean Air Temperature over Asian Area using GAC Data of NOAA AVHRR, Journal of Japan Remote Sensing Vol.13 No.1, 14-26(1993).
3)K. Nakane et al.; Application of Regional Hydrological Model to Huaihe River Basin in China and Ohyodo River Basin in Japan, The first PRC-JAPAN Workshop on the Asian Monsoon Mechanism, 13-16(1994).
4)K. Nakane et al.; Estimation of regional monthly mean air-temperature using NOAA AVHRR, Report on the 20th Remote Sensing Symposium, 103-104(1994).
5)K. Nakane ; Regional Water Balance Model, Proceedings of 1995 Annual Conference, Japan Society of Hydrology and Water Resources, (1995).

7. International Cooperation

These studies are being carried out cooperatively with RSTAC/MWS(Remote Sensing Technology ApplicationCenter, Ministry of Water Resources in China) and SMRI/SMR/CMA(Satellite Meteorology Research Institute, Satellite Meteorology Center, China Meteorological Administration). In this fiscal year, we had cooperated as follows:

(1) Invitation of Chinese researchers from Feb. 27 to March 23

NIED(National Research Institute for Earth Science and Disaster Prevention) had invited two researchers from RSTAC/MWS. We cooperated following studies: (a)We surveyed Ohyodo River basin for making data-set of the river system on the regional water balance model. (b)We investigated the possibility to apply both SAR data and OPS data on J-ERS1 to monitoring the soil wetness of the land surface and classification of the land. (c)We exchanged recent research works each

other.

Through these cooperative research, some results were obtained as follows: (a) we made data-set of the river system on the regional water balance model in Ohyodo River basin. (b) By examinations in both Jiling City and the mouth of Yellow River in China, we understood that OPS data are very useful to make land-use map, and NVI derived from OPS data and backscattering coefficients derived by SAR data has some relation with soil wetness on the land surface.

(2) Visit to China from Oct. 18 to Nov. 1

Nakane visited RSTAC/MWS and jointed field observations carried out by RSTAC. We surveyed soil moisture by using three kind of methods simultaneously with observation by air-borne SAR from Shijiazhuang to Suning in the west of Beijing. These method are portable micro-wave radar (C band), the soil moisture apparatus of the heat prove type, which measures the heat conductivity in the soil directly, and the weighing method (sampling and weighing, then drying and weighing). We had the data to compare among soil moisture, gray value of SAR image and back-scattering coefficients measured by polarized micro-wave radar.

Nakane also visited SMRI/SMR/CMA and maintain-ed the soil moisture apparatus installed at the agricultural observatory in Baoding in the west of Beijing. After that, we exchanged recent research works eachother in SMC.

和文抄録

本研究は広域にわたるアジアモンスーン地域を対象として、降水、積雪・融雪、蒸発散、河川流出等の水文過程を的確にモデル化し、アジアモンスーンの変動が地域の水資源及び土壌水分に与える影響を0.5°×0.5°(約50km×50km)の等緯度経度の計算密度で詳しく評価できる広域水収支モデルの開発を目的としている。この種の広域の計算には大気大循環モデルが使用されている。しかし、地表の分解能は2°×2°～5°×5°(低緯度地域において約4～25万km²)であり、また、複雑な地表の水文過程のモデル化が未だ不十分であることから、地域の水資源、植生と結び付いたより適合性の良いモデルの開発が望まれている。本研究で開発する広域水収支モデルは広域の地表を０.５度×０.５度の領域にメッシュ分割し、降水量、気温等から任意の地域の河川流量、水の流域貯留量（土壌水分量、地下水量など）、実蒸発散量等を計算するモデルである。この広域水収支モデルはタンクモデルの概念を基本とし用いている。初期的な広域水収支モデルは乾期と雨期のある熱帯域に位置するタイのチャオプラヤ川流域（解析対象面積１１万ｋｍ²）に適用し、良好な予測結果を得た。現在、このモデルは中国の淮河流域（解析対象面積１２万ｋｍ²）及び日本の大淀川流域（解析対象面積２千ｋｍ²）において検証・評価を行っている。

この広域水収支モデルは入力データとして膨大な観測データを使用するが、これら広域のデータを密に収集するのは困難である。特に、蒸発量データは困難である。そのため、衛星データを用いた蒸発量の推定研究も行っている。蒸発量は気温と密接に関係しており、NOAA AVHRR GACデータを用いた月平均気温の新しい推定手法を開発し、その一般化手法の検討を行っている。これら研究の今年度の主な成果は以下の通りである。

(1)中国の淮河流域及び日本の大淀川流域において、広域水収支モデルの検証・評価を行うための入力データセットを作成した。

(2)広域水収支モデルを中国の淮河流域に適用し、1984年から1988年の５年間について、予測実験を行った。その結果、雨の多い年は妥当な結果を得たが、雨の少ない年は良い結果は得られなかった。入力データがほとんど川沿いのものであり、山地のデータを使用できなかったのが原因と思われるが今後の検討課題である。

(3)月平均気温の推定に用いた回帰式は４つの定数を持ち、それらは地域依存性を有している。この地域依存性は大気中の水蒸気量に関係していることが新たに分かった。

III. Synthetic Study on the Atmosphere-Ocean-Land Interactions
大気・海洋・陸面間の相互作用に関する総合研究

1. Experiment of the Atmosphere-Ocean-Land Interactions by the Use of General Circulation Models
大規模モデルによる大気・海洋・陸面間の相互作用に関する実験研究

Meteorological Research institute,
Japan Meteorological Agency
A. Kitoh, Y. Nikaidou
気象庁気象研究所
鬼頭　昭雄、二階堂　義信

(Abstract)

In order to estimate the influence of sea surface temperature and land condition variabilities to the atmospheric ones, three sets of ten year integration are performed; the A-run where the observed sea surface temperature is specified, the B-run with the fixed sea surface temperature, and the C-run with the fixed land condition in addition to the fixed sea surface temperature. The land condition (snow and ground wetness) is predicted by the model in the A-run and the B-run.

The variabilities of the monthly mean 850 hPa air temperature are compared at each grid between the A-run and the B-run. Over the sub- and tropical ocean, the variabilities increase significantly not only in temperature but also in precipitation, wind speed and height field. No change in temperature variabilities is found over the mid-latitude ocean east of Japan. The variabilities over land are different between in Brazil and Africa. The variabilities in Brazil is affected more by the sea surface temperature. The increase in the variabilities is not significant in the mid-latitude land except for U.S.A.. This result indicates that El Niño gives the predictability in U.S.A..

By the comparison of the results between the B-run and the C-run, the effect of land condition variabilities on monthly mean 850 hPa air temperature is shown. That effect is large from Eurasia through Japan. The result indicates that the annual variabilities of land condition is important for the climate prediction in those regions.

1. Objectives

The monsoon is an essential part of climates in the Asian countries by contributing to establish an annual cycle in many meteorological elements. For some contries the monsoon is the climate. And the interannual variability of the Asian monsoon affects climate variations not only in Asia but also in larger parts of the globe because the Asian monsoon region is located close to the ocean with the warmest sea surface temperature and is the most vigorous heating source of the atmospheric general circulation.

The purposes of the present study are to clarify the mechanism of atmosphere-ocean-land interactions in an Asian monsoon region including the Pacific and the Indian Oceans and the Eurasian continent by performing a series of numerical experiments.

2. Methods

We use an atmospheric general circulation model (GCM) which includes interactive land surface processes (in the first phase of the program) and also an ocean-atmosphere coupled GCM (in the second phase). By a series of numerical experiments with atmospheric and/or coupled GCMs, roles of land surface conditions and SST in establishing the monsoon and its variability will be investigated.

It has been argued that deterministic forecasts from initial conditions are limited on the time scale of one month, while on the seasonal time scale boundary conditions (sea surface temperature (SST) and land surface conditions such as snow cover, soil moisture and surface albedo) become more important as external forcing to the atmosphere (Shukla, 1985).

This year, we try to assess relative roles of SST and land surface conditions on atmospheric variability. The model used is a 5-level version of the MRI atmospheric GCM (Kitoh, 1991). Three sets of 10 year integrations are performed. Exp-A allows interannual variability of both SST and land surface conditions, Exp-B allows land surface variations but with climatological SST, while Exp-C has no interannual variability on sea nor land surface conditions. Comparison between A and B yields effect of SST and that between B and C yields effect of land surface conditions. Ratio of variability is usually used as an index of predictability or reproducibility.

3. Results

Figure 1a shows geographical distribution of the ratio of standard deviations for monthly mean 850 hPa temperature between Exp-A and Exp-B in the interannual time scale. It is assumed that the larger the value, the greater the predictability. Over the tropical and the subtropical oceans, significantly large values are obtained not only for 850 hPa temperature as shown but for precipitation, wind speed and height fields. Small values over the ocean east of Japan are noted. Over the tropical continent, South America is more affected by SST variability than Africa. Values are generally small over the mid-latitude continent, except over US where predictability exists. The latter result may be related with El Niño/Southern Oscillation (ENSO) and is confirmed by statistical prediction study by Barnston (1994) and by ensemble seasonal prediction study with GCM by Stern and Miyakoda (1995).

Figure 1b is the ratio between Exp-B and Exp-C, showing the effect of land surface conditions. Interannual variability of 850 hPa temperature increases over land when land conditions are allowed to vary interannually. Areas with significantly increased variability are found over Eastern Eurasian continent. They extend towards Japan and over the western North Pacific.

Figure 2 shows the seasonality. Here standard deviations of monthly mean surface air temperature or precipitation are averaged over the Eurasian continent. Interannual variability of surface air temperature is large in winter, while that of precipitation is large in summer. Comparing three experiments, interannual variability of Exp-A and Exp-B are similar each other, and that of Exp-C is smaller than the other two experiments in summer.

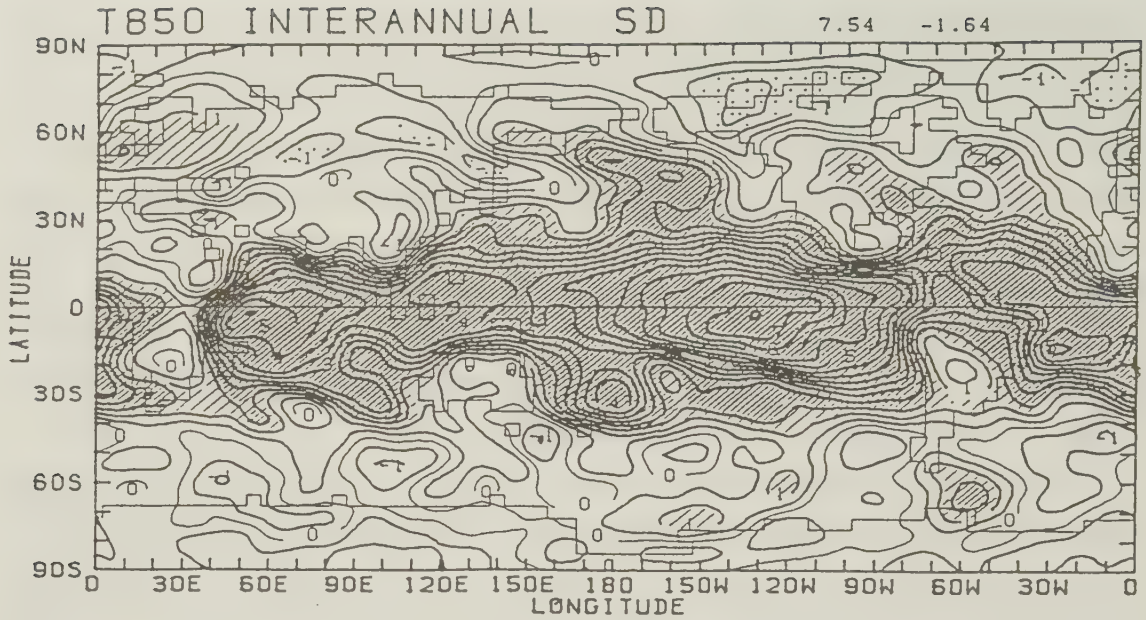

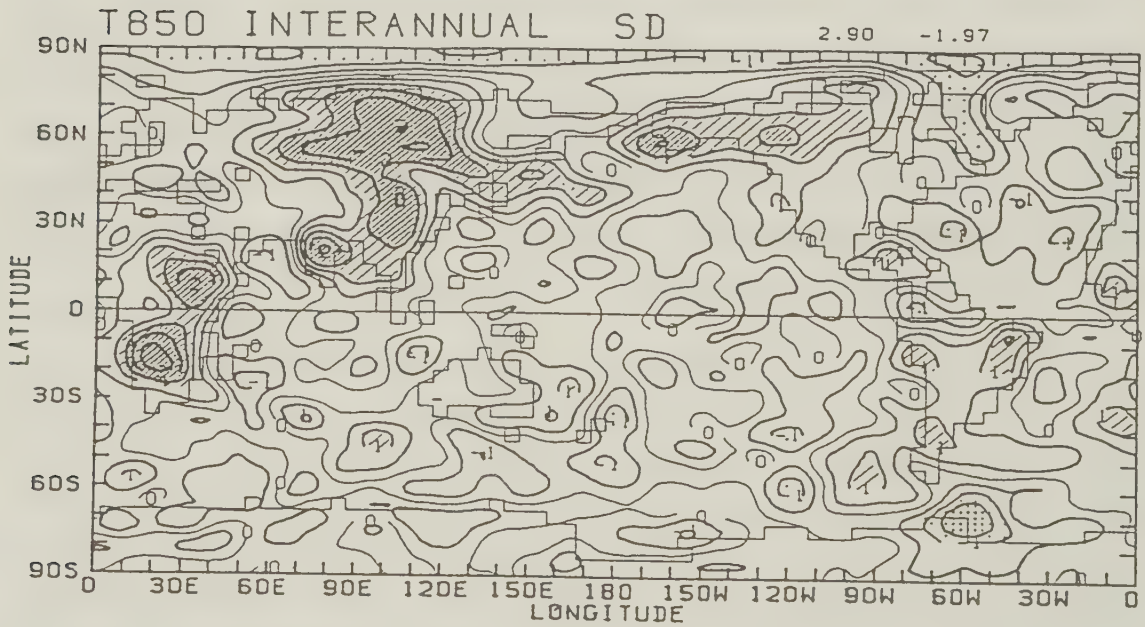

Fig. 1 (a) Ratio of interannual variability of monthly mean 850 hPa temperature for with and without interannual variations of SST. Values are shown in log2 scale with shadings for significant area. (b) As in (a), but for with and without interannual variations of land surface conditions.

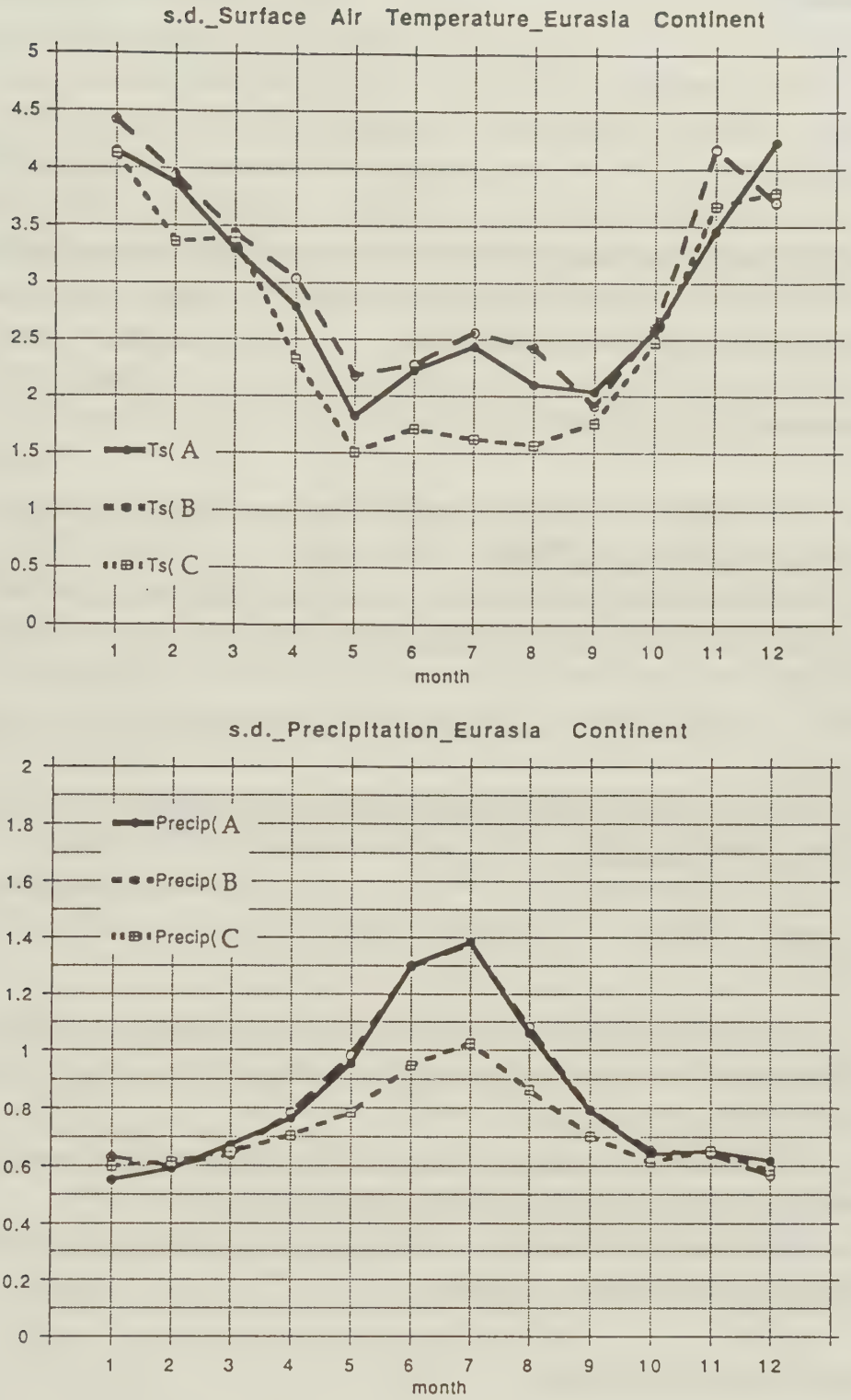

Fig. 2 (a) Seasonal change of standard deviations of monthly mean surface air temperature averaged over the Eurasia continent. Exp-A: solid line. Exp-B: dashed line. Exp-C: dotted line. (b) As in (a), but for precipitation.

4. Discussions

We have investigated relative roles of SST and land surface conditions on atmospheric variability. Results show a large effect of land surface variability over the Eurasia continent and to the east, particular in summer. This implies a relative importance of correctly forecasting land surface conditions over these areas than tropical or global SST, although land surface anomalies can be associated with SST anomalies through atmospheric circulation patterns. This latter question should be elaborated in further numerical experiments.

5. References

1) Barnston, A. G., 1994: Linear statistical short-term climate predictive skill in the Northern Hemisphere. J. Climate, 7, 1513-1564.
2) Kitoh, A., 1991: Interannual variations in an atmospheric GCM forced by the 1970-1989 SST. Part I: Response of the tropical atmosphere. J. Meteor. Soc. Japan, 69, 251-269.
3) Shukla, J., 1985: Predictability. Advances in Geophysics, Vol. 28B, Academic Press, 87-123.
4) Stern, W. and K. Miyakoda, 1995: Feasibility of seasonal forecasts inferred from multiple GCM simulations. J. Climate.

6. Publications

Kitoh, A., 1994: AGCM experiments on Tibetan snow and monsoon. Proceedings of the Interannual Conference on Monsoon Variability and Prediction. WCRP-84 (WMO/TD-No.619), 661-665.

Kitoh, A., 1994: Studies on atmospheric long-term variability with an atmospheric general circulation model. Tenki, 41, 447-458. (in Japanese)

Kitoh, A., 1994: Effect of SST variations on the atmospheric general circulation. Kisyou, 38, 13450-13454. (in Japanese)

7. International Cooperation

Two researchers, Dr. Zhang Xiangdong and Mr. Song Yukuan, of the Chinese Academy of Meteorological Sciences (CAMS) were invited to the MRI for 15 days from 1 September 1994 to 15 September 1994 for the exchange of the technical information.

One researcher, Mr. Tomoaki, Ose, of Japan Meteorological Research Institute

(MRI) was invited to Beijing and Guangzhou for 12 days from 27 October 1994 to 7 November 1994 to attend the Workshop and Symposium on the Asian Monsoon.

和文要旨

海面水温変動と陸面状態の変動のそれぞれが大気循環の変動に及ぼす影響を評価するために、Ａ：年々変動する実測海面水温を境界条件としたラン、Ｂ：Ａのランで使った海面水温の気候値を境界条件としたラン（海面水温の年々変動なし）、Ｃ：Ｂのランで得られた陸面状態の平均値を境界条件としたラン（陸面の年々変動もなし）をそれぞれ10年間積分した。ＡＢのランでは陸面状態（積雪・土壌水分）はモデルの予報変数である。

ランＡとランＢの各グリッドでの月平均850hPa気温の年々変動成分を比較した結果、海面水温の年々変動があることにより、熱帯・亜熱帯の海上は気温のみならず、降水量・風速・高度場とも有意に増加した。一方、中緯度の海上では日本東方で気温変動度に差がみられない。熱帯の陸上ではブラジルとアフリカでは様相が異なり、ブラジルの方が海面水温変化の影響を大きく受けている。中緯度の陸上ではおおむね増加は小さいが、米国は例外的に有意に変動度が増加しており、エルニーニョに関係した予測可能性の存在を示している。

ランＢとランＣの比較からで、陸面状態の年々変動を許すことによる月平均850hPa気温の年々変動度の増加を見積もると、ユーラシア大陸から日本付近にかけての領域で陸面状態の変動の影響が大きく現れた。このことはこれらの場所では陸面状態の年々変動を正しく評価しておかないと気候予測が出来ないことを示唆している。

III. 大気、海洋、陸面間の相互作用に関する総合研究
Synthetic study of the monsoon circulations

2. モンスーンのエネルギー収支に関する解析研究
Analysis of the energy balance of monsoon

気象庁気象研究所
尾瀬　智昭
Meteorological Research Institute
Japan Meteorological Agency
Tomoaki Ose

(Abstarct)

The seasonal change of the shortwave and longwave radiation at the top of the atmosphere in the Asian Monsoon is influenced by (1) snowcover in the continent, (2) clouds over the continent in spring, (3) clouds associated with monsoon disturbances, and (4) local ground condition. Therefore, the earth radiation budget in the Asia Monsoon regions is very different from that in the Southern Hemisphere which has the spacial and seasonal symmetry.

The above factors affect the shortwave and longwave radiation in the reverse sense. The contrast between land and ocean is rather remarkable in the net radiation field.

The net radiation has its maximum from May through July over the continent. That is evenly distributed in the extended regions from 20°N through 50°N. The even distribution over the continent of the net radiation during the Asian Monsoon is distinguished from the strong gradients in the latitudianl direction found in the net radiation over the North Pacific during the same season and the net radiation over the continent in April and August.

1. Objectives

Asia Monsoon is formed basically by the solar heat difference between land and ocean. In order to understand the mechanism of the Asian Monsoon activities including its onset, it is one way to analyze the spatial and temporal variabilities of the energy budget associated with the Asian Monsoon.

Earth Radiation Budget (ERB) is the budget of the shortwave radiation and the longwave radiation at the top of the atmosphere. ERB, especially the net radiation, is the most important factor in the whole energy budget of the Asian Monsoon. The seasonal change of the spacial ERB distribution over the Asia Monsoon regions is analyzed to study the important factors in controlling ERB. In addition, the radiative aspect of the Asia Monsoon is considered.

2. Methods

The used ERB data is the ERBE S-4 which consists of the monthly averaged upward shortwave/longwave radiation, planetary albedo, upward clear-sky shortwave/longwave radiation, clear-sky planetary albedo, and solar incident at the top of the atmosphere. The climatic monthly data is obtained from the period from '85 February through '88 January.

First, the seasonal march of ERB is studied in the latitude-time section, where the data is averaged within 70°E-100°E. The southern edge of the Eurasian Continent locates north of 20N. Tibet locates within 30°N-40°N. Second, ERB averaged between 30°N and 42°N is shown in the longitude-time section. Tibet is from 70°E through 100°E. Caspian Sea locates at 50°E, and the eastern edge of the Eurasian Continent locates at 120°E

Hereafter, upward longwave radiation, downward shortwave radiation, and downward net radiation are referred to as ULW,DSW and NET, respectively.

3. Results

(1) DSW and planetary albedo in the latitude-time section

Fig.1 (a) and (b) are DSW and planetary albedo in the latitude-time section, respectively. High planetary albedo over Tibet in spring is due to snowcover left from winter in addition to cloud albedo effect. In summer, both snowcover and cloudiness decreases, and DSW increases rapidly. But DSW is still small as comapared with other regions because the snowcover is found even in the summer season of Tibet. There is little cloud from winter to spring over the ocean, where planetary albedo is very low and DSW is over 340w/m^2. After the monsoon lower jet is strengthen, the clouds associated with the monsoon disturbances produce high planetary albedo north of the jet.

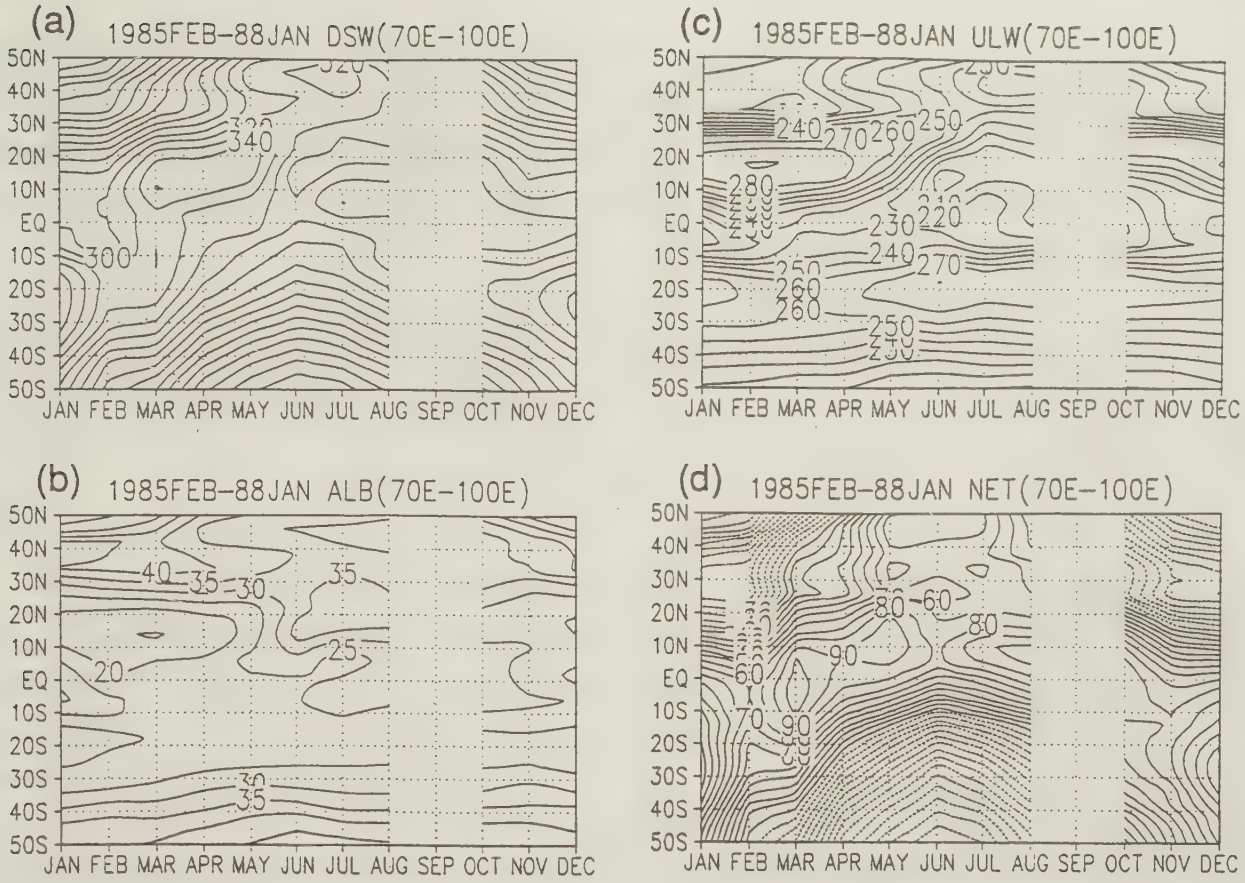

Fig.1 (a) downward shortwave radiation, (b) planetary albedo, (c) upward longwave radiation, and (d) downward net radiation in the latitude-time section. Those are averaged between 70°E and 100°E. Unit is w/m^2 except for % of planetary albedo.

Therefore, planetary albedo and DSW are not symmetric around summer in the Northern Hemisphere. In the Southern Hemisphere, DSW attains its maximum at 20°-30°S in December and January. The corresponding maximum locates at 10°-20°N over the ocean during spring in the Northern Hemisphere. Local maximum of DSW over the continent is found in July.

(2) ULW and NET in the latitude-time section

Fig.1 (c) and (d) are ULW and NET in the latitude-time section, respectively. The seasonal change of NET is relatively symmetric around June, that of DSW is not though. Large ULW cancels the DSW maximum at 10°-20°N over the ocean from spring to summer. Small ULW due to the monsoon clouds contributes to NET over the ocean during summer. NET over Tibet turns to be positive in March. The clouds and snowcover in spring tend to delay the seasonal change of

NET over Tibet as compared with the northern part of the continent. NET over Tibet has its maximum from May to July, that of DSW is in July though. Because ULW is relatively small from spring to summer as compared with that in mid-summer. It may be due to low ground temperature in spring.

The maximum of NET in the Northern Hemisphere locates at 10°N over the ocean. The maximum of NET in the Southern Hemisphere locates at 20°-30°S. NET over the continet is lower than NET over the ocean in mid-summer. This is not true for DSW. Large ULW over the continent in mid-summer contributes to small NET.

(3) DSW and planetary albedo in the longitude-time section

Fig.2 (a) and (b) show DSW and planetary albedo in the longitude-time section, respectively. The clouds produce high albedo over the continents in spring. In summer, high albedo due to the clouds is found east of Tibet at 100°-110°E. Low albedo is remarkable over the dry regions west of Tibet, especially at 60°E. The planetary albedo takes its minimum in August because of little snowcover and little clouds.

The seasonal change of DSW is small from May to August. The fine DSW distribution during summer is understood from the planetary albedo distribution. The maximum DSW appears in July when the solar incident is relatively large and the planetary albedo is relatively small.

(4) ULW and NET in the longitude-time section

Fig.2 (c) and (d) are ULW and NET in the longitude-time section, respectively. ULW has its maximum in late summer. ULW drastically increases from early summer over the dry regions west of Tibet. ULW increases slowly in the eastern parts of Tibet. The difference in the ULW seasonal change may be related to the ground condition. NET attains its maximum from May through July. This is because DSW is largely canceled by ULW in late summer. NET is relatively large around 100°E. The longitudinal distribution of NET is explained mainly from the distribution of DSW (or the planetary albedo) in the eastern part of the continent. Because ULW is very large from June through August over the dry and cloudless regions in the western part of the continent, NET is small in those regions. NET maximum appear in May at 60°E

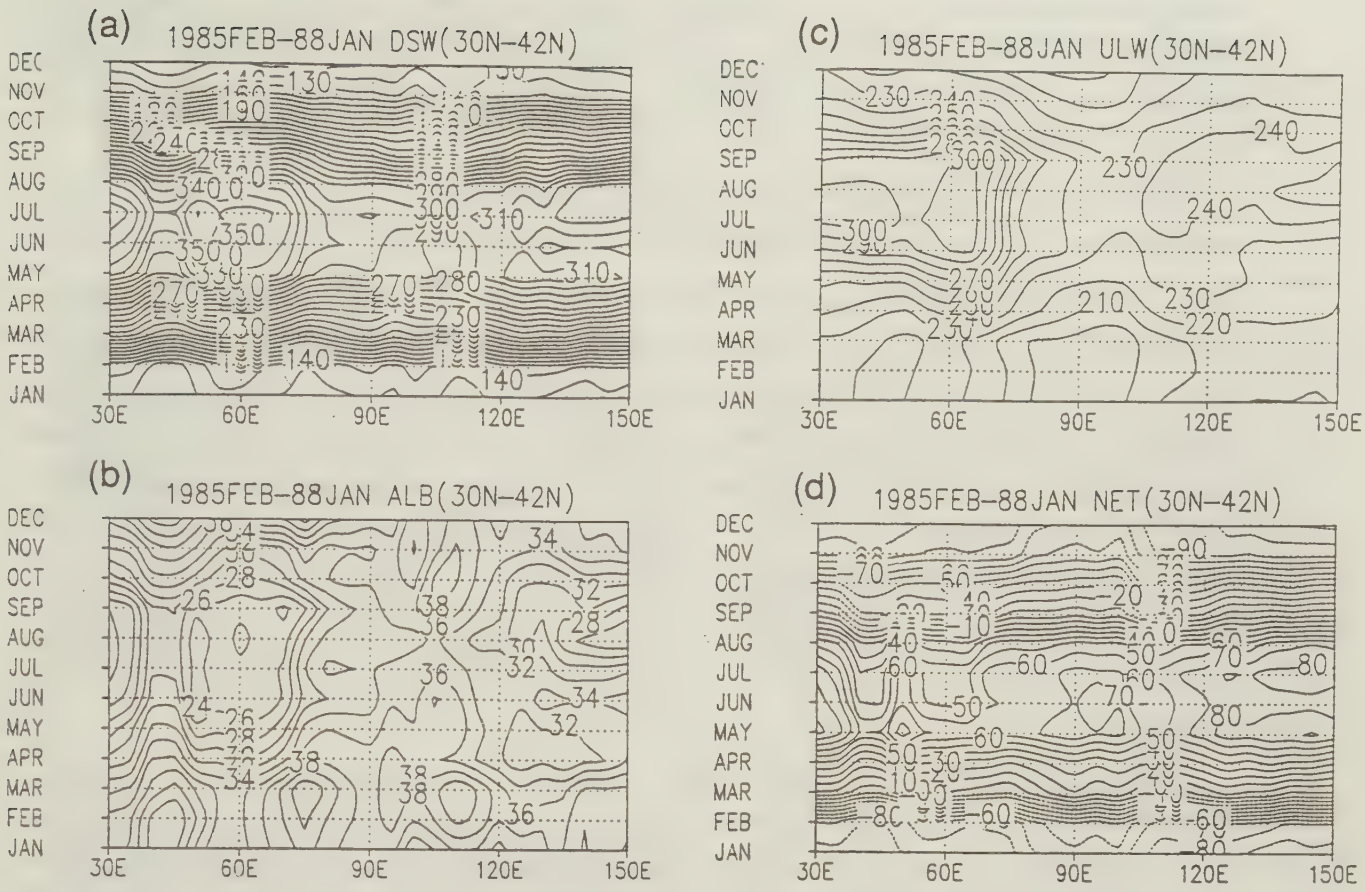

Fig.2 (a) downward shortwave radiation, (b) planetary albedo, (c) upward longwave radiation, and (d) downward net radiation in the longitude-time section. Those are averaged between 30°N and 42°N. Unit is w/m^2 except for % of planetary albedo.

(5) ERB during the Asian Monsoon period

We show that NET has its maxmum most of the regions from May through July. Fig.3 (a), (b), and (c) show DSW, ULW, and NET averaged from May through July, respecytively. DSW and ULW have the structure in the latitudinal and longitudinal directions. Large effect of cloud forcing characterized by low DSW and low ULW is apparent over South Asia. However, those structures found in DSW and ULW are not clear NET. DSW and ULW is well cancelled. The contrast between land and ocean is rather clear in those regions; NET is large in the tropical and the sub-tropical ocean, and small over the continent. NET is relatively even with the values between 60w/m^2 and 80w/m^2 over the Eurasian Continent from 20°N through 50°N. On the other hand, NET changes latitudinally over the Northern Pacific. The even distribution of NET

over the continent is the characteristics of the radiation during the Asian Monsoon season in May, June, and July. In fact, NET has large gradient in the latitudinal direction over the continent in April and August.

Fig.3 (d), (e), and (f) are the same as Fig.3 (a), (b), (c), respectively, except for those of '88 minus those of '87. Note the Asian Summer Monsoon is active/weak in '88/'87. The dominant anomalies are found over the oceans in DSW and ULW. Those are attributed to the anomalously strong cloud forcing of DSW and ULW. Though the effect of cloud forcing on NET is not clearly found, we may point out the tendency of positive NET over the ocean and negative NET over the continent. If it is the true NET difference between the strong and weak monsoon, anomalous NET radiation makes the sense to weaken the monsoon anomalies.

4. Discussions

ERB associated with the Asian Monsoon is influenced by a lot of factors like snowcover, the clouds over the continent in spring, and the clouds due to the monsoon disturbances and the ground condition. Those factors result in the complicated seasonal change of DSW and ULW. But NET over the continent, which is important as the energy source for the Asian Monsoon, is relatively simple. NET has its maximum from May to July when the solar incident is largest. NET has almost the same value over the extended regions of the continent during those season. This means that the energy input from the space is almost the same over the entire continent during the Asian Monsoon season. How these energy source is important is dependent on local land condition, other energy source like the energy flux through the atmosphere there.

Fig.3 (a) downward shortwave radiation, (b) upward longwave radiation, and (c) downward net radiation. Those are averaged between May and July. Unit is w/m^2. (d), (e) and (f) are the same as (a), (b) and (c), respecyively, except for the difference between those in '88 and in '87. The shaded area is negative in (d), (e) and (f).

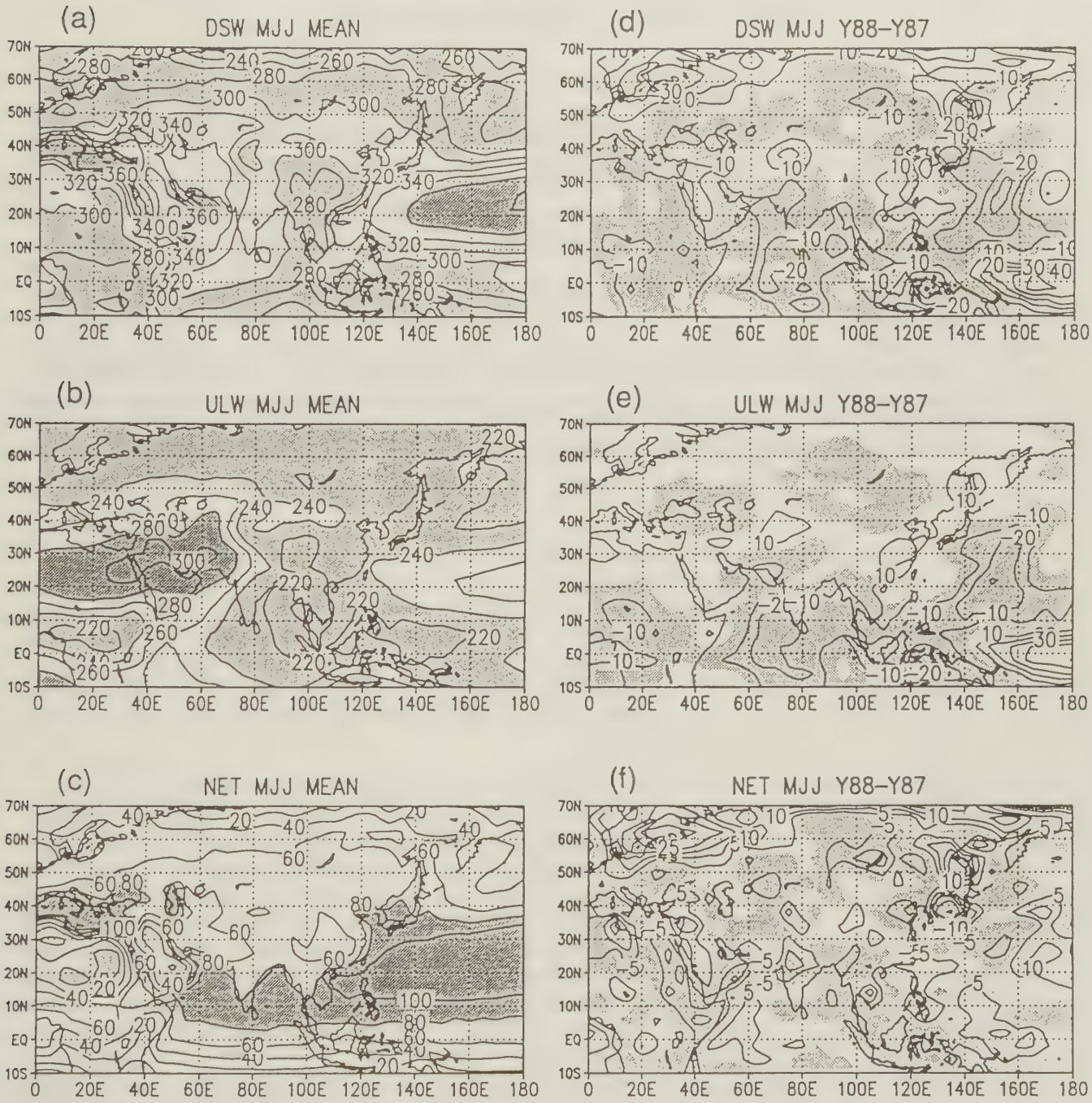

5. Publications

Aural presentation

speaker : Tomoaki Ose

Title : cloud factor obtained from the monthly averaged ERB data

Prints : Abstracts for Japanese Meteorological Society Spring Meeting in 1994 (in Japanese)

6. Abstract in Japanese

アジアモンスーン域の大気上端での短波および長波放射の季節変化には、（1）大陸の積雪、（2）春期の大陸上の雲、（3）モンスーン擾乱による雲、（4）地表面条件の地域性の影響が見られ、南半球の季節的空間的な対称性を持った季節変化とは大きく異なる。しかし、上記因子の短波放射と長波放射への影響はすべて逆センスであるため、正味放射ではむしろ大陸と海洋間のコントラストがより目立つ。

大陸上の正味放射は5月から7月にかけて年最大値を取り、北緯20度から50度の広い範囲で60 w/m^{2}から80 w/m^{2}のほぼ一定の値を取る。これは、同季節の海洋上での正味放射や、4月や8月の大陸上の正味放射の分布に見られる強い緯度依存性に比べた時、アジアモンスーン期の大陸での放射収支の特徴と言える。

Ⅲ. Synthetic study on the atmosphere-ocean-land interactions

3. Synthetic study of the monsoon circulations

Japan Meteorological Agency
Forecast Department
Long-range Forecast Division
H. Isobe and T. Aoki

(Abstract) For the purpose of understanding the atmosphere-ocean-land interactions, convective activity around the Philippines is correlated with 500hPa heights in the Asia. The relationships between the convective activity around the Philippines and the sea surface temperatures in the western Pacific and in the Indian Ocean are also studied by the correlation analysis. Following results are obtained by the analysis of data in August for the period from 1978 to 1993.

There are positive correlations between convective activity around the Philippines and 500hPa heights around Japan. On the other hand, negative correlations are found in sea surface temperatures in the Indian Ocean, while the correlations in the western tropical Pacific are not so high. Convective activity around the Philippines is highly correlated with the difference of sea surface temperatures in the western tropical Pacific from those in the Indian Ocean.

1. Objectives

The Asian monsoon circulation shows the variations on the time scales from several ten days to several years and has a significant influence on the climate in Japan and the world through the global atmospheric circulation. The purposes of this study are to clarify long-term variations of the monsoon circulation and to assess the influence on the climate in Japan and the world by the observational data analysis.

2. Method

We apply the correlation analysis to investigation into the relationship between convective activity around the Philippines and some factors, such as 500hPa heights in the Asia, sea surface temperatures in the western Pacific and in the Indian Ocean, and the difference of sea surface temperatures between in the western tropical Pacific and the Indian Ocean. Convective activity is defined as the area mean of high cloud amounts observed by Geostationary Meteorological Satellite in the area of HCPH shown in Fig. 1. Using the area means of sea surface temperatures at NINO.WEST and IND shown in Fig. 1, the difference (WEST-IND) of sea surface temperatures between the western tropical Pacific and the Indian Ocean is defined as subtracting IND from NINO.WEST. The data in August during the period 1978 to 1993 are used in this study.

3. Results

Figure 2 presents the distribution of correlation coefficients between convective activity and 500hPa heights. The area of a significant positive correlation stretches from the central Japan to the Korean Peninsula. This characteristic of correlation pattern agrees with the analysis performed by Kurihara and Tsuyuki (1987)[2].

Figure 3 presents the distribution of correlation coefficients between convective activity around the Philippines and sea surface temperature in the western Pacific and the Indian Ocean. The areas of negative correlation are located in the Indian Ocean, the South China Sea and the sea south of Japan. The correlation in the western tropical Pacific is low and the correlation coefficient between HCPH and NINO.WEST is a comparatively low value of 0.45.

Figure 4 shows a scatter diagram used to present a close correlation between WEST-IND and HCPH. The correlation coefficient is 0.74.

4. Discussion

It should be noted that the difference of sea surface temperatures between in the western tropical Pacific and in the Indian Ocean shows a significant correlation with convective activity around the Philippines in August. This result is consistent with the analysis presented by Graham and Barnett (1987)[1] and Lintzen and Nigam (1987)[3].

It would be interesting to study whether the relationship described here is applicable to another season or not. The mechanism of the relationship mentioned in this study requires a further investigation.

5. References

1) Graham, N.E. and T.P. Barnett, 1987: Sea surface temperature, surface wind divergence and convection over tropical oceans. Science, 238, 657-659.

2) Kurihara, K. and T. Tsuyuki, 1987: Development of the barotropic high around Japan and its association with Rossby wave-like propagations over the North Pacific, analysis of August 1984. J. Meteor. Soc. Japan, 65,237-246.

3) Lintzen, R.S. and S. Nigam, 1987: On the role of sea surface temperature gradients in forcing low-level winds and convergence in the tropics. J. Atmos. Sci., 44, 2418-2436.

6. Publications

Isobe, H., 1994: Relationship between convective activities around the Philippines and tropical SST pattern from the Pacific to the Indian Ocean. The first China/Japan Workshop on Asian Monsoon Studies, Beijing, China, 28-31 October,1994.

7. International Cooperation

none

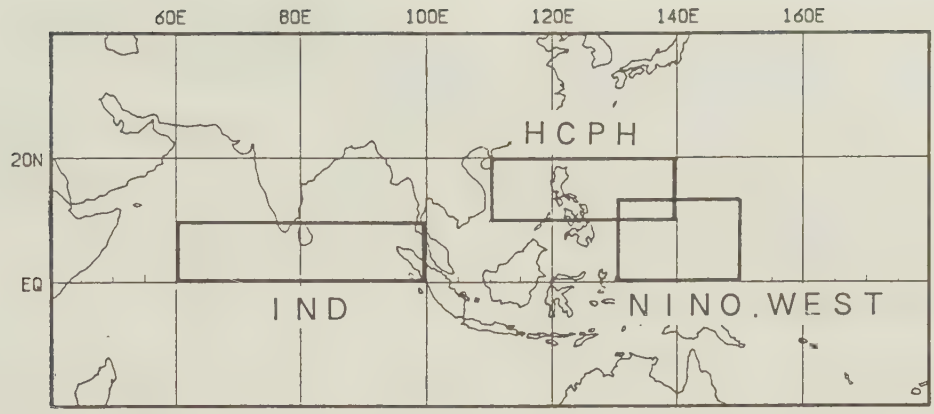

Fig. 1 Study area for the convective activity (HCPH) and the sea surface temperature (NINO.WEST and IND).

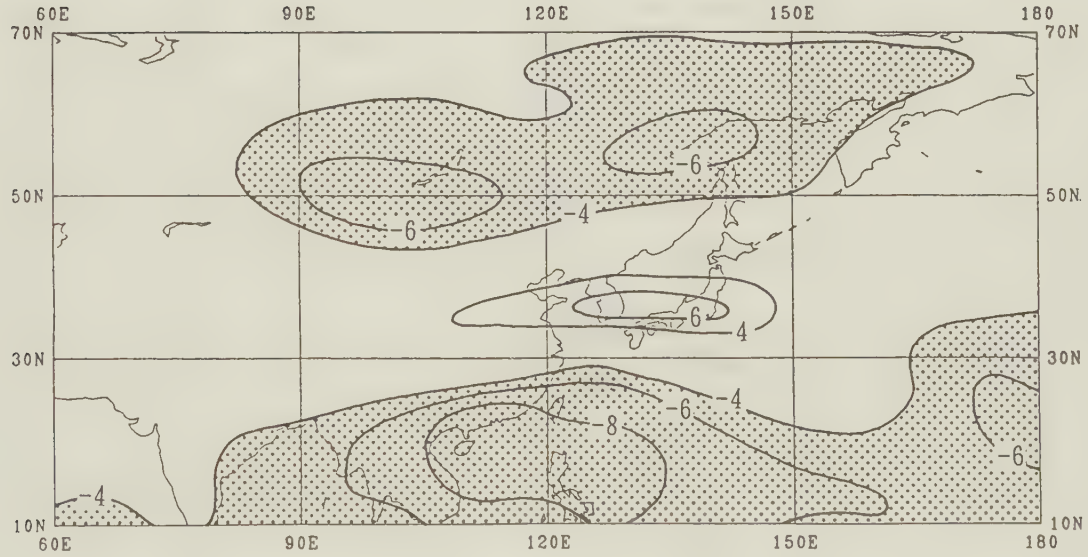

Fig. 2 Distribution of correlation coefficients between the convective activity (HCPH) and 500hPa heights. The contour interval is 0.2 and contours between -0.4 and 0.4 are excluded. Shading indicates areas where the correlation coefficient is less than -0.4.

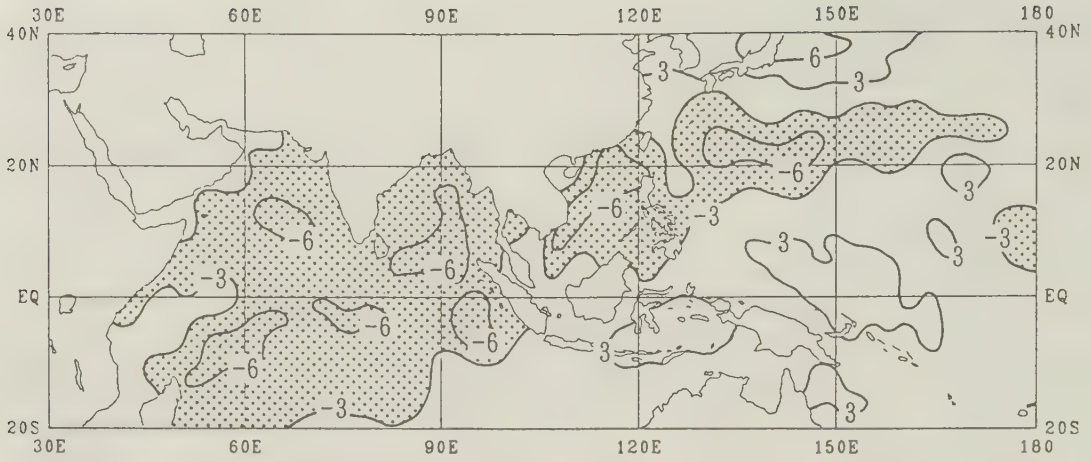

Fig. 3 Distribution of correlation coefficients between the convective activity (HCPH) and sea surface Temperatures. The contour interval is 0.3 and Contour of zero is excluded. Shading indicates areas where the correlation coefficient is less than -0.3.

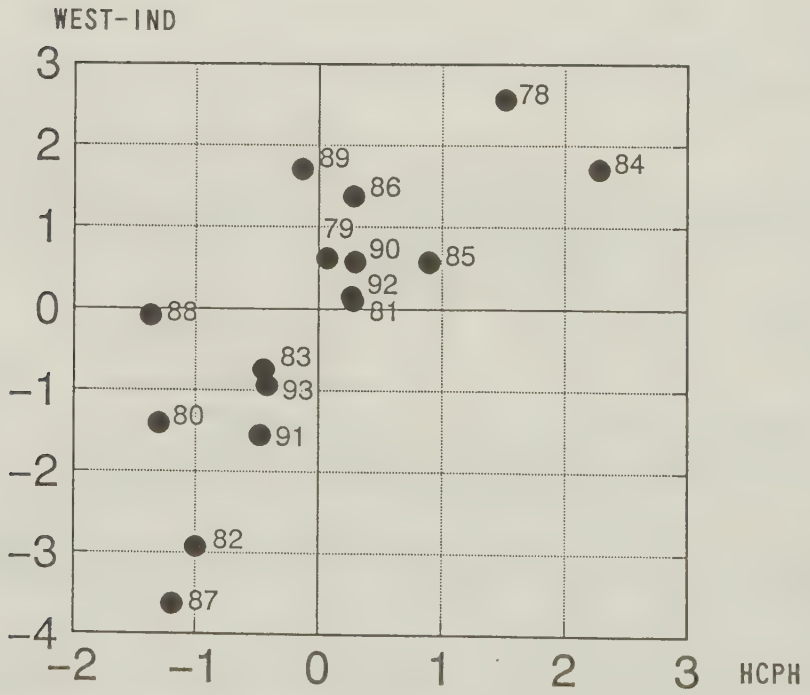

Fig. 4 Scatter diagram of the convective activity (HCPH) versus the difference (WEST-IND) of the sea surface temperatures between in the western tropical Pacific and in the Indian Ocean.
The number with dot indicates the year.

アブストラクト

フィリピン付近の対流活動とアジアの500hPa高度との相関解析を行った。またフィリピン付近の対流活動と西太平洋およびインド洋の海面水温との相関解析も行った。1978～93年の８月のデータに基づく解析で得られた結果は次のとおり。

フィリピン付近の対流活動と日本付近の500hPa高度は正の相関関係にある。インド洋や、南シナ海、日本の南の海域の海面水温とフィリピン付近の対流活動とは負の相関にあるが、熱帯太平洋西部の海面水温との相関は高くない。しかし熱帯太平洋西部とインド洋との海面水温の差は、フィリピン付近の対流活動と高い相関にあることが分かった。

観測・解析研究ディレクトリー

Directory of
Observation／Analysis Data Set

1. Directory Entry Title :
GMS IR Histogram

2. Directory Entry Start and Stop Date
Start Date : 1994-01-01
Stop Date : 1994-12-31

3. Sensor Name
VISSR

4. Source Name
GMS

5. Investigator, Technical Contact, and Author
(1) Investigator
Last name : Murakami
First name : Masato
Email : [M. MURAKAMI/MRI]ATI/JAPAN
Phone : +81-298-53-8668
Address : M.R.I., 1-1 Nagamine, Tsukuba, Ibaraki 305, Japan
(2) Technical Contact
Last name : Ohno
First name : Tomoo
Email :
Phone :
Address : Meteorological Satellite Center, Tokyo, Japan
(3) Author
Last name :
First name :
Email :
Phone :
Address :

6. Data Center
(1) Data Center Name : ＭＲＩ＞Meteorological Research Institute
(2) Dataset ID :
(3) Data Center Contact
Last Name :
First Name :
Email :
Phone :
Address :

7. Originating Center

8. Campaign or Project
ＪＥＸＡＭ＞Japanese Experiment on Asian Monsoon

9. Storage Medium

130 CCT's 13 G Bytes

10. Parameter Measured

Earth Radiative Process > IR equivalent black body temperature

11. Discipline Keywords

Earth Science > Atmosphere

12. Coverage

Minimum Latitude: 50S
Maximum Latitude: 50N
Minimum Longitude: 80E
Minimum Longitude: 160W

13. Location Keywords

Western Pacific

14. General Keywords

15. Revision Date

16. Science Review Date

17. Future Review Date

18. References

19. Summary

Available on the basis of cooperative research

1. Directory Entry Title :
Gridded Brightness Temperature from NOAA-11 AVHRR

2. Directory Entry Start and Stop Date
Start Date : 1991-05-01
Stop Date : 1991-08-31

3. Sensor Name
AVHRR > Advanced Very High Resolution Radiometer

4. Source Name
NOAA-11

5. Investigator, Technical Contact, and Author
(1) Investigator
Last name : Inoue
First name : Toshiro
Email :
Phone : +81-298-53-8669
Address : M.R.I., 1-1 Nagamine, Tsukuba, Ibaraki 305, Japan
(2) Technical Contact
Last name :
First name :
Email :
Phone :
Address :
(3) Author
Last name :
First name :
Email :
Phone :
Address :

6. Data Center
(1) Data Center Name : MRI>Meteorological Research Institute
(2) Dataset ID :
(3) Data Center Contact
Last Name :
First Name :
Email :
Phone :
Address :

7. Originating Center

8. Campaign or Project
JEXAM>Japanese Experiment on Asian Monsoon

9. Storage Medium

4 MT, 400M Bytes

10. Parameter Measured

Brightness Temperature of Split Window

11. Discipline Keywords

Earth Science

12. Coverage

Minimum Latitude : 40°S
Maximum Latitude : 40°N
Minimum Longitude: 40°E
Maximum Longitude: 150°E

13. Location Keywords

Indian Ocean, South Asia

14. General Keywords

15. Revision Date

16. Science Review Date

17. Future Review Date

18. References

19. Summary

This data set contains brightness temperature of split window data and satellite zenith angle data from AVHRR. These data are available at 0.1° latitude/longitude grid.

1.Directory Entry Title
XBT observation between the South China Sea and the Persian Gulf

2.Directory Entry Start and Stop Date
Start Date:07 Oct. 1990
Stop Date:

3.Sensor Name
XBT>Expendable bathythermograph

4.Source Name
Kashimasan Maru

5.Investigator,Technical Contact, and Author
(1)Investigator

		(Last Name)	(First Name)	(Middle Name)
Name	:	Mikawa	Tetsuya	
Email	:	ocean@hq.kishou.go.jp		
Phone	:	+81-3-3212-8341 Ext.5135		
Address	:	Oceanographical Division		
		Marine Department, Japan Meteorological Agency		
		1-3-4, Otemachi, Chiyoda-ku, Tokyo, 100		
		JAPAN		

(2)Technical Contact

Name	:	Yoshida	Takashi	
Email	:	ocean@hq.kishou.go.jp		
Phone	:	+81-3-3212-8341 Ext.5129		
Address	:	Oceanographical Division		
		Marine Department, Japan Meteorological Agency		
		1-3-4, Otemachi, Chiyoda-ku, Tokyo, 100		
		JAPAN		

6.Data Center
(1)Data Center Name: TOGA Subsurface Data Center
(2)Dataset ID :
(3)Data Center Contact

		(Last Name)	(First Name)	(Middle Name)
Name	:	Rebert	Jean	Paul
Email	:	rebert@orstom.fr		
Phone	:	+33-98-22-45-13		
Address	:	IFREMER/ORSTOM		
		PB 70		
		29280 Plouzane		
		FRANCE		

7.Originating Center

8.Campaign or Project
 Campaign : TOGA>Tropical Oceans and Global Atmosphere
 Campaign : WOCE>World Ocean Circulation Experiment

9.Storage Medium
 magnetic disks

10.Parameter Measured
 Ocean Dynamics>Temperature

11.Discipline Keywords
 Earth Science>Ocean

12.Coverage
 Minimum Latitude : 5N
 Maximum Latitude : 23N
 Minimum Longitude : 60E
 Maximum Longitude : 121E

13.Location Keywords
 Indian Ocean

14.General Keywords

15.Revision Date

16.Science Review Date

17.Future Review Date

18.References

19.Summary
 Japan Meteorological Agency is operating a voluntary ship for XBT observations at South China Sea, the Strait of Malacca to Sri Lanka, to the Persian Gulf. The ship, Kashimasan Maru, is a crude oil tanker.
 About 12 sections per year and 4 casts a day are observed.

1.Directory Entry Title
XBT observation between the Strait of Malacca and the Cape of Good Hope

2.Directory Entry Start and Stop Date
Start Date:25 Feb. 1990
Stop Date:

3.Sensor Name
XBT>Expendable bathyermograph

4.Source Name
Delmas Tourville

5.Investigator,Technical Contact, and Author
(1)Investigator

		(Last Name)	(First Name)	(Middle Name)
Name	:	Mikawa	Tetsuya	
Email	:	ocean@hq.kishou.go.jp		
Phone	:	+81-3-3212-8341 Ext.5135		
Address	:	Oceanographical Division Marine Department, Japan Meteorological Agency 1-3-4, Otemachi, Chiyoda-ku, Tokyo, 100 JAPAN		
Name	:	Rebert	Jean	Paul
Email	:	rebert@orstom.fr		
Phone	:	+33-98-22-45-13		
Address	:	IFREMER/ORSTOM PB 70 29280 Plouzane FRANCE		

(2)Technical Contact

Name	:	Yoshida	Takashi	
Email	:	ocean@hq.kishou.go.jp		
Phone	:	+81-3-3212-8341 Ext.5129		
Address	:	Oceanographical Division Marine Department, Japan Meteorological Agency 1-3-4, Otemachi, Chiyoda-ku, Tokyo, 100 JAPAN		

6.Data Center
(1)Data Center Name: TOGA Subsurface Data Center
(2)Dataset ID :
(3)Data Center Contact

		(Last Name)	(First Name)	(Middle Name)
Name	:	Rebert	Jean	Paul
Email	:	rebert@orstom.fr		
Phone	:	+33-98-22-45-13		
Address	:	IFREMER/ORSTOM PB 70 29280 Plouzane		

7.Originating Center

8.Campaign or Project
Campaign : TOGA>Tropical Oceans and Global Atmosphere
Campaign : WOCE>World Ocean Circulation Experiment

9.Storage Medium
magnetic disks

10.Parameter Measured
Ocean Dynamics>Temperature

11.Discipline Keywords
Earth Science>Ocean

12.Coverage
Minimum Latitude : 28S
Maximum Latitude : 5N
Minimum Longitude : 40E
Maximum Longitude : 94E

13.Location Keywords
Indian Ocean

14.General Keywords

15.Revision Date

16.Science Review Date

17.Future Review Date

18.References

19.Summary
Japan Meteorological Agency and ORSTOM Brest are operating a voluntary ship for XBT observations cooperatively on TWI Line No. IX6. The ship, Delmas Tourville, is equipped with a XBT launcher and a satellite transmitter by ORSTOM Brest, and JMA provides T-6 XBT probes.
About 8 sections per year and 4 casts a day are observed.

1. Directory Entry Title : JEXAM drifting buoy data in teh tropical Indian Ocean

2. Directory Entry Start and Stop Date
Start date : Feb. 2, 1990
Stop date :

3. Sensor Name : Surface drifter with SST sensor

4. Source Name : ARGOS

5. Investigator, Technical Contact and Author
(1) Investigator
Last Name : Michida
First Name: Yutaka
Email : ymichida@osman.jhd.go.jp (internet)
Phone : +81-3-3541-4387 FAX : +81-3-3545-2885
Address : 5-3-1 Tsukiji, Chuo-ku, Tokyo 104 Japan
(2) Technical Contact
Last Name : Michida
First Name: Yutaka
Email : ymichida@osman.jhd.go.jp (internet)
Phone : +81-3-3541-4387 FAX : +81-3-3545-2885
Address : 5-3-1 Tsukiji, Chuo-ku, Tokyo 104 Japan
(3) Author
Last Name : Michida
First Name: Yutaka
Email : ymichida@osman.jhd.go.jp (internet)
Phone : +81-3-3541-4387 FAX : +81-3-3545-2885
Address : 5-3-1 Tsukiji, Chuo-ku, Tokyo 104 Japan

6. Data Center
(1) Data Center Name : Japan Oceanographic Data Center
(2) Data Set ID :
(3) Data Center Contact
Last Name : Tatsuno
First Name: Tadao
Email : jodc@osman.jhd.go.jp (internet)
Phone : +81-3-3541-4295 FAX : +81-3-3545-2885
Address : 5-3-1 Tsukiji, Chuo-ku, Tokyo 104 Japan

7. Originating Center

8. Campaign or Project
Project : Japanese Experiment on Asian Monsoon (JEXAM)

9. Storage Medium : Magnetic Tape, 5 Mbyte

10. Parameter Measured : Locations of drifters, SST

11. Discipline Keywords Earth science > Tropical Indian Ocean > Oceanic currents
12. Coverage Minimum latitude : 33S Maximum latitude : 6N Minimum longitude : 38E Maximum longitude : 135E
13. Location Keywords Indian Ocean > Tropical Region
14. General Keywords Heat Transport
15. Revision Date March 31, 1995
16. Science Review Date
17. Future Review Date
18. References Surface Currents and Upper Oecan Thermal Structure in the Indian Ocean, 1994.

1. Directory Entry Title: Lower Atmosphere Observation by Wind Profiling Radar

2. Directory Entry Start and Stop Date

Start Date: 1992-11-24

Stop Date: Measurements are continued

3. Sensor Name: Wind profiler and Wind profiler/RASS

4. Source Name: Atmospheric Turbulence and Acoustic Wave

5. Investigator, Technical Contact, and Author

(1) Investigator

(Last Name) (First Name) (Middle Name)

Name: Yuji Ohsaki

Email: ohsaki@crl.go.jp

Phone: +81-98-895-2045

Address: 829-3, Daigusukubaru, Aza-Kuba, Nakagusuku-son, Nakagami-gun,
Okinawa 901-24, Japan

(2) Technical Contact

(Last Name) (First Name) (Middle Name)

Name: Yuji Ohsaki

Email: ohsaki@crl.go.jp

Phone: +81-98-895-2045

Address: 829-3, Daigusukubaru, Aza-Kuba, Nakagusuku-son, Nakagami-gun,
Okinawa 901-24, Japan

(3) Author

(Last Name) (First Name) (Middle Name)

Name: Yuji Ohsaki

Email: ohsaki@crl.go.jp

Phone: +81-98-895-2045

Address: 829-3, Daigusukubaru, Aza-Kuba, Nakagusuku-son, Nakagami-gun,
Okinawa 901-24, Japan

6. Data Center

(1) Data Center Name: CRL (Communications Research Laboratory)

(2) Dataset ID:

(3) Data Center Contact:

(Last Name) (First Name) (Middle Name)

Name: Yuji Ohsaki

Email: ohsaki@crl.go.jp

Phone: +81-98-895-2045

Address: 829-3, Daigusukubaru, Aza-Kuba, Nakagusuku-son, Nakagami-gun,
Okinawa 901-24, Japan

7. Originating Center:

8. Campaign or Project: JEXAM (Japanese Experiment on Asia Monsoon)

9. Storage Medium: DOS Formatted 5 inch Magneto Optical Disk

10. Parameter Measured: Backscattered Signals from Atmospheric Turbulence and Acoustic Wave

11. Discipline Keywords: Radar Remote Sensing of Atmosphere

12. Coverage

Minimum Latitude: 26° 16.9´N

Maximum Latitude:

Minimum Longitude: 127° 48.4´E

Maximum Longitude:

13. Location Keywords: Subtropical region

14. General Keywords: Asian monsoon

15. Revision Date:

16. Science Review Date:

17. Future Review Date:

18. Reference

19. Summary

This data set is composed by the Doppler spectrum measured with a wind profiler. A wind profiler is a Doppler radar to measure the signals scattered by clear air turbulence, and estimates the profile of the three-dimensional wind vectors.

全般の問い合せ先

〒１００　東京都千代田区霞ケ関２－２－１

科学技術庁研究開発局
総合研究課
地球科学技術推進室

Inquiries to:

Office of Earth Science & Technology,
Research and Development Bureau,
Science and Technology Agency,
2-2-1, Kasumigaseki, Chiyoda-ku, Tokyo 100
Japan